University of Glasgow

Virtual Prototyping and Optimisation of Microwave Ignition Devices for the Internal Combustion Engine

by

Christoph Schöning

Thesis Submitted to the
School of Engineering
University of Glasgow
for the degree of
DOCTOR OF PHILOSOPHY

July 09, 2014

Abstract

The internal combustion engine (ICE) has been used in automotive vehicles without any significant improvement in energy efficiency for over a hundred years. There are several possibilities for developing a 'greener' and more powerful engine such as the homogeneous charge microwave ignition (HCMI) system. In this thesis, the HCMI system is analysed and investigated through simulation based 'virtual prototyping' in combination with an intelligent optimisation and a Computer-Automated Design (CAutoD) framework. The intention is to analyse and develop designs which could be used to transform the existing ICE ignition system to the HCMI system with minimal modifications to the existing engine.

With the help of the finite element method (FEM), the microwave induced electromagnetic field in the engine cylinder is first simulated for 'virtual prototyping' using a computer model. This then takes the prototyping methodology one step further, by replacing the process of human tuning of the prototypes with a computer-automated search process using computational intelligence.

To realise this, an interface between the FEM model and the CAutoD framework is designed using the Application Programming Interface (API) of the FEM simulation software. This connection facilitates a rapid exchange of data between the simulation model and the search algorithm. Thus, rendering it possible to accommodate a wider exploration or a higher simulation resolution for superior and more accurate prototyping.

Another contribution of this thesis is the improvement of the search performance, including the combination of deterministic and non-deterministic search algorithm as well as using a new technique to solve optimisation problems without using the frequency as an input variable. The knowledge gained from the analysis of nature-inspired algorithms is used to perform a pre-evaluation and hence to provide a population which guides a non-deterministic search towards potentially optimal directions for the global maximum.

A CAutoD system is then developed to optimise digital prototyping on various aspects of the ignition device for the HCMI system. This helps deepen the understanding of relationships between the characteristic outputs of a design, and the input parameters that affect the performance of the device. The CAutoD system is first applied to a basic cylinder model, with one single antenna in the middle, to analyse the single variable changes for the antenna designs. It is discovered that the inner antenna length has a significant impact on the maximum electric field intensity inside the engine cylinder. Then it is applied to the design process involving multiple variable changes for the global optimum electromagnetic performance. The results are presented in multi-dimensional graphs, which illustrate the relevant relationships between the different input variables. For example, it is revealed that the resonance frequency is affected more by the piston position than by the antenna length, which underlines the importance of the correct and exact timing advance and control of the ignition event.

Subsequent to the extensive and systematic analysis of different antenna designs and input variables, Computer-Automated Design (CAutoD) has been applied to various designs to expand the understanding and virtual prototyping of the HCMI system. The criterion for the best design is to first provide the highest possible electromagnetic propagation performance within the cylindrical cavity by using the lowest microwave input power. With this, the reflection of the microwave energy from the cylinder back to the microwave source, under the geometric conditions of the cylinder and antenna model, will also be minimised. During the search process, the default antenna model was extended with an additional antenna, which leads to a dramatic decrease in the field, once the additional antenna is introduced. This determines, that any antenna at the outer shield of the coaxial cable and inside the cylinder head, interferes with the electromagnetic propagation inside the cavity and lowers the propagation performance.

The results show that this field will break down the air-fuel mixture inside the cylinder because the field strength is comparable to that, created by a spark plug. Hence, a HCMI system can be designed to replace a spark ignition system without requiring physical modifications to the engine cylinder.

List of Publications

Schöning, Christoph and Yun Li (2011). "Review electromagnetic field ignition system for Internal Combustion Engine". In: *Proceedings 17th International Conference Automation and Computing (ICAC'11)*. Huddersfield UK: IEEE, ISBN: 978-1-4673-0000-1, pp. 306–309.

Schöning, Christoph and Yun Li (2012). "Multivariable Simulations on a Homogeneous Charged Microwave Ignition System". In: *Proceedings 18th International Conference Automation and Computing (ICAC'12)*. Loughborough, UK: IEEE, ISBN: 978-1-4673-1722-1, pp. 50–55.

Schöning, Christoph and Yun Li (2013). "Multivariable optimisation of a Homogeneous Charge Microwave Ignition system". In: *Proceedings 19th International Conference Automation and Computing (ICAC'13)*. London, UK: IEEE, ISBN: 978-1-9085-4908-2, pp. 1–5.

Schöning, Christoph and Yun Li (2014). "Finite Element Simulation of Electromagnetic Properties for a Homogeneous Charge Microwave Ignition ICE System". In: *To be confirmed*. In Progress.

Contents

List of Figures

List of Abbreviations

AFR Air-Fuel Ratio . . . 8
API Application Programming Interface . . . 17
BDC Bottom Dead Centre . . . 4
CAD Computer-Aided Design . . . 36
CAutoD Computer-Automated Design . . . iii
CI compression ignition . . . 7
CNG Compressed Natural Gas . . . 12
CSV comma-separated values . . . 38
DC Direct Current . . . 21
DNA Deoxyribonucleic acid . . . 32
EA Evolutionary Algorithm . . . 30
EM Electromagnetic . . . 18
EOS equation-of-state . . . 16
FEM finite element method . . . 17
GA Genetic Algorithm . . . 17
HA Heredity Algorithm . . . 32
HCCI homogeneous charge compression ignition . . . 7
HCMI homogeneous charge microwave ignition . . . 7
ICE internal combustion engine . . . 1
LISI Laser Induced Spark Ignition . . . 16
LI laser ignition . . . 7
LNG Liquefied Natural Gas . . . 50
LPG Liquefied Petroleum Gas . . . 12
MI microwave ignition . . . 13
MWI Micro Wave Ignition GmbH . . . 15

NM Nelder–Mead . . . 29

PGA Predefined Genetic Algorithm . . . 95

PSO Particle Swarm Optimization . . . 30

QWCCR Quarter Wave Coaxial Cavity Resonator . . . 15

RF Radio-Frequency . . . 21

RF resonance frequency . . . 21

SI spark ignition . . . 7

TDC Top Dead Centre . . . 4

TE transverse electric . . . 19

TM transverse magnetic . . . 19

Nomenclature

B	Magnetic flux density
D	Electric displacement field
E	Electric field intensity
H	Magnetic field intensity
J	Current density
c	Speed of light
Z	Impedance of coaxial cable
n_a	Number density of neural atoms
n_i	Number density of ions
ρ	Electric charge density
ε_r	Relative permittivity

Chapter 1

Introduction

1.1 Current Challenges

Since its invention over a hundred years ago, the internal combustion engine (ICE) has been used in automotive vehicles with the ignition principle mostly unchanged. There have not been any significant improvements in energy efficiency or exhaust emission ever since the system was introduced, despite the increased demand for 'greener' and more powerful engines over the last few decades.

Currently, there exists two types of ICE ignition systems: the spark ignition (SI) and the compression ignition (CI). The ignition device of the SI system contains two electrodes with a small gap. A high discharge voltage generates the spark which ignites the air-fuel mixture inside the engine cylinder. The ignition is initiated from the gap between the two electrodes. The flame ball needs around 0.6 ms to grow to 25.4 mm and then to turn into combustion and thus the combustion is unlikely to be thorough (Taylor 1985; Jacobs 1996). These are the causes of low combustion efficiency and high emissions for the SI system. The CI system improved the ignition and fuel efficiency through a compression ignition; however the improvements are limited. Researchers have been actively working on alternatives and solutions to improve the efficiency of an internal combustion engine (ICE) and reduce emissions. Especially, at this time when the number of vehicles on the road has increased rapidly, and with it fuel consumption and harmful pollutants.

1.2 Existing Alternatives

Several possibilities to have been developed. One such example is the homogeneous charge compression ignition (HCCI) engine. A HCCI system aims to auto-ignite the homogeneous air-fuel mixture inside the engine cylinder at multiple locations simultaneously. Unfortunately, the closed-loop control of the system is difficult to realise, since pressure and temperature need to be monitored and adjusted for the successful initiation of combustion. The auto-ignition of the HCCI system leads to a much higher heat and pressure inside the combustion cylinder, which requires modifications to the engine and results in a faster wearing of the engine. So far, the HCCI has only been demonstrated successfully in concept in the laboratory, but has not been a success on the road (Epping et al. 2002; Johansson et al. 2008).

1.3 Objectives and Methodology of This Research

Furthering upon the idea of the HCCI system, this work focuses on the investigation of a microwave ignition (MI) based ignition system and the homogeneous charge microwave ignition (HCMI) system. So far, the microwave ignition system has not been implemented on the road either, and the development is ongoing (Gesche, Kühn, and Andrei 2008; Pertl and J E Smith 2009). The developing process requires fundamental theoretical analysis and simulation studies of the electromagnetic field in the engine cylinder, the reaction of the field to the homogeneously mixed air-fuel, the combustion properties, the mechanical effects, the exhaust emissions, and the prototyping of the ignition device and system. Unfortunately, the manufacture of physical prototypes is expensive and time consuming. Hence, developing a software based virtual prototype of the microwave ignition device is a critical step towards understanding and experimenting with the HCMI, which is the main objective of this research. The HCMI system combines the advantages of the SI and CI systems, as the ignition event is straightforward to control and the air-fuel mixture inside the cavity will ignite simultaneously. Several papers have shown the potential of the HCMI methodology, but the crucial dilemma of the HCMI is the generation of a sufficient electromagnetic field strength inside the engine cylinder to break down the air-fuel mixture simultaneously. To successfully build up resonance inside the engine cylinder, a very precise ignition timing, supply frequency, and emitter geometry is mandatory. The microwave emitter is called an antenna during this work. Each of these can be analysed using intelligent computer-automated search for optimum system parameters. For this reason, the virtual prototype model can be modified easily and offers the opportunity to run several different designs of microwave ignition devices over a short period of time at a mini-

mal cost in comparison with a physical prototyping process, if the simulation tool is validated. Hereinafter, a series of simulations can then be carried out to analyse the influences of HCMI parameters to the electromagnetic field strength inside the cavity. In this way, it is possible to understand more about the electromagnetic performance inside the engine cylinder. The simulation method to analyse the virtual engine cylinder is the finite element method (FEM). The first step in the prototyping process is to change only a single input variable of the simulation model to understand the relationship between said variable, the maximum electric field intensity inside the cylinder, the resonance frequency, and the bandwidth of the microwave signal. By applying a computer-automated search and using computational intelligence, the simulation model of the microwave ignition device can be analysed systematically in practical time and be modified automatically for the best performance.

1.4 Thesis Outline

Chapter 2 gives an overview about the commonly used ignition systems for ICEs and summarises the existing problems in order to illustrate the potential of a microwave ignition system. In chapter 3, the main focus lies on the design stage of the computer aided cylinder model of an internal combustion engine. This cylinder model is the foundation of all further investigations. Furthermore, the necessary components for the generation of a Computer-Automated Design system are outlined. Primary to any simulation, this chapter also validates the finite element method software package COMSOL Multiphysics for use in this thesis. Chapter 4 simulates and analyses the microwave distribution inside different cylinder models with various microwave ignition antenna designs. Following the extensive analysis using existing search methods, chapter 5 develops new search techniques to avoid the high influence of the resonance frequency on the propagation performance. These search techniques render it possible to solve optimisation problems with a minimum frequency range or even without using the frequency as an input parameter of the search process.

Chapter 2

Background and Literature Review

2.1 Ignition Principles

Modern petrol vehicles are fitted with an engine design which was derived from the Otto engine. The Otto engine was developed and designed in Germany, by the engineer N. Otto in 1876 (Taylor 1985). Although the principle of an ICE was described and patented by Barsanti and Matteucci in 1854 and some years later by Rochas in 1862, but Otto was the first engineer with the ability to successfully build the four stroke engine (Rajput 2005; Starikovskaia 2006). Today's modern petrol engines have exactly the same four strokes proposed by Otto (illustrated in Fig. 2.1). The process is divided into the following: the intake stroke, the compression stroke, the power stroke, and the exhaust stroke (Taylor 1985).

The four stroke cycle starts with the intake stroke which moves the piston from Top Dead Centre (TDC) to Bottom Dead Centre (BDC) inside the engine cylinder. Concurrently, the inlet valves open, the exhaust valves close, and the air-fuel mixture is sucked in to the cylinder due to the piston motion and the resulted depression inside the enclosed cavity. Once the intake stroke finishes, the compression stroke starts and the inlet valve closes. The piston moves in the opposite direction back from BDC to TDC. The air-fuel mixture inside the cylinder compresses and the pressure rises to its maximum of eighty bars (Taylor 1985). After that pressure rises, the power stroke starts and provides external usable energy. This stroke, also called the combustion or ignition stroke, is the main criteria for defining the engine's efficiency. Now the compressed air-fuel mixture ignites and drives the piston back from TDC to BDC. The resulted energy of the combustion will be transformed and temporarily stored in the flywheel of the engine. The inlet valves as well as the exhaust valves remain closed

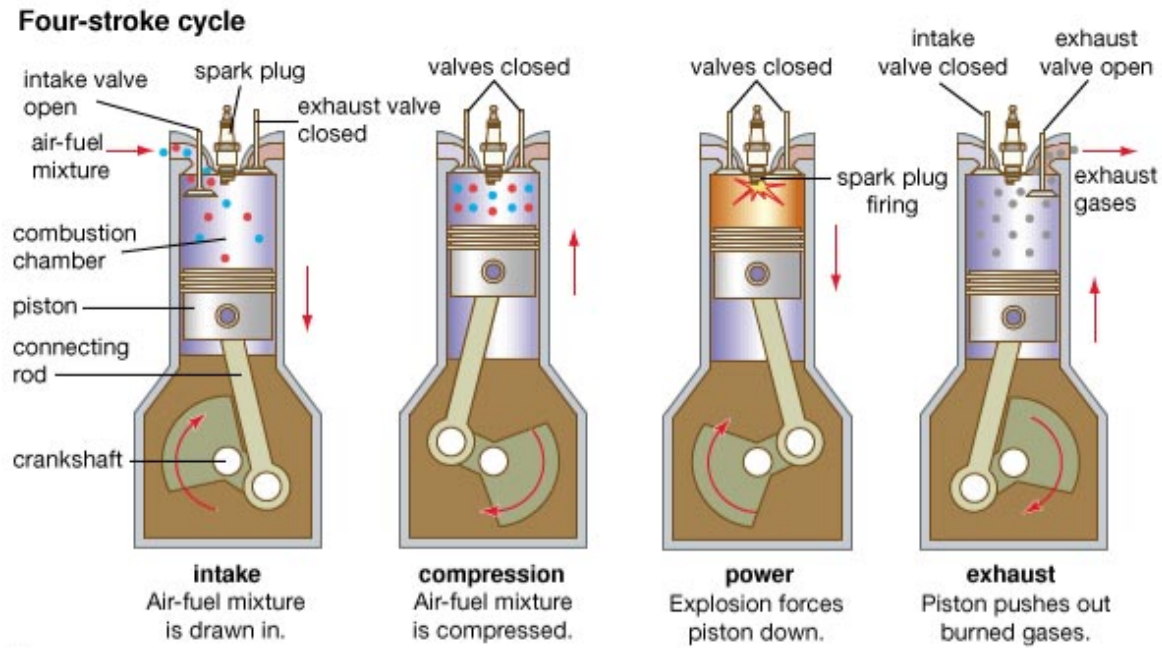

Figure 2.1: Four stroke cycle (Britannica Encyclopædia Online 2011)

during the combustion while the pressure reaches its maximum.

The last and fourth stroke, the exhaust stroke, removes the used gas from the engine cylinder. The piston moves again from BDC to TDC and the used gas will be pushed out of the cavity through the open exhaust valves (Rajput 2005). The exact position of the piston in the cylinder is expressed by the crank angle degree or the length to TDC.

In the following, the piston position is always measured in mm instead of degree. It describes the distance between the piston and the cylinder head, which is known as distance to TDC. Figure 2.2 shows this relationship.

The rod length is described by l, r is the crank radius, α is the crank angle, and x is the distance between the piston and the crank centre. The piston position to TDC can also be expressed as the angle by the approximate proportional relationship to the cosine of the crank angle. The reciprocating motion created by the continuously rotating crank and the connected rod can be simplified as a harmonic motion.

$$x = l + r \cdot cos(\alpha) \tag{2.1}$$

$$d = h - (l + r \cdot cos(\alpha)) \tag{2.2}$$

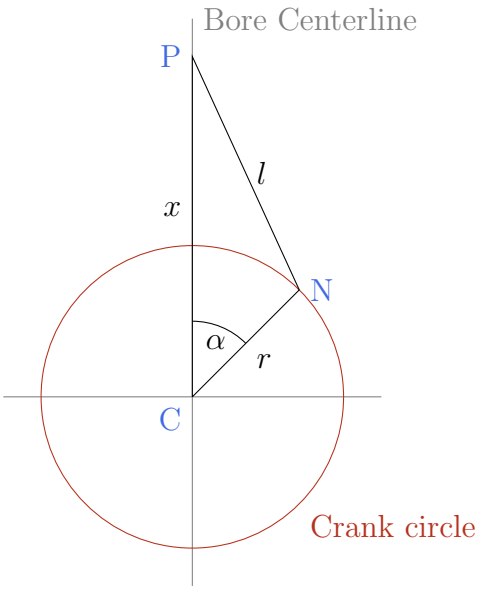

Figure 2.2: Piston motion

The distance to TDC is marked by d, and h is the total height of a single engine cylinder. A standard 90 mm cylinder, requires a range of $\pm 10°$ before and after TDC. This range is equivalent to a variation of the distance to TDC of approximately 0 mm to 5 mm.

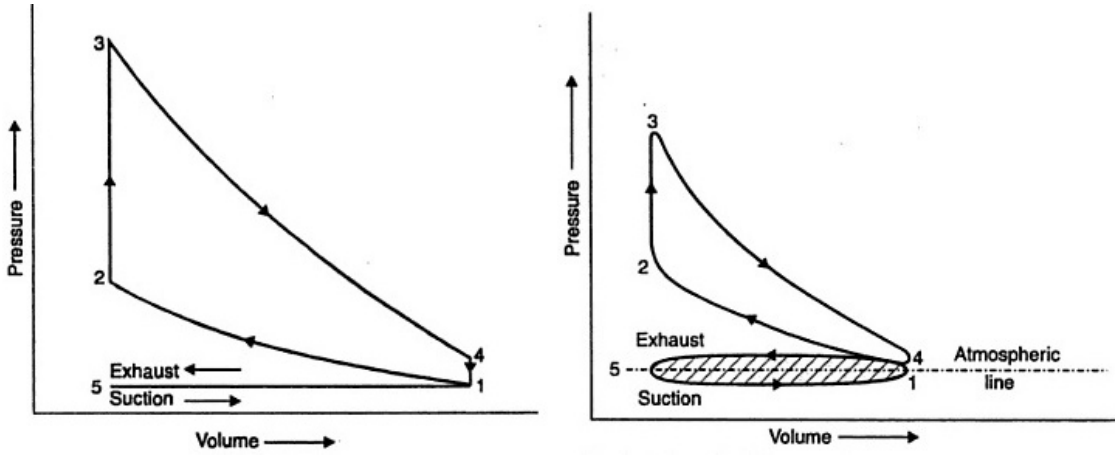

(a) Theoretical (b) Practical

Figure 2.3: Pressure against cylinder position (Rajput 2005)

Figure 2.3a shows the theoretical pressure-volume diagram of the four different strokes of an Otto engine. The piston volume can also be converted directly into the piston position, this is shown on the x-axis and the cylinder pressure on the y-axis. '1' shows the intake stroke, '2' the compression stroke, '3' the power stroke, and '4' the exhaust stroke. The combustion energy turns into mechanical usable energy during the power stroke. Unfortunately, approximately only 30 % to 35 % of the combustion energy can be used as effective power to move the vehicle. The other 65 % to 70 % appear as losses, which are mechanical, exhaust gas, and thermal losses of the combustion engine

(Jacobs 1996; U.S. Department of Energy 2013). The real pressure-volume diagram appears to be considerably different to the theory, shown in Fig. 2.3b.

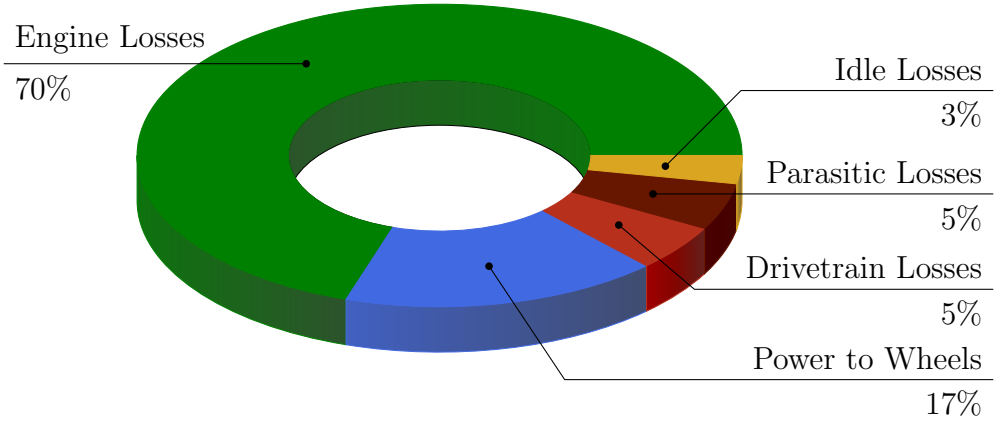

Figure 2.4: Fuel economy (U.S. Department of Energy 2013)

The energy losses of the engine depend on the driving style, therefore it is important to know the driving cycle used to determine the efficiency. Figure 2.4 shows the energy distribution of an ICE for a combination of city-highway driving. Approximately 14 % of the potential fuel energy reaches the wheels of the vehicle during city driving, this value increases to 26 % for highway driving.

The diagram plots the exact losses of the process related to the vehicle during combined city-highway driving. As can be seen, the main loss occurs due to the engine which means the engine has a huge impact on the overall efficiency. The other losses, not related to the engine, occur as drive train, transmission, idle (stop and go traffic), and parasitic losses such as power steering. Therefore, the potential of improving the fuel efficiency of an ICE with advanced engine technologies is enormous.

There are a number of different ignition systems available on the market, each with its advantages and disadvantages. Some systems like the spark ignition (SI)- or compression ignition (CI) system have been successfully used for decades in personal vehicles. Other systems, such as the laser ignition (LI) system, are more theoretical concepts and first field tests have partially demonstrated their insufficient ability to increase the performance significantly in comparison to the well established ignition systems (further discussion of the LI in section 2.5).

A completely new idea is the homogeneous charge compression ignition (HCCI) system. This system is still under active research and development and could have the potential to replace the common SI system. The priority of the homogeneous charge microwave ignition (HCMI) system is to increase the overall engine efficiency and yet being financially and economically attractive. Each system will be further described and discussed in the following sections. These reviews will focus on their individual

weaknesses and illustrate their potential to increase their performance and efficiency.

2.2 Spark Ignition

The SI system is one of the most commonly used systems in the world. Typically, the SI system transforms about 30 % of the combustion energy into usable mechanical energy. This is known as fuel efficiency (Jacobs 1996; Kutlar, Arslan, and Calik 2005; U.S. Department of Energy 2013). This low efficiency is based on the fact that the combustion of the air-fuel mixture is initiated by a spark at a single point inside the combustion chamber (see Fig. 2.5).

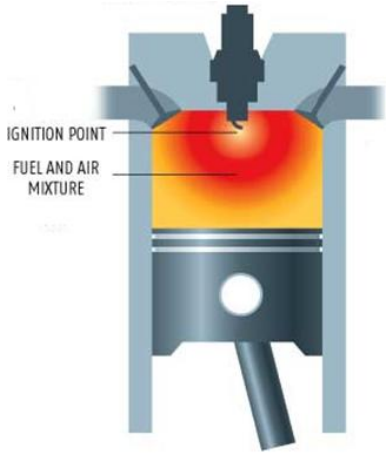

Figure 2.5: Spark ignition (Jalopnik 2007)

The spark plug is connected to the ignition coil which converts the battery voltage of 12 V into the necessary voltage needed to generate a reliable strong spark. The plug of a SI system requires two main components: the centre electrode which supplies new free electrons and the ground electrodes which collects the electrons. Once the spark is generated, it ignites the air-fuel mixture inside the engine cylinder.

Free electrons and ions participate in the random thermal movement of molecules. If an electric field exists in gas, the charged particles will accelerate in the field and gain extra kinetic energy. As a result of this additional kinetic energy, electrons would bounce off a gas molecule and hence the gas is ionised. The gap between the two electrodes of a common spark plug is within the range of 0.9 mm to 1.8 mm. The required discharge voltage proportionally rises due to the distance between the two electrodes. The prolonged use of the spark plug widens the gap incrementally as the electrode wears, thus a higher discharge voltage is required which heightens the probability of misfiring. The discharge voltage ranges between 10 kV to 25 kV but also depends on other factors such as the Air-Fuel Ratio (AFR), compression pressure, air-

fuel mixture temperature, electrode temperature, and humidity. The discharge voltage also rises proportionally to the compression pressure.

The AFR of the mixture affects the discharge voltage. In fact, there is clear tendency for the discharge voltage to be higher for a leaner air-fuel mixture. Vice versa, a leaner air-fuel mixture needs a lower discharge voltage and therefore this combination is more likely to cause misfire inside the cylinder. The last major factor which affects the discharge voltage, is the temperature of the air-fuel mixture. The discharge voltage drops down with a rising temperature, therefore a lower engine temperature increases the possibility of misfire during combustion.

The ignition process is divided into two phases: the first phase builds the flame core and the second phase includes the quenching effect, which contains the absorption of the heat and extinguishes the flame inside the engine cylinder. The gap between the electrodes can determine the relationship between these phases. If the plug gap is wider, the flame core is bigger and the quenching effect smaller in order to obtain a reliable ignition. In case the gap is too wide, a substantial discharge voltage would be required. If the discharge voltage exceeds the operation range of the coil, a reliable generation of a spark would become impossible.

The high voltage impulse is generated by the ignition system and applied between the two electrodes of the spark plug, the insulation between these electrodes breaks down. The current flows from the centre electrode to the ground electrode and an electrical spark is generated. The spark triggers the ignition and the combustion of the compressed air-fuel mixture inside the combustion chamber. The discharge process is extremely short, within just about a single ms and yet extraordinarily complex. The general role of the spark plug is to supply a reliable and strong spark between the two electrodes at a specified time, to trigger the combustion of the compressed air-fuel mixture. When the combustion is initiated by the spark, the air-fuel mixture inside the cylinder cannot ignite simultaneously. The time from the start of ignition until the flame ball grows to 25.4 mm is about 0.6 ms (Taylor 1985; Jacobs 1996).

Once the supplied voltage exceeds the dielectric strength of the air-fuel mixture, the matter becomes ionised between the gap of the two electrodes. The recently ionised mixture becomes a conductor and allows the electrons to flow across the gap between the centre and ground electrode of the spark plug. As the flow of electrons surges across the gap, the temperature of the spark channel rises to 60 000 K. The intense heat in the spark channel causes the ionised mixture to expand rapidly and to produce a small explosion, which is know as the start of ignition.

The high pressure and resulting heat inside the engine cylinder forces the gas in the combustion chamber to react. The spark plug initiates a small fireball in the spark gap which burns the gas. The dimension of the fireball mostly depends on the exact composition of the mixture inside the combustion chamber but also on the level of combustion turbulences at the time when the spark was initiated. The correct ignition time advance is essential for the general engine performance, and therefore needs to be optimised. A too small ignition timing advance would lead into a delayed combustion and dramatically decrease the usable power of the engine. A too large timing advance would result in misfiring and the combustion energy would be used to push the piston back before reaching TDC. This also decrease the ignition performance and overall engine efficiency.

2.3 Compression Ignition

The CI system is used in diesel engines, developed by R. Diesel in 1893. The philosophy behind this design was to invent an engine that has a higher efficiency than the ordinary SI engine (Moon 1974).

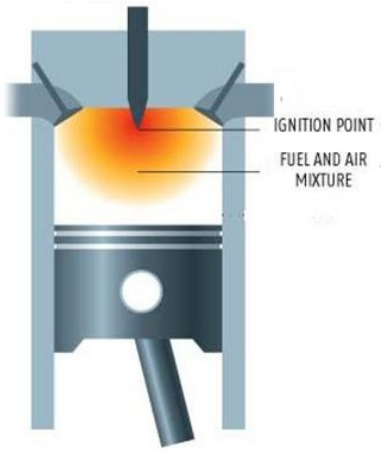

Figure 2.6: Compression ignition (Jalopnik 2007)

The diesel ICE is based on compression. In contrast to the gasoline powered SI engine, the CI system uses highly compressed hot air instead of a spark to ignite the fuel inside the engine cylinder. While the piston moves from BDC to TDC the air inside the combustion chamber will compress and the pressure increase. The pressure inside the combustion chamber is significantly higher in comparison to a SI engine. The ignition will occur when fuel is injected into the combustion chamber near TDC. Due to the high pressure and temperature the fuel ignites once it comes into contact with the pre-compressed air inside the engine cylinder. To optimize the burning process and reduce pollutant emissions, researchers are currently trying to develop the HCCI system.

2.4 Multi-Spark Ignition System

The multi-spark ignition system is another possible solution to the reduction of fuel consumption and pollutants. This system replaces the common spark plug of a SI system with a cylinder head which is fitted with at least three spark plugs.

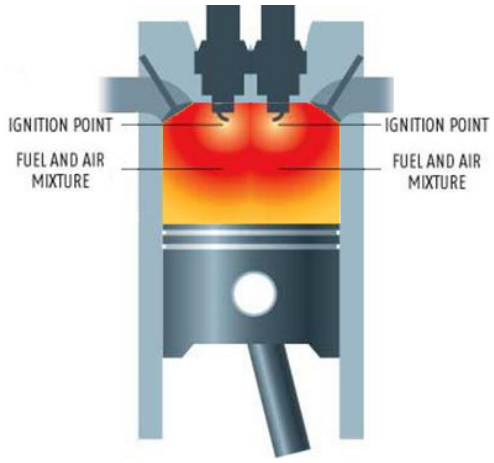

Figure 2.7: Multi-Spark ignition

A multi-point ignition system makes it possible to initiate the ignition at multiple points inside the engine cylinder simultaneously. Theoretically this system should increase the engine efficiency but can also cause misfiring during the combustion (J. A. Davis 1989; Schaus 2003).

2.5 Laser Ignition

Laser ignition is another type of a one point ignition system. The procedure for changing a spark ignition system into a laser ignition system is to replace the spark plug

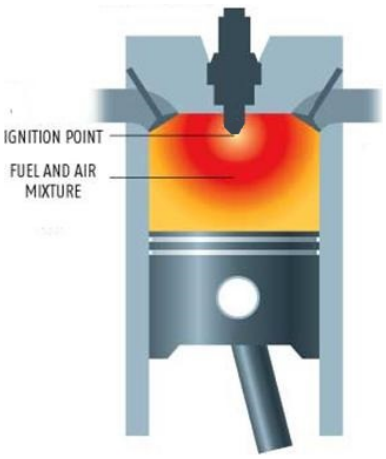

Figure 2.8: Laser ignition

with a laser plug. Once the laser beam is generated, it induces the air-fuel mixture breakdown at its focal point. The ignition efficiency improvement by using a laser ignition system instead of a spark ignition system is negligible because it is still only initiates the ignition at a single point (Bradley et al. 2004).

2.6 Homogeneous Charge Compression Ignition

The aim of a HCCI system is to achieve a more efficient ignition than the common SI and CI systems. The advantage of the HCCI is a volume ignition and not a single point ignition like for the SI system. HCCI combines the homogeneous charge (spark ignition) of a SI engine with the stratified charge (compression ignition) of a CI engine.

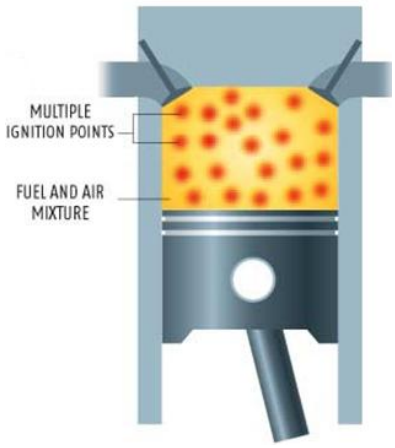

Figure 2.9: Homogeneous charge compression ignition (Jalopnik 2007)

With HCCI systems it is possible to save up to 30 % on fuel consumption compared to traditional SI engines. A HCCI engine can operate on most kind of fuels such as gasoline, diesel, and the majority of alternative fuels, like Compressed Natural Gas (CNG) or Liquefied Petroleum Gas (LPG) (Epping et al. 2002). Through the homogeneous mixture the auto-ignition occurs at multiple locations simultaneously throughout the cylinder. The result of a homogeneous air-fuel mixture is a cleaner combustion and a lower emission. The peak temperature is significantly lower than it would be during a typical spark ignition and the NOx level is negligible (Warnatz, Maas, and Dibble 2006).

The control of the system is difficult since pressure and temperature need to be monitored and adjusted at any time of the process. The constantly changing engine load requires a close loop system which is elementary to adjust the exact position of the inlet and outlet valves, to control pressure and heat inside the engine cylinder to obtain ignition. The auto-ignition of the HCCI system brings a much higher peak pressure inside the engine cavity, which results in a faster wearing of the engine.

2.7 Microwave Ignition

The microwave ignition (MI) system was first proposed and patented in 1974 by M. Ward. This patent describes a microwave transmission line and a microwave emitter, which transmits microwave energy into the engine cylinder. The microwave resonance inside the combustion chamber generates a strong electric field. This field breaks down the injected air-fuel mixture inside the cylinder (Ward 1974).

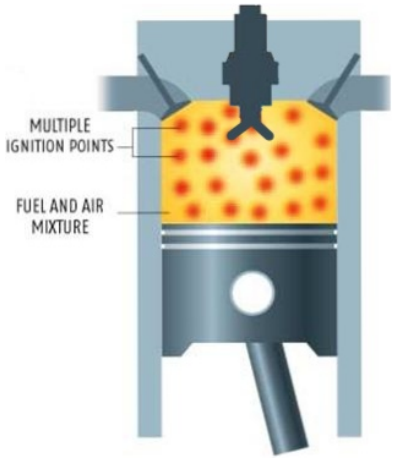

Figure 2.10: Microwave ignition

The MI system is a relatively new approach combining the aforementioned advantages of the spark ignition system as well as the compression ignition system to make a significant impact on the fuel consumption of the engine and the pollutant emissions. A MI system works as a multipoint ignition system, shown in Fig. 2.10. It is comparable with the HCCI (section 2.6) but its main disadvantage, the complex control of the ignition event, is eliminated with the MI system. The control of the ignition event is theoretically as simple to achieve as for the common SI system. Most of the issues occur through the constantly fluctuating resonance frequency inside the combustion chamber of the engine. This project will model one single engine cylinder and simulate the electromagnetic field proportion inside this cavity. To build various physical prototypes is time consuming and expensive, so to save costs and time, virtual prototyping has been developed and used to obtain the best possible electromagnetic field propagation performance.

Figure 2.11 shows the basic concept of a MI system. A control signal (ignition event) triggers the microwave generation which builds an electric field. The microwave signal is then transferred to the engine cylinder through the transmission line (for the engine application is a coaxial cable). A MI system provides a volume ignition and starts the breakdown of the air-fuel mixture at multiple points throughout the combustion chamber, like a HCCI or CI system.

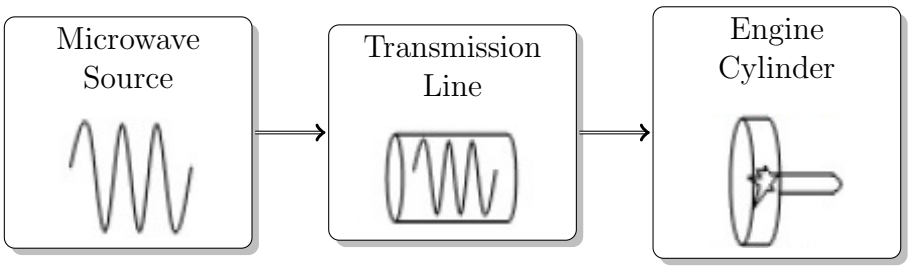

Figure 2.11: Microwave ignition concept

To initiate the breakdown of the homogeneous mixed air-fuel inside the engine cylinder a strong electric field is required. For a spark plug the gap between the two electrodes is around 1 mm to 2 mm and the applied voltage on the electrodes between 15 kV to 25 kV. Employed these two values, the used electric field intensity between the two electrodes is approximately 1×10^7 V/m.

Existing experiments have shown that the equivalent electric field intensity for the microwave breakdown of the air-fuel mixture is slightly lower than 1×10^7 V/m for the spark ignition. The minimum required electric field intensity of this process is around 777×10^3 V/m and will be simplified as 1×10^6 V/m in this thesis (Hagen, Venot, and Wiesbeck 2001).

2.8 Critical Review of Existing Research on Microwave Ignition ICEs

Since Ward's initial idea in 1974, several patents and research papers have been published and submitted in this area. All of these publications and ideas can be separated into two groups. The first group uses the engine cylinder as a resonator as described in section 2.7 (Katsuhiro, Endo, and Takezaki 1981; Ward 1991; Schleupen 2002; Schmidt, Linkenheil, et al. 2003; Schmidt and Ruoss 2003). The second group wants to develop an independent resonator and then ignite the air-fuel mixture inside the cylinder (Manning and P 1995; Pertl and J E Smith 2009).

DeFreitas patented an ignition apparatus for a combustion device which included a microwave energy source (DeFreitas et al. 1997). The microwave energy was transmitted into the combustion chamber at a fixed resonance frequency. This is not suitable for an engine where the movement of the piston continuously changes the natural frequency of the cavity. The main challenge is to design a system that is independent of engine cylinder geometry or can adapt easily to the given circumstances (Ward 1991;

Katsuhiro, Endo, and Takezaki 1981; Schleupen 2002; Schmidt and Ruoss 2003). In response to this challenge, researchers at the West Virginia University developed a Quarter Wave Coaxial Cavity Resonator (QWCCR) (Pertl and J E Smith 2009). The QWCCR works as an independent resonator and was developed with the aim to replace the spark plug without any mechanical change to the engine cylinder. The QWCCR creates a strong electric field generated inside the resonator and then ignite the air-fuel mixture inside the combustion chamber. Unfortunately, with the QWCCR the ignition occurs just around the centre electrode of the resonator, which dissipates the advantage of using the microwave ignition system. Comparable to the QWCCR, a RF plasma ignition device for ICE with a frequency range from 800 MHz to 1500 MHz was developed by Smith (James E Smith, Stile, and Thompson 1997) in 1997. In 2002, Schleupen (Schleupen 2002) patented an ignition device for a high frequency ignition.

In 2003, Schmidt and Ruoss published a patent for a plug which was designed to replace the common spark plug without any mechanical changes to the engine cylinder (Schmidt and Ruoss 2003). Dana Corporation demonstrated in 2005 a technology which uses pulsed microwave energy to initiate engine combustion, also called AtmoPlas(TM). AtmoPlas(TM) combines microwave source feeds with short microwave pulse which flow into the engine through a modified spark plug. Ignition occurs at an atmospheric pressure and with a plasma temperature of around 1200 degrees Celsius (no known upper practical level); nevertheless there has not been any detailed information on AtmoPlas(TM) published (Dana Corporation 2005).

Micro Wave Ignition GmbH (MWI) published several patents for a MI system between 2003 and 2005 (V. Gallatz 2004; A. Gallatz and Hirsch 2010). In 2006, MWI was planning to build a prototype in cooperation with different vehicle manufacturers within two years. They had an ultimate goal of supplying every new vehicle with their technology within ten years (V. Gallatz, Hirsch, and Tarasova 2010).

Makita and Ikeda patented 2010 an apparatus for ignition or plasma generation (Makita and Ikeda 2010). The purpose is to eliminate the need for resonance in the combustion chamber. The past research shows the feasibility and advantages of an MI system. The potential of using a volume based ignition for the combustion efficiency and fuel consumption is high but at present, there has not been a working MI system successfully realised.

Potts experimented in 2000 with partially ionised plasma generated by microwaves with the frequency of 2.45 GHz. Various working gases where employed, including air, nitrogen and noble gas at pressures up to 2×10^5 Pa. The partially ionised plasma can be sustained inside a high-Q cavity within various gases at pressures up to approximately twice atmospheric, using 1.4 kW of microwave power at 2.45 GHz (Potts and

Hugill 2000). The article by Starikovskaia (2006) summarized the results and observations of researchers over the previous decades (Starikovskaia 2006). They confirmed the existence of the artificial initiation of chemical chains by low temperature plasma from gas discharges. Unfortunately, all the results were obtained by experiments and needed further investigation into the "class-by-class" impact on ignition and combustion. When a certain class of particles is separately injected into a system, it will ensure a deeper understanding of chemical kinetics under ignition by non-equilibrium plasma. In relation to this project, Starikovskaia article shows that a plasma assisted ignition is possible but for the development of a new ignition model insufficient details are provided.

The study by Yasar (2001) reported the preliminary analysis of an integrated plasma-enhanced ignition and combustion model for SI as well as for a Laser Induced Spark Ignition (LISI) combustion chamber. Yasar focused on developing a new ignition sub-model. The KIVA-III program was used for this investigation in combination with the expanded equation-of-state (EOS) tables. The ignition temperature obtained in the plasma-enhanced simulation was significantly higher (70 %) than the temperature of a classic ignition (Yasar 2001). Liu in 2005, showed that using transient plasma or pulsed corona discharge provided a shorter ignition delay time and pressure rise times (J. Liu et al. 2005). In these experiments, a high-voltage electric pulse generator provided an average pulse of 60 kV peak voltage and a suitable time pulse. The plasma occurred during the formative phase of an arc discharge and persisted for around 50 ns.

Jimenez (2007) produced a simulation of low pressure plasma discharge typical of a DC magnetron sputtering process that used a Monte Carlo-fluid-Poisson hybrid model (Jimenez, Ekpe, and Dew 2007). The densities of the plasma electrons and ions and the electrical potential of the discharge space were calculated by using COMSOL Multiphysics. Although this simulation model included the effects of gas heating, it made gross assumptions for the electrical conductivity of the process gas. In turn, these assumption make it useful for illustration purposes but not for building a physical and chemical model.

Chapter 3

Simulation Based Methodology

The design of a microwave ignition device for ICEs requires several steps. First, models need to be made of the engine cylinder and the electromagnetic field distribution inside the cavity simulated. For this purpose, the finite element method (FEM) simulation software COMSOL was employed. The combustion cylinder will work as a resonator for the MI system. The FEM simulation software calculates the microwave propagation throughout the cylinder as well as the resonance condition of the enclosed cavity.

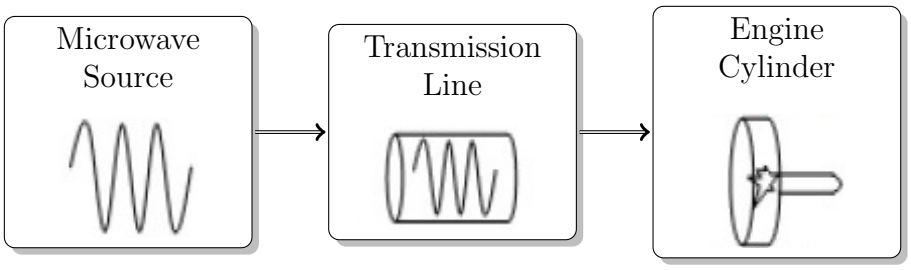

Figure 3.1: Microwave ignition concept

In order to optimise the given model, the software COMSOL has an optimisation toolbox but does not possess sufficient equipment to optimise complex systems such as adjusting the used search algorithm. In the past, COMSOL was connected with MATLAB by using the MATLAB Live Link extension to exchange data between the simulation model and algorithm. Unfortunately, this tool combination possesses the problem of a slow communication speed between both components. It makes it impractical to run a Genetic Algorithm (GA) optimisation with a large number of evaluations to gain sufficient results for a particular antenna design.

To address this problem a new framework was designed focussing on communication speed. The Java Application Programming Interface (API) of COMSOL was utilised to combine the FEM simulation software with variable algorithms. The use of this

newly designed CAutoD has many advantages and can solve the given problems with a higher simulation and search resolution to obtain more accurate results.

3.1 Microwave Resonance in a Cavity

The Electromagnetic (EM) field can be seen as a combination of an electric field and a magnetic field while the electric field is produced by stationary charges and the magnetic field by moving charges with a current. The microwave breakdown in the combustion chamber of an ICE is caused by the electric field. In correlation with this breakdown of the air-fuel mixture, the electric field also induces plasma in the engine cylinder.

The following Maxwell equations are used to describe the EM field inside a combustion chamber (Seely and Poularikas 1979).

$$\nabla \bullet D = \rho \tag{3.1}$$

$$\nabla \bullet B = 0 \tag{3.2}$$

$$\nabla \times E = -\frac{\partial B}{\partial t} \tag{3.3}$$

$$\nabla \times H = J + \frac{\partial D}{\partial t} \tag{3.4}$$

where D is the electric displacement field in $[C/m^2]$, ρ is the electric charge density in $[C/m^3]$, B is the magnetic flux density $[T]$, E is the electric field intensity in $[V/m]$, H is the magnetic field intensity in $[A/m]$, and J is the current density in $[A/m^2]$.

In a regularly shaped cylinder under practical boundaries, Eq. (3.1) to 3.4 can be used to solve the electric field distribution. The resolution of these equations depends on the primary propagation mode, while this mode depends on the shape of the enclosure and its dimensions. For most real engine cylinders the boundary conditions are complex and in combination with the irregular geometric shape of the combustion chamber,

the calculation becomes very complicated. The use of computer simulations is the most effective way to resolve this particular problem thus this project utilises the FEM simulation software COMSOL.

Resonance is mandatory in any MI system in order to breakdown the air-fuel mixture inside the cylinder. Resonance occurs when the system achieves a suitable configuration of frequency and geometric dimensions. Microwave resonance occurs at a frequency greater than 1 GHz. The resonator is usually a metallic enclosure and the energy in the resonator is generated from an electric and magnetic field.

A cylindrical cavity can have two different types of resonance: transverse magnetic (TM) and transverse electric (TE) mode. The dominant mode is TM_{010}, when a cylindrical cavity matches the following condition (Seely and Poularikas 1979):

$$\frac{d}{a} < 2 \tag{3.5}$$

where d is the depth of a cylinder and a is the radius of the cylinder. The microwave energy can be applied by using different methods to the cavity shown in Fig. 3.2.

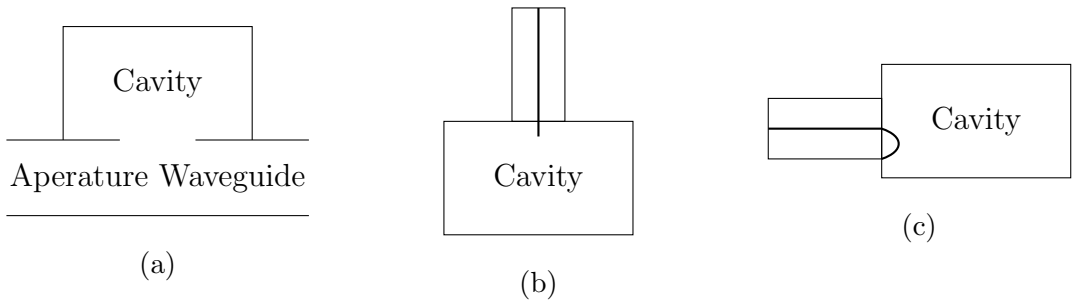

Figure 3.2: Coupling methods

The microwave energy can be coupled into the cavity by a small opening in the walls (Fig. 3.2a), a coaxial cable with a probe shape antenna (Fig. 3.2b), or a coaxial cable with a loop antenna (Fig. 3.2c). To implement a MI system on existing engines, with the aim of making the least modifications to the engine, requires that the coupling apparatus can fit into the engine cylinder without any modification to the cylinder body. Therefore the solution shown in Fig. 3.2b is the most suitable coupling method for a HCMI system. Another important aspect and a major reason for optimising the microwave coupling efficiency into the combustion cylinder is the impedance match between the output of the coaxial cable, using Eq. (3.6), and the input of the resonator (Seely and Poularikas 1979). If the input impedance of the cavity matches the output impedance of the coaxial cable, the microwave energy can be transmitted into the resonator with minimum reflections and the optimum efficiency.

$$Z = \frac{60}{\sqrt{\varepsilon_r}} \ln \frac{b}{a} \tag{3.6}$$

where Z is the impedance of the coaxial cable, ε_r is the relative permittivity, a the radius of the centre core of the coaxial cable, and b the outer radius of the coaxial cable.

The resonance frequency of a regular shaped cylinder can be calculated with Eq. (3.7) for TM_{mnp} propagation mode and by using Eq. (3.8) for TE_{mnp} propagation mode.

$$f_{mnp} = \frac{c}{2\pi\sqrt{\mu_r \varepsilon_r}} \sqrt{\left(\frac{X_{mn}}{r}\right)^2 + \left(\frac{p\pi}{L}\right)^2} \tag{3.7}$$

$$f_{mnp} = \frac{c}{2\pi\sqrt{\mu_r \varepsilon_r}} \sqrt{\left(\frac{X'_{mn}}{r}\right)^2 + \left(\frac{p\pi}{L}\right)^2} \tag{3.8}$$

If the dominated mode in a cylinder is the TM_{010} mode, Eq. (3.7) can be simplified to the following:

$$f_{010} = \frac{c \cdot X_{01}}{2\pi r\sqrt{\mu_r \varepsilon_r}} \tag{3.9}$$

where c is the speed of light, X_{01} the first root of the zero order Bessel function, r the radius of the cylinder, and ε_r, μ_r respectively the permeability and permittivity of the material inside the cylinder.

3.2 Plasma

The definition of plasma dates back to 1928 (Langmuir 1928). Plasma is similar to gas but the ions and electrons are fully or partially separated and a certain portion of the particles need to be ionised. Scientists have found that more than 99% of all materials in the universe are plasma (Gurnett, Bhattacharjee, and Zita 2006).

Each ordinary gas atom has an equal number of positive and negative charges. This

means each atom is electrically neutral if the positive charges in the nucleus are surrounded by an equal number of negatively charged electrons in the atomic shell. By supplying an external energy such as electromagnetic waves, gas can become plasma. To create plasma a significant number of atoms needs to release some or all of their electrons. The remaining parts of those atoms are left with a positive charge and the detached negative electrons are free to move. Those atoms and the resulting electrically charged gas is now ionised. The gas becomes plasma after enough atoms are ionised to significantly affect the electrical characteristics of the gas. The plasma is electrically conductive and therefore responds strongly to EM fields.

Plasma can be induced by different methods: direct current (*direct current plasma*), electromagnetic waves with frequencies around kHz (*radio-frequency plasma*), electromagnetic waves with frequencies around MHz (*microwave plasma*), and electromagnetic waves with frequencies around PHz (*laser plasma*). The most common methods of producing plasma are Direct Current (DC), resonance frequency (RF), and microwave.

The synergy between the charged particles and the neutral particles are important in determining the behaviour of the plasma. The wide spectrum of plasma types, characteristics, and behaviours are attributed to the type of atoms along with the ratio α of ionised particles to neutral particles, as well as the particle energies. A large and growing number of applications exploit these different features.

Plasma is separated in to classes and fundamentally defined by its temperature and its number density. For an ignition system, combustion represents a burning process which leads to a plasma class characterised by a flame with a maximum temperature of 5000 K and a density up to 1×10^{17} electrons/m^3. The degree of ionisation, α is defined as:

$$\alpha = \frac{n_i}{n_i + n_a} \tag{3.10}$$

where n_i is the number density of ions in $[cm^{-3}]$ and n_a the number density of neural atoms in $[cm^{-3}]$.

Plasma induced by microwaves has a noticeable advantage over plasma generated by direct current or radio-frequencies. The degree of ionisation, the ion density, and the level of dissociation are higher using microwave induced plasma in comparison with the other methods (Qiao et al. 2003). Therefore microwaves have a stronger capacity to dissociate electrons from their atoms.

ICE air-fuel mixtures consist primarily of N_2, O_2, NO, NO_2, C_2H_6, CO, CO_2, H_2O, and non-combusted fuel feedstock (Qiao et al. 2003; Starikovskaia 2006). The associated plasma is then obtained as follows:

$$O_2 + e^- \rightarrow O\bullet + O\bullet + e^- \tag{3.11}$$

$$O\bullet + HC \rightarrow RO, RO_2, OH\bullet \ldots \tag{3.12}$$

$$NO + O\bullet \rightarrow NO_2\bullet \tag{3.13}$$

$$NO + RO_2 \rightarrow NO_2 + RO \tag{3.14}$$

where R is an organic species and $\bullet$ denotes radical species. Ozone is formed as an intermediary of the reaction described below (Qiao et al. 2003):

$$O\bullet + O_2 \rightarrow O_3 \tag{3.15}$$

Equations (3.11) to (3.15) describe the ignition process of a common petrol internal combustion engine. Below, the chemical equations of the different fuel types (Eq. (3.16) propane, Eq. (3.17) methane, Eq. (3.18) pentane) and their chemical reaction during the combustion (Lackner, Winter, and Agarwal 2010).

$$C_3H_8 + 5O_2 \rightarrow 3CO_2 + 4H_2O \tag{3.16}$$

$$CH_4 + O_2 \rightarrow CO + H_2 + H_2O \tag{3.17}$$

$$2C_8H_{18} + 25O_2 \rightarrow 16CO_2 + 18H_2O \tag{3.18}$$

The pressure inside a cylinder affects the breakdown voltage. Paschen's curve can be used to determine the breakdown voltage of a gas (Paschen 1889). At higher pressures and gap length, the breakdown voltage is approximately proportional to the product of the pressure and gap length. This approximation is only valid over a limited range of the curve.

$$V = \frac{B \cdot p \cdot d}{C + \ln(p \cdot d)} \tag{3.19}$$

$$E = \frac{V}{d} \tag{3.20}$$

To express the breakdown voltage as electric field intensity Eq. (3.20) can be used. After inserting Eq. (3.19) into Eq. (3.20), Eq. (3.21) can be applied for an immediate evaluation of the electric field intensity.

$$E = \frac{B \cdot p}{C + \ln(p \cdot d)} \tag{3.21}$$

where p is the pressure in the cylinder, d the gap between the two electrodes, B a constant depending on the used material, and C can be calculated by using Eq. (3.22).

$$C = \ln\left(\frac{A}{\ln\left(1 + \frac{1}{y}\right)}\right) \tag{3.22}$$

where A is a constant depending on the used material and y the secondary ionisation coefficient.

3.3 Finite Element Method Simulations of Electromagnetic Fields

FEM is a numerical engineering tool developed in the 1960's by the nuclear power and aerospace industries. It was developed in order to find usable, even just approximate, solutions to problems with many complex variables. The FEM analysis is a numerical

technique for finding approximate solutions to partial differential equations. For the past half century, FEM has been widely utilised in different disciplines for example, the design and development of commercial products. The analysis has also become an indispensable technology in the design and modelling of complex engineering systems (Rao 2005; G. Liu and Quek 2013).

During the research process of this project the FEM simulation software COMSOL was used to design and develop a representative model of a MI system and engine cylinder. Initially, the research started by modelling the irregularly shaped cylinder of an ICE. The changing geometry of a running engine affects the propagation performance of a MI system more than for a SI system, since the resonance condition is crucial for a clean and complete combustion. The simulation of the electric field finds the solutions to the Maxwell equations by applying certain boundary conditions. Due to the major impact of the cylinder's geometry on the resonance conditions, it is very difficult to find the correct solution by using a FEM simulation software with parameters and through "trial and error". Therefore it is essential to combine the electric field simulation into a CAutoD system to search for the optimum solution for the given problem.

The simulation of the EM field propagation performance inside the combustion chamber is the essential part of this research. The EM field inside the cavity is generated by a microwave source and the resonance condition of the irregularly shaped cylinder needs to reach a maximum electric field. In the past, the major problem during the design process was the search resolution of the simulation, due to the slow communication speed between the simulation and the optimisation search algorithm. It was impossible to simulate enough points in an acceptable time scale for a reliable observation of the results. It is also important to respect the practical boundaries during the design of a HCMI system, e.g. the material thickness cannot be assigned to a negative value.

3.4 Simulation Environment

The implementation of a CAutoD optimisation search for the HCMI system requires different connected software components. The idea of a CAutoD system is to go one step further than the trial and error method and improve the general search performance and investigation details. The required parts are the FEM simulation model of the engine cylinder, enabled by using COMSOL, and the optimisation algorithm. The used optimisation algorithm is implemented using the MATLAB optimisation toolbox. It is necessary to find a universal communication platform between the optimisation algorithm and the simulation model. The optimisation algorithm needs to be able

to communicate with the simulation model to exchange data and perform a detailed search.

3.4.1 COMSOL Multiphysics

COMSOL Multiphysics is a well established FEM simulation software on the market and can be used for a wide range of applications (Pepper and Heinrich 1992). In the past, COMSOL Multiphysics was widely used in many different research areas, due to the basic program being supplemented by commercial extensions to adapt to a particular area. For the modelling process of a HCMI system, COMSOL Multiphysics has been used and applied to simulate the electromagnetic field propagation inside the combustion chamber of an ICE (Comsol 2011b; Comsol 2012). To implement a CAutoD system it is critical to connect the optimisation search with the simulation model. COMSOL Multiphysics offers several ways to interact with other software products, such as the commercial MATLAB Live Link extension or the use of the Java API. The use of the MATLAB Live Link is easy and straight forward but brings disadvantages like a slow communication speed. Therefore the Java API was chosen and implemented for the optimisation search with a view to a faster and more efficient communication between the simulation model and optimisation search.

3.4.2 MATLAB Live Link and Java API

To evaluate COMSOL Multiphysics models in connection with other software tools, the use of the MATLAB Live Link extension is one possible solution. This connection between MATLAB and COMSOL Multiphysics is realised by using the COMSOL server (Comsol 2011a). There are some advantages by using this method such as the immediate presentation of the results during the search process or after the simulation. The MATLAB Live Link extension also provides some practical MATLAB functions for example, the plotting of the model geometry or simulation results with just a single command. Furthermore, available functions like “mphnavigator(model)” are effective for examining the implemented model details and for debugging purposes. In any case, these advantages are not important for the implementing a CAutoD system. The communication speed between both software products is the crucial issue for a CAutoD system. Unfortunately the communication speed of the MATLAB Live Link extension is unreasonably slow and often takes some seconds for just one single evaluation.

Another way to communicate with the FEM simulation software is the access of COM-

SOL models via the Java API. To implement the simulation model a fundamental and deep knowledge of the model structure is necessary before using this method. It requires a runnable COMSOL installation with all mandatory extensions for the calculation of the model but no additional extension is needed, like for example the MATLAB Live Link. The implementation is based on Java without any graphical interface but for the evaluation of the simulation model, Java offers advantages and disadvantages. The communication rate is significantly faster compared to the MATLAB Live Link extension and the implementation more flexible but more complex. During the implementation of the simulation as Java model, it is possible to choose between the use via the COMSOL server or as a standalone application. The first option does not offer any significant advantages compared to the described MATLAB solution but the second option, to implement a standalone application, increases the communication speed. This advantage makes a standalone application as a way of implementation indispensable. A CAutoD system requires thousands of evaluations and thus through the use of the Java API's rapid communication speed the total simulation time decreases noticeably.

Aforementioned, this way of implementation requires a wider knowledge of the programming language Java along with the ability to read and understand the COMSOL API documentation. Through the gained flexibility for the model implementation and the significantly increased simulation and communication speed, this method has more advantages than disadvantages for the designing of a CAutoD system.

3.5 Validation of Simulation

A FEM simulation software is required for the calculation of the electric field intensity inside a cylindrical cavity. This divides up the complicated equations of the electric field distribution calculation into small elements which can be solved in relation to each other. Especially for complex multidimensional geometries it is required to apply a suitable mesh to the model and solve it with an FEM simulation software. The mesh used for the validation process is shown in Fig. 3.3 and contains 240 elements. Due to the regular cylinder dimensions and the correlated linear behaviour of the field this value could be further decreased and still deliver sufficient results. For the advanced simulations with irregular shaped cylinder models in chapter 4 and chapter 5 a mesh with 465 elements was established to be suitable to deliver stable results.

To validate the FEM simulation software for the particular application of modelling a HCMI system engine cylinder, a sequence of test simulations is required. Once the

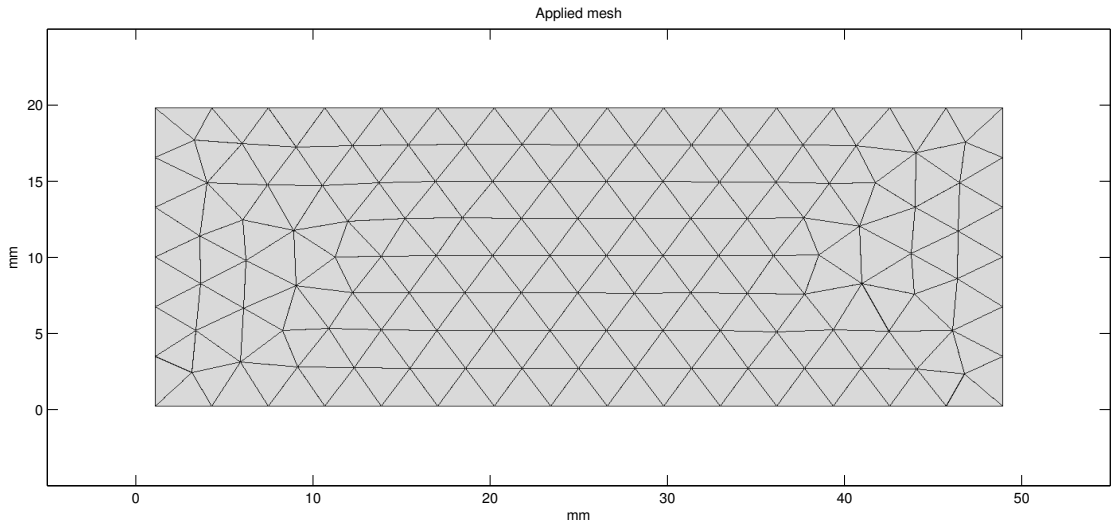

Figure 3.3: Applied mesh to the validation

validation is completed the FEM simulation software can be used for further modelling. In this thesis, the COMSOL Multiphysics modelling and simulation software is used to calculate the electric field distribution inside the combustion chamber (Comsol 2011b). In order to validate these simulation methods, the resonance frequency and electric field propagation performance inside a regularly shaped cylinder will be simulated and the response compared with the theoretical results.

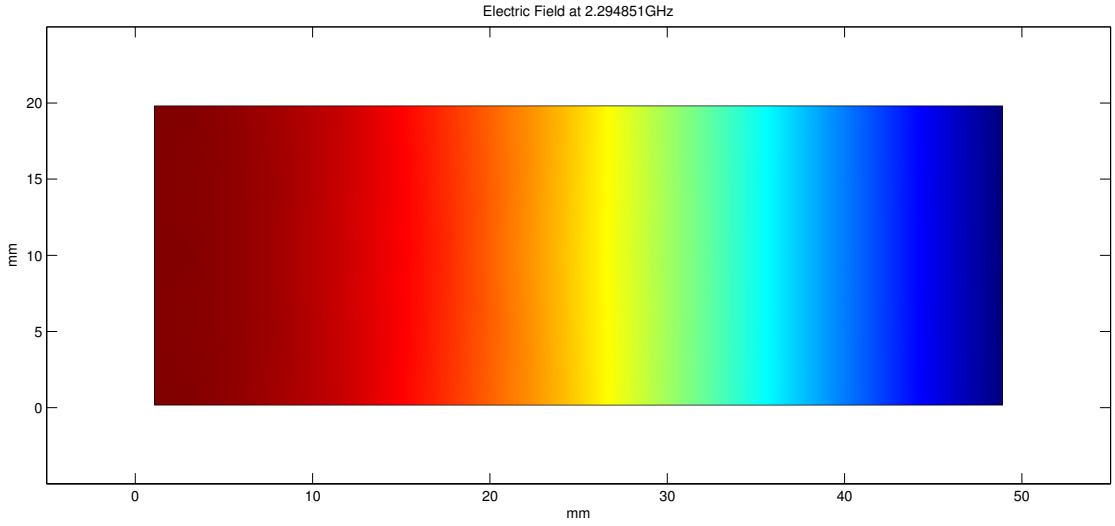

Figure 3.4: Electric field inside a cylindrical cavity

Figure 3.4 exemplifies the geometrical dimensions of the model used for this simulation. It is modelled in a two dimensional axis symmetrical pattern. The centre of the cylindrical wave guide is shown on the left side and according to the figure during the resonance condition, the electric field reaches the maximum near the centre of the cylinder. In accordance with the theory, the wavelength inside a cylindrical cavity can be calculated with Eq. (3.23) below. After converting the wavelength into a equivalent frequency, Eq. (3.25) can be used to calculate the resonance frequency of a cylindrical cavity (Sequeira 2011).

$$\lambda = \frac{2\pi \cdot r}{p_{mn}} \tag{3.23}$$

$$f = \frac{c}{\lambda} \tag{3.24}$$

$$f = \frac{p_{01} \cdot c}{2\pi \cdot r} \tag{3.25}$$

where r is the radius of the cylinder, c is the speed of light, and the variable p_{mn} is determined by the propagation mode inside the cavity. In this case, the TM_{010} is present and so the first root of zero order Bessel function will be used. According to the simulation result obtained by using COMSOL Multiphysics, the resonance frequency of this cavity in TM_{010} mode is 2.294 851 GHz. To compare the simulation result with the theory, the resonance frequency of this cylindrical cavity in TM_{010} mode using Eq. (3.25) is 2.295 02 GHz.

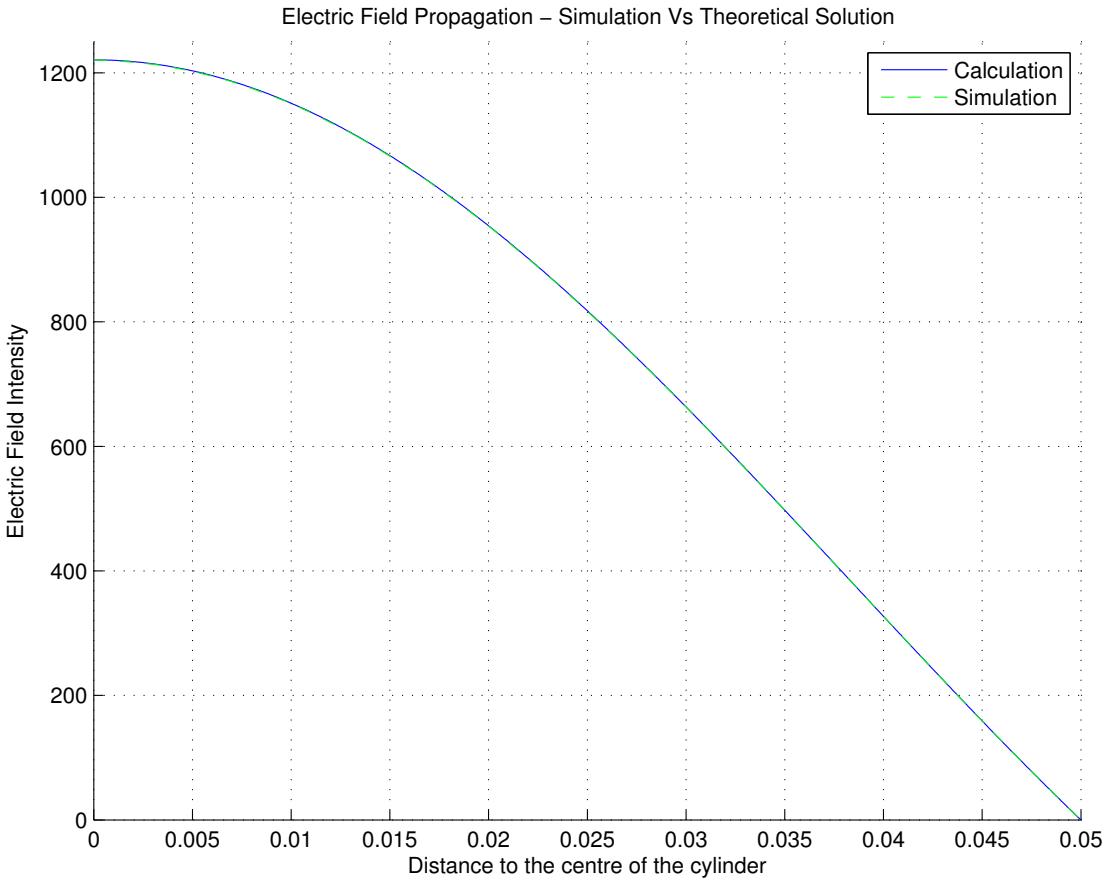

Figure 3.5: Compare the electric field propagation performance

$$E_z(r) = E_0 \cdot J_0\left(\frac{p_{01} \cdot r}{a}\right) \tag{3.26}$$

$$J_0(z) = \sum_{k=0}^{\infty} (-1)^k \frac{\left(\frac{1}{4} \cdot z^2\right)^k}{(k!)^2} \tag{3.27}$$

The second part of the validation process is to simulate and analyse the microwave propagation performance throughout the combustion chamber. This simulation's purpose is to show that the distribution of the electric field inside the cavity is valid and can give reliable values throughout the cavity. The same model, as in the first part of the validation process, is used and the result is shown in Fig. 3.5. The illustrated field in this figure is measured at the top of the cavity while the excitation of microwave was assigned to the cylinder at the bottom. It can be seen that the electric field near the symmetrical axis is the strongest and that the amplitude of the field drops down by increasing the distance to the centre.

To compare the simulation with the theory, the propagation of the electric field at the top of the cavity is calculated by Eq. (3.26). E_0 is the initial electric field intensity, r the variable in horizontal direction, and a is the total radius of the cylinder. J_0 represents the zero order Bessel function and can be calculated by the infinity series in Eq. (3.27) (Stegun, Abramowitz, and Miller 1965). By comparing the two lines in Fig. 3.5 it is demonstrated that the simulation and theoretical results of the electric field distribution inside the cylindrical cavity are almost identical.

3.6 Search and Optimisation

The different search methods used in this thesis have been widely employed in various fields for many years. In consideration of the electric field signal characteristics inside the resonance cavity of an ICE, it can be useful to combine different search algorithms. One possible way it to generate a more suitable initial population for the GA. In particular, this shows that combining deterministic and non-deterministic search algorithms within one single optimisation search helps to find the strongest electric field intensity for a given HCMI system simulation model.

3.6.1 Trial and Error Based Simplex Search

The Nelder–Mead (NM) simplex method is a posteriori and deterministic search algorithm. This method makes it possible to search and calibrate several design parameters

at once. During hardware experiments, it is difficult to calibrate several parameters at the same time by using an automated search method. Proposed by Nelder and Mead in 1965, the Nelder-Mead simplex method (also called the Downhill Simplex Method), is a non-linear optimisation algorithm which minimises an object function in a multi-dimensional space (Nelder and Mead 1965). This method uses the concept of simplexes, which are a special polytope $N+1$ vertices in N dimensions. Some examples of simplexes are a line segment in one-dimensional space, a triangle in two-dimensional space, and a tetrahedron in three-dimensional space. The method finds a locally optimal solution to a problem with N variables if the objective function varies smoothly (R. L. Haupt and S. E. Haupt 2004).

Although the NM simplex method is a local search method, it still has some advantages over other search methods. For example, the NM simplex method works without calculating the function derivatives of the particular search points and achieves significant improvements of the function value at a very early stage of the search process. The NM algorithm only requires a few function evaluations per iteration. In comparison to the Evolutionary Algorithm (EA) search method, the NM algorithm requires less function evaluations to find a solution, potentially saving a great amount of time. Conversely, an EA based or Particle Swarm Optimization (PSO) search algorithm is far less likely to find local extrema.

EA and NM searches have been used to find the right design parameters for the optimum electric field propagation inside the cylindrical cavity of a HCMI system. The performance of the NM algorithm is inadequate if the search includes the frequency as a parameter, or if the correct starting point is not chosen for the individual optimisation problem. The NM search requires a rough knowledge of the solution range along with multi-optimisation searches.

3.6.2 Evolutionary Algorithm

The EA is a non-deterministic search method, with the basic idea proposed in the 1960's by several computer scientists, to solve practical non-linear problems. Similar to Darwin's theory of evolution, the EA includes three steps: selection, crossover, and mutation. These three steps mimic the natural evolution of the human being and have been employed in various fields of research.

The EA begins with the creation of a random population with a defined number and size of individuals. Each individual of the population is then evaluated. The evaluation function or fitness function is provided by the programmer and ascribes each

individual a score, depending on how well they perform at the given task. After the evaluation process two individuals are selected. The selection process can be based on their individual fitness value or just on a random selection. The selected individuals apply the crossover and mutation steps in order to generate new offspring. This procedure continues until a suitable solution has been found or the maximum number of evaluations are completed (L. D. Davis 1999; Spears 2000; Ghanea-Hercock 2003).

The most common type of selection method is the "roulette wheel selection". This method provides a selection probability of each individual based on the individual's fitness value. The higher the fitness, the higher the chance of selection. Another way is the selection of two random individuals and eliminating the individual fitness value from the selection process (L. D. Davis 1999; Deb 2001).

During the crossover process two individuals are selected and a new individual will be created. There are multiple ways to perform the crossover of two individuals but the most common way is a single point crossover. For this the parents are separated at one point and then both children take one part of each parent (shown in Fig. 3.6) (Deb 2001).

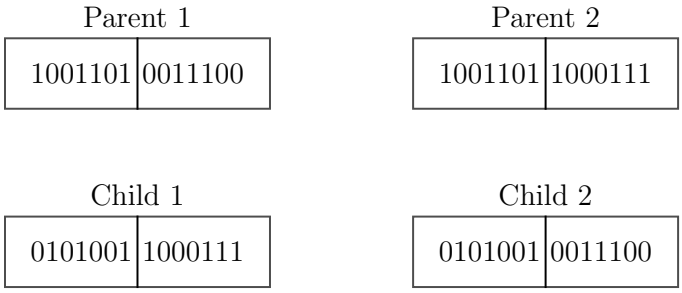

Figure 3.6: One point crossover

The crossover step can also include that some children are directly copied from their parents. The whole crossover process can be improved by developing another split and crossover process. The mutation process is applied by each individual of the population. Some individuals are changed by the crossover step, while others remain the same. Mutation assures that the individuals are not all homogeneous as they were before, crossover occurred.

Figure 3.7: Mutation

The mutation procedure (Fig. 3.7) loops all the genes of every individual. If one gene

is selected for mutation, the value will be replaced by a new value (Spears 2000). This thesis will utilise various implementations of the GA such as from the MATLAB genetic optimisation toolbox.

3.6.3 Heredity Algorithm

The Heredity Algorithm is an attempt to improve the overall performance, especially the convergence speed in comparison to the original Genetic Algorithm in section 3.6.2. As shown in chapter 5 the GA is known to be very efficient at of finding the global optimal solution for complex multidimensional optimisation problems. Prior to Darwin's theory of evolution by natural selection, Lamarck proposed a multifaceted theory of evolution. The idea behind this theory is the speculation that specific organism characteristics are inheritable by its offspring. Lamarck proposed this with the meaning that organisms can pass specialised characteristics, which are required to survive in the given environment, on to its offspring. This is known as Lamarckian evolution or Lamarckism (Dawkins 1996). A typical Deoxyribonucleic acid (DNA) of organisms can have hundreds of millions of genetic variations. The physical characteristics of a phenotype are the result of combined interactions between many components of the DNA. Although discredited in biology, the implementation in intelligence algorithms has proven that Lamarckian evolution is an effective concept for improving convergence characteristics (Mitchell 1997; Ross 1999).

Ross (1999) gave an example of Lamarckian evolution: "If a horse developed especially adept leg muscles for negotiating mountainous terrain, Lamarckian evolution suggests that its offspring would inherit similarly muscular legs. Lamarckian inheritance of acquired characteristics maintains that the acquired development of strong legs, through years of exercise in a mountainous environment, will influence the actual genetic makeup of the horse. This altered genetic information is inheritable by the horse's offspring. This contrasts with the Darwinian tenet that a horse that is genetically predisposed to having muscular legs will probably have offspring with a similar genetic tendency" (Ross 1999).

Based on Lamarck's theory of evolution, the Heredity Algorithm (HA) implements this alternative idea of how organisms can evolve through learning from one generation to another. The newly proposed algorithm in this section needs several benchmark functions to analyse, validate, and measure the performance against the existing GA optimisation method. The search algorithms used are non-deterministic optimisation methods and therefore must be executed several times in order to obtain realistic and representable results. Each benchmark function shown in Table 3.1 was executed

100 times for every optimisation algorithm; each time with the exact same individual algorithm configurations. To generate the final results for the graph's the average of all available simulation results were used.

Table 3.1: Test functions

Test function	**Dimensions**	**Search Space**
$f_1(x) = \sum_{i=1}^{D} x_i^2$	10	[-100, 100]
$f_2(x) = \sum_{i=1}^{D} \left(\sum_{j=1}^{i} x_j \right)^2$	10	[-100, 100]
$f_3(x) = \sum_{i=1}^{D} \left(\lvert x_i + 0.5 \rvert \right)^2$	10	[-100, 100]

Table 3.1 shows the different benchmark functions used in this section. Each benchmark function is executed in multiple dimensions for both algorithms. The algorithms applied comparable settings like a population size of 101, a fixed generation count of 50, and the limits mentioned in Table 3.1. To obtain comparable results, it is required to keep the number of generations constant. The selection function for all the chromosomes is identical for both algorithms and the number of evaluations is fixed for each generation as well as for the whole search process. The termination criteria to end the optimisation search is defined by the number of generations and the equivalent number of evaluations. In the application to a HCMI system, it is ideal to have as few function evaluations as possible, due to the slow evaluation of the FEM simulation model. This is the reason behind a convergence speed being the main criteria and objective of the HA design.

Figure 3.8 shows the most suitable and mean score for the whole population over 50 generations by using the first benchmark function. In Fig. 3.8a the blue line represents the convergence speed of the best score within the population by using the GA, whereas the green line shows the convergence speed by using the HA. The demonstrates that the best score converges faster within the first 20 generations. Figure 3.8b illustrates the mean score over 50 generations for both algorithms, the HA converts significantly faster than the GA within the first 10 generations. In Fig. 3.9, the performance comparison of the second testing function is shown. It can be seen in Fig. 3.9a, that the convergence speed of the best score for the first 15 generations is slightly faster for the HA in comparison to the GA although they have the same starting conditions. Figure 3.9b displays the mean score for 50 generations for both algorithms. After 5 generations, the HA had already reached the same value as the GA after 15 generations. This confirms the same tendency as the first testing function and a noticeable advantage of employing the HA over the GA. Figure 3.10 shows the performance comparison for the third and last testing function in this section. The convergence speed for the best score in Fig. 3.10a, and the mean score in Fig. 3.10b, establishes the advantage of the HA in comparison to the GA.

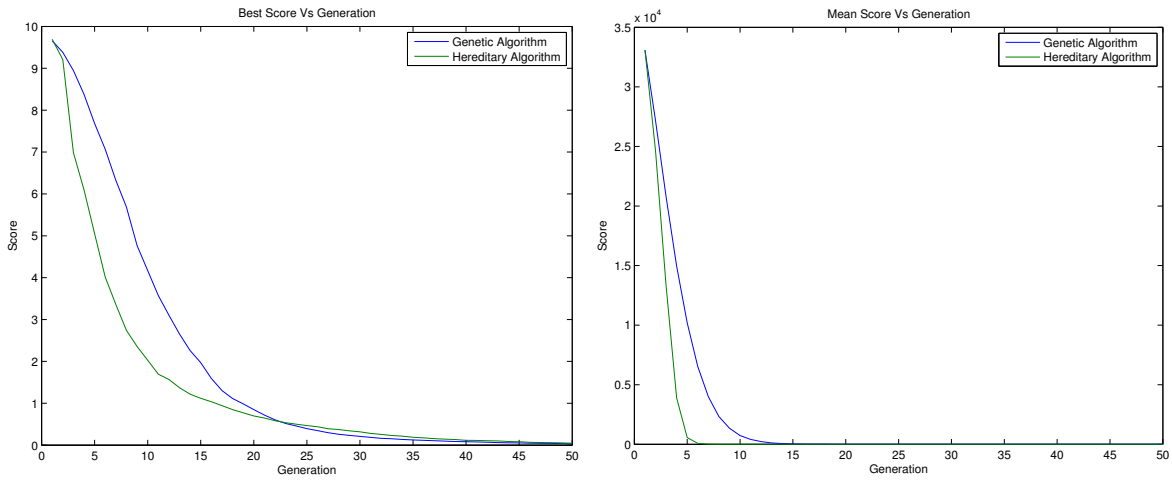

(a) Best (b) Mean

Figure 3.8: Test function 1 - convergence speed

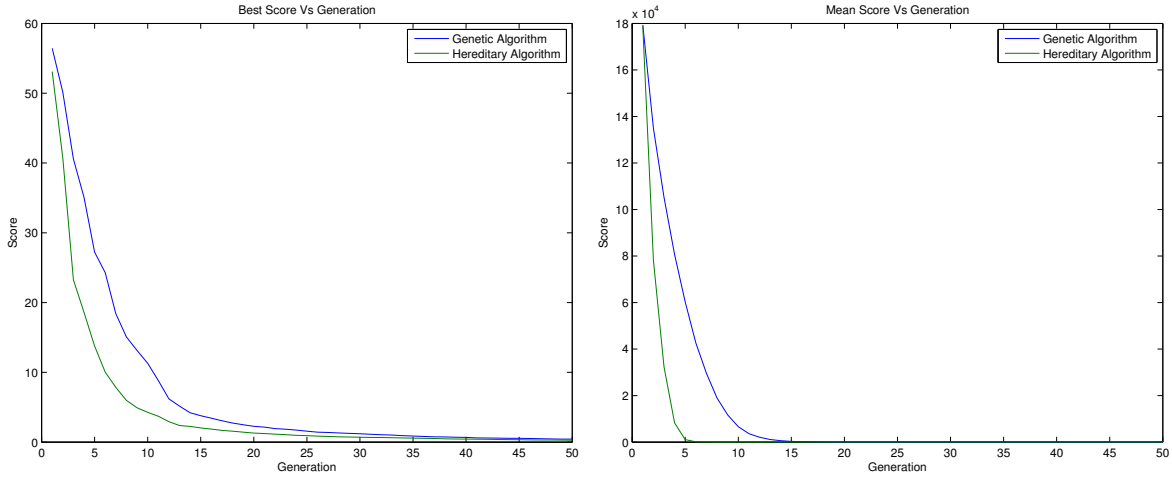

(a) Best (b) Mean

Figure 3.9: Test function 2 - convergence speed

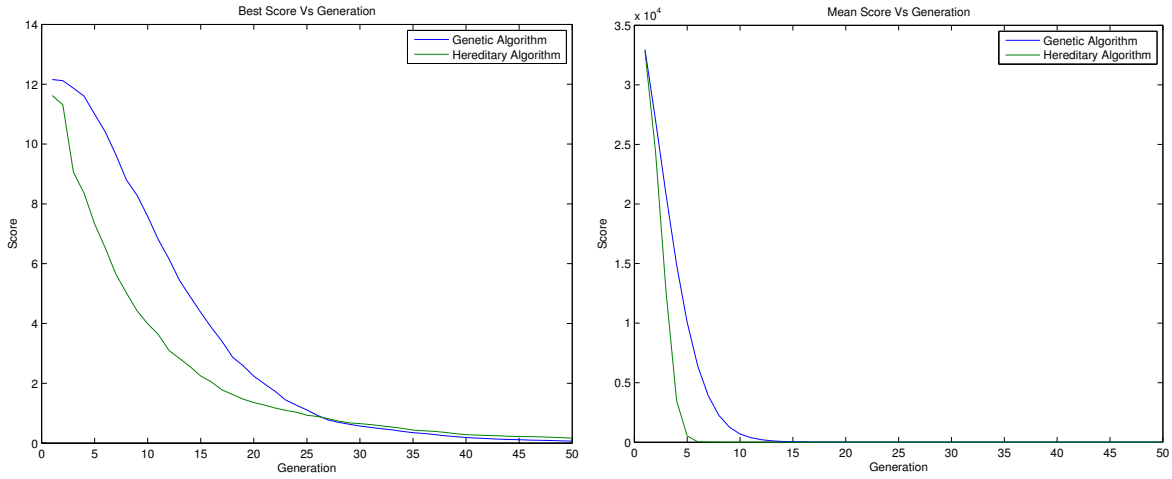

(a) Best (b) Mean

Figure 3.10: Test function 3 - convergence speed

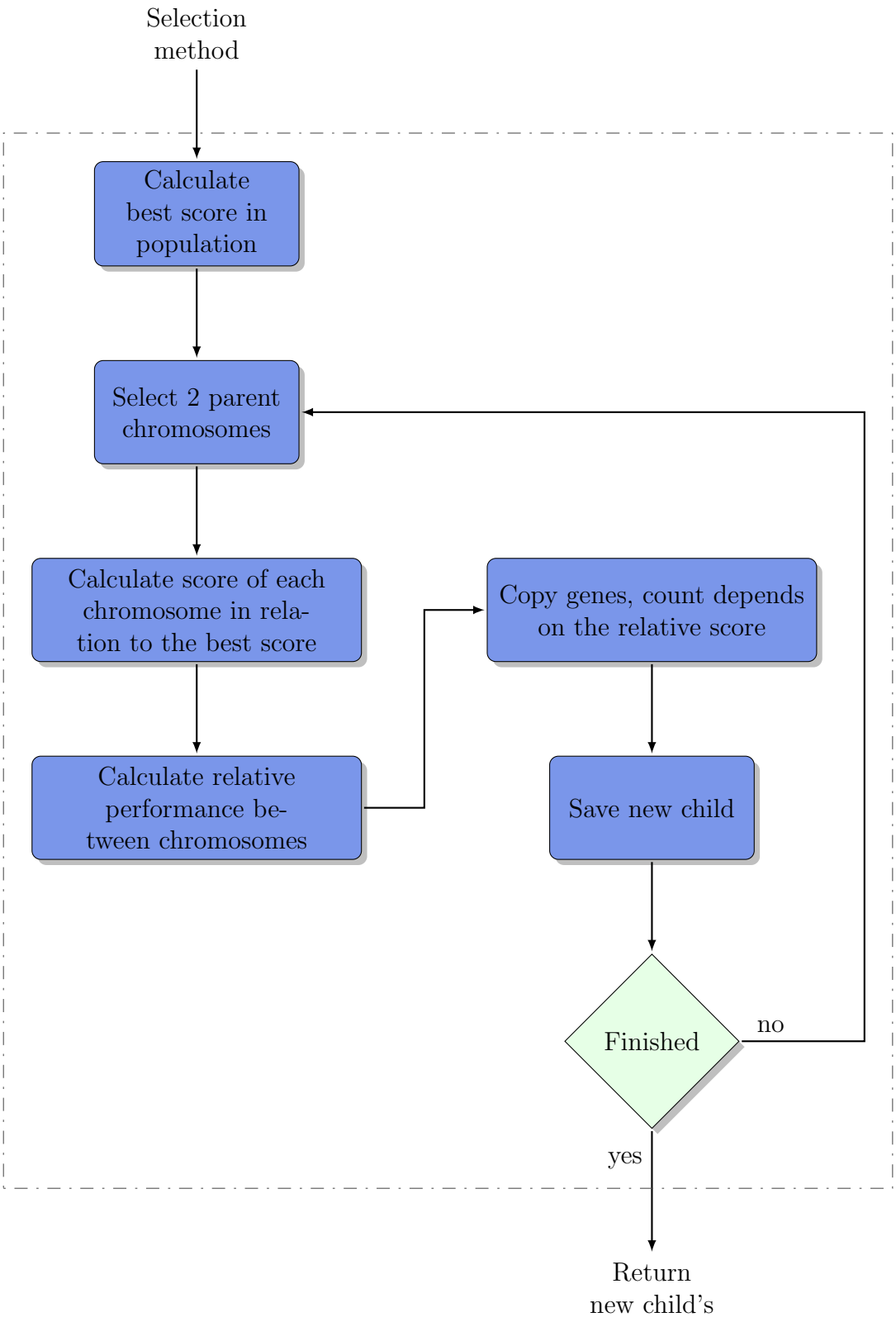

Figure 3.11: Heredity algorithm workflow

The HA is very similar to the GA and to better understand the process of the algorithm improvement Fig. 3.11 was created. The process can be explained as the following: At first the best score inside the whole population will be picked as reference. Based on the used selection method, two parent chromosomes are going to be selected to generate a new child. Then the algorithm will use the relative score of each chromosome compared to the best score in the population, to decide how many genes should be kept. Therefore this process is similar to the natural process proposed by Lamarck; the strongest will survive. The HA search will then pick variable genes of the weaker chromosome and overwrite the same amount of genes in the stronger chromosome. In this way, the crossover process is dynamic and aids in the improvements of the convergence speed of the optimisation problem as shown.

This section, used three testing functions (Table 3.1) to compare the convergence performance of the Heredity Algorithm and Genetic Algorithm. The advantage of using the HA over the GA is significant, it can has been determined that the convergence speed is faster throughout all the benchmark functions. Regardless of this early success, this area requires more investigation than done in this thesis. The further research will be included as a separate article from a journal paper with more tests and benchmark functions.

3.7 CAutoD Framework and Simulation Software

A CAutoD system can be applied to any random simulation problem. This will combine the computational intelligence of the search algorithm and the simulation model. The results from the simulation model will be obtained by using a Computer-Aided Design (CAD) system. The algorithm will execute several design parameters to find the most suitable solution for the given problem. This process can be computationally intensive and if multiple simulations need to be carried out the execution time can grow exponentially.

The software COMSOL was used to design a CAD system of the combustion chamber of an ICE. The combustion cylinder will work as a resonator for the MI system. The FEM simulation software calculates the microwave propagation throughout the cylinder as well as the resonance condition of the enclosed cavity. Figure 3.12 illustrates the system design used and the relationship between the simulation and search algorithm. The FEM simulation software calculates the electric field distribution inside the engine cylinder for the given search parameters. After each evaluation, the search algorithm will predict based on the previous results, new parameters to achieve the

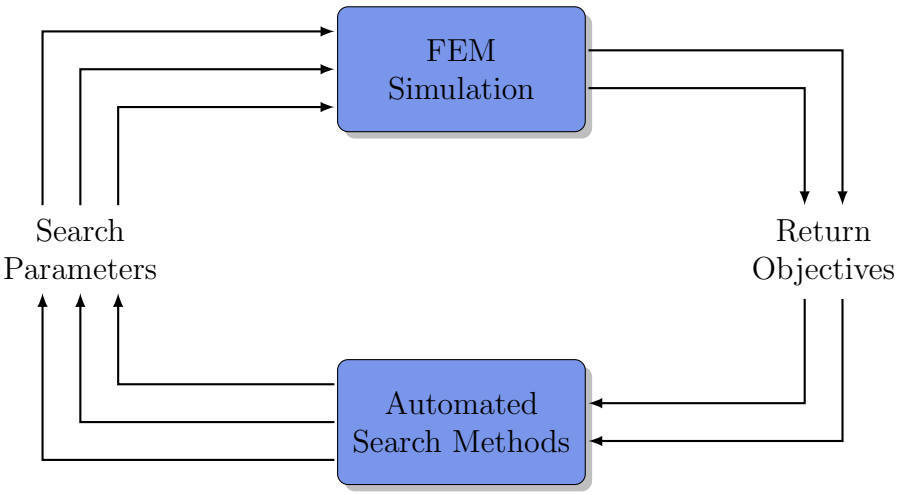

Figure 3.12: Connection between the optimisation algorithm and the simulation model

search objectives of the problem.

To optimise the CAutoD design it is important that both algorithms, the simulation and optimisation algorithm, are chosen carefully and thoroughly investigated for possible improvements. Section 3.6 describes the advantages and disadvantages of the the different search algorithms and their usability for the practical application of this project. In chapter 4, various algorithms are used to perform multiple evaluations on one particular cylinder design with variable antenna designs in order to discover the best propagation performance for the MI system.

Theoretically, a CAD model with ten variables could be solved without an optimisation algorithm by calculating all possible combinations but the calculation time would be inefficient. For example, if every calculation needs one second and 10^{10} steps, the entire process would require more than 300 years. The first step is to generate the initial parameters and transfer them to the simulation. After the simulation receives the parameters, the objectives are calculated and transferred back to the automated search algorithm.

At this point, the search algorithm needs to check for the stopping criteria for the search. If the criteria does not match, new search parameters need to be generated and the simulation process must to be restarted. The differences between the variable optimisation searches are mainly in the generation of the search parameters and the variable termination criteria.

3.7.1 FEM Solver

For the investigation of the microwave propagation performance inside the combustion chamber of an ICE, a flexible software is required to cover the whole spectrum of possible alternations. Therefore, during this project, the simulation software "FEM Solver" was developed to combine the advantages of using the COMSOL Java-API with different optimisation techniques like the MATLAB optimisation toolbox or the individual designed search algorithms.

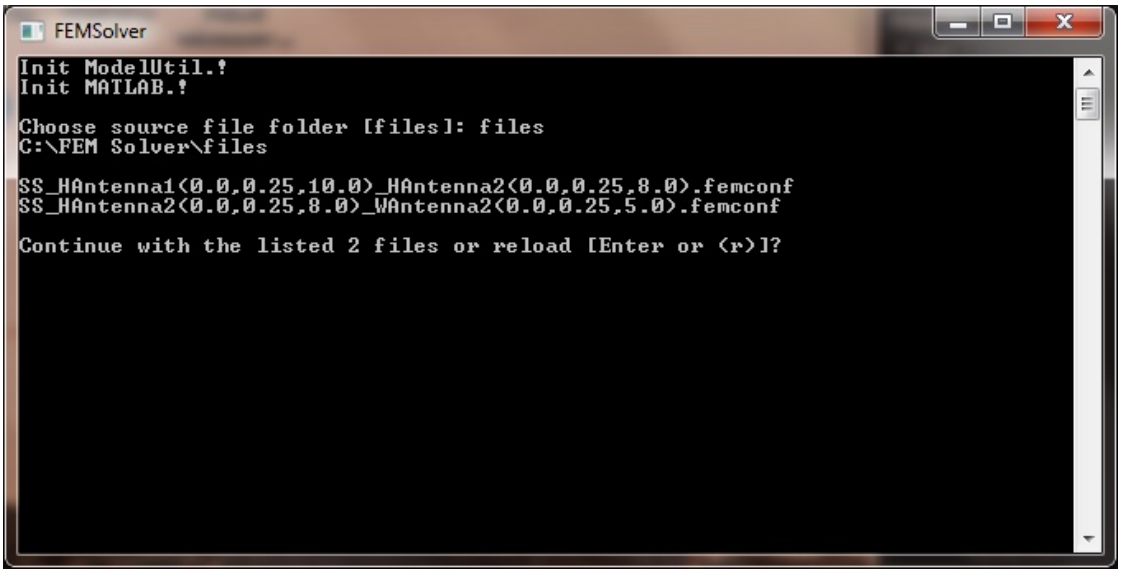

Figure 3.13: FEM Solver

The software (Fig. 3.13) can perform different simulation requests by using the most suitable simulation mode. The simulation results are saved as a comma-separated values (CSV) file, which can be directly read by for example MATLAB, to interpret and compare the results of different simulations after the search. Additionally, for each simulation the software creates a meta file which keeps all relevant simulation settings to reproduce the search process at a later stage. The structure of the meta and the CSV file depends on the performed kind of simulation. During the optimisation simulation, a backup file will be created after every evaluation to give an overview of the search progress as well as to backup the data in case of any unexpected problem. The solver can be extended by new COMSOL simulation models for different antenna designs without changing the source code or recompiling the software itself.

3.7.2 Simulation Modes

The **range frequency** mode simulates a defined spectrum of frequencies for a fixed set of parameters. The aim of this simulation mode is to gain knowledge of the electric

field intensity signal characteristics inside the combustion cylinder. Unfortunately, the quality of the results strongly depends on the search resolution. As shown in section 4.2, resonance occurs at a very narrow frequency range around the natural frequency of the cylinder. A successful run of this simulation mode requires an approximate estimation of the resonance frequency in order to successfully determine a suitable frequency range without missing the global extrema.

The **resonance frequency** search mode helps to find the resonance frequency of a given cylinder model. In contrast to the range frequency search, this mode uses a deterministic search algorithm to find the characteristic points of the signal rather than to apply a defined frequency range to the model and to analyse the results afterwards. The first step of this search mode is to calculate the Eigenfrequency of the given geometry with the FEM simulation software by supplying a starting value but without any input signal. On this way a frequency almost identical to the resonance frequency of the model will be obtained. The found Eigenfrequency will be used as a starting value for the single variable simplex optimisation search (more details in section 4.3.7). The calculated starting value will make it possible to find the resonance frequency of the cylinder model within a few iterations. The algorithm used in this mode is the "fminsearch" method provided by the MATLAB optimisation toolbox which was ported to Java in order to use the COMSOL API. Additional to the resonance frequency, this search mode can determine the bandwidth of the electric field intensity signal by running another deterministic search after finding the maximum electric field intensity. This search mode is used in sections 4.3.2, 4.4.1 and 4.4.2.

The **surface search** will obtain all required data to build a surface plot for the understanding of the relationship between multiple inputs. It is useful to gain information about the output signal characteristics depending on multiple input parameters. On this way, it is possible to understand the relationships of the variables and to acquire a wider knowledge of the system within the search range. During the implementation the following needed to be considered: If the search range covers an antenna length of 5 mm to 25 mm with a resolution of 0.1 mm and a piston position between 0.5 mm to 5 mm with the same resolution, the number of parameter pairs are 9000. Each of these 9000 parameter pairs would require several hundreds of evaluations and the simulation mode would require several days of calculation for one single search. This is impractical and was therefore never used in other research papers. To solve this problem the performance between the Eigenfrequency and the resonance frequency of the cylinder was analysed in section 4.3.7. The Eigenfrequency is not exactly, but nearly identical to the resonance frequency of the cylinder. This advantage can be used to minimise the simulation time for this search mode by using the Eigenfrequency instead of locating the resonance frequency by applying a deterministic search. Therefore just one single evaluation is required to reach a frequency close enough to the resonance

frequency of the cylinder which generates a representable electric field intensity for the given configuration. The use of the Eigenfrequency improves the simulation time to less than a few hours which makes this simulation mode and this kind of representation practical and useful in the illustration of the important relationships between multiple variables. After the simulation is finished, the data needs to be analysed and processed by MATLAB to generate a three dimensional surface or a contour plot.

The different search modes presented up to this point are essentially static and require assistance in the improvement of the propagation performance of the antenna design. The **Nelder–Mead** optimisation mode is implemented by utilising the NM Simplex Search algorithm of MATLAB to find the maximum electric field intensity using a various number of parameters. This optimisation search works without boundary conditions, therefore a well defined starting point is mandatory, to obtain a sufficient field strength. It is also important to validate the found solution for a feasible real world application. The settings for this optimisation mode are the maximum number of evaluations and iterations as well as the function and variable tolerance. In order to accelerate the execution time it is possible to use the frequency as a normal input variable or as a combination of Eigenfrequency and single frequency simulation to perform the optimisation of the problem. The performance of both searches will be compared in chapter 5.

The **Genetic Algorithm** optimisation mode implements a non-deterministic search technique. The advantage of the GA mode is that it fully supports boundary conditions during the search. On this way, it is possible to avoid for example a negative length for an antenna which might give mathematically the best solution but not a practical solution for a real world application. In order to provide similar results, as achieved with the NM search algorithm, more evaluations are required but the chances of finding the global maximum are superior using the GA technique. The total evaluation time of the GA optimisation mode is in average fundamentally higher than the NM mode, but will eventually produce more favourable results. The algorithm used for this mode is also provided by the MATLAB optimisation toolbox and ported to use within the newly developed framework for communication with COMSOL via the API.

Chapter 4

Simulation and Analysis of Microwave Distribution

Virtual prototyping is a technique used in the process of developing and producing a novel product. It involves using a CAD and CAutoD software to validate and predict the results of an idea before building a physical prototype. In this project virtual prototyping uses the FEM simulation software COMSOL Multiphysics to design a single combustion chamber and incorporates this model into a CAutoD system. Using this method makes it possible to assemble different antenna designs in order to find the best suitable solution for the optimum propagation performance inside the enclosed cavity of an ICE within a relatively short time. Effective virtual prototyping now incorporates the computer model of the given problem with an algorithm which is applied to the simulation model in order to find the most suitable design for the given parameters.

The most favourable design of a HCMI system needs to match two principal parameters. The first parameter is to provide the maximum electric field propagation performance inside the engine cylinder of the ICE. This will potentially result in a more complete combustion and therefore lead to fuel saving along with an improvement of the engines efficiency. The second parameter is the consideration of economic and financial factors, this will have the most impact on the successful design and implementation of a HCMI system. The most economical antenna design would require minimum modifications to the existing engine cylinder of an ICE. Considering both parameters, it would be possible to improve the general engine performance and efficiency with minimal physical modifications to the engine cylinder of a SI system as well as at minimum financial expense while upgrading an existing system.

A HCMI system requires a microwave generator, the microwave energy will be transferred via a transmission line into the combustion chamber of the ICE. This can be realised with several coupling methods, here used coupling mean, a probe antenna (illustrated in Fig. 3.2b), will fit into the spark plug hole of an ordinary SI cylinder head. The antenna type of this HCMI design would require minimum physical modifications to the engine cylinder of the existing SI system and therefore matches the aforementioned economical criteria.

Prior to the virtual prototyping of the antenna model and the search for the optimum design in terms of electromagnetic field propagation, it is required to evaluate the used approximated cylinder model of the ICE. Section 4.1 shows the evolution from a regularly shaped cylindrical cavity to the used approximated cylinder model for the virtual prototyping in chapters 4 and 5. Aforementioned, the used microwave coupling apparatus will be designed to replace the ordinary SI plug and must fit in the existing opening at the cylinder head. Both components, the geometric model of the cylinder and the microwave coupling apparatus, are designed with the FEM based simulation software COMSOL Multiphysics and analysed for different behaviours. The main research focus of this project is the optimisation of the electric field intensity inside the combustion chamber prior to combustion occurring.

As discussed in section 3.1 TM_{010} is the dominant resonance mode inside the engine cylinder of an ICE. The natural frequency of the cylinder changes while the piston moves up and down. Once this happens, and the supplied frequency is fixed, the resonance inside the cavity will be weakened or completely disappear. This summarises the flaw in all previous MI designs and needs to be further investigated to gain a wider understanding of the elements contributing to this phenomenon. Some possible factors affecting the natural frequency of the resonator are the piston position, the air-fuel mixture, the cylinder dimension, and the coupling mean dimensions.

4.1 Geometry Models of Engine Cylinders

A four stroke Otto engine cylinder primarily consists of the cylinder head, the cylinder body, the inlet and outlet valves, the spark plug, and the moving piston. The typical cylinder diameter varies and ranges between 80 mm and 100 mm while the diameter of the cylinder head is approximately 10 mm smaller. During the simulations, in order to investigate the electromagnetic field propagation performance inside the combustion chamber, the inlet and outlet valves are completely closed. This circumstance will simulate the power stroke of a four stroke engine and allows to simplify the enclosed

cavity for the design of the geometric irregularly shaped cylinder model of the ICE. After the successful generation of the electric field, the air-fuel mixture inside the combustion chamber will ignite and push the piston back towards to BDC.

The engine cylinder can be varied and quite complex. This section will investigate several cylinder models for their electromagnetic propagation performance and compare their characteristics in order to choose a suitable model for later use in the CAutoD system. The enclosed dimensions of an irregularly shaped ICE cavity are complicated and difficult to implement as an exact computer model. Regrettably, this project was not in cooperation with an engine manufacturer and therefore no actual and reliable CAD model of a physical engine cylinder was available prior to the design stage. For the search and optimisation this is not an issue, the steps would be the same even if the results would be different for a different simulation model. In consideration of both aspects, the complexity and the simplification, the development of a suitable engine cylinder model for the simulation of the prototyping process starts with a regular cylindrical cavity (illustrated in Fig. 4.1) in combination with a basic coaxial cable in the middle.

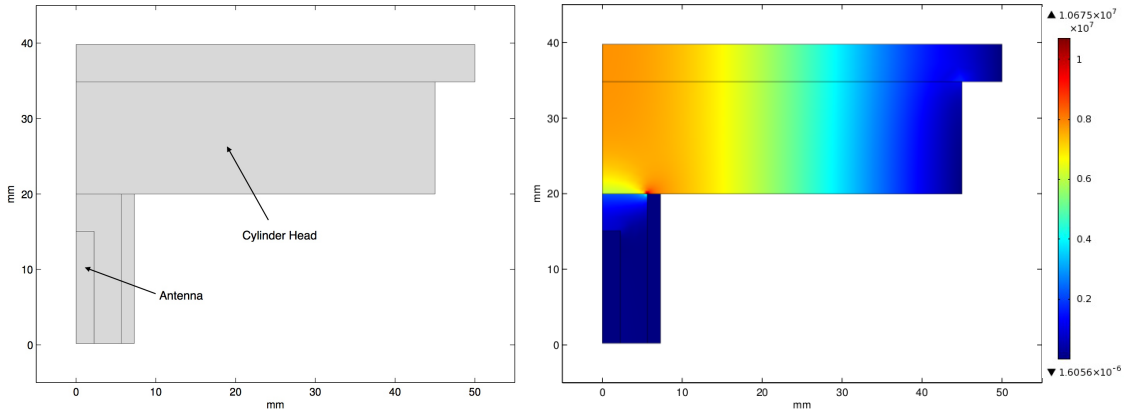

(a) (b)

Figure 4.1: Cylinder model (a)

Figure 4.1a shows the geometric dimensions of a regularly shaped cylinder with an antenna in the middle. This simple model will be further used in section 4.3.1 and 4.3.2 in aid of discovering the relationships between the air-fuel mixture as well as the cylinder radius with the electromagnetic field propagation performance. The geometric dimensions of the cylinder model in Fig. 4.1a are a piston radius of 50 mm, a cylinder head radius of 45 mm, a inner coaxial cable radius of 2.25 mm, an outer radius of 7.3 mm, and a dielectric radius of 5.65 mm. The used radius for the coaxial cable matches the dimensions of most commonly used cables. The outer radius of the ignition device is equal to the default size of a common spark plug in order to transform the existing SI system to the HCMI system with minimal modifications to the existing engine.

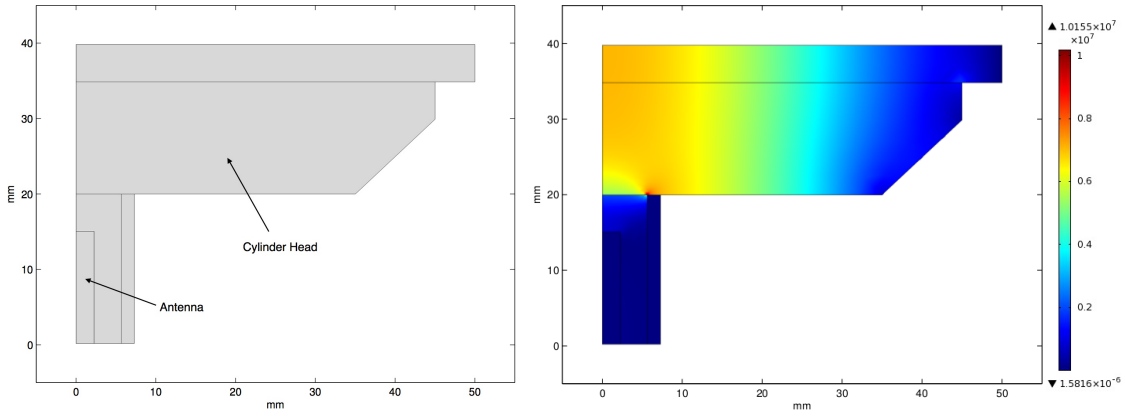

(a) (b)

Figure 4.2: Cylinder model (b)

Figure 4.1 shows a regularly shaped cylinder with a radius of 50 mm and a piston position to TDC of 5 mm. The generated microwave energy is transmitted from the source into the engine cylinder through an ordinary coaxial cable in all four models in this section. It can be seen in Fig. 4.1b that the dominant propagation inside the model's cavity is vertical to the horizontal axis. In the next model (Fig. 4.2) the shape of the cylinder is altered, it can be seen in Fig. 4.2b that the propagation mode changes and the generated electric field throughout the cylinder increases slightly due to the alternation. In comparison to the first model in Fig. 4.1, the second model (in Fig. 4.2) is one step closer to a real world engine cylinder.

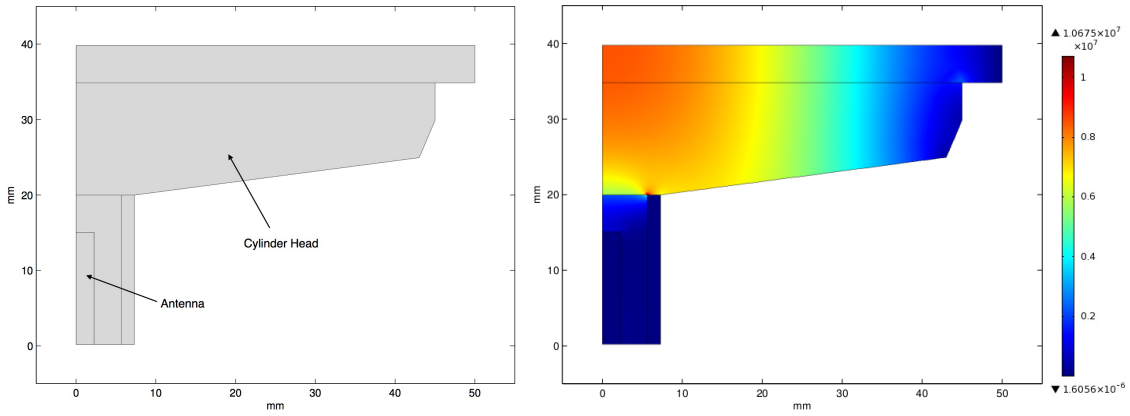

(a) (b)

Figure 4.3: Cylinder model (c)

Figures 4.3 and 4.4 show further changes to the geometric design of the engine cylinder model. In figs. 4.3b and 4.4b it can be seen that the electromagnetic field propagation performance further improved. The propagation is through the cylinder but based on the geometric changes the generated field intensity concentrates its maximum at the centre of the cylinder near TDC.

Table 4.1 summarises the results of the four different models in this section. The table compares the maximum electric field measured at the top of the cylinder head (at

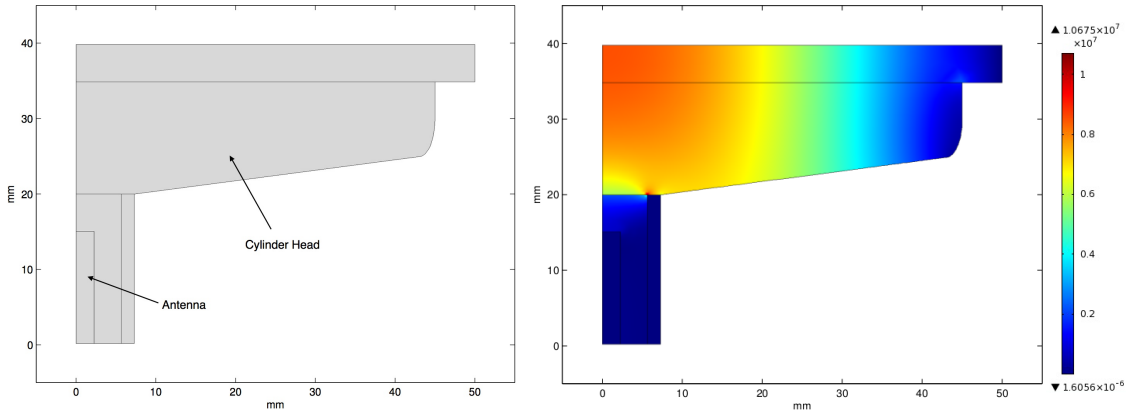

(a) (b)

Figure 4.4: Cylinder model (d)

TDC), and the resonance frequency required to generate the electric field intensity. The table confirms the initial observation, that the last two models (Fig. 4.3 and Fig. 4.4) deliver practically the same results and possess the best electromagnetic field propagation performance.

Table 4.1: Performance of different cylinder models

Model Name	**Resonance Frequency** (Hz)	**Maximum Electric Field Intensity** (V/m)
Model 2D (a)	2.4810×10^9	7.178×10^6
Model 2D (b)	2.6104×10^9	6.784×10^6
Model 2D (c)	2.6059×10^9	7.837×10^6
Model 2D (d)	2.5962×10^9	7.872×10^6

The fundamental objective for the most suitable antenna design is to possess the most effective distribution of the strongest electric field intensity inside the engine cylinder. In order to find the most suitable design, the ignition performance will be measured for each model and a detailed comparison made. Figure 4.5 shows the volume propagation performance inside the combustion chamber for the different models. To obtain this graph, the resonance frequency of each configuration was determined by using the search mode "Resonance Frequency" (see section 3.7.2) and set as the fixed input frequency for the generator. The input power varies between 1 W to 1000 W for the whole search range to attain the volume propagation performance inside the cylinder. The electric field intensity was captured along the cylinder head (TDC) of the CAD cylinder model. Also the distance between the cylinder centre and the point where the maximum electric field becomes lower 1×10^6 V/m was measured.

It can be seen that the propagation performance of the regular cylinder model (a) is in comparison preferable than of the extended model (b) but clearly deficient to the more

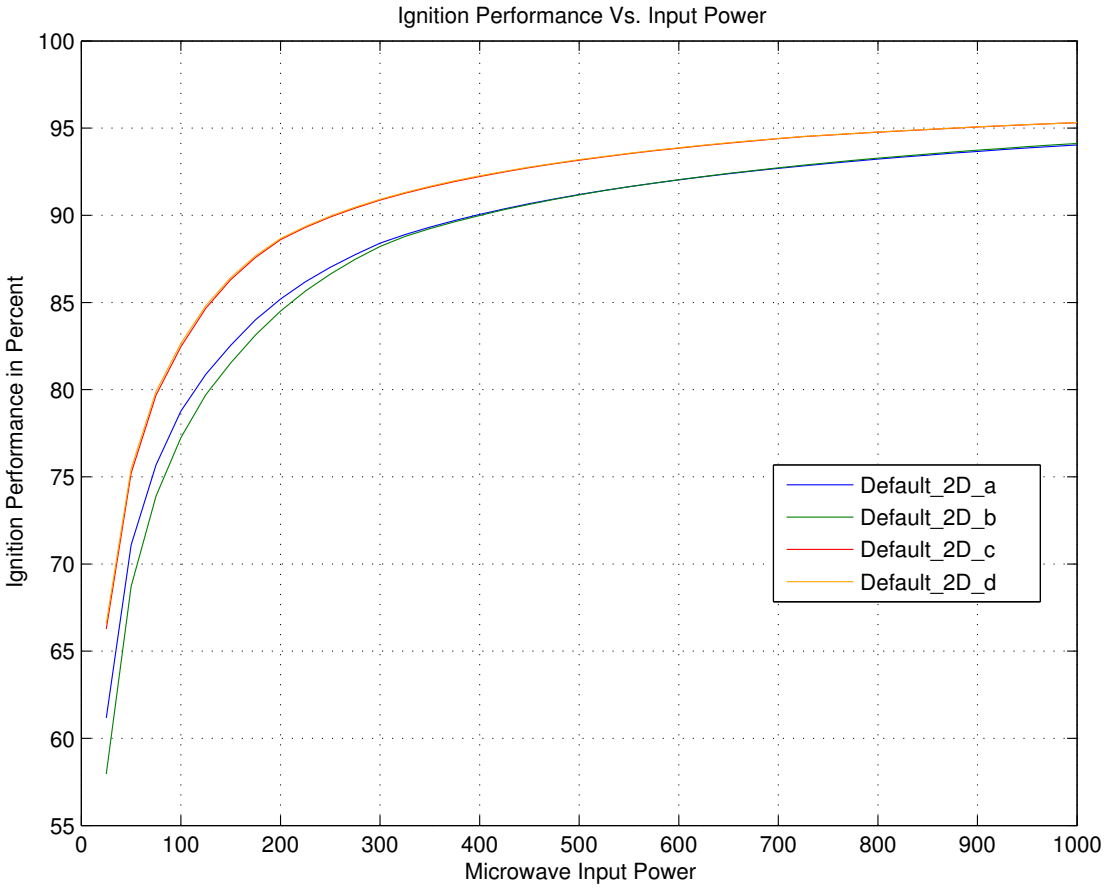

Figure 4.5: Ignition performance for default cylinder models

detailed models (c and d). The geometric difference between the detailed models (c and d) is trivial and therefore the difference in their volume propagation performance inside the cylinder as well. Using an input power of 330 W for the cylinder model d will lead to a volume propagation performance of 92 % while the regular cylinder model (a) would provide 87 % using the same input power. Based on the performance comparison between the different cylinder models in this section, the last cylinder model (shown in Fig. 4.4) will be used as the virtual prototype model for all further investigations. With a view to finding the suitable antenna design the given cylinder model needs to be extended with various antenna designs. The best suitable antenna design's purpose will be to obtain a maximum electromagnetic field propagation performance inside the combustion chamber which correlates with a maximum total combustion efficiency of an ICE.

4.2 Signal Characteristics

Figure 4.6 shows the maximum electric field intensity at the top of the cylinder head against a variable supply frequency. In the figure the point with the maximum electric

field intensity occurs at resonance condition, at around 2.7317×10^9 Hz. The reflections between the source and the cylinder are minimal at this particular frequency and the generated electric field intensity is at its maximum.

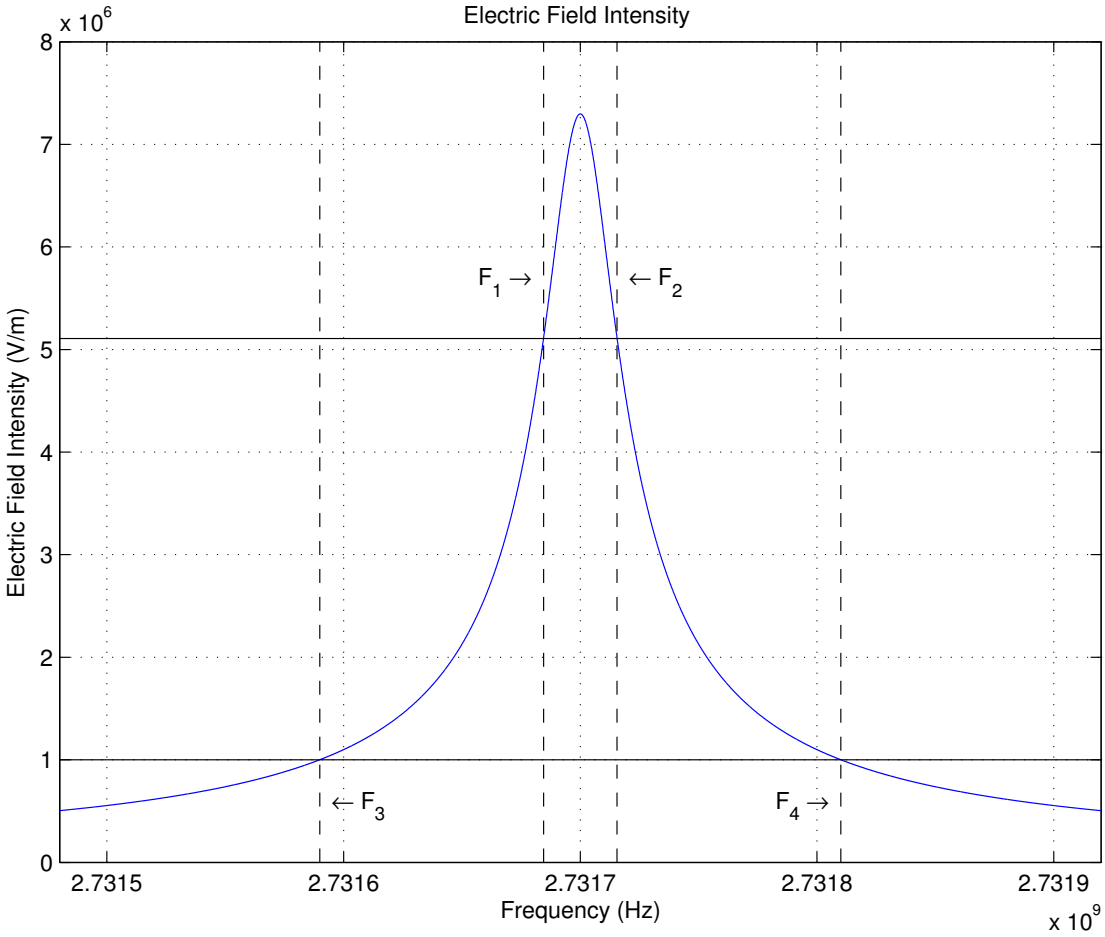

Figure 4.6: Electric field

The resonance inside the combustion chamber occurs at a very narrowed frequency close to the resonance frequency. Immediately, even with a small frequency change, the resonance will be weakened or disappear completely inside the cavity. Therefore, the electric field inside the cylindrical combustion chamber of an ICE changes significantly with every slight frequency fluctuation near the resonance frequency. To initiate the breakdown of the air-fuel mixture inside the combustion chamber a minimum electric field intensity of 1×10^6 V/m is required, as analysed in section 2.7. To simulate a real world application, the used input power of the microwave generator is set to 330 W for all simulations in this thesis, which could operate within an automotive system. This input power could be increased further if the generated field is not strong enough to break down the air-fuel mixture during the first field tests.

To obtain Fig. 4.6 the default cylinder model was used for the simulation with a fixed piston position of 0.5 mm to TDC. In section 4.3.6, it is shown that the piston motion significantly affects the resonance frequency of the resonator due to the explicit impact on the geometric dimensions of the cavity. Hence, the piston position could also alter

the dominant microwave propagation mode TM_{010}.

It can be seen that the signal is sharp and the bandwidth very small. Resonance occurs quite close to the actual resonance frequency of the cavity. To guarantee a volume ignition and therefore further improve the ignition performance along with the engine efficiency, a wider bandwidth would be beneficial. To address this problem, section 4.3.6 analyses the impact of the piston motion during the ignition on the maximum electric field inside the combustion chamber and the propagation performance. The bandwidth in general is defined as 0.7 times the maximum electric field, which leads to the frequencies $F_1 = 2.731\,64 \times 10^9\,\text{Hz}$ and $F_2 = 2.731\,67 \times 10^9\,\text{Hz}$ in Fig. 4.6. Aforementioned, a MI system requires a minimum electric field intensity of around $1 \times 10^6\,\text{V/m}$ to breakdown the air-fuel mixture inside the cavity. In consideration of that requirement, the bandwidth amplitude can be lowered to $1 \times 10^6\,\text{V/m}$ which then produces the two frequencies $F_3 = 2.731\,54 \times 10^9\,\text{Hz}$ and $F_4 = 2.731\,76 \times 10^9\,\text{Hz}$, and a total bandwidth of 31 000 Hz.

4.3 Default Prototype Antenna Model

The antenna model used in this section is the basic model of a cylinder with a single antenna in the centre of the cylinder and will be extended later by additional antenna designs (4.28). The changeable parameters in this model are shown in Table 4.2. The number of variables are kept to a minimum while still allowing maximum flexibility.

Table 4.2: Changeable values of default antenna model

Name	**Value**
HAntenna1	10 mm
HPlug	20 mm
HPiston	5 mm
AirEps	1.00
ZProb	35 mm

The cylinder head and the cylinder body are not modified throughout this simulation, as there is not any need to. These conditions are predefined through the geometric dimension of the engine model. Variable “HPiston” represents the piston position and more precisely the distance between piston head and the TDC.

There are four different materials used for this antenna design. The material inside the cylinder head and the cylinder body represents the homogeneous air-fuel mixture

which is alterable during the simulations with the parameter "AirEps". The inner material of the antenna, in this case antenna 1, is copper and represents a standard coaxial cable with a radius of 2.25 mm. The bound on the outside is steel with a fixed width of 2 mm for this model. A dielectric material fills the gap between the steel and copper, according to a standard coaxial cable.

The initial single variable change simulations are very similar to the simulations carried out in section 4.3.2. Instead of applying a frequency range to the model, like in section 4.3.1, and simulate several thousand different frequencies, this simulation will use a deterministic optimisation search. This will aid in the identification of the most suitable supply frequency for the microwave generator in order to create the most effective electric field propagation inside the combustion chamber.

4.3.1 Influence of the Air-Fuel Mixture

The AFR is the quotient between the air and fuel inside the combustion chamber and fluctuates when the engine is in use. Before the ignition of the mixture and plasma generation, the medium inside the combustion chamber is a pure mixture of air and fuel. The resonance frequency or natural frequency of the cavity depends on the relative permittivity of the material. One of the requirements for the successful and reliable design of a HCMI system is to investigate and expose the influence of a wide range of AFRs. For petrol engines, the AFR can be tuned approximately from 11:1 to 16.2:1, strongly depending on the engine status, load, and power that needs to be achieved (Taylor 1985). The most economical efficiency is reached at 15.4:1, while the maximum power point is at 12.6:1. The boundary between a rich and a lean mixture is located at an AFR of 14.7:1 (Hartman 2004; Gilles 2011).

The air and fuel for HCMI system are always well and homogeneously mixed before the ignition starts. The AFR is the factor that affects the dielectric of the mixture on the cylinder cavity and can be calculated by the approximation of the following equations. If material 1 with the permittivity ε_1 is located randomly in a homogeneous environment, material 2, with the permittivity ε_2 the power-law model can be used to calculate the resulted effective permittivity of the mixture (Johansson et al. 2008).

$$\varepsilon_{eff}{}^{\beta} = f\varepsilon_1{}^{\beta} + (1-f)\varepsilon_2{}^{\beta} \tag{4.1}$$

The parameter β is a dimensionless parameter and depending on the mixing model

used for the particular calculation, the value can be different. For example, the Birchak formula ($\beta = \frac{1}{2}$) (Birchak et al. 1974) or Looyenga formula ($\beta = \frac{1}{3}$) (Looyenga 1965) as well as the Lichtenecker formula ($\beta \to 0$) (Lichtenecker and Rother 1931):

$$\ln \varepsilon_{eff} = f \ln \varepsilon_1 + (1 - f) \ln \varepsilon_2 \tag{4.2}$$

The Lichtenecker equation is a special case of the power law models and can be used if $\varepsilon_1 > \varepsilon_2$. The distinct mixing models predict various effective permittivity values for a given mixture. However, for all the different mixing models, there are bounds that limit the range of predictions. The loosest bounds are the Wiener bounds (Wiener 1910). These permittivity bounds are:

$$\varepsilon_{eff,min} = \frac{\varepsilon_1 \varepsilon_2}{f\varepsilon_2 + (1 - f)\varepsilon_1} \tag{4.3}$$

$$\varepsilon_{eff,max} = f\varepsilon_1 + (1 - f)\varepsilon_2 \tag{4.4}$$

These bounds calculate the minimum and maximum permittivity independently of the mixing model and will always give the minimum and maximum for $\varepsilon_1 < \varepsilon_2$ as well as for $\varepsilon_1 > \varepsilon_2$.

$$f = \frac{1}{AFR + 1} \tag{4.5}$$

The volume fraction f represents the AFR in these equations and can be calculated by using Eq. (4.5). The following investigation will cover a suitable range for AFRs from 10:1 to 20:1. The fuel permittivity can be varied for different types of fuels. Propane, the main component for LPG, has a permittivity of 1.6. Methane, the main component of CNG or Liquefied Natural Gas (LNG), has a permittivity of 1.7. The main component is Pentane for the common petrol engine, which has a permittivity of 1.8 (Controls 2012).

Figure 4.7 shows the mixture permittivity inside the combustion chamber for different fuel types by using Eq. (4.2). The figure demonstrates that a fuel with a higher permittivity results in a higher permittivity of the homogeneous air-fuel mixture irrespective of the AFR. This is based on Eq. (4.2) and it is evident that the mixture permittivity

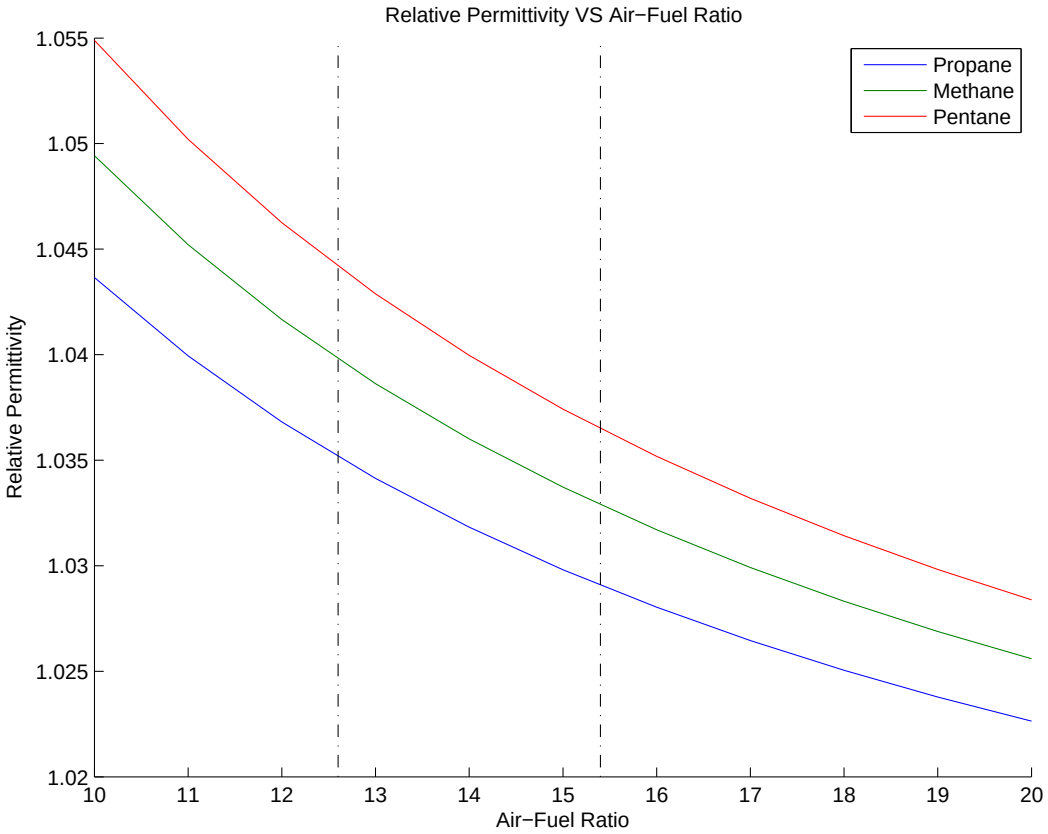

Figure 4.7: Relative permittivity for different AFRs

grows by increasing ε_1 of the monotonically increasing natural logarithm function and a constant variable ε_2 and f which represents the AFR.

The maximum power point occurs at a rich mixture AFR of 12.6:1 and the best fuel consumption condition with a lean mixture of 15.4:1, these points are indicated by vertical lines at the corresponding values (Hartman 2004; Martin 2012). The best fuel consumption condition is required by the catalytic converter to operate at maximum efficiency. According to the Lichtenecker specifications (Eq. (4.2)) the equation can be applied for $\varepsilon_1 > \varepsilon_2$, where ε_1 is the permittivity of the injected material. This agrees with the application requirements but to spread the investigation range at this point, the Wiener bounds are used. With eqs. (4.3) and (4.4) the loosest permittivity bounds are 1.0216 and 1.0636 for the AFR search range.

Regarding to the AFR search range, the mixture permittivity will span from 1.00 to 1.07 which encompasses the Wiener bounds. The default model is used here without any additional antenna modifications. It is assumed that the air and fuel are well mixed before being injected into the cylinder and evenly distributed within the cylinder during a compression stroke.

To obtain Fig. 4.8 a frequency range from 2.35 GHz to 2.5 GHz was applied to the simulation model. This frequency range contains distinct resolutions for the various

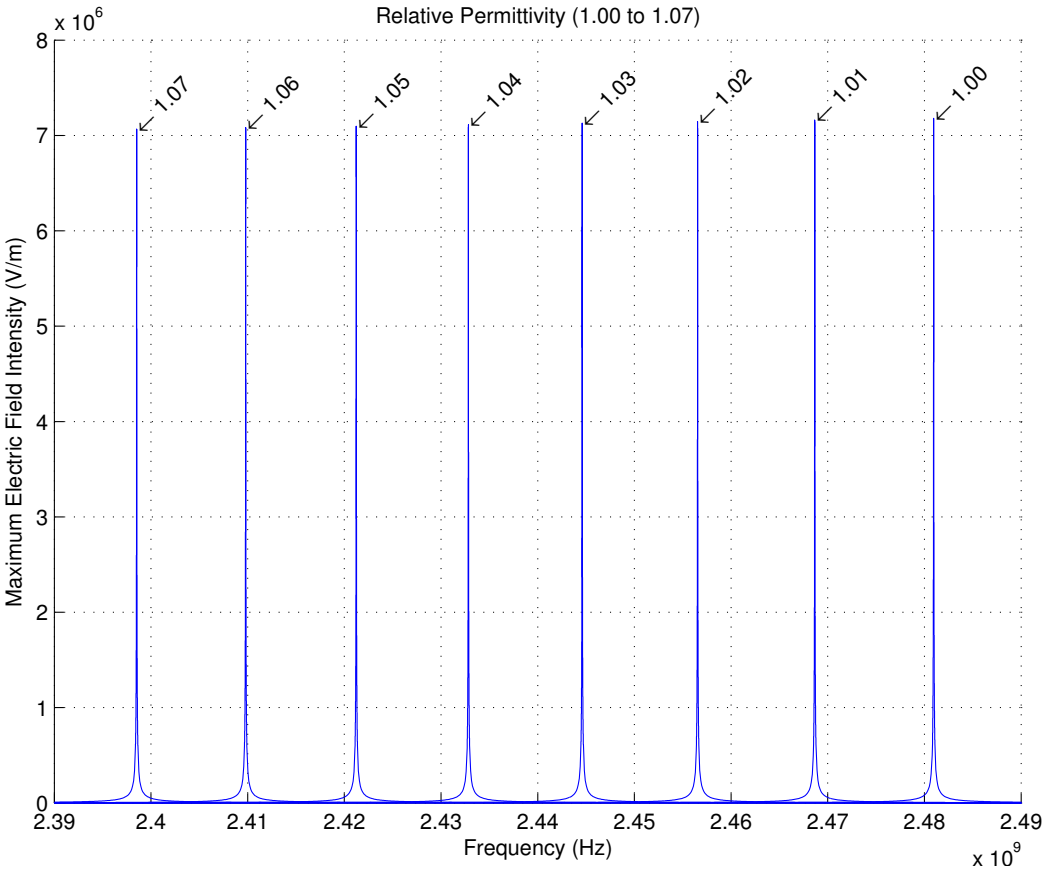

Figure 4.8: Influence of the AFR

Table 4.3: Relative permittivity from 1.00 to 1.07

AirEps	**Resonance Frequency** (Hz)	**Bandwidth** (Hz)	**Maximum Electric Field Intensity** (V/m)
1.00	2.4810×10^9	155 430	7.178×10^6
1.01	2.4687×10^9	154 299	7.161×10^6
1.02	2.4565×10^9	153 135	7.145×10^6
1.03	2.4446×10^9	151 948	7.128×10^6
1.04	2.4328×10^9	150 821	7.112×10^6
1.05	2.4212×10^9	149 682	7.096×10^6
1.06	2.4098×10^9	148 628	7.081×10^6
1.07	2.3985×10^9	147 529	7.065×10^6

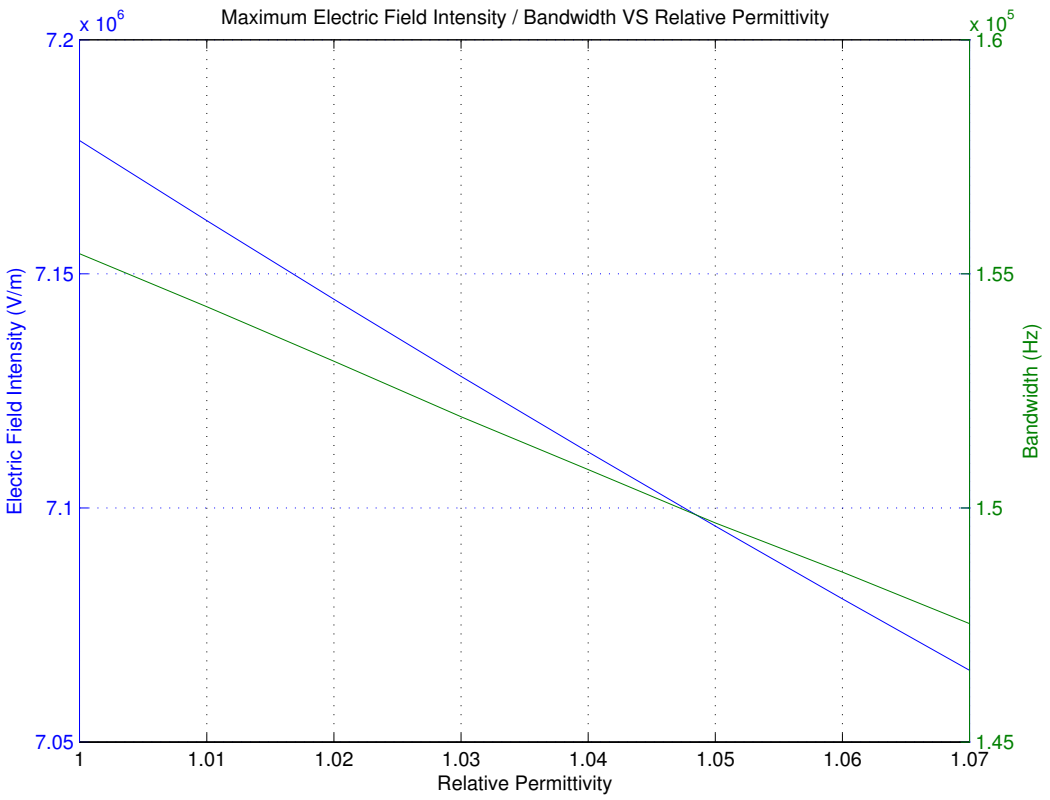

Figure 4.9: Electric field and bandwidth against the relative permittivity

frequencies and AFRs. This means that for an AFR of 1.03 the search frequency range must be more detailed around 2.445 GHz and can be less detailed further away from the resonance frequency which lowers the resolution and therefore saves calculation time. Figure 4.8 illustrates the electric field intensity inside the combustion chamber by varying the AFR. The maximum electric field intensity change is insignificant. When the relative permittivity increases from 1.00 to 1.07, the field strength decreases from 7.178×10^6 V/m to 7.065×10^6 V/m. This implies that the AFR does not notably affect the maximum electric field intensity or the Q factor. In contrast, the resonance frequency changes significantly from 2.3985 GHz up to 2.481 GHz) as a result when using a variable AFR. This results in an increasing permittivity which leads to a decreasing natural frequency of the combustion cavity. Figure 4.9 summarises the tendency of the maximum electric field intensity inside the cavity as well as the bandwidth of the signal. To obtain the bandwidth of the signal is was required to further analyse the results shown in Fig. 4.8.

It can be seen that the maximum electric field intensity decreases from 7.178×10^6 V/m to 7.065×10^6 V/m with a linear behaviour within the search range. Similar to the field, the bandwidth of the electric field signal is decreasing linearly from 155 kHz to 147 kHz for the given search range and search direction. The effects on the resonance frequency and bandwidth can be used later during the design of a MI system to manipulate and adjust the resonance frequency and bandwidth performance. The sensitivity of the resonance frequency can become a major complication in the realisation of a practical

HCMI system. In order to define the AFR, the behaviour of the electric field intensity performance allows a free adjustment of the AFR. A lean mixture with a high AFR would lead to a better propagation performance but for the ignition process a richer mixture gives a higher combustion performance.

Table 4.4: AFR at maximum power point and best fuel consumption condition

AirEps	**Resonance Frequency** (Hz)	**Bandwidth** (Hz)	**Maximum Electric Field Intensity** (V/m)
1.0365	2.4369×10^9	151 169	7.118×10^6
1.0442	2.4279×10^9	150 375	7.105×10^6

To complete the investigation of the AFR, it is required to simulate and measure the resonance frequency, bandwidth, and maximum electric field intensity fluctuations between the maximum power point at a rich mixture of 12.6:1 and the best fuel consumption condition with a lean mixture of 15.4:1. An AFR of 12.6:1 is equal to a relative permittivity of 1.0442 and 15.4:1 can be expressed as a relative permittivity of 1.0365. By applying these two AFRs to the simulation model, the details given in Table 4.4 have been obtained. The resonance frequency changes by 8.992 MHz, the bandwidth by 793.413 Hz, and the maximum electric field intensity by 1.2306×10^3 V/m. This demonstrates that for the resonance condition it is essential to know the exact AFR inside the cylinder in order to determine the suitable supply frequency needed to match the natural frequency of the cavity.

4.3.2 Effect of a Variable Engine Cylinders Radius

One principal factor which affects the geometric dimensions of a cylinder directly and therefore also influences the resonance mode and natural frequency, is the radius of the combustion chamber. The simulation of the radius of the engine cylinder includes a value from 40 mm to 50 mm which encompasses all commonly used systems. The cylinder radius can change the dominant microwave propagation mode inside the combustion chamber. The radius impacts the matching condition for the dominant TM_{010} mode in Eq. (3.5) directly, therefore it is important to understand this relationship. However, for the the running system it is not important, since the engine cylinder is fixed. During the design stage understanding the relationship might offer some advantages for increasing the bandwidth and general propagation performance.

This simulation uses a slightly different method for obtaining the results in comparison to section 4.3.1, but uses the identical cylinder model. Instead of applying a defined

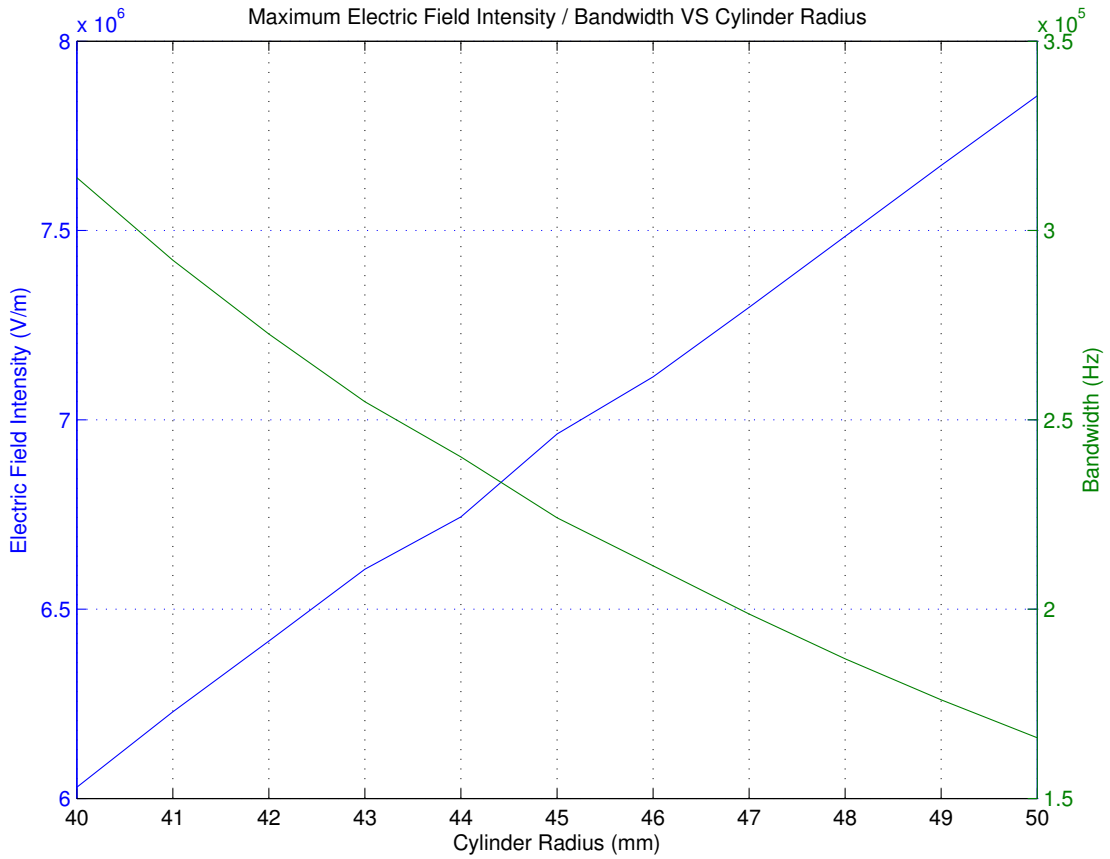

Figure 4.10: Electric field and bandwidth against the piston radius

frequency range to the simulation and measuring the electric field intensity at the top of the cylinder of every single frequency, a deterministic optimisation method will be utilised to find the maximum electric field intensity. The advantage of this method is the computing speed. Instead of calculating thousands of frequency points, which takes several hours, this method only requires the start of the simulation at a frequency nearby the resonance frequency. It then calculates approximately 100 further frequencies to find the most suitable one that will provide the strongest electric field intensity inside the combustion chamber. The simulation can also measure the bandwidth of the signal to calculate the Q factor of the cylinder. In order to do so, another deterministic search will be used to find the needed frequencies to calculate the bandwidth of the signal.

Table 4.5 summarised the simulation results for the cylinder radius and the results are illustrated in 4.10. It shows that the resonance frequency decreases while the radius of the engine cylinder increases and in contradiction, increases the maximum electric field intensity. The slightly non linear behaviour between 43 mm to 50 mm can be explained by the signal shape and the used search resolution (see section 4.2 for more information on the signal shape and bandwidth). This confirms the relationship between cylinder radius and resonance frequency given by Eq. (3.9). The supplied frequency is essential for the designing of a HCMI system. Since the bandwidth decreases while increasing

the radius of the cylinder, it is necessary to find a compromise between the maximum electric field intensity and the bandwidth of the signal.

Table 4.5: Piston radius from 40 mm to 50 mm

WPiston (mm)	**Resonance Frequency** (Hz)	**Bandwidth** (Hz)	**Maximum Electric Field Intensity** (V/m)
40	2.8720×10^9	313 976	6.030×10^6
41	2.8018×10^9	292 136	6.229×10^6
42	2.7350×10^9	272 652	6.416×10^6
43	2.6712×10^9	254 787	6.606×10^6
44	2.6104×10^9	240 184	6.744×10^6
45	2.5523×10^9	224 098	6.963×10^6
46	2.4967×10^9	211 439	7.113×10^6
47	2.4435×10^9	198 729	7.297×10^6
48	2.3925×10^9	186 879	7.485×10^6
49	2.3436×10^9	176 029	7.672×10^6
50	2.2967×10^9	166 036	7.856×10^6

Section 4.3.6 explored the behaviour of the electric field while the piston moves and the minimum required bandwidth of the signal for a complete combustion. Therefore, the default value 50 mm for the radius used in the previous simulations is a suitable value and does not necessitate any further adjustments prior to the next simulations. The chosen value offers a bandwidth of 148 kHz which is approximately 70 % more than the minimum required bandwidth shown section 4.3.6.

4.3.3 Influence of the Piston Motion

The piston motion is a chief component which considerably affects the natural frequency of a cylinder cavity in TM_{010} mode. It directly alters the geometric dimension of the resonator and thus the resonator volume. The piston of an internal combustion engine moves continuously and due to this the geometry of the combustion chamber is in constant flux. This results in the natural frequency of the resonator being in constant fluctuation. The variable "HPiston" represents the distance (in mm) between the piston and the cylinder head TDC in all the simulations.

Some of the literature uses degrees to describe the piston position instead of mm to TDC. Both approaches can be directly converted into the other value by knowing

Table 4.6: Relationship between TDC and degree

Cylinder height (mm)	**TDC** (mm)	**Degree**
90	5.0	10°
90	0.5	1°
100	5.0	9°
100	0.5	0.9°

the cylinder height. In application to a 90 mm engine cylinder, a range from 0.5 mm to 5 mm would be approximately from 1° to 10° (see chapter 2). The simulation in Fig. 4.11 covers a range of piston positions between 0.5 mm and 5 mm to TDC which would be approximately from 1° to 10° for a 90 mm engine cylinder (Table 4.6).

Table 4.7: Relationship between rpm and piston speed

Cylinder height (mm)	**rpm** (r/min)	**Speed of piston** (m/s)
90	650	1.95
90	7200	21.6
100	650	2.17
100	7200	24.0

Several research papers have shown that the ignition time of a MI system is considerably shorter in comparison to a SI system. In numbers, the microwave based ignition occurs in 30 to 100 ns (Gundeisen 2004; Gundeisen 2007). Research on Corona Discharge Plasma Ignition also shows that the MI combustion is at least 25 % faster than a SI system (Bellenoue, Labuda, and Engles 2005). Table 4.7 shows the relationship between the revolutions per minute ($^{\circ}$/min) and the piston speed, therefore if the engine speed reaches 7200 $^{\circ}$/min the piston speed can be up to 21.6 m/s. A timing advance is required due to the time taken by the ignition and the speed of the piston. For every 0.5 mm in a 90 mm cylinder the piston needs between 256 ms at 650 $^{\circ}$/min and 0.023 ms at 7200 $^{\circ}$/min. Due to the fast ignition of a MI system, a significantly less time advantage is possible for the ignition event compared to a SI system and subsequently maximises the power used by pushing the piston.

For every piston position in this simulation, a variable frequency range was applied to the cylinder model. The electric field intensity was measured for each frequency at every piston position value. Table 4.8 gives the resonance frequency, bandwidth, and maximum electric field intensity at the top of the engine cylinder. Figure 4.12 is a graphical presentation of the resonance frequency in Table 4.8. The electric field intensity in the combustion cylinder is shown on the y-axis against the frequency on the x-axis while the piston moves from 0.5 mm to 5 mm to TDC in 0.5 mm steps. This

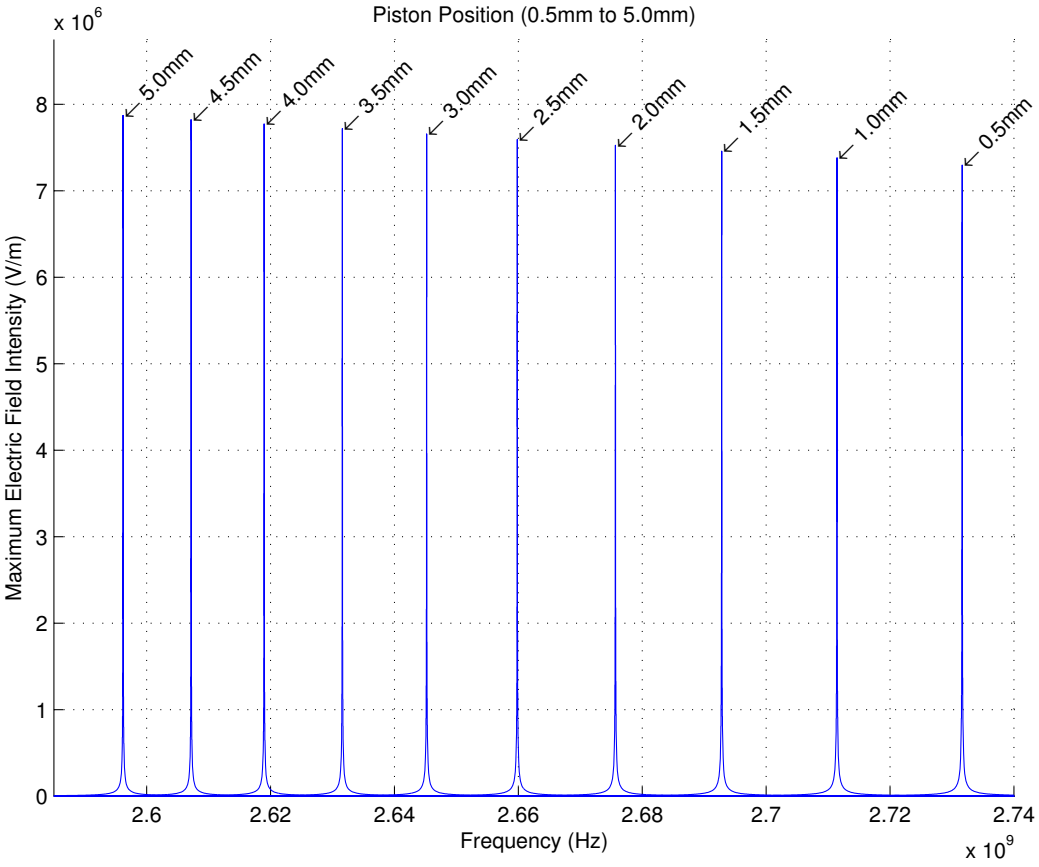

Figure 4.11: Electric field against the piston position

Table 4.8: Results piston position from 0.5 mm to 5.0 mm

Distance to TDC (mm)	**Resonance Frequency** (Hz)	**Bandwidth** (Hz)	**Maximum Electric Field Intensity** (V/m)
0.5	2.7317×10^9	2.20×10^5	7.297×10^6
1.0	2.7114×10^9	2.09×10^5	7.380×10^6
1.5	2.6928×10^9	1.99×10^5	7.458×10^6
2.0	2.6757×10^9	1.90×10^5	7.526×10^6
2.5	2.6598×10^9	1.82×10^5	7.592×10^6
3.0	2.6452×10^9	1.74×10^5	7.656×10^6
3.5	2.6316×10^9	1.67×10^5	7.717×10^6
4.0	2.6190×10^9	1.60×10^5	7.772×10^6
4.5	2.6072×10^9	1.54×10^5	7.822×10^6
5.0	2.5962×10^9	1.48×10^5	7.872×10^6

demonstrates that the field appears sharp and close around the resonance frequency, and that the bandwidth to resonance frequency ratio is small for the signals. Figure 4.12 indicates a slightly declining field if the distance between the piston and the cylinder head decreases. In regard to these first results, it can be concluded that the piston position affects the Q factor of the resonator. The natural frequency of the cavity increases from 2.595 GHz up to 2.73 GHz for this search range of the piston movement. This would make it necessary to adjust the supply frequency in case the running engine piston moves significantly enough to let the cylinder resonance disappear. Section 4.3.6 simulates the field change and disappearance during the piston movement and therefore further addresses this problem.

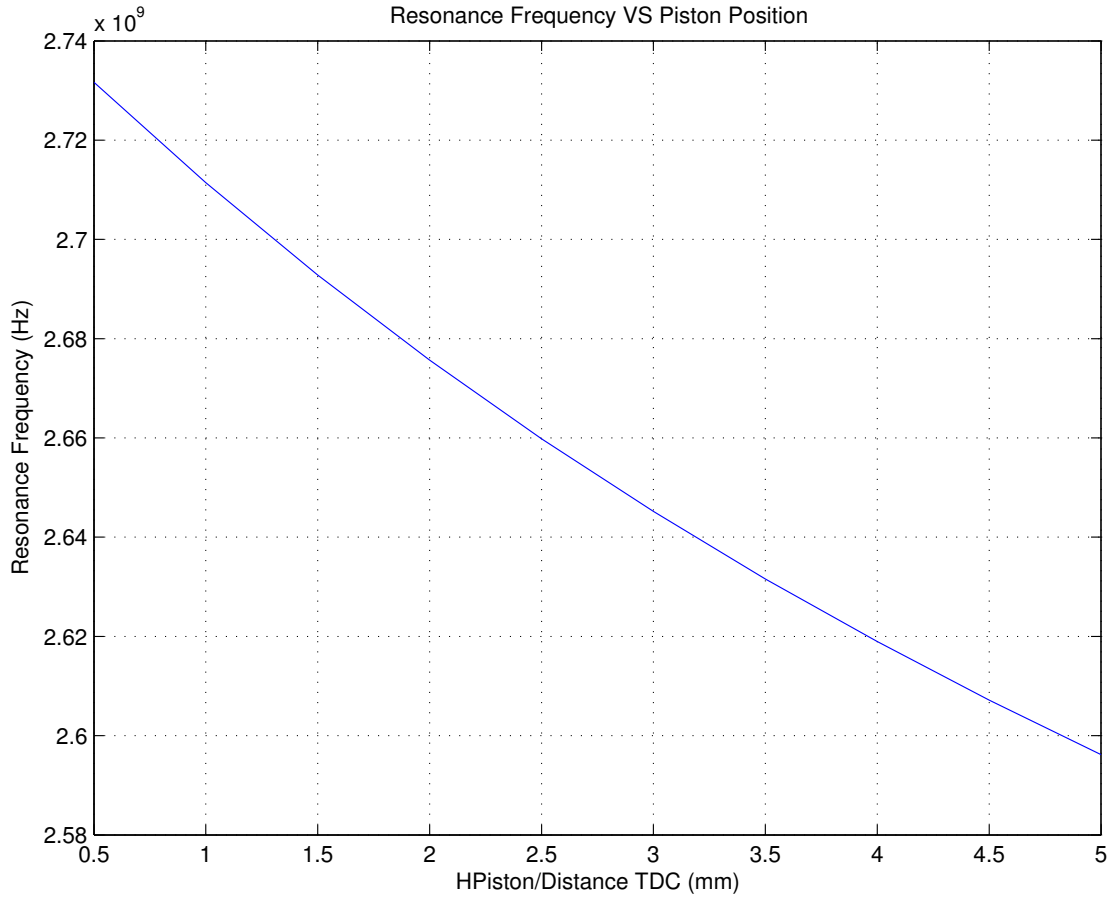

Figure 4.12: Resonance frequency against the piston position

To maximise the power used to push the piston, the time advance needs to be minimised which correlates with a smaller distance to TDC. The data from Table 4.8 was used to create Fig. 4.12 which shows the behaviour of the resonance frequency of the cylinder as previously mentioned. Figure 4.13 demonstrates the electric field intensity and bandwidth of the signal inside the combustion chamber, the electric field intensity declines from 7.872×10^6 V/m to 7.297×10^6 V/m while the distance to TDC decreases. This tendency also confirms the observation during the investigation of the measuring point inside the combustion chamber in section 4.3.5. The larger the distance from the source as the larger the electric field intensity grows. Consequently, the bandwidth which is an essential component for a successful, complete, and clear ignition, expands

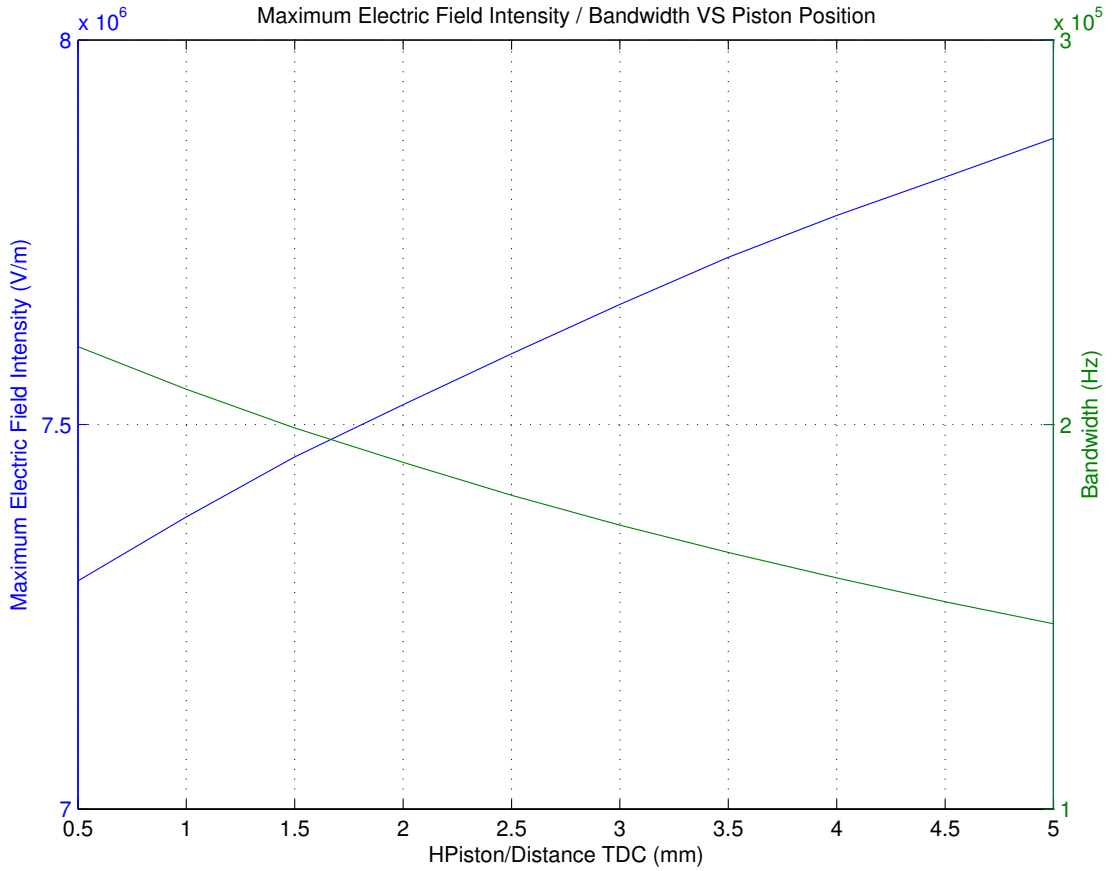

Figure 4.13: Electric field and bandwidth against the piston position

from 148 kHz to 220 kHz which is an increase of 50 %. If the distance to TDC decreases further the bandwidth will expand to 231 kHz with 0.05 mm to TDC. Whether the bandwidth can cover the piston motion during the time of the ignition is investigated in section 4.3.6.

4.3.4 Influence of the Antenna Length

The transfer of the microwave signal from the generator in to the combustion chamber is the fundamental component to improving the electric field propagation performance inside the cylinder. Figure 3.2 presents the possible available coupling methods while this simulation will use the probe antenna. The basic model, also called the default model, is a simple antenna in the middle of the coaxial cable. The material of the inner core is copper and in this simulation the only variable parameter in this model is the antenna height "HAntenna1" (see also section 4.3).

The height of the plug, "HPlug", is fixed to 20 mm and the antenna varies from 0 mm up to 30 mm. The chosen plug and antenna geometric dimensions are defined under the condition of replacing the current spark plug of an ICE with the minimal modification

to the engine cylinder head. Initiated by a variable antenna length, the geometric shape of the coupling element alters. This leads to a shift in the impedance of the microwave chamber and thus the electromagnetic field distribution characteristics. For every antenna length, a deterministic search algorithm was executed in order to obtain the characteristic values of the given parameters. The search objectives are the maximum electric field intensity, resonance frequency, and bandwidth of the signal. Once the resonance frequency is found, two further optimisations are started in order to locate the lower and upper limit for the bandwidth of the signal (see section 4.2).

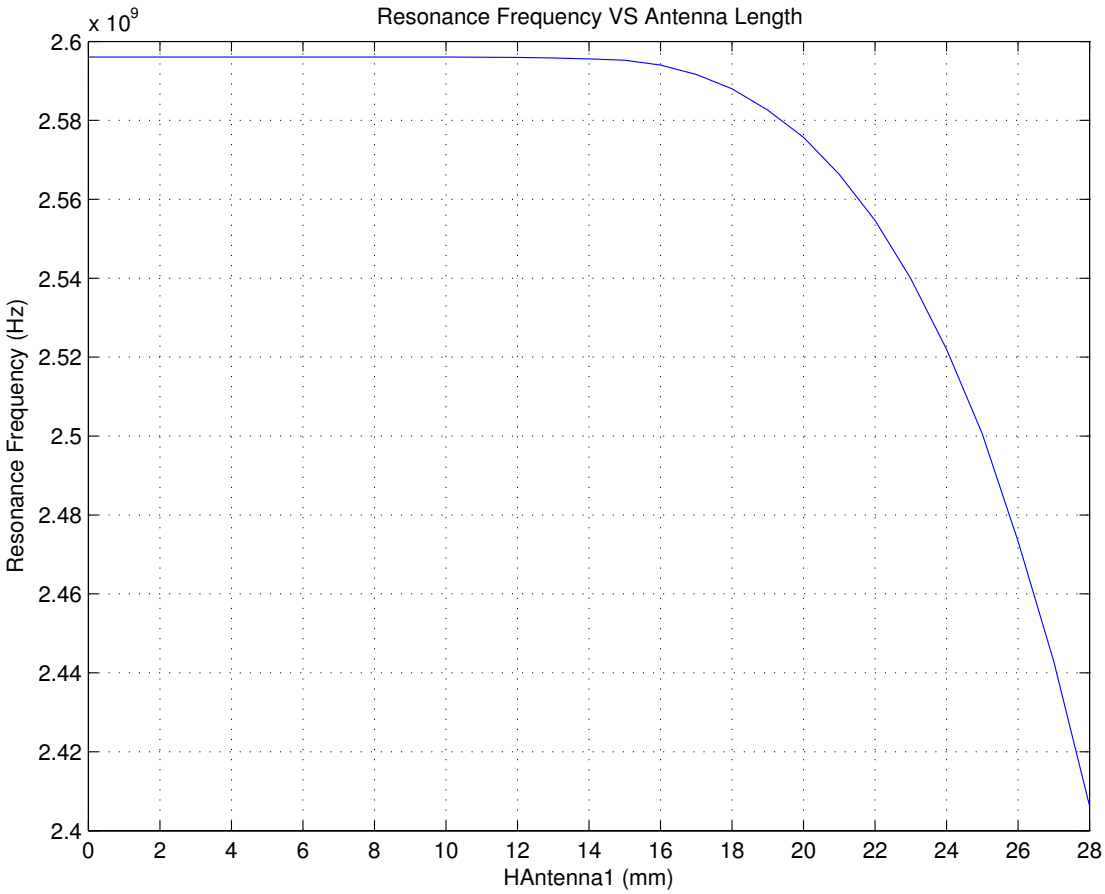

Figure 4.14: Resonance frequency against the antenna length

Table 4.9 gives an overview of the maximum electric field intensity, resonance frequency, and bandwidth of the signal for the various antenna lengths. These values were used to generate figs. 4.14 and 4.15. After the first run, it was established that the maximum electric field occurs around an antenna length of 1.25 mm. The search resolution was then adjusted to obtain more detailed information about the exact values for the antenna length. The correct values will lead to the attainment of the optimum electric field propagation performance inside the cylinder. Figure 4.14 shows that the resonance frequency is not greatly affected within the antenna length range of 0 mm to 14 mm. After raising the antenna length from 14 mm to 24 mm, the resonance frequency of the cavity declines by approximately 200 MHz. This decrease in the resonance frequency is not an issue even if a small alternation of the supply frequency would be required in case the antenna geometric dimensions distort over time. Figure 4.15 illustrates the

Table 4.9: Results antenna length from 0 mm to 14 mm

Antenna length (mm)	**Resonance Frequency** (Hz)	**Bandwidth** (Hz)	**Maximum Electric Field Intensity** (V/m)
0.00	2.5961×10^9	2.29×10^3	1.274×10^8
0.25	2.5961×10^9	2.55×10^3	1.336×10^8
0.50	2.5961×10^9	2.87×10^3	1.390×10^8
0.75	2.5961×10^9	3.12×10^3	1.431×10^8
1.00	2.5961×10^9	3.51×10^3	1.459×10^8
1.25	2.5961×10^9	3.87×10^3	1.473×10^8
1.50	2.5961×10^9	4.33×10^3	1.471×10^8
1.75	2.5961×10^9	4.77×10^3	1.452×10^8
2.00	2.5961×10^9	5.31×10^3	1.418×10^8
2.25	2.5961×10^9	5.91×10^3	1.371×10^8
2.50	2.5961×10^9	6.60×10^3	1.312×10^8
2.75	2.5961×10^9	7.25×10^3	1.247×10^8
3.00	2.5961×10^9	8.05×10^3	1.176×10^8
3.25	2.5961×10^9	8.94×10^3	1.100×10^8
3.50	2.5961×10^9	9.98×10^3	1.023×10^8
3.75	2.5961×10^9	1.10×10^4	9.488×10^7
4.00	2.5961×10^9	1.22×10^4	8.739×10^7
4.25	2.5961×10^9	1.34×10^4	8.082×10^7
4.50	2.5961×10^9	1.50×10^4	7.360×10^7
4.75	2.5961×10^9	1.69×10^4	6.649×10^7
5.00	2.5961×10^9	1.87×10^4	6.064×10^7
6.00	2.5961×10^9	2.83×10^4	4.103×10^7
7.00	2.5961×10^9	4.31×10^4	2.725×10^7
8.00	2.5961×10^9	6.51×10^4	1.809×10^7
9.00	2.5961×10^9	9.80×10^4	1.203×10^7
10.00	2.5960×10^9	1.48×10^5	7.930×10^6
11.00	2.5960×10^9	2.19×10^5	5.316×10^6
12.00	2.5959×10^9	3.19×10^5	3.562×10^6
13.00	2.5958×10^9	4.36×10^5	2.492×10^6
14.00	2.5956×10^9	5.45×10^5	1.817×10^6

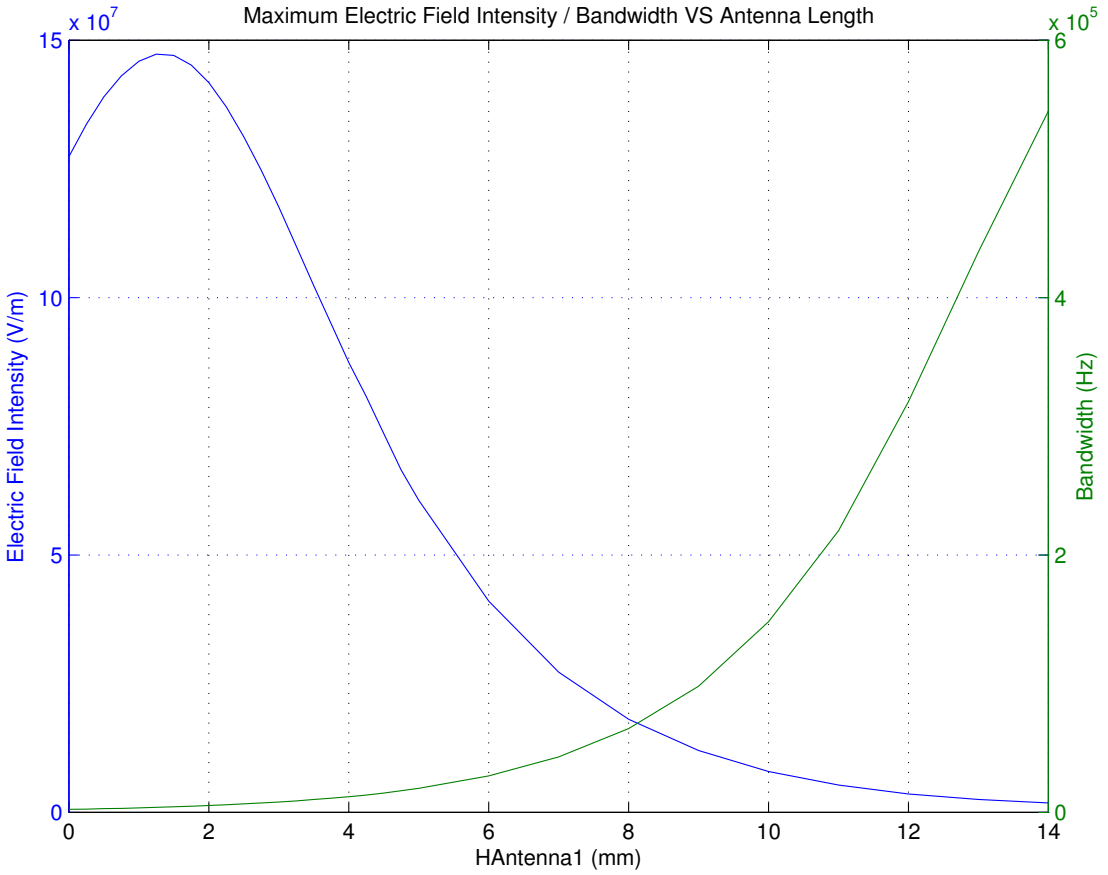

Figure 4.15: Electric field and bandwidth against the antenna length

found maximum electric field intensity and bandwidth for the given antenna length range. The maximum electric field intensity occurs at a length of 1.25 mm while the bandwidth is constantly expanding with an increasing antenna length. To determine the optimum antenna design, it is necessary to find a compromise between field strength and antenna length. Section 4.3.6 illustrates the problem of a signal with an insignificant bandwidth. The investigation shows that it would be beneficial to sacrifice the optimum electric field intensity for a wider bandwidth in order to increase the overall volume propagation performance inside the combustion chamber. To illustrate the influence of the fluctuating bandwidth Fig. 4.15 was created. In this graph, the antenna length varies from 4 mm to 10 mm while the frequency range is predefined and constant for all simulations. This search is quite similar to the range frequency simulation in section 4.3.3.

Figure 4.16 shows the electric field intensity inside the combustion chamber for an antenna length from 4 mm to 10 mm. The simulated frequency range is 2.596 GHz to 2.5961 GHz with a resolution of 50 Hz, these are 2000 simulation steps. It demonstrates that within this search range all extrema for the given antenna lengths were obtained. The signal characteristics are dynamic when the antenna length varies. The signal of an antenna length of 3 mm is a sharp peak while the bandwidth of the signal expands with a longer antenna length.

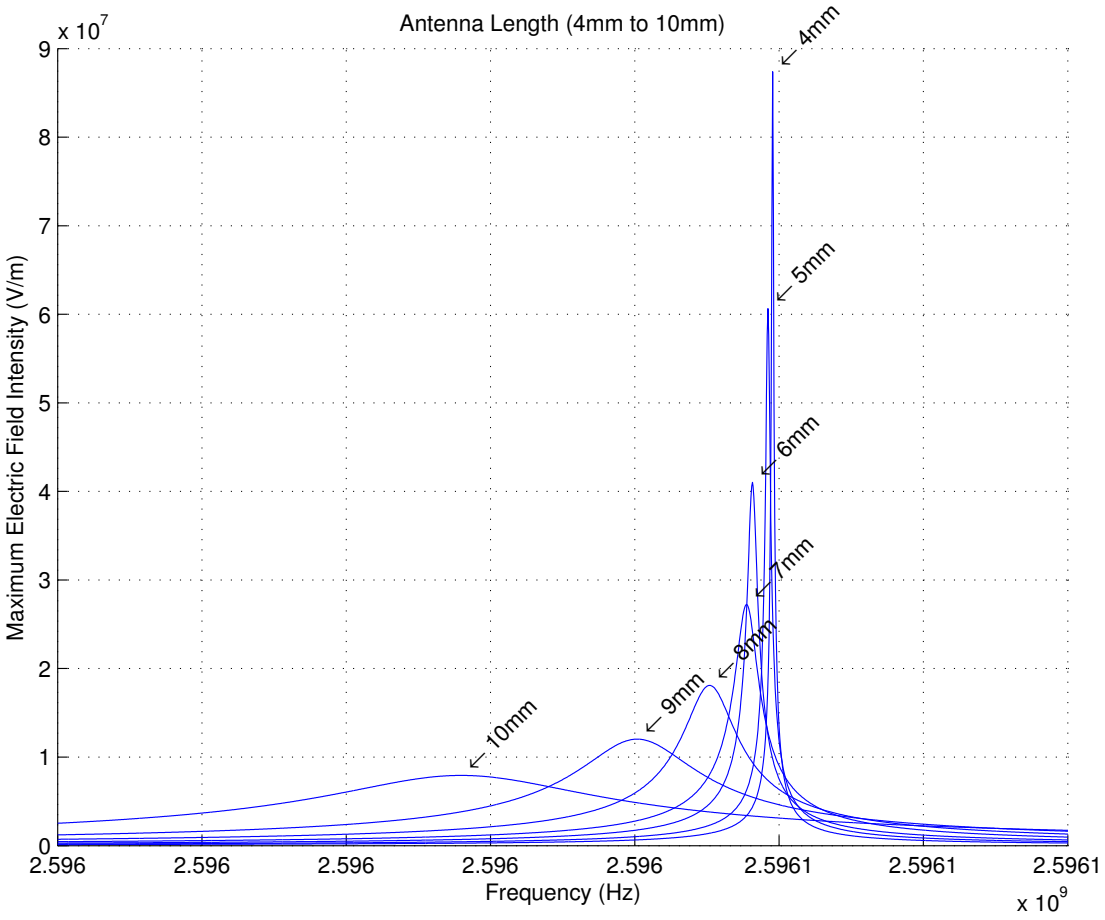

Figure 4.16: Electric field against the antenna length

In conclusion, the inner core of the coaxial cable, which is antenna 1 in this model, significantly affects the resonance condition. The maximum electric field intensity increases significantly with a lesser length, while the bandwidth of the signal noticeably decreases. The lower bandwidth could lessen the durability of the system and an exact supply frequency is required. The possible decrease in durability requires further investigation through real world testing once the experimental phase is concluded in this research area.

4.3.5 Measuring Position in Combustion Chamber

The microwave propagation performance is a principal element in the successful design of a HCMI system. The microwave energy in the simulation of this section will be induced at the top of the plug by using a coaxial cable. The propagation performance throughout the cylinder will be investigated, furthermore the electric field intensity is illustrated.

By applying the previous results, the supplied frequency for this simulation will be the

resonance frequency of the combustion cylinder. Figure 4.17a represents the electric field with the red arrows inside the two dimensional combustion chamber model. This demonstrates that the field decreases while moving further away from the centre of the cylinder. The blue arrows simplify the illustration of the field by showing the intensity at the boundaries of the cavity with the corresponding conclusion that the field at the centre is the strongest.

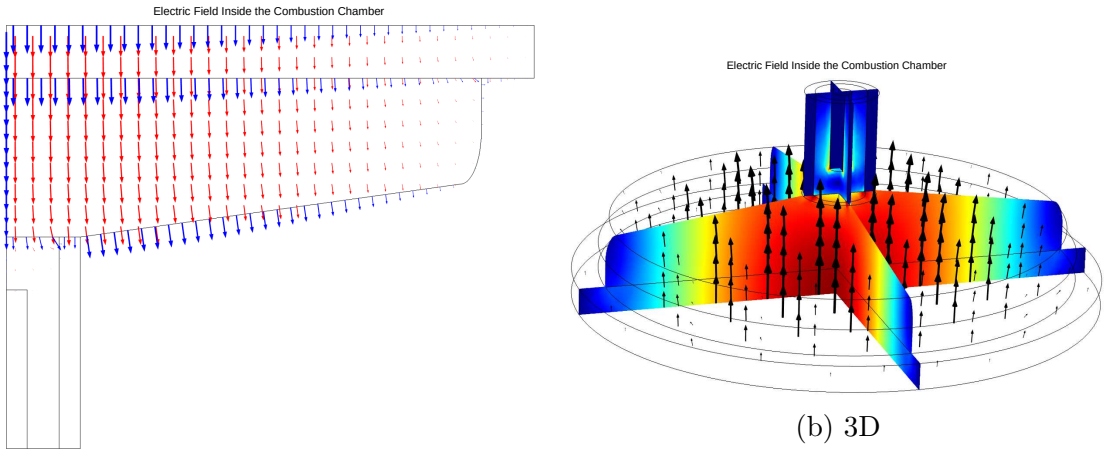

(a) 2D

(b) 3D

Figure 4.17: Electric field propagation inside the cylinder model

Figure 4.17b shows in further detail, the three dimensional model of the cylinder. It displays that the electric field near the inner material of the coaxial cable is high but not near to the maximum amplitude throughout the centre of the cylinder. The figure also shows that at the head of the cylinder, near TDC, the electric field intensity is the strongest (shown in dark red). The initial assumption after observing the two and three dimensional results is that the electric field increases inside the cylinder in vertical direction and necessitates further investigation. Some additional simulations are required and the electric field intensity will be measured with 1 mm steps along the symmetric axis inside the combustion cylinder.

To examine the propagation characteristics and the propagation performance throughout the cylinder, a series of different measuring points were used to interpret the simulation results illustrated in Fig. 4.18. The figure shows that the electric field intensity grows when increasing the distance between the measuring point and the start of the antenna. This led to the conclusion that the electric field intensity near the symmetric axis increases within the y-axis. For the distance range from 20 mm (the cylinder head top) to 30 mm (the cylinder head bottom) the maximum electric field intensity increases from 5.208×10^9 V/m up to 7.391×10^9 V/m which is an improvement of approximately 40 %.

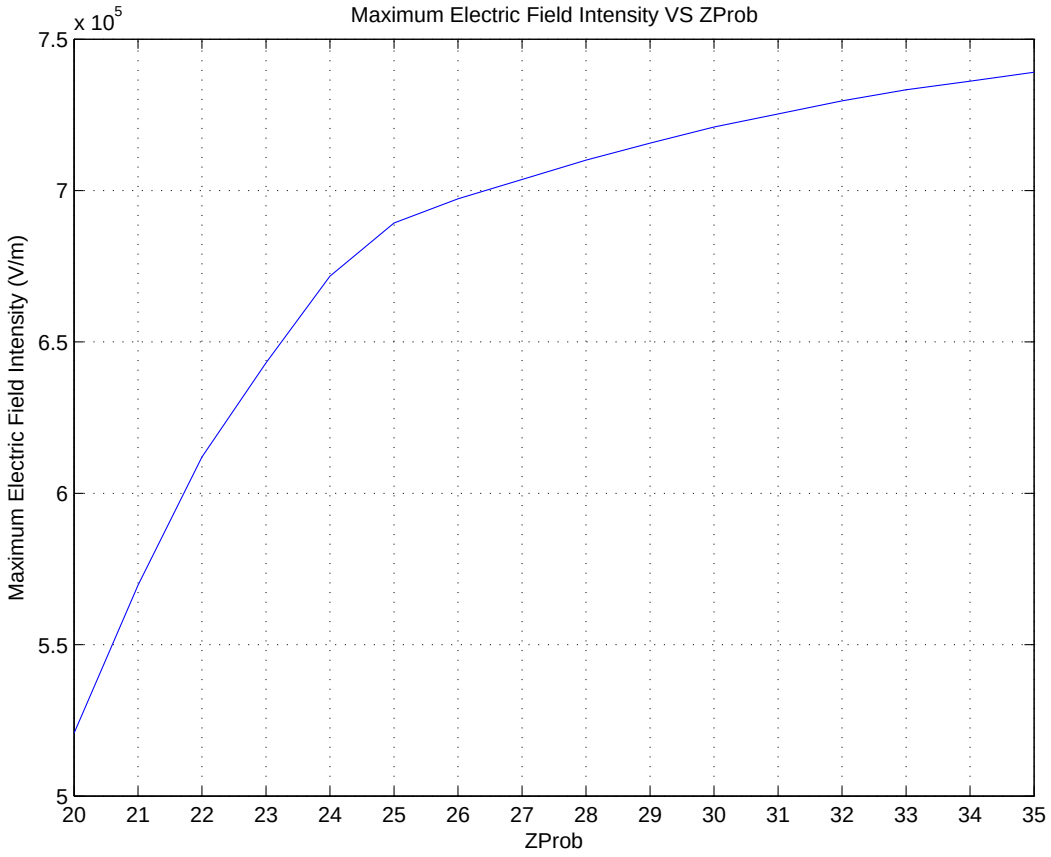

Figure 4.18: Electric field against the measuring point

4.3.6 Piston Motion During the Ignition

Section 4.3.3 shows that the piston position directly influences the resonance frequency of the combustion chamber. Therefore this section will focus on the change of the resonance frequency after the ignition event and during the combustion occurs. In general, the ignition of an MI system takes between 30 and 100 ns. Due to the constant motion of the piston, the natural frequency of the combustion chamber shifts. As a result, the

Table 4.10: Approximate piston motion during the ignition

Cylinder Height (mm)	**Engine Speed** (rpm)	**Distance to TDC per** 30 ns (µm)	**Distance to TDC per** 100 ns (µm)
90	650	0.059	0.195
90	3000	0.270	0.900
90	7200	0.648	2.160
100	7200	0.065	0.217
100	3000	0.300	1.000
100	7200	0.720	2.400

frequency change during the duration of the ignition needs to be investigated. The reason behind this search is to explore whether a time simultaneous ignition throughout the whole cavity with just one single supply frequency is possible. If not, the development of a different design with multi supply frequencies may be mandatory in order to achieve a clean and complete combustion.

Table 4.10 shows the approximate piston motion during the microwave ignition event while the engine is running. In general occurs this behaviour non-linear, as shown in 2.2, but to calculate the losses boundaries in this chapter this approximated values are suitable. Two different cylinder heads are shown, 90 mm and 100 mm. The average speed of an engine is considered as 3000 rpm. The piston inside a 90 mm engine cylinder displaces at a speed of 3000 rpm between 0.270 µm to 0.900 µm.

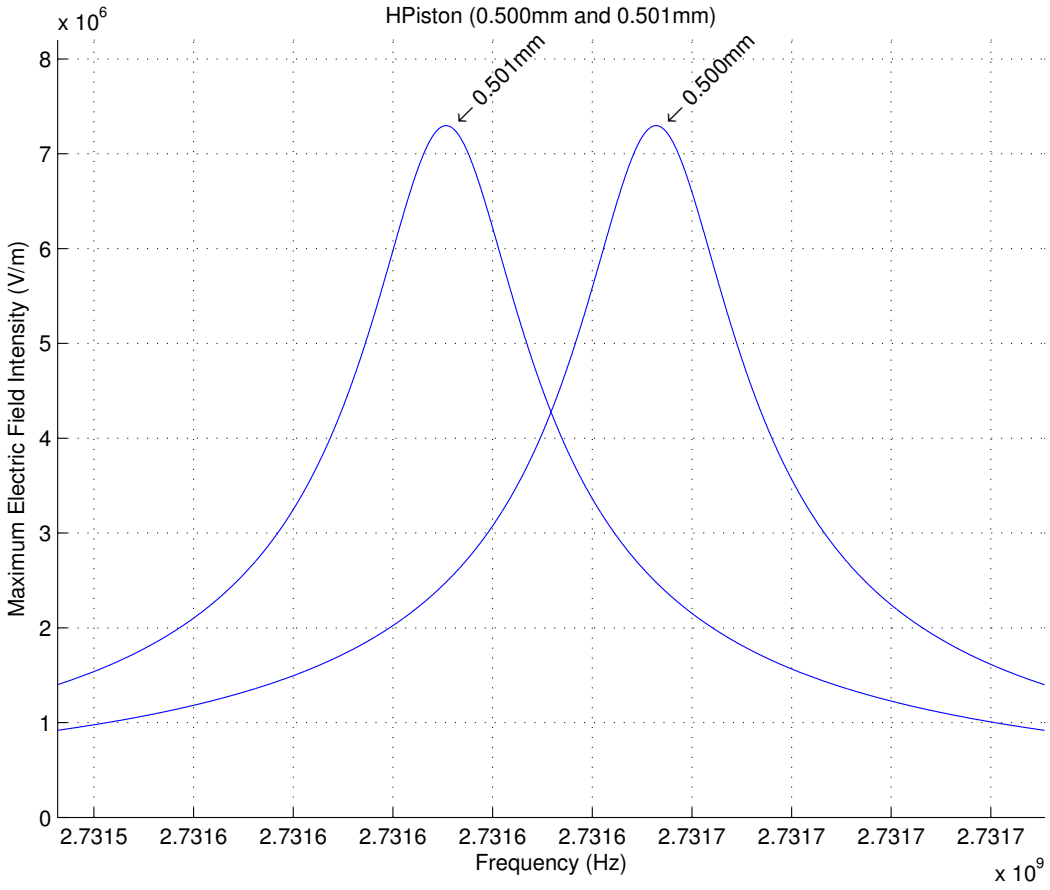

Figure 4.19: Electric field for a variable piston position

The MI ignition starts with a minimum required electric field intensity of 1×10^6 V/m (see section 2.7). The main consideration in calculating the moving distance of the piston is the exact ignition time of the MI system with the particular air-fuel mixture and the exact speed of the engine. A piston movement of 1 µm during the ignition occurs is assumed for the following simulation. This covers an ignition time of 100 ns at an engine speed of 3000 rpm. In case the engine runs faster, a higher input power can compensate for the quicker movement of the piston.

Figure 4.19 shows the electric field intensity for 0.5 mm and 0.501 mm to TDC over the given frequency range. The resonance frequency shifts by around 42 kHz while the piston moves by 1 µm, this frequency change is significantly smaller than the extended bandwidth of the signal itself, which is 220 kHz under these conditions. The figure also shows that the signals have an overlay in the middle which generates a sufficient electric field inside the cavity to ignite the air-fuel mixture simultaneously.

In case the ignition cannot be completed while the piston moves the given distance, one possible solution to cover higher ignition times would be to extend the bandwidth of the signal through the utilisation of various antenna designs. Another way would be to modify the geometric dimensions of the resonator, the possibilities of changing the cylinder's diameter are investigated in section 4.3.2. The final way of providing a complete ignition, such as for higher engine speeds, would be to increase the input power of the microwave source. This would result in a lower total efficiency of the system.

4.3.7 Eigenfrequency Performance

The simulation of the electric field propagation inside the engine cylinder of a HCMI consumes a large amount of computational weight. This fact makes it difficult to perform feasible multivariable simulations in terms of time for the range frequency simulation mode. The Eigenfrequency of the cylinder is used as a suitable starting point for the deterministic search to find the resonance frequency inside the cylinder. The Eigenfrequency of the cylinder is not equal to the resonance frequency but they are located close to each other. This section will investigate and validate the use of the Eigenfrequency in some simulations. Using the Eigenfrequency will save calculation time and therefore make it possible to apply a more detailed mesh and resolution during the search process. The Eigenfrequency represents the Eigenvalue of the enclosed cavity, the combustion chamber of an ICE. The Eigenfrequency is the natural frequency of the cavity without the application of any input power to the cylinder model. One additional simulation would be required at this found frequency to get the corresponding maximum electric field intensity with the found Eigenfrequency as input for the microwave generator.

As mentioned above, the Eigenfrequency of the engine cylinder is not identical to the resonance frequency, shown in Fig. 4.20. In this example, the Eigenfrequency misses the resonance frequency by just a fraction of the total value of 268 Hz. This offset can vary from one simulation to another, demonstrated in Fig. 4.21. Therefore it is impossible to define a frequency range around the Eigenfrequency in order to find the

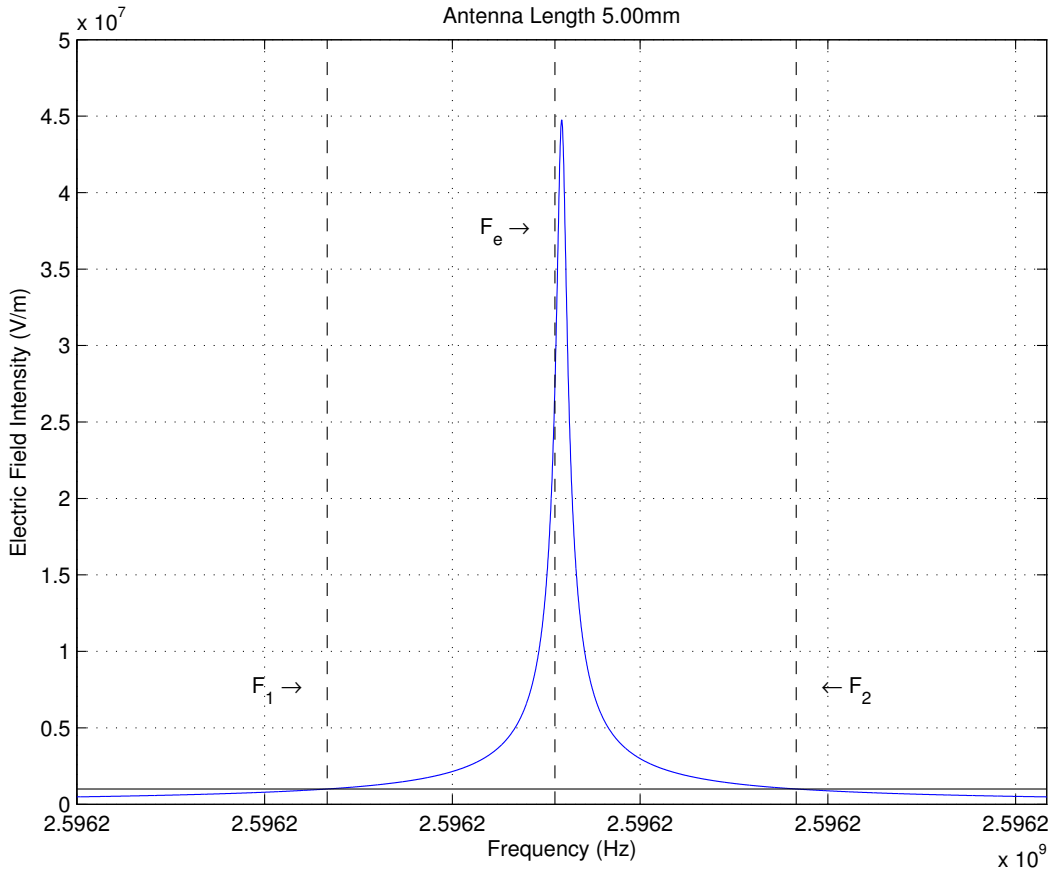

Figure 4.20: Location of resonance frequency again Eigenfrequency

resonance condition of the cylinder. To solve this dilemma, the Eigenfrequency value will be applied as the starting point for a deterministic optimisation search find the resonance frequency of the cylinder and thus the maximum electric field intensity.

Figure 4.21 exhibits the resonance frequency and the Eigenfrequency of the cylinder against the antenna length. The default model was used for this simulation with the default parameters given in section 4.3. The antenna length will be varied from 0 mm to 28 mm. It is established that until an antenna length of 14 mm the difference between both frequencies is negligible. Once the antenna exceeded the length of 14 mm, the difference between the Eigenfrequency and the resonance frequency increased. Figure 4.22 applies the given frequencies of Fig. 4.21 to calculate the corresponding maximum electric field intensity inside the combustion cylinder.

Figure 4.22 shows the maximum electric field intensity inside the cylinder for varying antenna lengths. On one occasion, the Eigenfrequency was used as the supply frequency of the microwave generator. On the other occasion, the deterministic search was applied previously and the found resonance frequency used as the input frequency of the microwave generator. The deterministic optimisation method requires approximately 100 evaluations for each antenna length after applying the Eigenfrequency as the starting value. The number of evaluations of the search algorithm is nearly con-

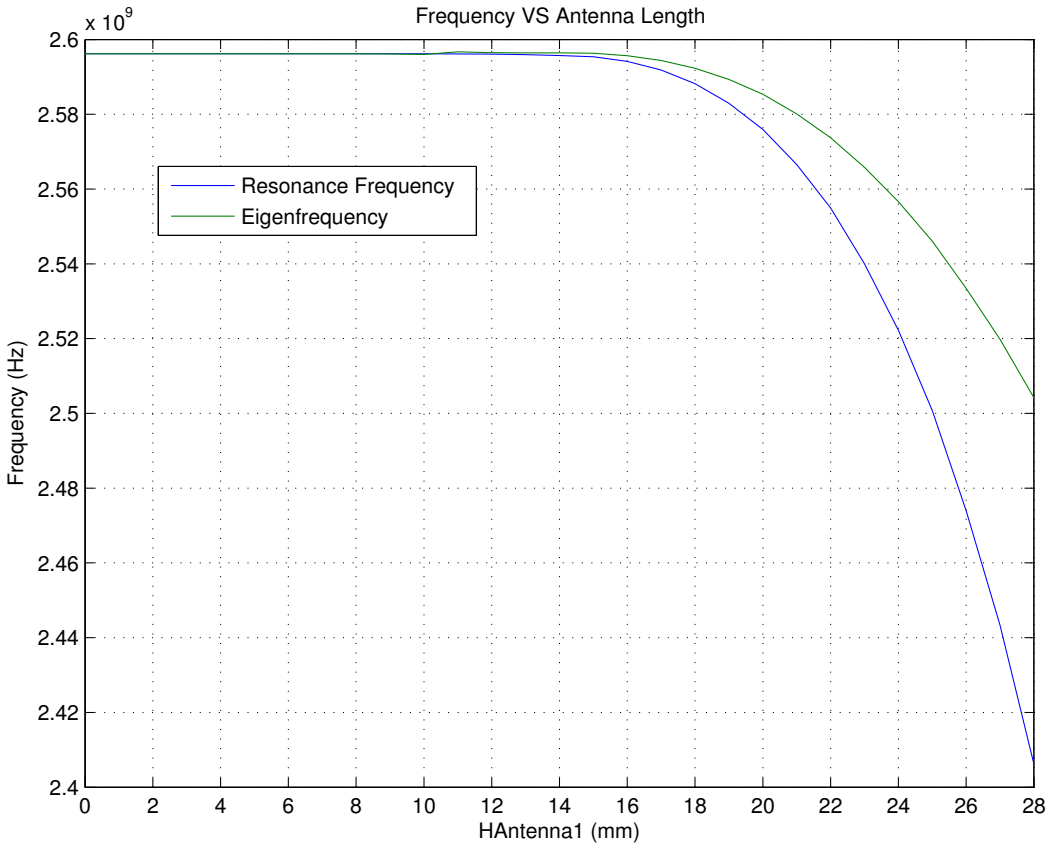

Figure 4.21: Comparison resonance frequency against Eigenfrequency (Frequency)

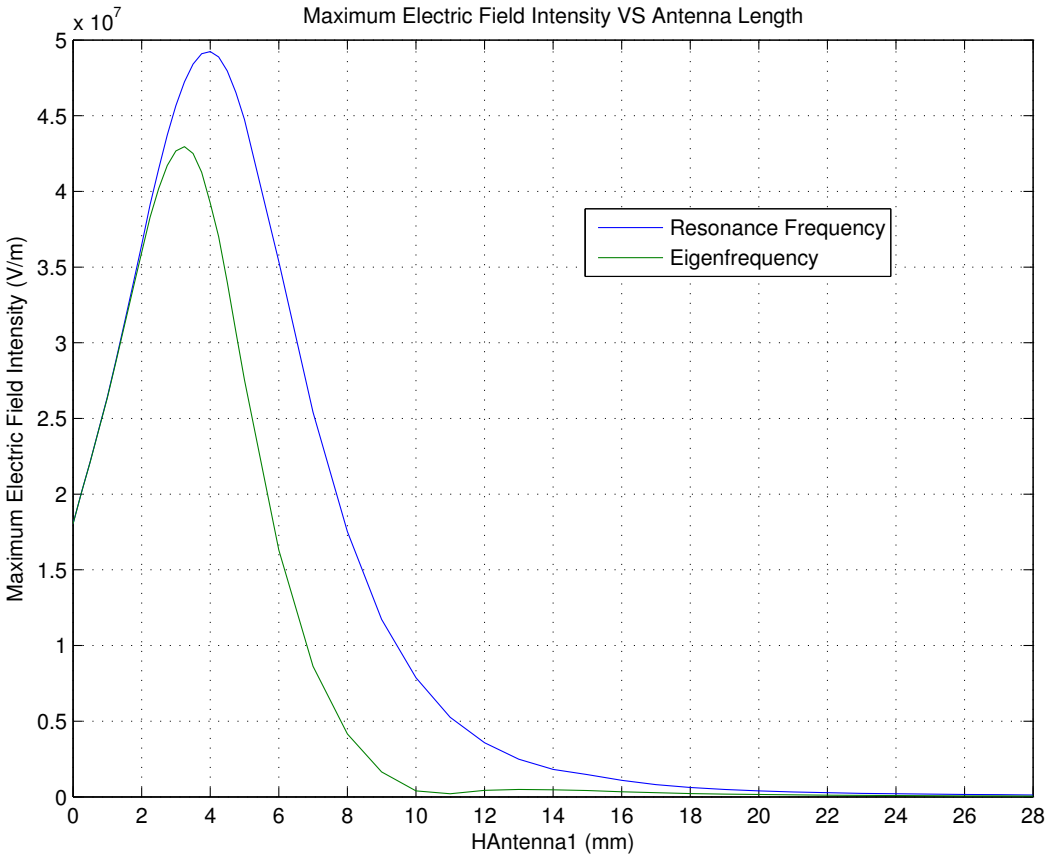

Figure 4.22: Comparison resonance frequency against Eigenfrequency (Field strength)

stant for the different simulations. This is due to the starting point being defined by the Eigenfrequency of the cylinder and this frequency is, as shown above, always near to the resonance frequency.

Figure 4.22 established that the maximum electric field intensity signal has a slight offset using the different frequencies. While using the Eigenfrequency, the maximum electric field intensity occurs at 3.5 mm but when using the resonance frequency the maximum field occurs at 4 mm. Figure 4.20 shows the offset between these frequencies at an antenna length of 5 mm, this gives evidence to the fact that even a small offset of 268 Hz results in a significant decrease in the maximum amplitude of the signal.

This section shows that the Eigenfrequency can be employed to detect the characteristics of the maximum electric field intensity at resonance frequency inside the combustion chamber. The offset is negligible at this point since a decrease in the electric field by applying the wrong frequency is more significant than accepting a small offset from the Eigenfrequency calculation. In chapter 5, the multivariable optimisation searches are applied to find the best field distribution inside the combustion chamber and to compare the performance against an ordinary search algorithm.

4.3.8 Influence of Antenna Length and Piston Position

Sections 4.3.3 and 4.3.4 analysed the influence of a variable antenna length and the piston position on the electric field distribution inside the combustion chamber by employing the default antenna model (described in section 4.3). The single variable simulation results have already demonstrated that the antenna length affects the maximum electric field intensity inside the cylinder directly. The results also established that the best field strength was generated with an antenna length of 4 mm. The piston position also affects the electric field intensity but its influence is smaller in comparison to the antenna length. As already known, a small distance to TDC would be preferred to obtain the best field strength.

This section focuses on multivariable simulations which are used to generate a three dimensional plot in furtherance of understanding and illustrating the relationships between the different input parameters, for the HCMI system. Aforementioned, the piston is in continuous motion inside the cylinder of an ICE system and the maximum electric field intensity along with the natural frequency of the cavity are in constant flux. The effect of the single variable change by the piston position was investigated in section 4.3.3 and by the antenna length in section 4.3.4. This section will examine the combined effect of the piston position and the antenna length on the resonance

frequency and the maximum electric field intensity inside the combustion chamber.

The antenna length ranges from 5 mm to 15 mm and the piston moves from 0.5 mm to 5.0 mm. Figure 4.23 presents the maximum electric field intensity for the antenna length against the piston position.

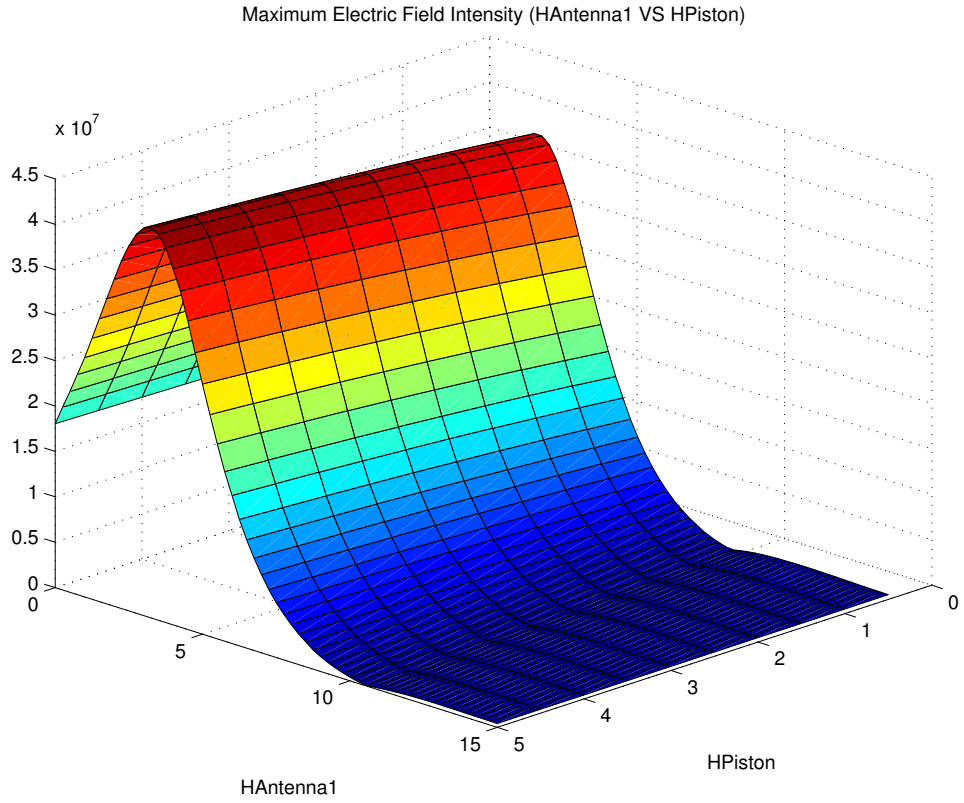

Figure 4.23: Electric field of antenna length against piston position

It confirms that the maximum electric field intensity grows while the distance to TDC increases, as previous discovered in section 4.3.3. The committed change of the maximum electric field intensity by the piston position is inconsequential in comparison to the shift due to the antenna length. The maximum electric field intensity occurs at an antenna length of around 7.8 mm and decreases considerably through movement away from the global maximum. Figure 4.24 illustrates the same data from the maximum electric field intensity inside the combustion chamber as a contour plot. In the figure, the bandwidth of the field expands whilst the distance of the piston increases to TDC. This behaviour is confirmed by the single variable investigations in section 4.3.3.

Figure 4.25 displays the behaviour of the natural frequency in this simulation. The natural frequency of the cavity fluctuates during the simulation and this change is mostly affected by the alternation of the piston position. This reveals that the antenna length has a limited affect on the resonance frequency in this given search range. In contract, the motion of the piston has a significant impact on the resonance frequency. This indicates that the ignition timing has an important influence on the successful

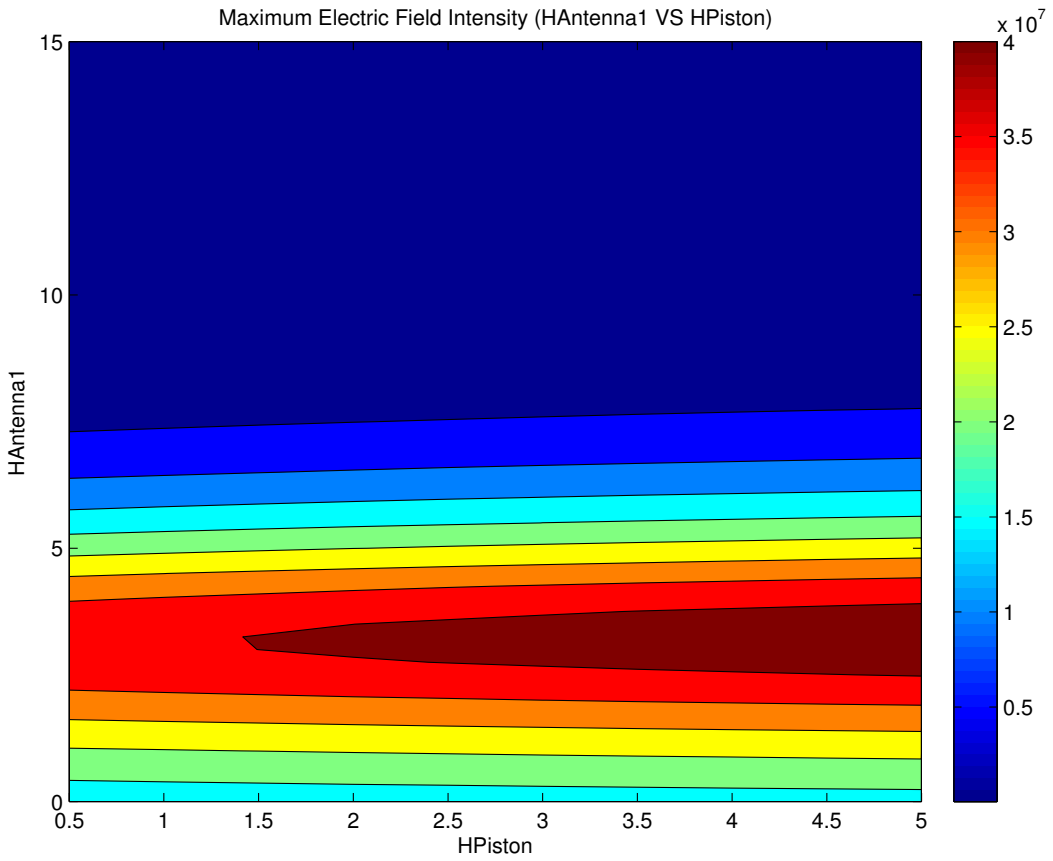

Figure 4.24: Electric field of antenna length against piston position (Contour)

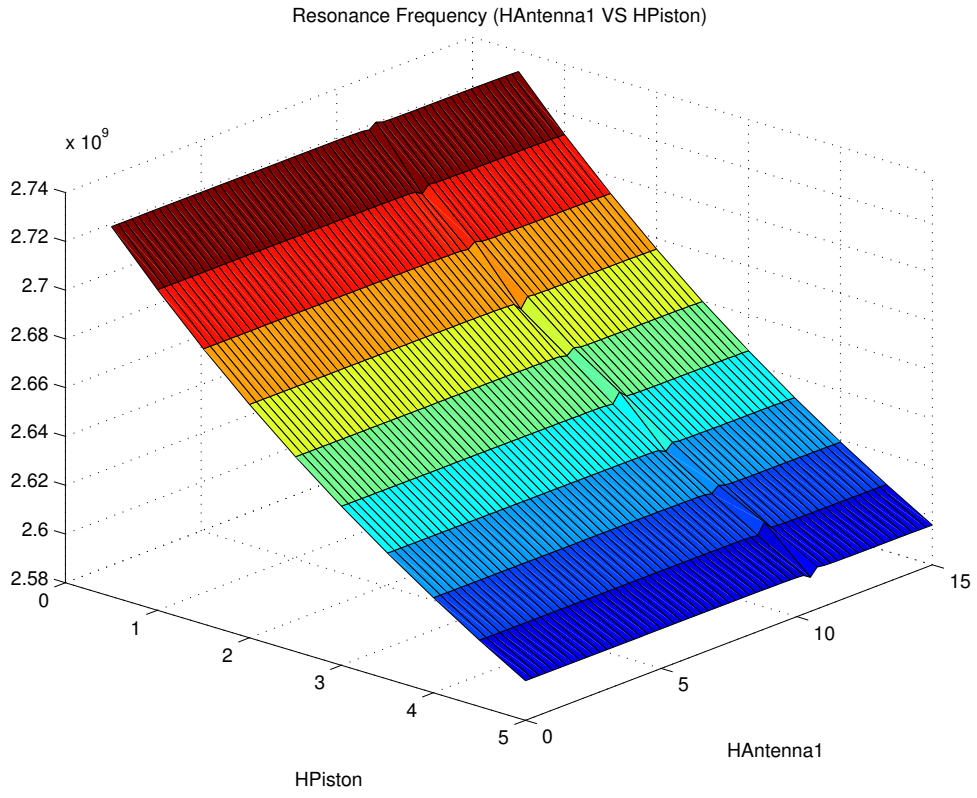

Figure 4.25: Resonance frequency of antenna length against piston position

design of a HCMI system. This is relevant in the avoidance the probable of running off-resonance due to the position of the piston.

4.3.9 Influence of Piston Position and Cylinder Diameter

The diameter of a cylinder for an ICE is fixed and therefore it is not necessary to include this input variable in the optimisation search in chapter 5. Regardless to this precondition, this section uses a multivariable simulation to discover the relationship between the piston position to TDC and the diameter of the cylinder on the electric field intensity inside the combustion chamber. The influence of the input variables on the simulations will be illustrated as a three dimensional plot. The effect of the single variable piston position and cylinder radius shift was researched in section 4.3.6 and section 4.3.2. These results are going to be used to confirm partial results within this section.

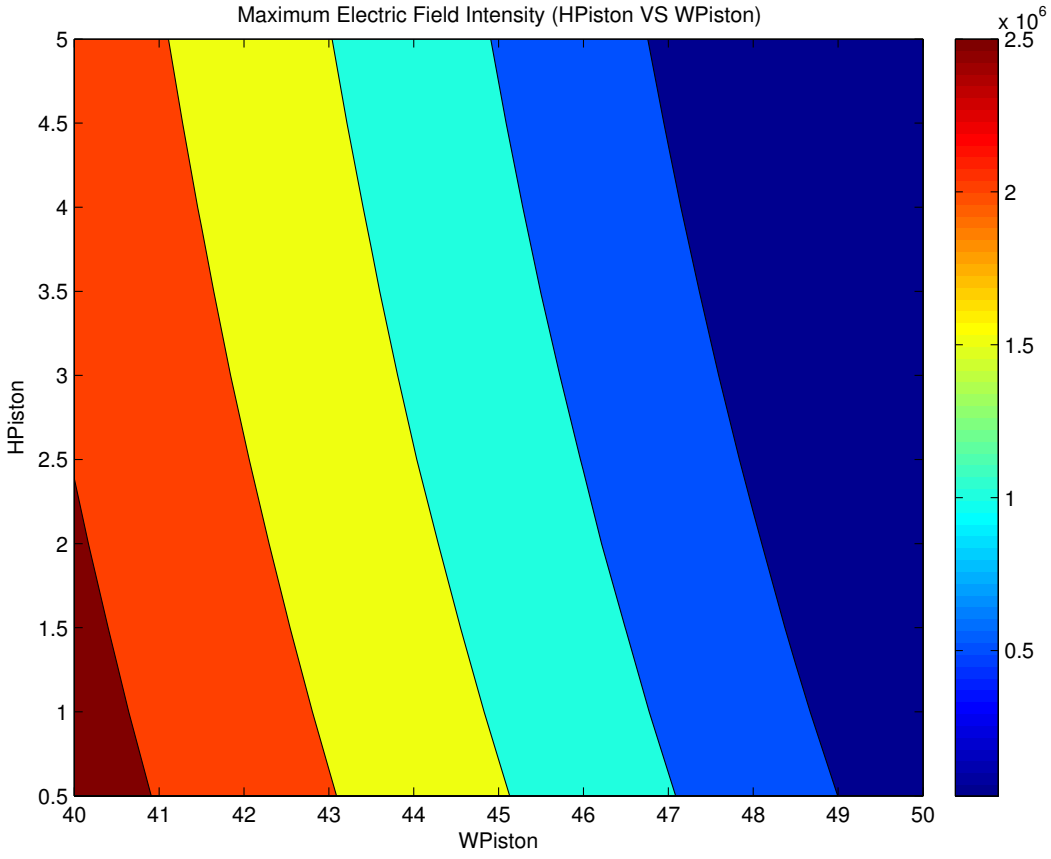

Figure 4.26: Electric field of piston position against cylinder diameter

The piston position ranges from 0.5 mm to 5 mm while the cylinder radius fluctuates between 40 mm and 50 mm. Figure 4.26 shows the maximum electric field intensity for the piston position from 0.5 mm to 5 mm versus the diameter of the cylinder as a contour plot.

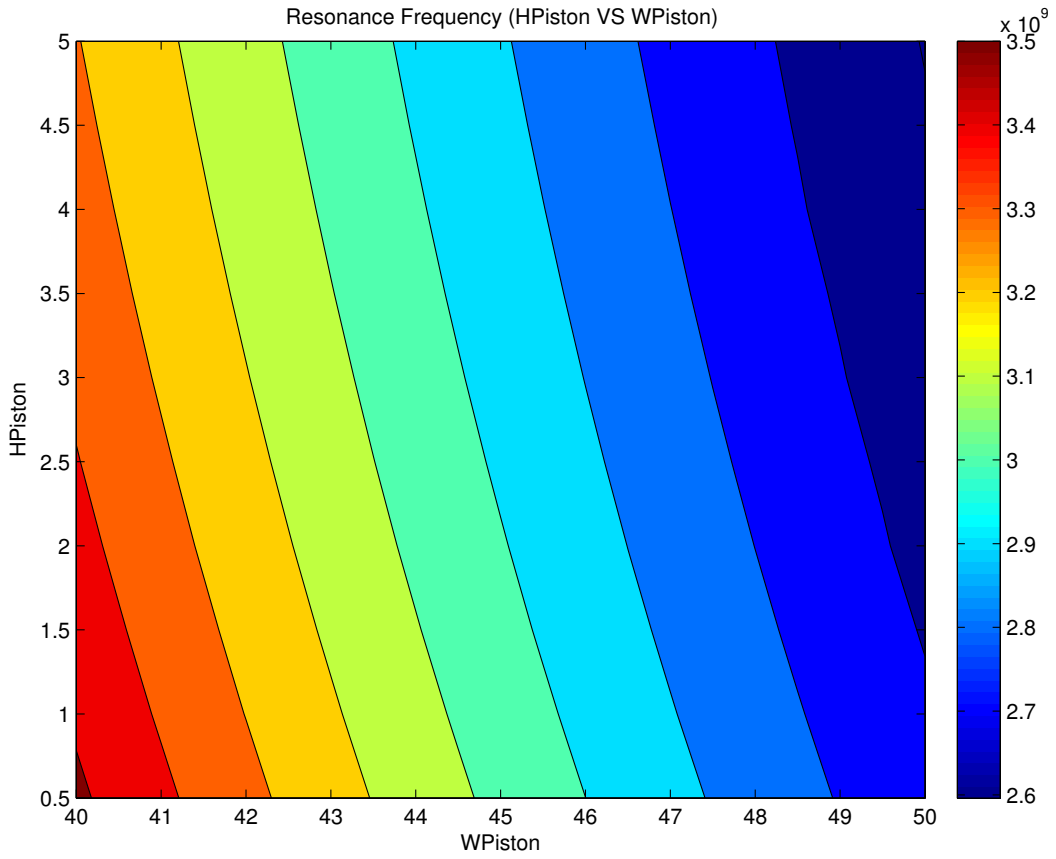

Figure 4.27: Resonance frequency of piston position against cylinder diameter

Figure 4.26 displays the maximum electric field intensity increasing while the distance to TDC is decreasing, confirming the findings in section 4.3.3. The contour plot indicates that the initiated shift in the maximum electric field intensity by the piston position is insignificant in comparison to the change, due to a variable cylinder diameter. Figure 4.27 shows the resonance frequency behaviour of this multivariable simulation. The natural frequency of the cavity alters during this simulation and as shown the change is primary affected by the fluctuating cylinder radius. This establishes that the piston position also affects the resonance frequency but insignificantly in comparison to the cylinder radius in the given search range. Therefore the cylinder radius has a meaningful impact on the resonance frequency what does not create any real barriers of a HCMI system. Section 4.3.2 already established that a variable cylinder radius also influences other factors (e.g. the bandwidth) rather than just the maximum electric field intensity.

4.4 Extended Prototype Antenna Model

The model used in section 4.3 was simplified and used to show the basic ideas and reliability of the tools and search algorithms in this thesis. The extended model shown

in Fig. 4.28 enhanced the default antenna model with an additional antenna, mainly to provide more possibilities for the search algorithm. Essentially, the objective of the design is to investigate if an additional antenna can lead to improved propagation characteristics of the electric field intensity inside the engine cylinder. Also to analyse the influence on the field strength due to the alternation of both antenna dimensions. The parameters for the additional antenna are the height "HAntenna2" and width "WAntenna2".

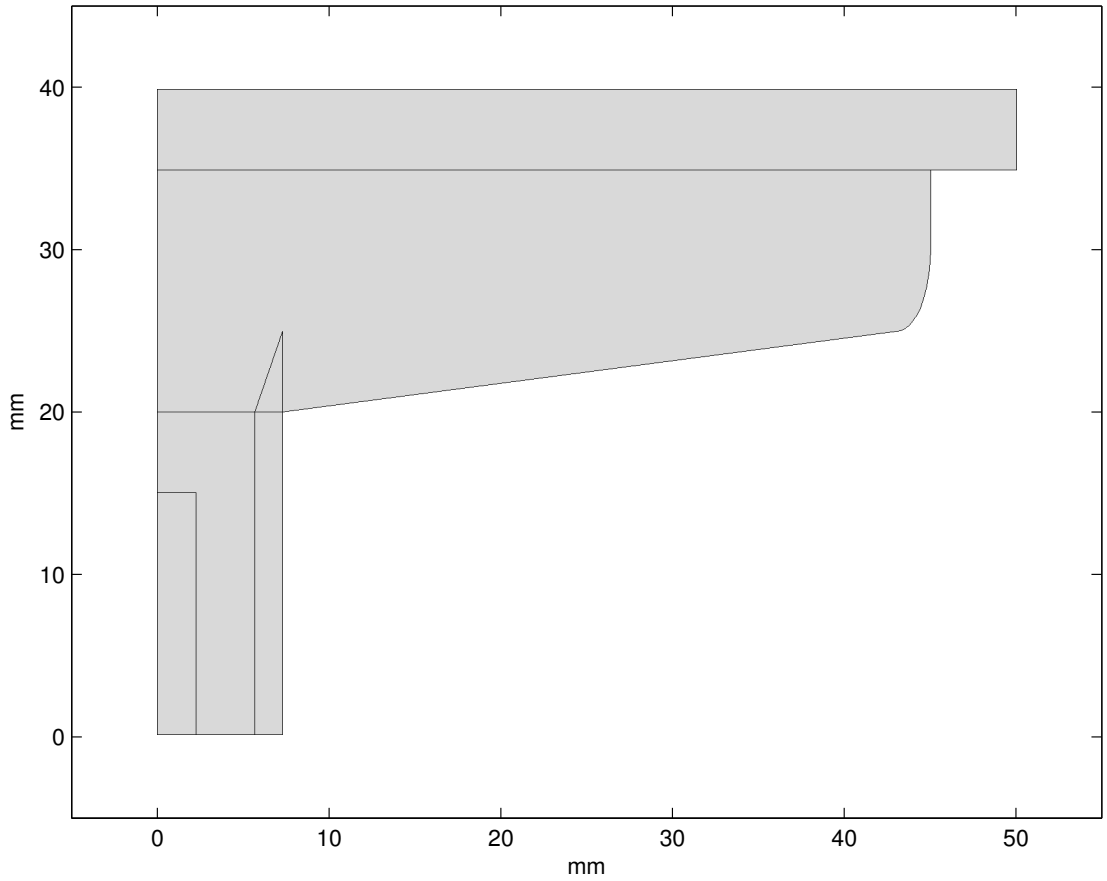

Figure 4.28: Extended antenna model

The materials of the extended antenna model are similar to the default model described in section 4.3. The additional antenna is made of steel and connected to the outer shield of the microwave ignition device. Table 4.11 shows the initial values for the extended antenna design and all variable parameters within this antenna model. The height of the antenna starts at the top of the plug and can be in the range from 0.5 mm to 15 mm (the height of the cylinder head). The width of the antenna is limited, due to the dimensions of the cylinder and the plug radius, to a maximum of 7.35 mm. This particular model keeps the number of variables to a minimum. Its flexibility can be further increased by adding more adjustable dimensions or by introducing irregular three dimensional antenna designs.

In the description of the various simulations, the variable "HAntenna1" is referred to as the antenna length since it represents the length of the inner antenna, the core of

Table 4.11: Changeable values of extended antenna model

Name	Value
HAntenna1	10 mm
HAntenna2	5 mm
WAntenna2	0 mm
HPlug	20 mm
HPiston	5 mm
AirEps	1.00
ZProb	35 mm

the coaxial cable. The variable "HAntenna2" is referred to as the antenna height and describes the height of the second antenna, "WAntenna2" is referred to as the antenna width.

4.4.1 Influence of the Antenna Height

The transfer of the microwave signal from the generator into the combustion chamber is the essential part and main factor in improving the electric field propagation performance inside the cylinder. The effect of the antenna length in the middle has been investigated in 4.3.4 and since this part of the MI device has previously been described, it can be summarised that the input variable "HAntenna1" has a significant impact on the propagation performance inside the combustion chamber.

For this simulation the default antenna model was extended by an additional antenna at the outer radius of the MI device. As mentioned in Fig. 4.28 the additional antenna is made of steel. The purpose of this section is to investigate the influence of the antenna height, input variable "HAntanna2". The antenna height will range from 0 mm to 8 mm during the simulations. This should cause a shift in the impedance of the microwave chamber and thus the characteristics of the electromagnetic field distribution. A deterministic search algorithm was executed for every antenna height, in order to obtain the characteristic values of the given parameters. The search objectives are the maximum electric field intensity, resonance frequency, and bandwidth of the signal. Once the resonance frequency is found, two further optimisations need to take place in furtherance of locating the lower and upper limit for the bandwidth of the signal (see section 4.2).

Table 4.12 gives a numerical overview of the maximum electric field intensity, the

Table 4.12: Results antenna height from 0 mm to 8 mm

Antenna Height (mm)	**Resonance Frequency** (Hz)	**Bandwidth** (Hz)	**Maximum Electric Field Intensity** (V/m)
0.00	2.5960×10^9	1.48×10^5	7.930×10^6
0.25	2.5957×10^9	1.47×10^5	8.001×10^6
0.50	2.5952×10^9	1.44×10^5	8.158×10^6
0.75	2.5945×10^9	1.40×10^5	8.392×10^6
1.00	2.5936×10^9	1.37×10^5	8.635×10^6
1.25	2.5925×10^9	1.33×10^5	8.916×10^6
1.50	2.5911×10^9	1.28×10^5	9.251×10^6
1.75	2.5893×10^9	1.23×10^5	9.692×10^6
2.00	2.5875×10^9	1.18×10^5	1.014×10^7
2.25	2.5852×10^9	1.12×10^5	1.075×10^7
2.50	2.5828×10^9	1.07×10^5	1.129×10^7
2.75	2.5801×10^9	1.02×10^5	1.193×10^7
3.00	2.5771×10^9	9.65×10^4	1.262×10^7
3.25	2.5738×10^9	9.13×10^4	1.339×10^7
3.50	2.5702×10^9	8.63×10^4	1.419×10^7
3.75	2.5666×10^9	8.18×10^4	1.497×10^7
4.00	2.5624×10^9	7.72×10^4	1.600×10^7
4.25	2.5581×10^9	7.29×10^4	1.691×10^7
4.50	2.5534×10^9	6.88×10^4	1.787×10^7
4.75	2.5489×10^9	6.51×10^4	1.838×10^7
5.00	2.5432×10^9	6.10×10^4	1.901×10^7
5.25	2.5377×10^9	5.73×10^4	1.965×10^7
5.50	2.5319×10^9	5.41×10^4	2.021×10^7
5.75	2.5245×10^9	5.05×10^4	2.062×10^7
6.00	2.5185×10^9	4.77×10^4	2.081×10^7
6.25	2.5113×10^9	4.48×10^4	2.083×10^7
6.50	2.5045×10^9	4.22×10^4	2.068×10^7
6.75	2.4968×10^9	3.96×10^4	1.953×10^7
7.00	2.4890×10^9	3.74×10^4	1.884×10^7
7.25	2.4827×10^9	3.54×10^4	1.569×10^7
7.50	2.4744×10^9	3.33×10^4	1.456×10^7
7.75	2.4657×10^9	3.13×10^4	1.340×10^7
8.00	2.4558×10^9	2.93×10^4	1.221×10^7

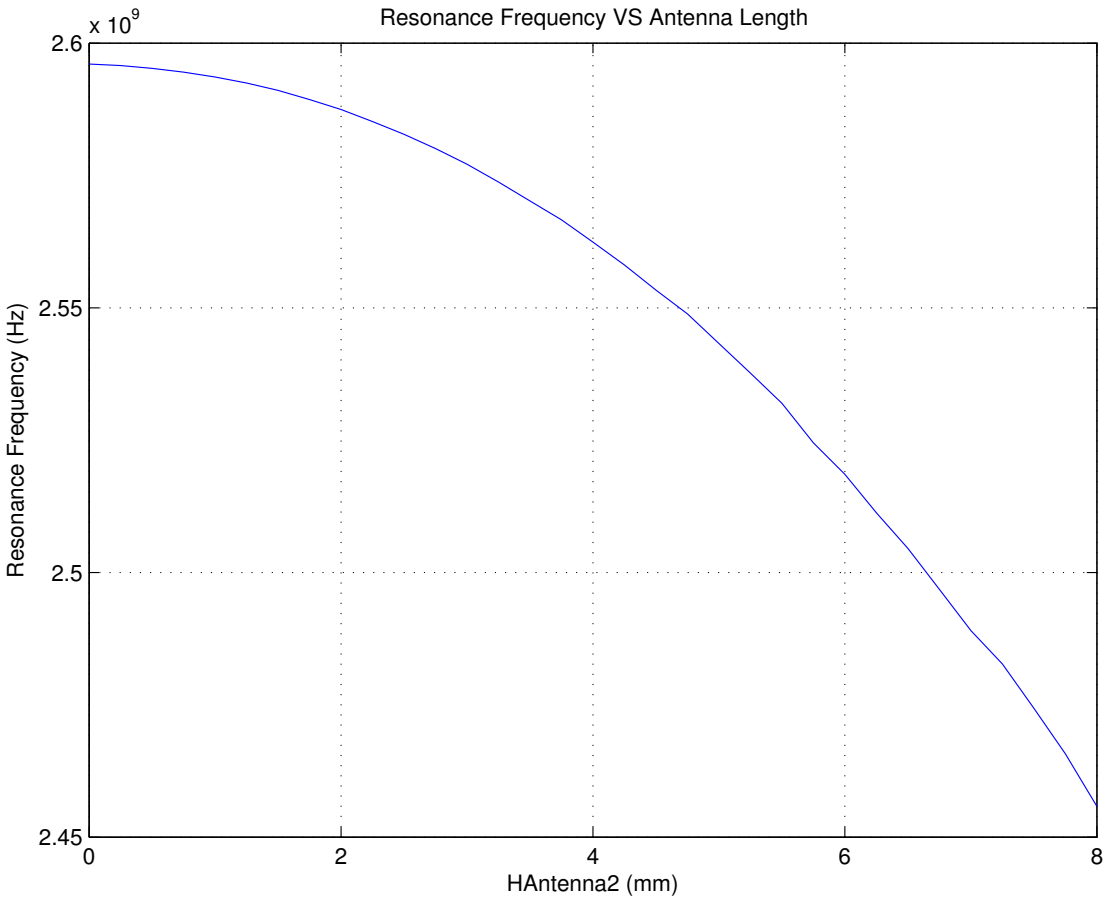

Figure 4.29: Resonance frequency against the antenna height

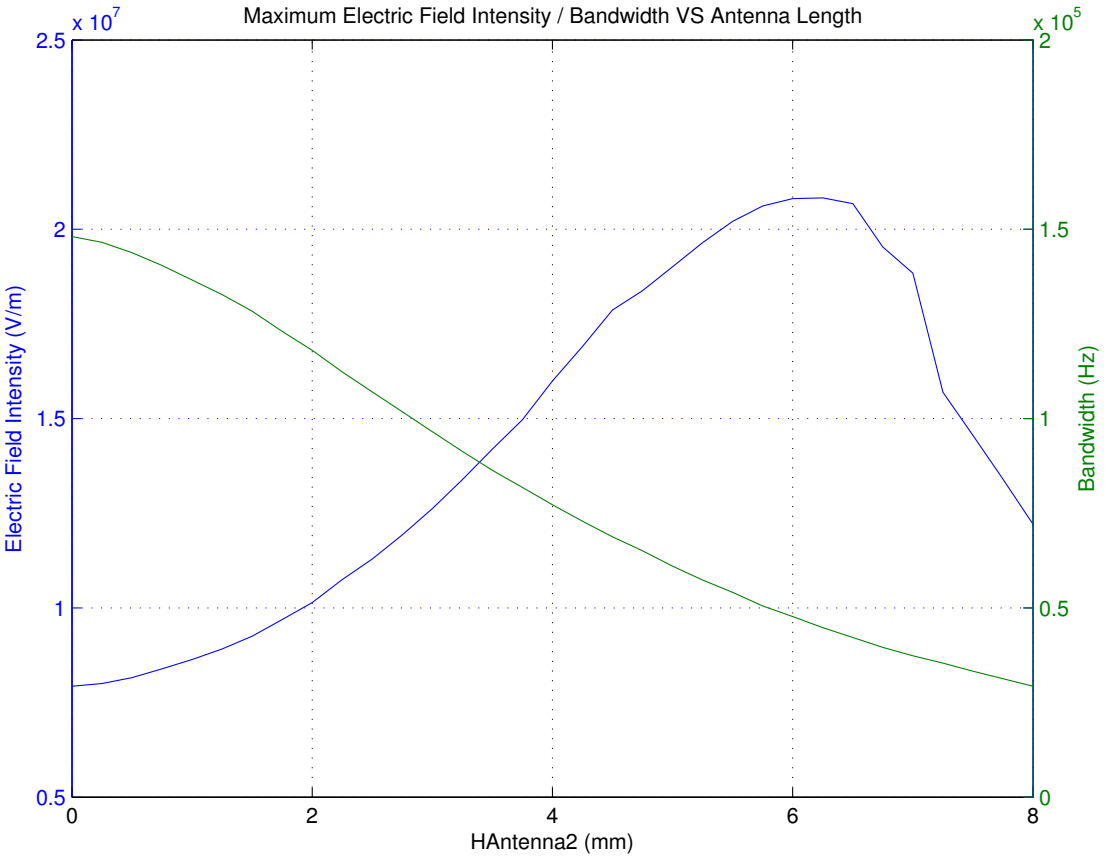

Figure 4.30: Electric field and bandwidth against the antenna height

resonance frequency, and the bandwidth of the signal for the various antenna heights. These values were used to generate Fig. 4.29 along with Fig. 4.30.

Figure 4.30 shows the maximum electric field intensity inside the cylinder. To obtain the maximum field strength, an antenna height of about 6 mm would be required. The effect of the antenna height on the maximum electric field intensity is non-linear. It can be seen that the maximum electric field intensity at first increases and then decreases while the antenna height extends further. Figure 4.29 displays the resonance frequency inside the combustion chamber. This demonstrates how the frequency changes significantly while the antenna height extends from 0 mm to 8 mm. Figure 4.30 also illustrates the bandwidth of the electric field intensity near the top of the cylinder. The results establish that the bandwidth is affected by the maximum electric field intensity, a higher electric field results in a lower bandwidth.

4.4.2 Influence of the Antenna Width

The investigation of the effect of the antenna length "HAntenna1" in section 4.3.4 and antenna height "HAntenna2" in section 4.4.1 gives evidence to their influence on the electric field intensity and the propagation performance inside the combustion chamber. This section will research the influence of the antenna width "WAntenna2" on the propagation performance. The series of simulations with different antenna widths attempts to locate the maximum electric field intensity depending on the single variable search. The starting conditions of the simulation are the default values of the extended antenna model in Table 4.11.

For this simulation the default antenna model was, like in section 4.4.1, extended by an additional antenna at the outer radius of the MI device. As before in Fig. 4.28, the additional antenna is made of steel. The antenna width will span from 0 mm to 6 mm during the simulations. This should create a change in the impedance of the combustion chamber and thus the electromagnetic field distribution characteristics. For every antenna width, a deterministic search algorithm was executed in order to obtain the characteristic values of the given parameters. The search objectives are the maximum electric field intensity, resonance frequency, and bandwidth of the signal. Once the resonance frequency is found, two further optimisations are required to locate the lower and upper limit of the signal's bandwidth (see section 4.2).

Table 4.13 displays a numerical overview about the maximum electric field intensity, the resonance frequency, and the bandwidth of the signal for the various antenna heights. These values were used to generate Fig. 4.31 as well as Fig. 4.32.

Table 4.13: Results antenna width from 0 mm to 6 mm

Antenna Width (mm)	**Resonance Frequency** (Hz)	**Bandwidth** (Hz)	**Maximum Electric Field Intensity** (V/m)
0.00	2.5432×10^9	6.10×10^4	1.901×10^7
0.25	2.5433×10^9	5.80×10^4	1.707×10^7
0.50	2.5410×10^9	5.37×10^4	1.883×10^7
0.75	2.5389×10^9	4.95×10^4	2.086×10^7
1.00	2.5373×10^9	4.55×10^4	2.327×10^7
1.25	2.5356×10^9	4.15×10^4	2.345×10^7
1.50	2.5340×10^9	3.74×10^4	2.501×10^7
1.75	2.5332×10^9	3.39×10^4	2.495×10^7
2.00	2.5320×10^9	3.02×10^4	2.560×10^7
2.25	2.5310×10^9	2.66×10^4	2.623×10^7
2.50	2.5300×10^9	2.32×10^4	2.614×10^7
2.75	2.5290×10^9	1.98×10^4	2.560×10^7
3.00	2.5284×10^9	1.71×10^4	2.334×10^7
3.25	2.5278×10^9	1.43×10^4	2.180×10^7
3.50	2.5272×10^9	1.19×10^4	1.977×10^7
3.75	2.5266×10^9	9.55×10^3	1.740×10^7
4.00	2.5265×10^9	7.56×10^3	1.483×10^7
4.25	2.5260×10^9	5.61×10^3	1.161×10^7
4.50	2.5258×10^9	4.30×10^3	9.298×10^6
4.75	2.5255×10^9	2.96×10^3	6.611×10^6
5.00	2.5254×10^9	2.05×10^3	4.072×10^6
5.25	2.5250×10^9	1.32×10^3	2.892×10^6
5.50	2.5249×10^9	7.37×10^2	1.797×10^6
5.75	2.5247×10^9	1.74×10^2	1.113×10^6
6.00	2.5247×10^9	0.00×10^0	5.618×10^5

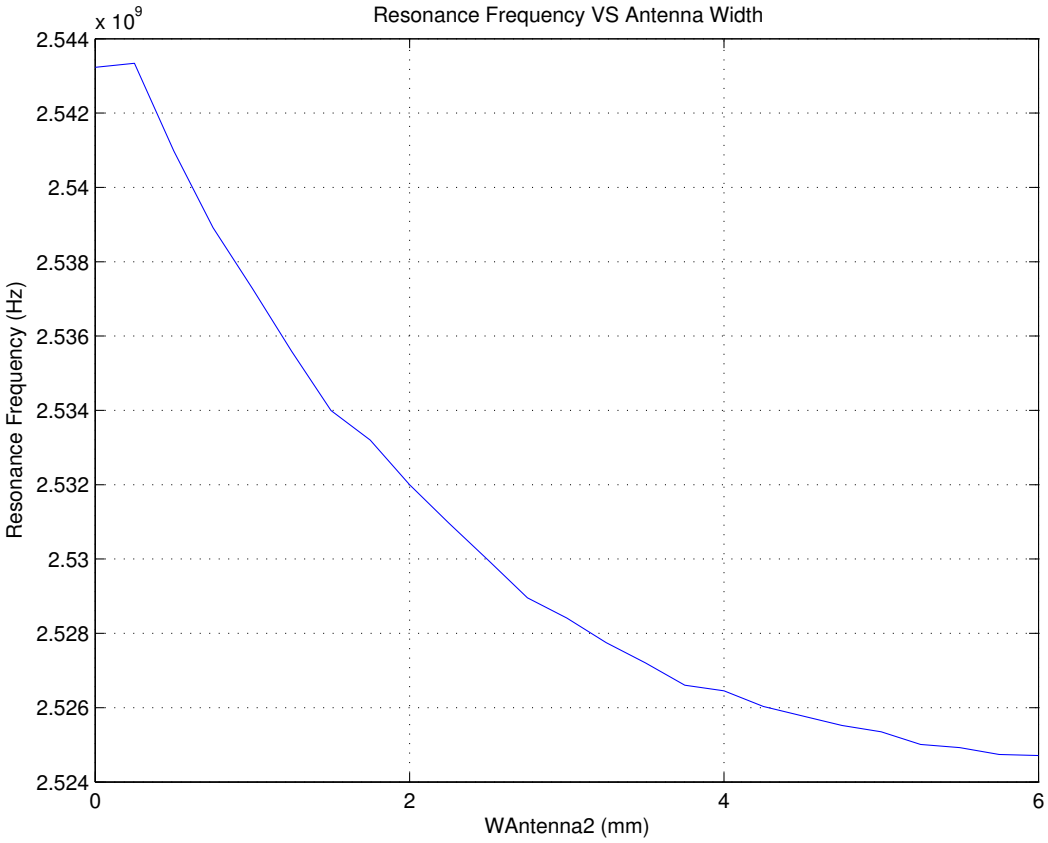

Figure 4.31: Resonance frequency against the antenna width

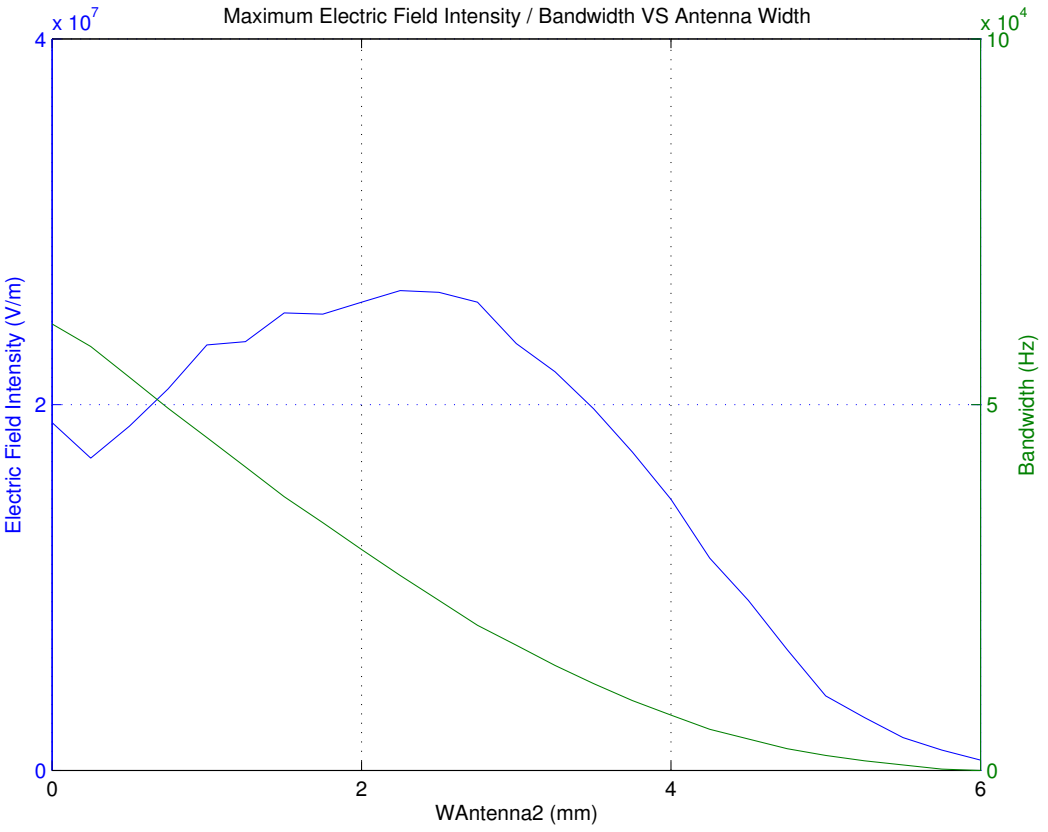

Figure 4.32: Electric field and bandwidth against the antenna width

Figure 4.32 shows the maximum electric field intensity inside the cylinder. To obtain the maximum electric field intensity an antenna width of 2.5 mm is required. The figure demonstrates that the maximum electric field intensity is alternating and declining towards zero while the antenna width increases. Figure 4.31 concludes that the resonance frequency is not affected significantly within the antenna width range of 0 mm to 6 mm. Figure 4.32 illustrates the bandwidth of the electric field intensity near the top of the cylinder.

4.4.3 Influence of Antenna Length and Antenna Height

Sections 4.3.4 and 4.4.1 analysed the influence of varying antenna length in the middle of the cylinder and the antenna height respectively, on the electric field distribution inside the combustion chamber by using the extended antenna model (described in Fig. 4.28). The single variable simulation results have already established that the antenna height directly affects the maximum electric field intensity inside the cylinder. The highest field strength was generated with an antenna length of 4 mm. The antenna height also affects the electric field intensity but the influence is limited in comparison to the antenna length.

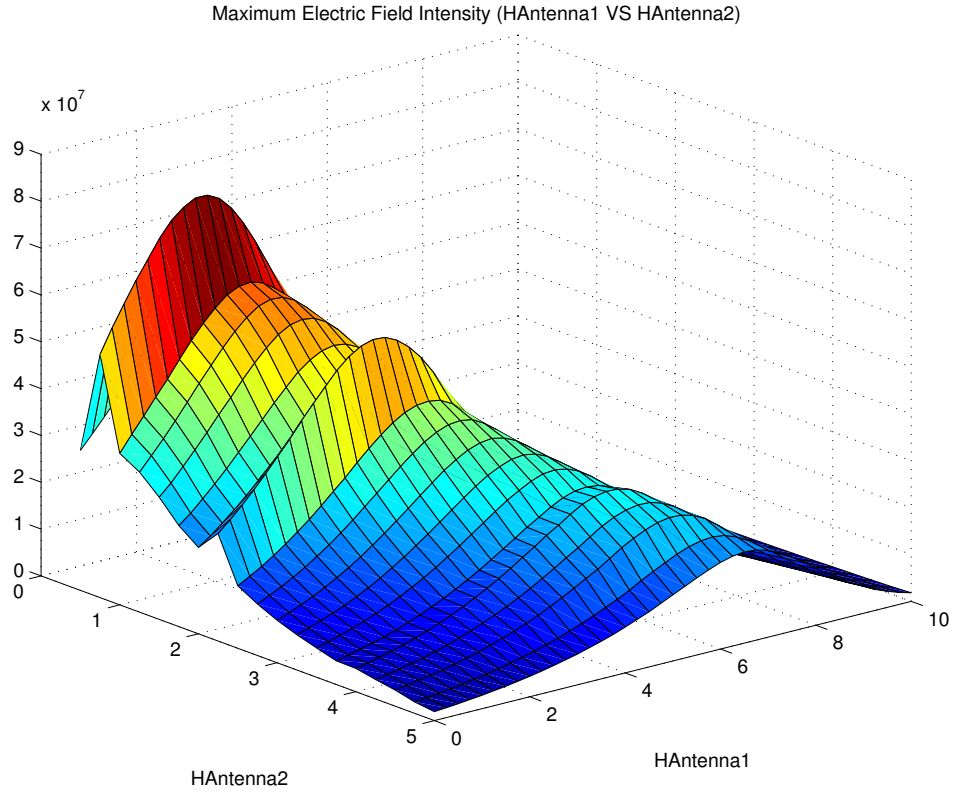

Figure 4.33: Electric field of antenna length against antenna height

The antenna length ranges from 0 mm to 10 mm and the antenna height from 0.5 mm to 5.0 mm. Figure 4.33 demonstrates the maximum electric field intensity for the antenna

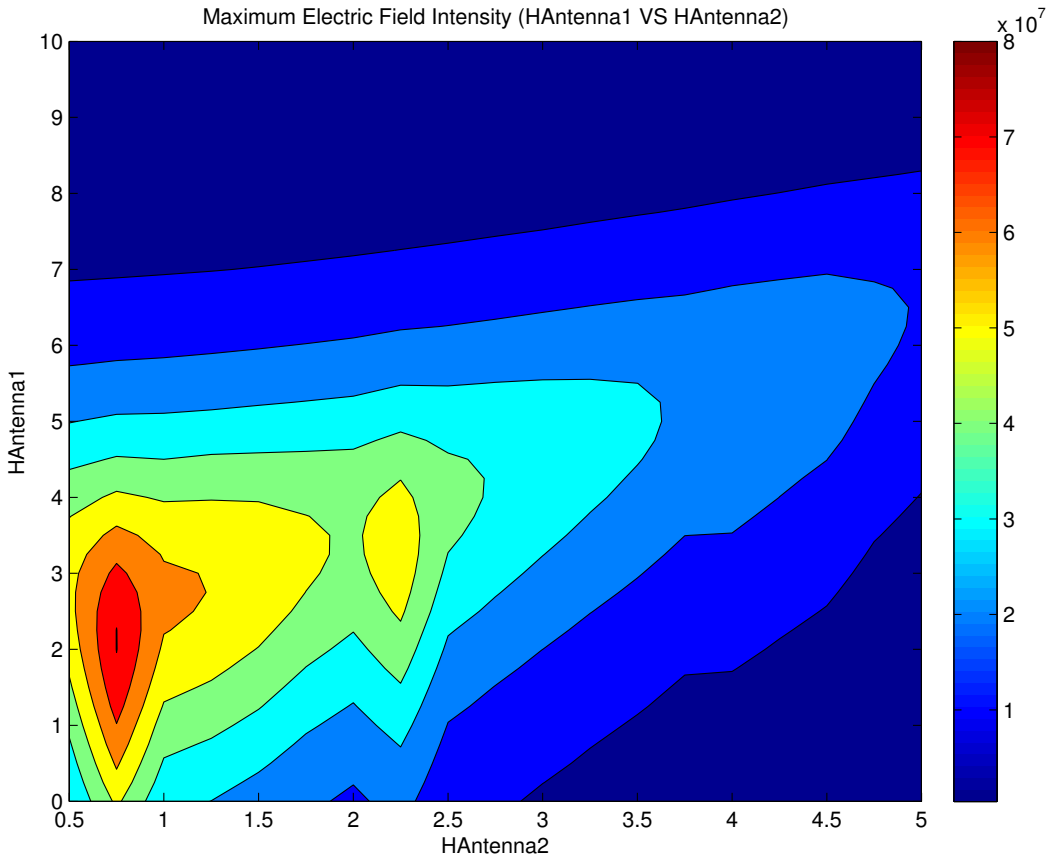

Figure 4.34: Electric field of antenna length against antenna height (Contour plot)

length against the antenna height. The electric field intensity reaches its maximum at an antenna length of 2 mm. This confirms the findings in section 4.4.1 with the single variable change. The committed change of the maximum electric field intensity by the extended antenna height is limited in comparison to the shift due to the antenna length. The maximum electric field intensity occurs at approximately 0.75 mm and decreases considerably when moving from the global maximum. Figure 4.34 illustrates the same data as Fig. 4.33 as a contour plot. They show the maximum electric field intensity inside the combustion chamber.

4.4.4 Influence of Antenna Height and Antenna Width

Sections 4.4.1 and 4.4.2 have analysed the effect of varying single antenna heights and antenna widths on the electric field distribution and signal characteristics inside the combustion chamber. The CAD simulation model employed for these simulations is the extended antenna model (described in Fig. 4.28). The one dimensional single simulation results give evidence that the antenna height as well as the antenna width directly affect the maximum electric field intensity inside the cylinder within the given search range. The highest field strength was found by applying an antenna height of about 6 mm and an antenna width of 2.25 mm. As before in sections 4.4.1 and 4.4.2 only

a single input parameter of the model was changed for these simulations. Therefore the solutions found for the highest field strength are static and not usable for multivariable changes of the antenna height and width.

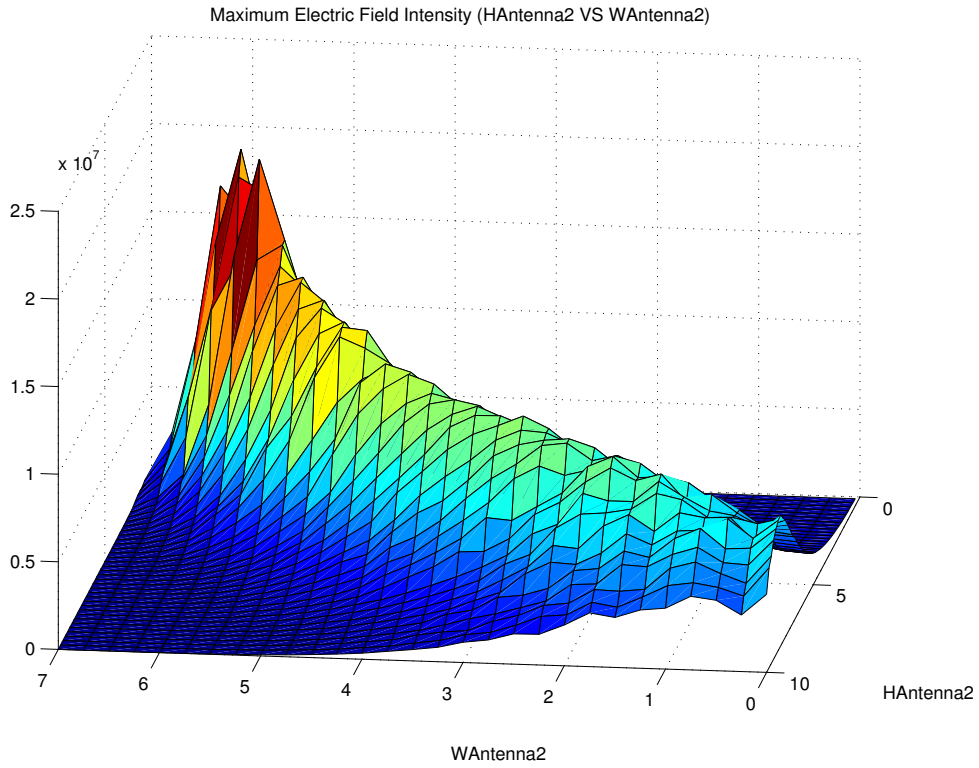

Figure 4.35: Electric field of antenna height against antenna width

The antenna height for this simulation search spans from 0.5 mm to 10 mm while the antenna width ranges from 0 mm to 7 mm. Figure 4.35 shows the maximum electric field intensity for the antenna height versus the antenna width, Fig. 4.36 represents the same data as a contour plot. It is established that the maximum electric field intensity was achieved at multiple points by using the correct combination of the antenna height and width. The results in section 4.4.1 for the single variable change of the antenna height have been obtained by using a fixed antenna width of 0 mm. Section 4.4.2 uses a constant antenna height of 5 mm while alternating the antenna width. However this simulation varies both dimensions simultaneously to illustrate the multivariable behaviour. The relationship discovered between the antenna height and width can be summarised by the following: a longer antenna height with a thinner antenna width is required to archive the highest electric field intensity inside the cylinder.

4.5 Effect of Microwave Induced Plasma

The generation of plasma can influence the resonance frequency in the cavity and therefore the propagation performance of a HCMI system. The plasma in the combustion

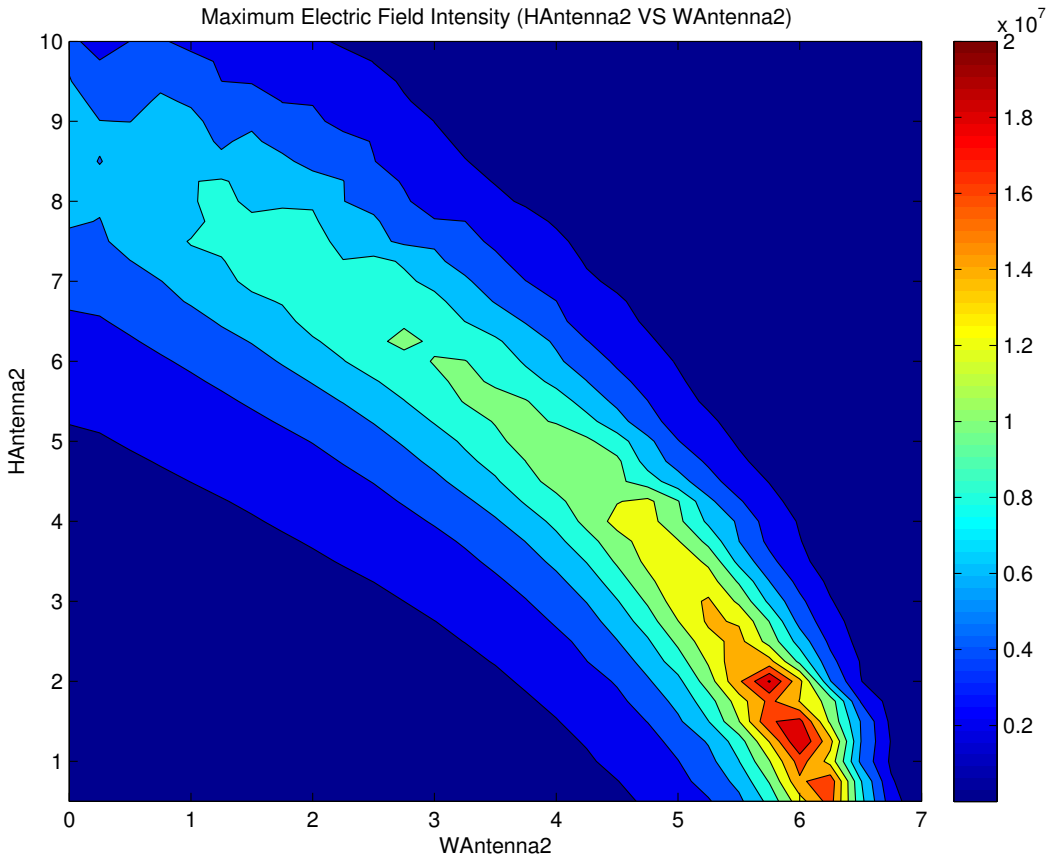

Figure 4.36: Electric field of antenna height against antenna width (Contour plot)

chamber will be induced by high frequencies and is therefore called microwave plasma.

Plasma is separated into classes and fundamentally defined by its temperature and number density. For an ignition system, the combustion represents a burning process which causes the plasma class to be a flame with a maximum temperature of 5000 K and a density of up to 1×10^{17} electrons/m^3. The degree of ionization, α is defined as:

$$\alpha = \frac{n_i}{n_i + n_a} \tag{4.6}$$

The dilemma in this kind of simulation is the creation of a feasible model of the ignition process for an ICE and then to combine it with the electromagnetic field simulation. The air-fuel mixture contains a number of miscellaneous materials, therefore the design and modelling of the chemical reactions is an extensive and intricate process.

At the current stage, Argon gas will be used as the material in the cylinder to simplify the design process. This will test the general effect of microwave induced plasma inside the combustion chamber for the microwave propagation. A preliminary simulation shows that the propagation performance of the air-fuel mixture and Argon gas is nearly

identical thus it is possible to use this simplified model with Argon gas for the following simulations. Other researchers also used Argon gas for their designs due to its similar behaviour to the air-fuel mixture (Starikovskaia 2006; Gesche, Kühn, and Andrei 2008).

4.5.1 Electric Field Propagation Performance

An investigation is required as to whether plasma has a significant impact on the microwave propagation performance inside the combustion chamber while plasma is induced. Figure 4.37 shows an ordinary propagation of the electric field at the top of the cylinder with a supplied frequency of 2.59 GHz. The given geometry of the cylinder and antenna design are constant for all simulations in this section. This is to achieve a comparison of the shift in performance while plasma is induced. The electric field intensity is measured at TDC, but as shown in section 4.3.5, the position is irrelevant and behaves linearly to the measuring point and input power. Aforementioned, the natural frequency is not completely identical to the resonance frequency of the combustion chamber. The importance of the frequency is secondary in this simulation and therefore the supplied frequency, the natural frequency, is close enough to ensure a strong electric field intensity inside the cylinder in furtherance of discovering the influence of microwave induced plasma.

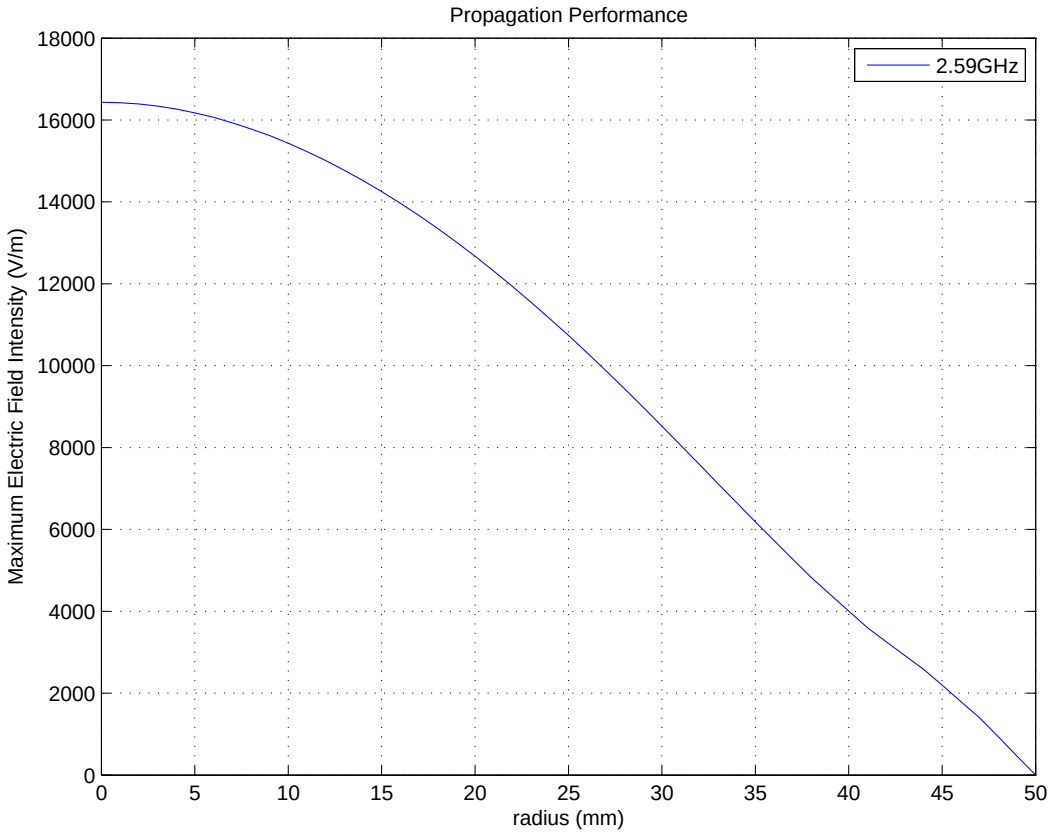

Figure 4.37: Propagation performance without plasma

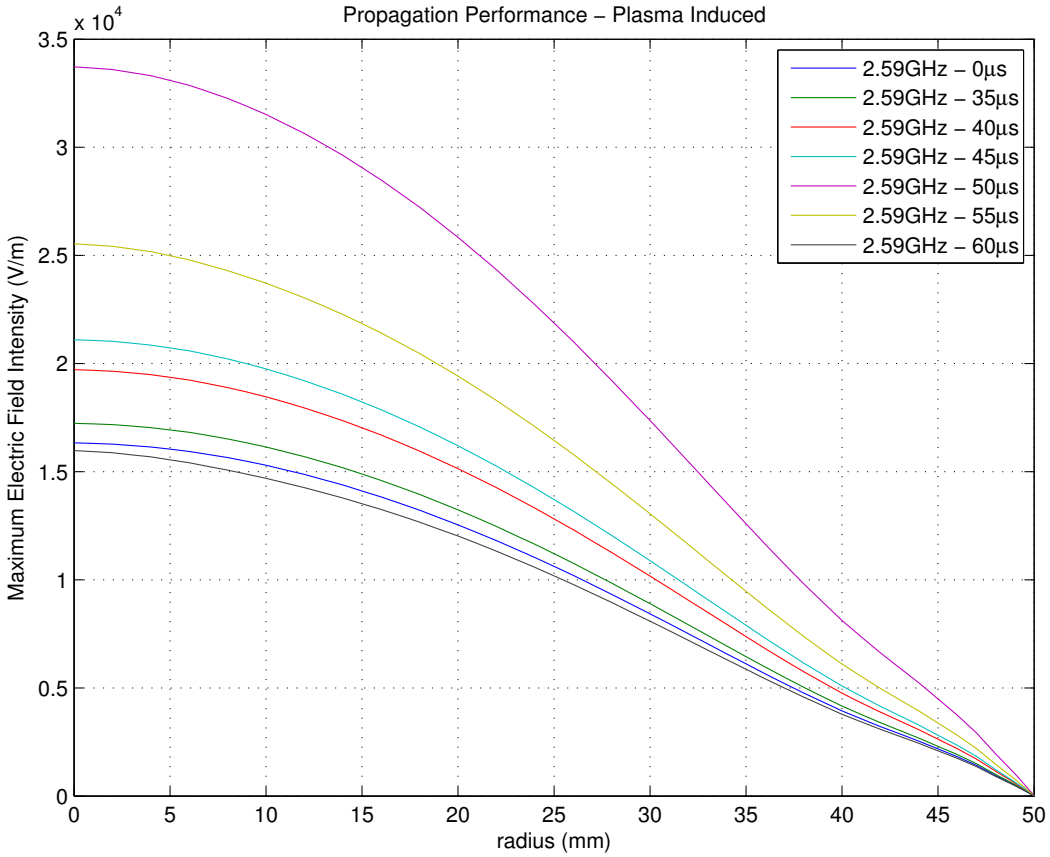

Figure 4.38: Propagation performance with microwave induced plasma

The initial electric field intensity starts at the centre of the cavity with approximately 16.5×10^3 V/m. This intensity declines while travelling out to the frame of the combustion chamber until the field decreases to zero at a distance of around 50 mm from the cylinder centre. Figure 4.38 exhibits the initial propagation performance and also the corresponding propagation while inducing microwave plasma. Inside the cavity, plasma is induced and the performance at the supplied frequency alters over time. This will be examined later but for now it is established that the tendency of the propagation does not shift significantly while inducing plasma. The blue line in Fig. 4.38 shows the propagation at 0 µs, this is before any plasma was induced. Gradually, more molecules are ionised and the initial electric field intensity increases. The general propagation performance looks similar in relation to the distance between the centre of the cavity and the measuring point. The electric field intensity always decreases over distance, declining to zero at the outer frame of the cylindrical cavity at 50 mm.

The maximum initial field intensity appears at 50 µs after the supplied frequency was enabled. Before and after 50 µs the initial field intensity is lower than the maximum value. There are two possibilities for this; one could be that the resonance frequency alters and so after 50 µs the supplied frequency of 2.59 GHz does match the natural frequency the closest in this simulation. The other possibility is that the propagation performance of the ionised material inside the combustion chamber decreases after a

defined electron density is reached. The first possibility can be investigated through another simulation with a marginally different frequency.

4.5.2 Influence of Mixture Temperature for the Propagation Performance

The gas mixture can be injected into the combustion chamber with a variable temperature. Consequently the variable temperature could affect the electric field propagation performance. This section is going to investigate the variable mixture injection temperature for the performance of the ionised material inside the chamber and the total propagation performance of the electric field while building plasma. The material inside the combustion chamber is Argon gas. Table 4.14 illustrates the chemical collisions and reactions required for this model. For this simulation, it is necessary to implement these chemical reactions with the FEM simulation software COMSOL Multiphysics for building the microwave plasma. The simulation of plasma is computationally intensive and therefore it is necessary to limit the resolution and simulation mesh before starting to compute the simulation.

Table 4.14: Collisions and reactions modelled

Reaction	**Formula**
1	e + Ar ⇒ e + Ar
2	e + Ar ⇒ e + Ars
3	e + Ars ⇒ e + Ar
4	e + Ar ⇒ 2e + Ar+
5	e + Ars ⇒ 2e + Ar+
6	Ars + Ars ⇒ e + Ar + Ar+
7	Ars + Ar ⇒ Ar + Ar

where e are the electrons and Ar the Argon atoms. Reaction 2 describes how to create the electronically excited Argon atoms and reaction 3 the opposite along with the thermal energy the gas gains back. The ionisation of the Argon atoms are described in reaction 4 and 5 for low pressure Argon discharges.

Originally, the simulation was executed with an initial temperature of 297.15 K, represented by the blue line in Fig. 4.39. To compare the behaviour with a different initial temperature, the second value was increased to 350.15 K which is represented by the green line. Figure 4.39 shows the maximum electric field intensity at the centre of the combustion cylinder on the y-axis against the time on the x-axis. The maximum electric field intensity is illustrated in V/m and the elapsed time since the microwave

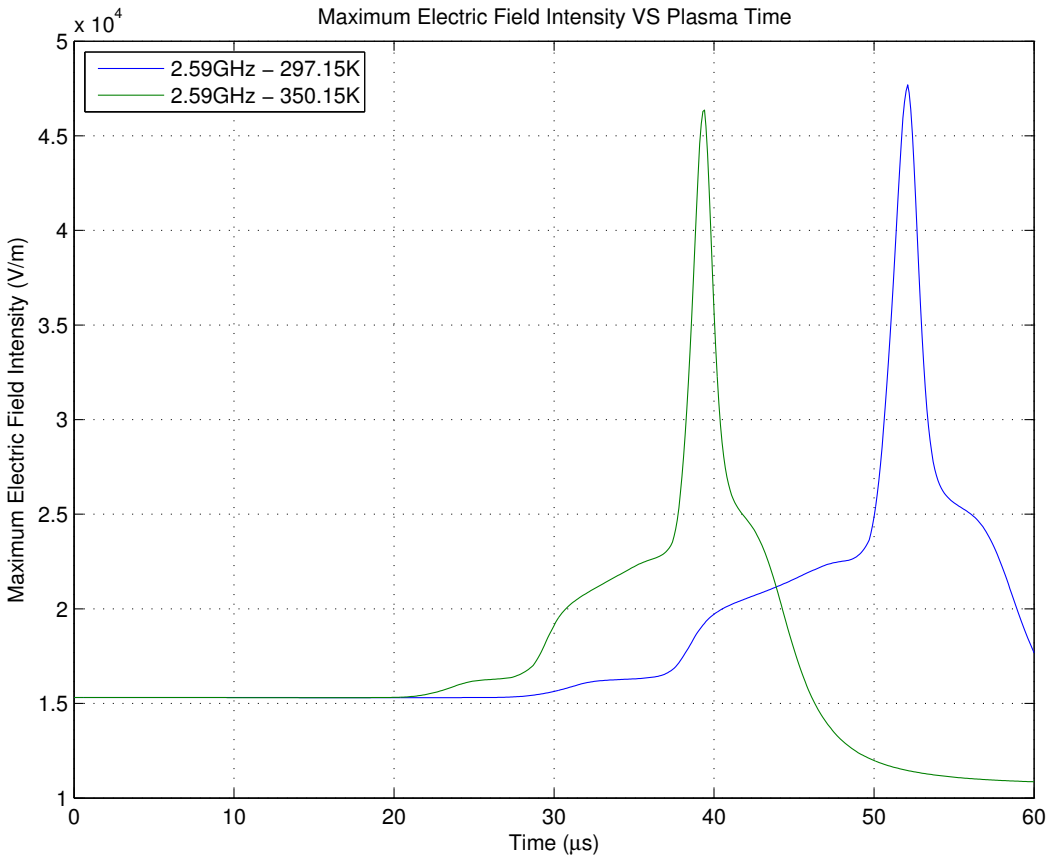

Figure 4.39: Electric field for different initial temperatures 2.59 GHz

source was activated is pictured on the horizontal axis. The most effective way to see the difference in the electric field intensity between the two initial temperatures is to capture both graphs in one figure. The initial field strength and the field up to a time of 20 µs are on the same level for both temperatures. The electric field intensity of the premixed gas with 350.15 K increases faster to the maximum peak compared to the one with just 297.15 K. The maximum electric field peak intensity is lesser for the higher initial temperature. The reason behind this is the simulation resolution because the peak is very narrowed around the resonance frequency.

Figure 4.40 shows a case of the same initial temperature of the medium inside the combustion chamber with varied supply frequencies applied. For the first case the previously used frequency of 2.59 GHz is set. The second case applies a frequency, 2.596 GHz, which is closer to the resonance frequency for the used cylinder model and material. The initial electric field intensity with a supply frequency of 2.596 GHz is 82×10^3 V/m and decreases while the microwave plasma is induced. Compared to the blue graph, which represents the electric field with the initial frequency of 2.59 GHz, the maximum field intensity nearly doubles. Reasons for this could be an insufficient search resolution for the first simulation or that the propagation of a high ionised material is less efficient.

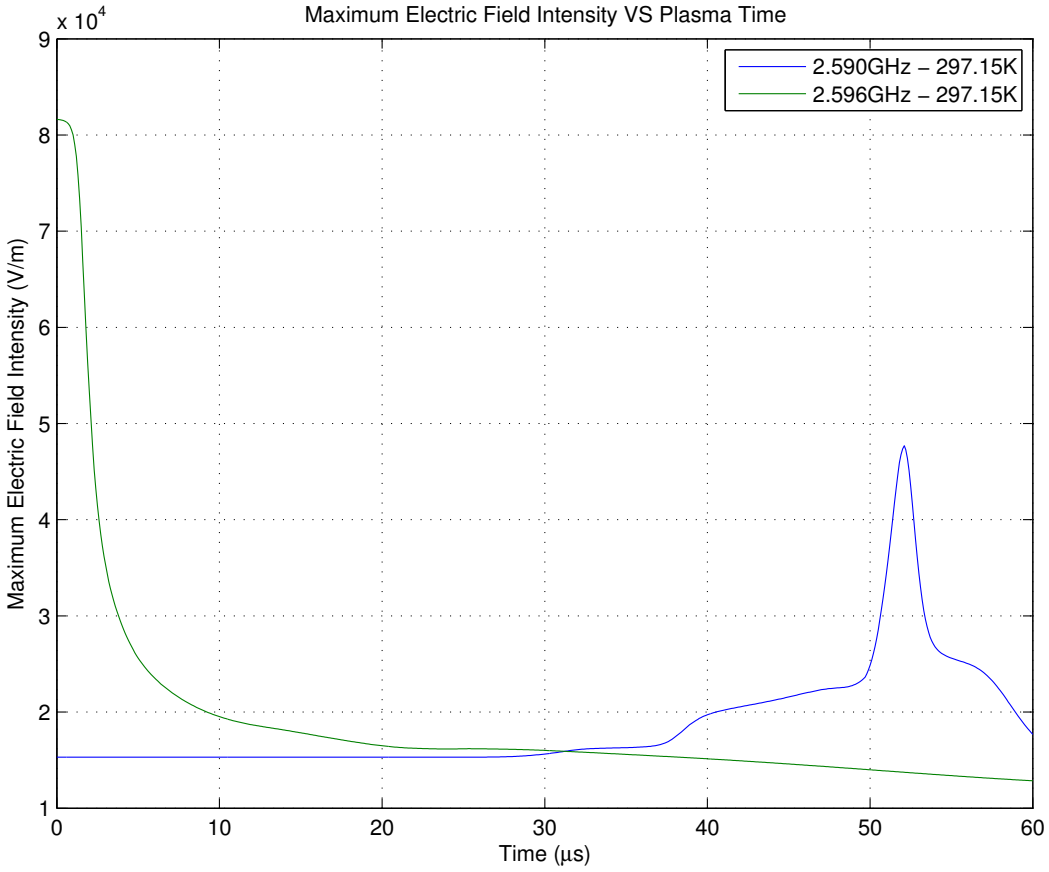

Figure 4.40: Electric field for different frequencies

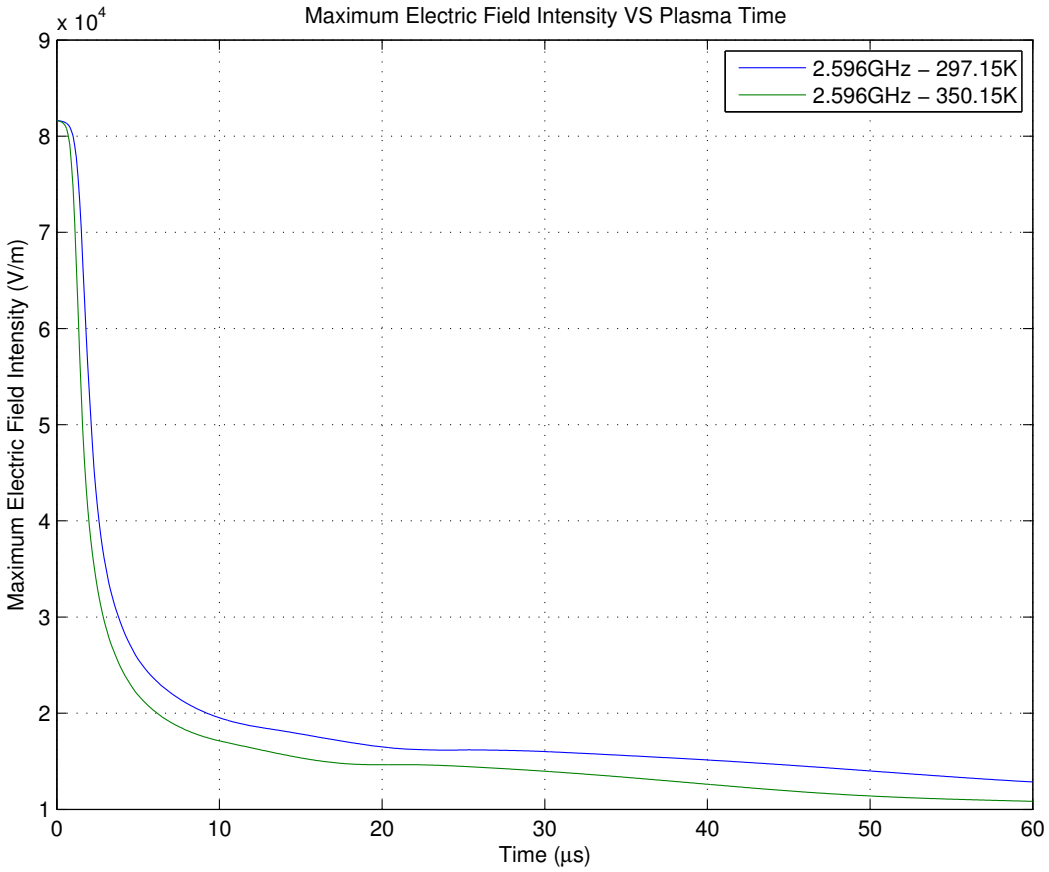

Figure 4.41: Electric field for different initial temperatures 2.596 GHz

The final simulation, illustrated in Fig. 4.41, covers a simulation setting with a frequency close to the resonance condition and two different initial temperatures. The initial electric field intensity for both mixtures is the same but over time, the propagation of the simulation with the initial temperature 350.15 K is less favourable in comparison to the one at 297.15 K. This gives evidence that the initial temperature does not affect the propagation performance itself but during the plasma building process and ionisation of the mixture inside the combustion chamber, the performance does shift.

In summary, it has been determined that the initial electric field intensity does not alter with a variable injection temperature of the mixture. Figures 4.39 and 4.41 demonstrate that the initial electric field intensity of both temperatures are identical even with a difference of 53.15 K. When the observation also included the plasma building process, the performance difference is present for variable initial temperatures. At the current stage, a preheated injection temperature does not produce a better propagation performance, but to the contrary the propagation performance decreases. This is shown in figs. 4.39 and 4.41. Figure 4.39 displays that the preheated gas reaches the maximum faster but also decreases the maximum electric field intensity at the peak. Figure 4.38 illustrates that the ionisation of the material affects the propagation performance and initial electric field intensity with a constant supply frequency, but not the behaviour of the field reduction over the distance of the cylinder.

Conclusion

This chapter investigated the influence of various input parameters for the default and extended antenna model of a HCMI system. At first single variable changes have been performed for both antenna models. After these the exhaustive search was further carried out for multiple variables. It was discovered in section 4.3.1 that the AFR cannot be used as an optimisation parameter in chapter 5 to locate the maximum electric field propagation performance inside the engine cylinder. The maximum electric field intensity as well as the bandwidth of the signal is monotonically decreasing while increasing the AFR of the mixture. The results of the antenna dimensions ("HAntenna1", "HAntenna2", "WAntenna2") have shown at least a single extrema over the applied search range. Therefore these variables can be further used for the digital prototyping in chapter 5. The investigation of the antenna length "HAntenna1" shows the highest influences on the propagation performance inside the engine cylinder of all searches.

Chapter 5

Virtual Prototyping

So far, the CAD cylinder and antenna model have been used and investigated by the trial and error method. This means the simulation was started with a given set of parameters and the search following these predefined values. This chapter takes the virtual prototyping one step further by applying a CAutoD search in furtherance of finding the most suitable antenna design for the default cylinder model (described in Fig. 4.4). The advantage of using an automated search with a computer based simulation module is the possibility of modifying the virtual prototype of the MI device during the search process. The CAutoD system is able to execute multiple geometric dimensions of the engine cylinder and antenna design model in a minimal amount of time at low expense. This makes it possible to investigate and predefine several successfully simulated antenna designs before starting the physical prototyping.

5.1 Optimisation Search with Eigenfrequency

The systematic searches in chapter 4 along with the further investigations in chapter 5 have demonstrated the dilemma in the realisation of the HCMI system. While applying different optimisation techniques it was established that the supplied frequency for a HCMI system is the most practical input parameter. The frequency affects the electric field propagation performance inside the engine cylinder significantly more than any other input variable. Due to this fact it is clear that the resonance condition must be the priority for every search. Ideally every search would involve an embedded optimisation search to determine the corresponding resonance frequency but Unfortunately this would involve too many evaluations. This problem needs to be addressed and solved in the following in order to find a reliable virtual prototype of the antenna model.

Especially as the deterministic NM search has difficulty locating the optimum design due to the high possibility to find a local extrema while the frequency is included as an input for the FEM CAD model, shown in sections 5.3.1 and 5.4.1. This section introduces a new search for discovering the maximum electric field intensity inside the combustion chamber while excluding the frequency as an input parameter. The technique shown below is similar to the algorithm used to calculate and create the three dimensional surface plots (see section 3.7.2).

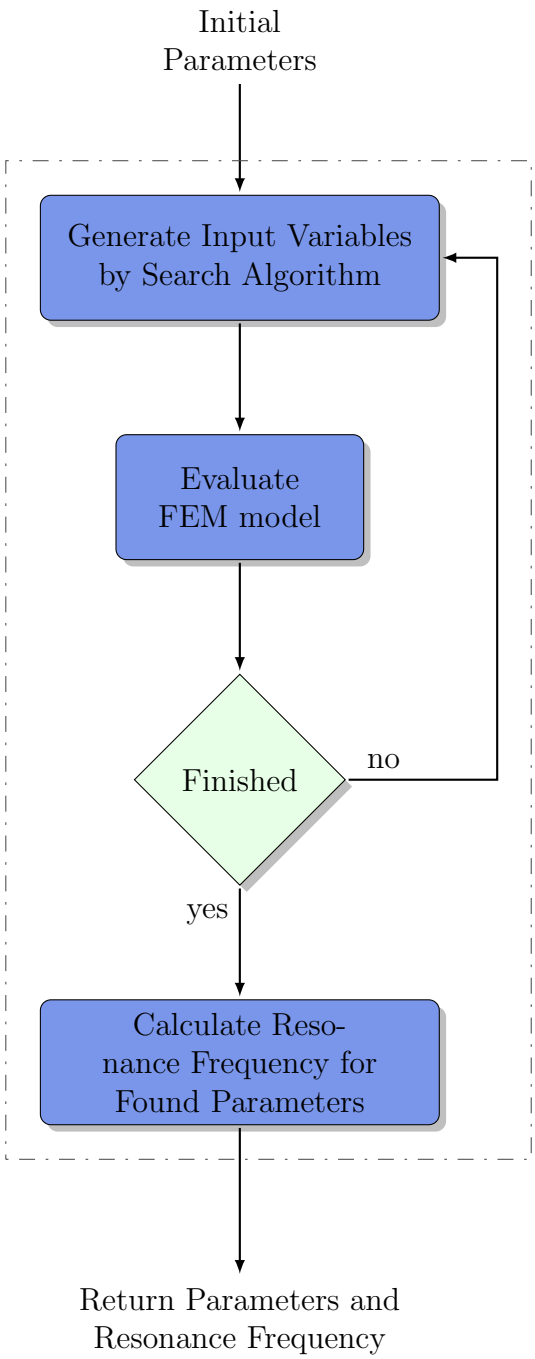

Figure 5.1: Optimisation search with Eigenfrequency

Every optimisation search that involves multiple input variables is getting more difficult to optimise when the frequency is involved as an input variable. This is due to the

fact that the frequency has a high influence on to the propagation performance inside the cylinder. A shift of a few kHz can significantly weaken the maximum electric field intensity or lead to a complete disappearance of the resonance inside the combustion chamber and with it the electric field intensity. In theory, the ideal solution would be to evaluate a separate optimisation search for each input variable configuration in order to find the related resonance frequency inside the combustion chamber. Unfortunately, considering the time consumed by each optimisation search, it is impossible to implement this theory. This would involve too many evaluations and is impractically at the current stage. As shown in sections 5.3.1 and 5.4.1 the NM optimisation search requires a well defined starting point in order to find a suitable solution. This is the main weakness of this algorithm and therefore the possibility of reaching a local extrema is most probable. The GA search could find the solution for a supplied search range but needs significantly more evaluations compared to the NM optimisation search. If the supplied search range of the non-deterministic GA search is too loose, the algorithm will also lead to local extrema, shown in sections 5.3.2 and 5.4.2.

Section 5.1 demonstrates the search for the maximum electric field intensity by using the Eigenfrequency instead of the supply frequency as an input variable. The search can be executed with the deterministic NM algorithm or the non-deterministic GA search technique. Section 4.3.7 investigated the performance of the Eigenfrequency in relation to the resonance frequency of the cylinder and determined that the Eigenfrequency is very close to the resonance frequency and behaves similarly. The small offset shown in Fig. 4.21 is negligible for the general performance of the search algorithm. After the successful optimisation search, the found parameters are applied to another optimisation search to calculate the corresponding resonance frequency. These often provide a slightly higher maximum electric field intensity inside the cylinder than the Eigenfrequency.

5.2 Predefined Genetic Algorithm

The dilemma of the HCMI system have already be mentioned in section 5.1, this section will propose a new search which will use a combination of NM algorithm and the GA search technique.

Section 5.2 illustrates the new search technique, as evidenced in sections 5.3.2 and 5.4.2, it is required to supply a frequency range close to the resonance frequency in order to obtain acceptable results of the HCMI system optimisation problem. To address this issue, and narrow down the frequency range, the Predefined Genetic Algorithm (PGA)

will analyse the given input parameters. The algorithm will also generate an initial population, and calculate the frequency range before starting the non-deterministic optimisation search. To calculate the frequency range, the algorithm will select characteristic values out of the initiated population and locate the resonance frequency for this values. Additional to the characteristic values, the algorithm will also select a defined number of random parameters out of the initial population and evaluate their corresponding resonance frequency. The frequency range will be calculated from the found minimum and maximum resonance frequency and expanded by a defined boundary. Therefore the defined frequency range will be near to the minimum required range for the given search parameters.

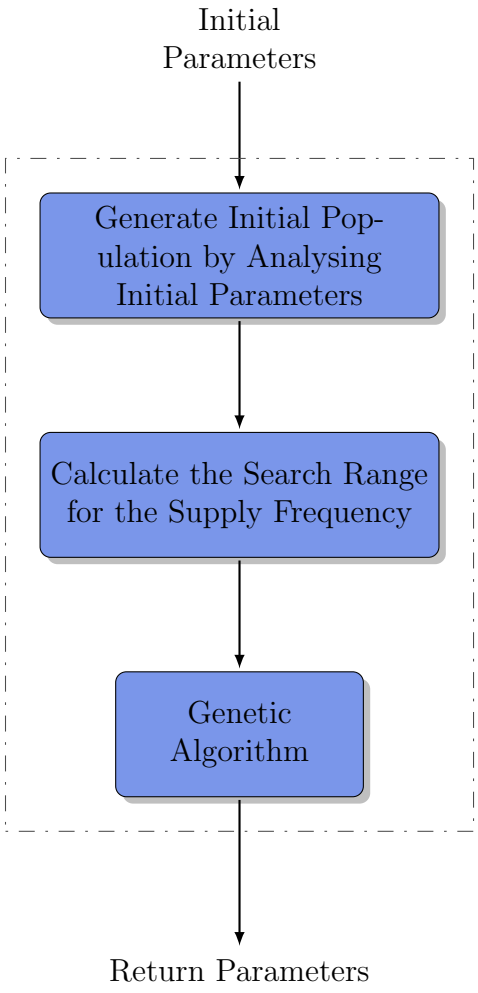

Figure 5.2: Predefined Genetic Algorithm

The PGA search is used in sections 5.3.3 and 5.4.3 to find the best antenna design. The performance will be compared with the NM and ordinary GA optimisation.

5.3 Combination of Frequency and Antenna Length

The combination of the frequency and the antenna length demonstrates a multivariable optimisation problem in context of the HCMI system. The supply frequency is the most sensitive input variable of the system and even a small alteration, results in a weaker propagation performance or a complete disappearance of the resonance inside the combustion chamber of the ICE. The input variables for the systems are the supply frequency and the antenna length. The single variable influence of the antenna length for the maximum electric field intensity and propagation performance was investigated in section 4.3.4.

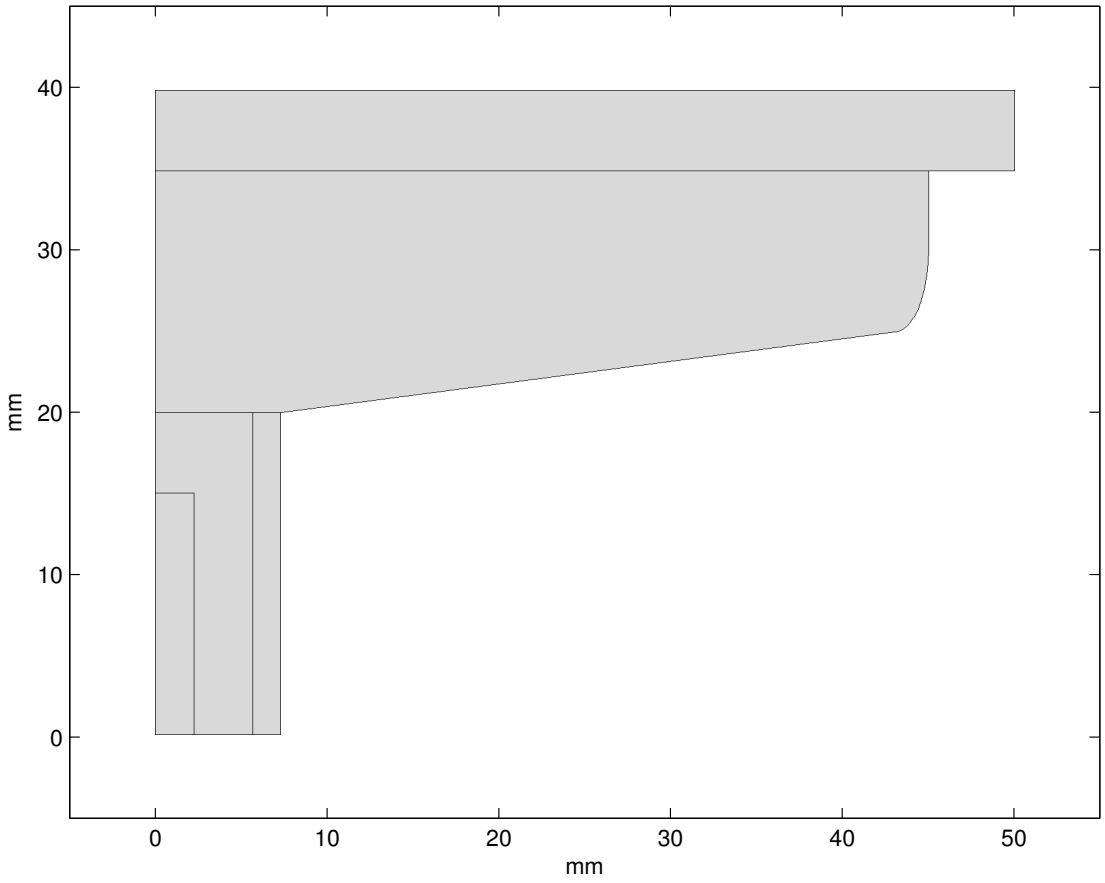

Figure 5.3: 2D Default antenna model

Figure 5.3 displays the antenna model used for this optimisation search. In section 5.3.1, the deterministic NM algorithm will be used to find the best propagation performance inside the combustion chamber. This section presents the problems of using the deterministic search algorithm for a HCMI system. For further investigations, this section will analyse the same optimisation problem by using non-deterministic search algorithms, such as the standard GA and the PGA, described in section 5.2. The HA search technique will not be used for the optimisation problems in this chapter. Section 3.6.3 presents the performance of the HA by using generic optimisation problems.

The results of the search in section 4.3.4 have already determined the best solution for the antenna length. The optimum solution, for the best propagation performance, was achieved by applying an antenna length of approximately 1.25 mm with a correlated supply frequency of 2.5961 GHz. This outcome helps to compare the performance of the different searches after a detailed investigation of the optimisation problem.

5.3.1 Deterministic search

The deterministic optimisation search in this section is implemented by using the NM simplex algorithm. The advantages and disadvantages of the NM algorithm are reviewed in section 3.6.1. In order to find the most suitable solution, the optimisation search will vary the supply frequency of the microwave generator and the antenna length ("HAntenna1") of the given simulation model in section 5.3. The whole investigation process includes four different searches with the following starting conditions:

Table 5.1: Starting conditions of NM searches

Search	**Frequency** (GHz)	**Antenna length** (mm)
1st	2.5	2
2nd	2.59	2
3rd	2.5	10
4th	2.59	10

The chosen starting conditions for the supply frequency as well as the antenna length were influenced by the results of the single variable search for the antenna length in section 4.3.4. The optimisation settings and stopping criteria for the algorithm used were set to the following values:

- Display = final
- MaxFunEvals = 500
- MaxIter = 500
- TolFun = 1E-4
- TolX = 1E-4

These values are the default settings of the algorithm provided by the MATLAB optimisation toolbox. At a later stage, altering these conditions can improve the convergence speed, search performance, or the overall search resolution.

1st Search

The first search employing the NM algorithm, uses the starting conditions defined in Table 5.1. In this case, the initial value for the frequency was defined as 2.5 GHz and the antenna length started at 2 mm. The initial value for the antenna length is very close to the known value that delivers the best propagation performance inside the engine cylinder, shown in section 4.3.4. The chosen starting value for the supply frequency is approximately 100 MHz lower than the known frequency that causes resonance of the cavity.

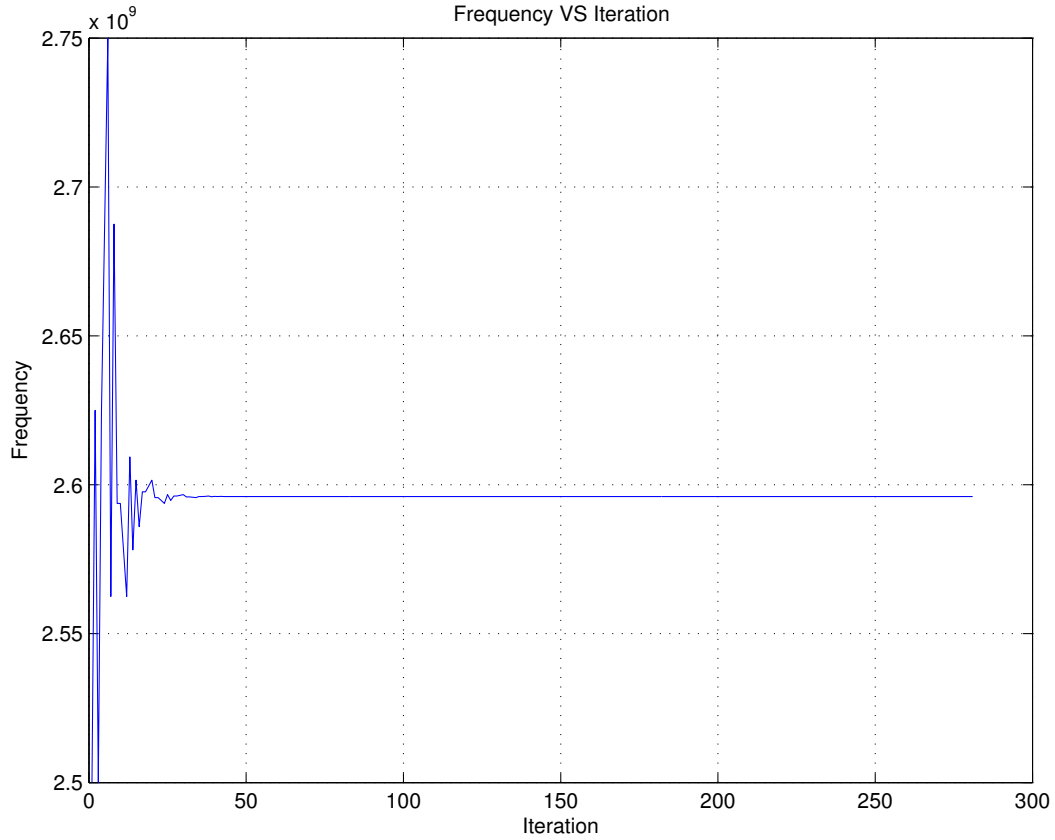

(a) Search trace for the supply frequency with the NM search method

Figure 5.4: NM search for the 1st set of initial parameters of Table 5.1

Figure 5.4 shows the search trace and the development of the different input variables and objectives and objectives by applying the first set of initial parameters of Table 5.1. The search trace of the supply frequency, with an initial value of 2.5 GHz, is displayed in Fig. 5.4a. The figure was created by connecting the value after each evaluation during the search process. Figure 5.4b shows the search trace for the antenna length starting at 2 mm for each step in the search process. The search point distribution between supply frequency and antenna length is presented in Fig. 5.4c. Figure 5.4d demonstrates the maximum electric field intensity inside the cylinder during the search process.

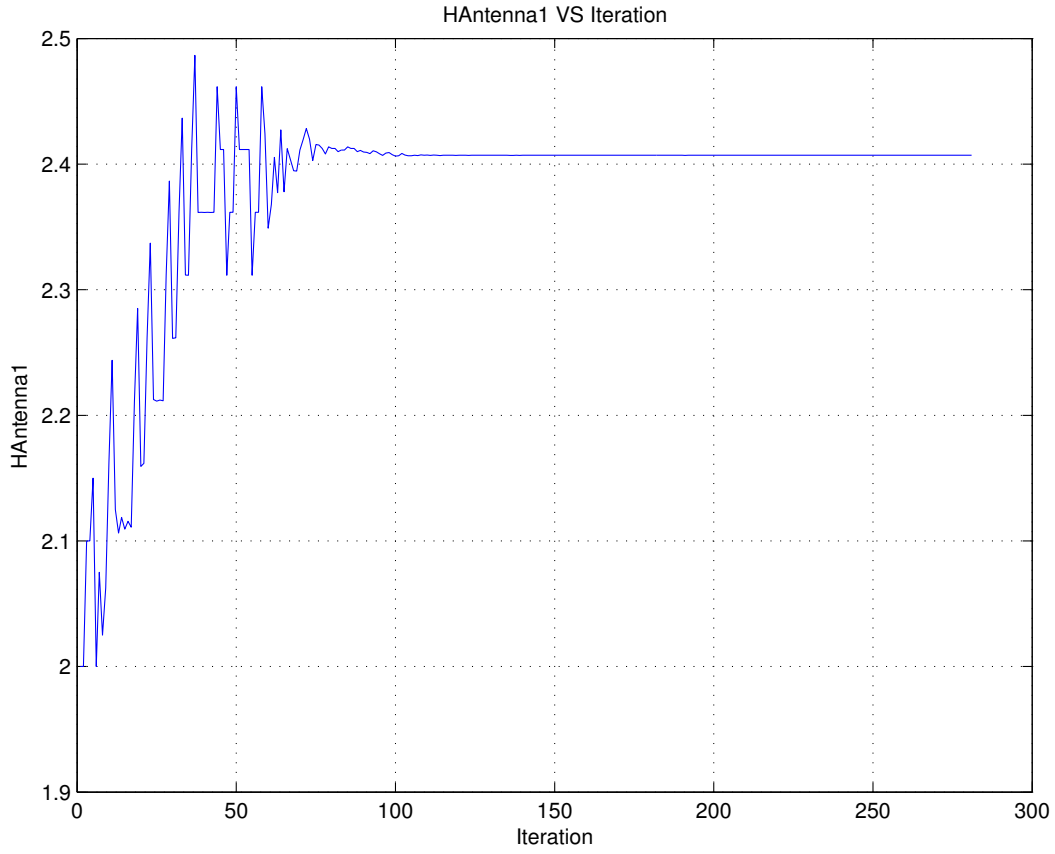

(b) Search trace for the antenna length with the NM search method

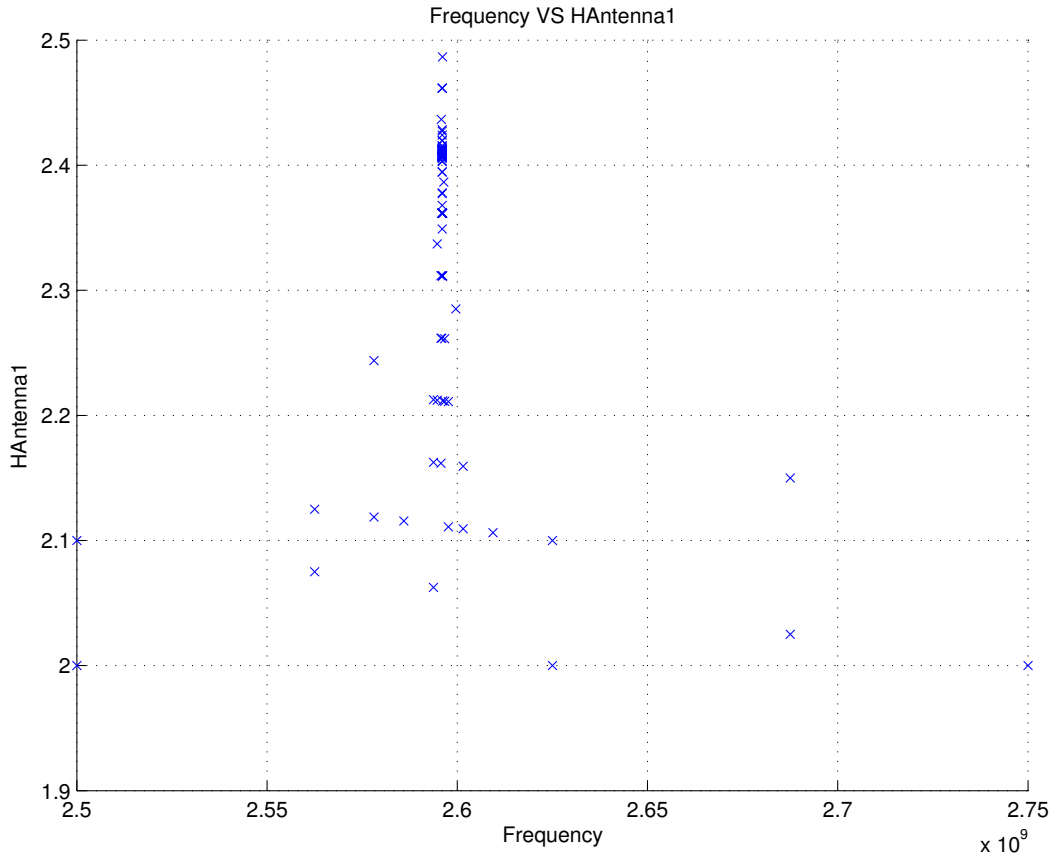

(c) Distribution of the search points of the supply frequency and antenna length

Figure 5.4: NM search for the 1st set of initial parameters of Table 5.1

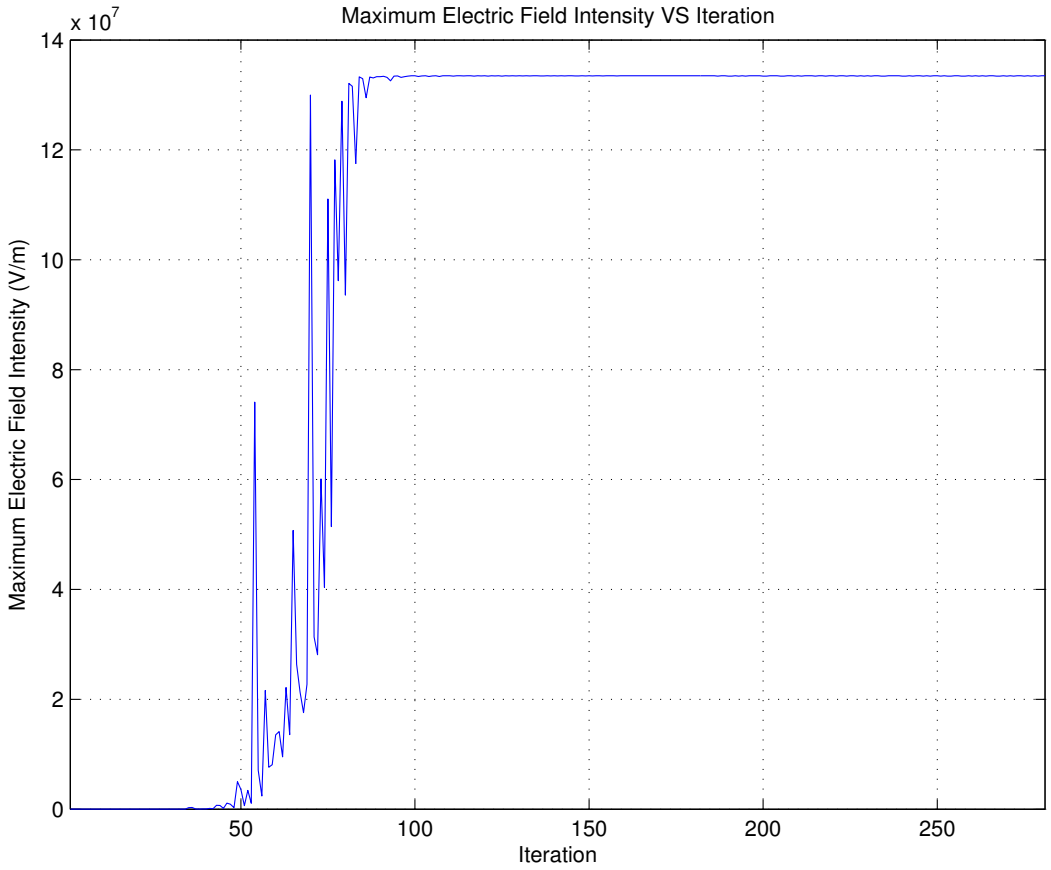

(d) Search trace for the maximum electric field intensity

Figure 5.4: NM search for the 1st set of initial parameters of Table 5.1

2nd Search

The second search employing the NM algorithm, uses the starting conditions defined in Table 5.1. The initial value for the frequency was defined as 2.59 GHz and the antenna length started at 2 mm. The initial value for the antenna length is near to the known antenna length that delivers the best propagation performance, shown in section 4.3.4. The chosen starting value for the supply frequency is close to the frequency which generates resonance inside the cavity.

Figure 5.5 shows the trace of search and the development of the different input variables and objectives and objectives by using the second set of initial parameters of Table 5.1. The search trace of the supply frequency with an initial value of 2.59 GHz, is displayed in Fig. 5.5a. The figure was created by connecting the value after each evaluation during the search process. Figure 5.5b demonstrates the search trace for the antenna length starting at 2 mm for each step on the search process. The search point distribution between supply frequency and antenna length is presented in Fig. 5.5c. Figure 5.5d shows the maximum electric field intensity inside the cylinder during the search process.

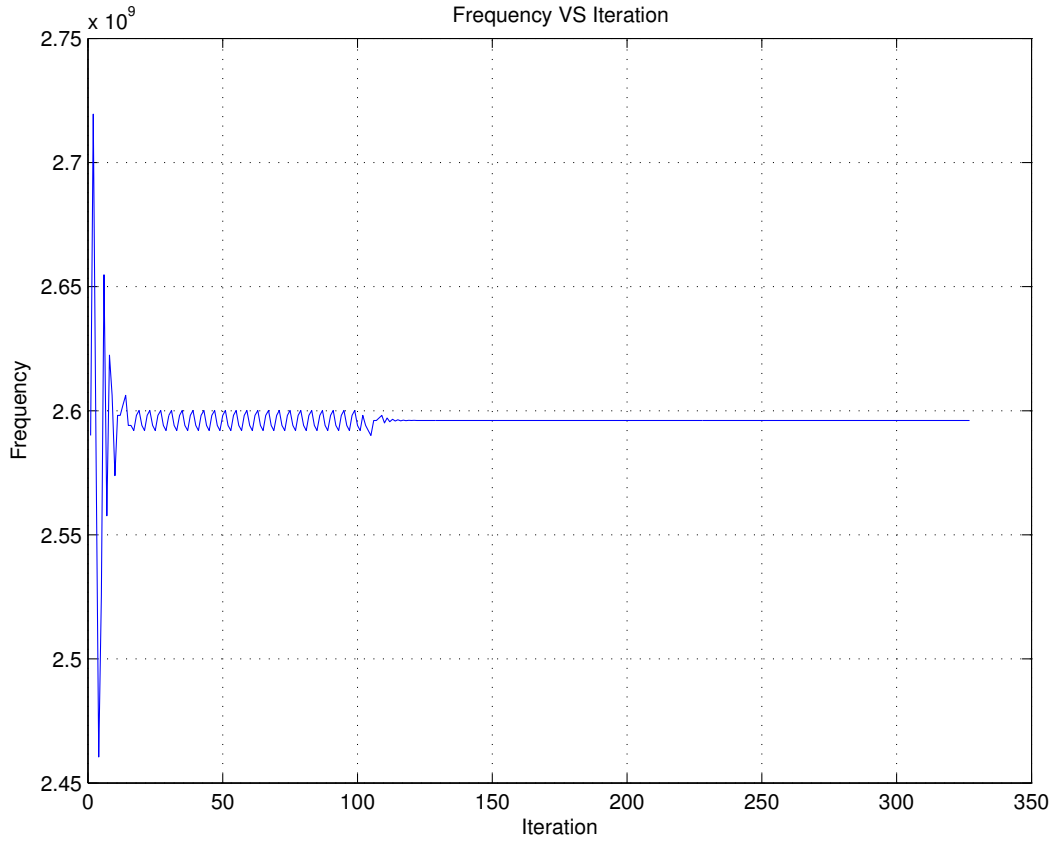

(a) Search trace for the supply frequency with the NM search method

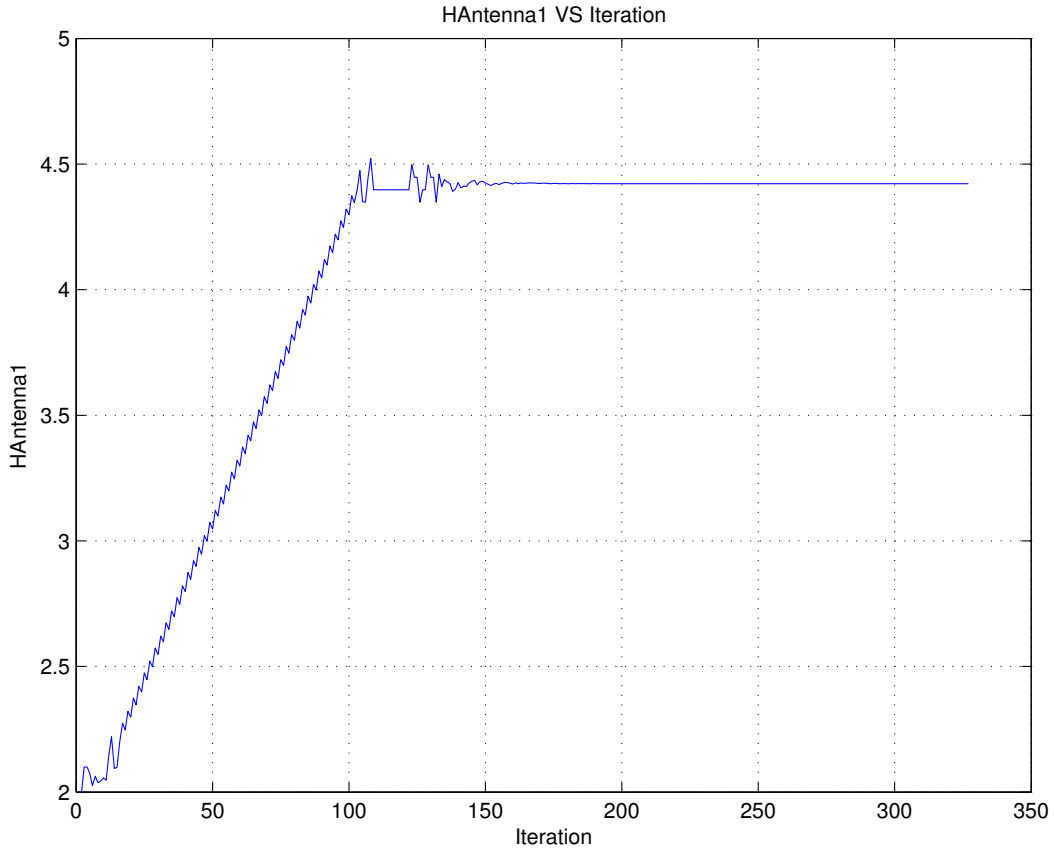

(b) Search trace for the antenna length with the NM search method

Figure 5.5: NM search for the 2nd set of initial parameters of Table 5.1

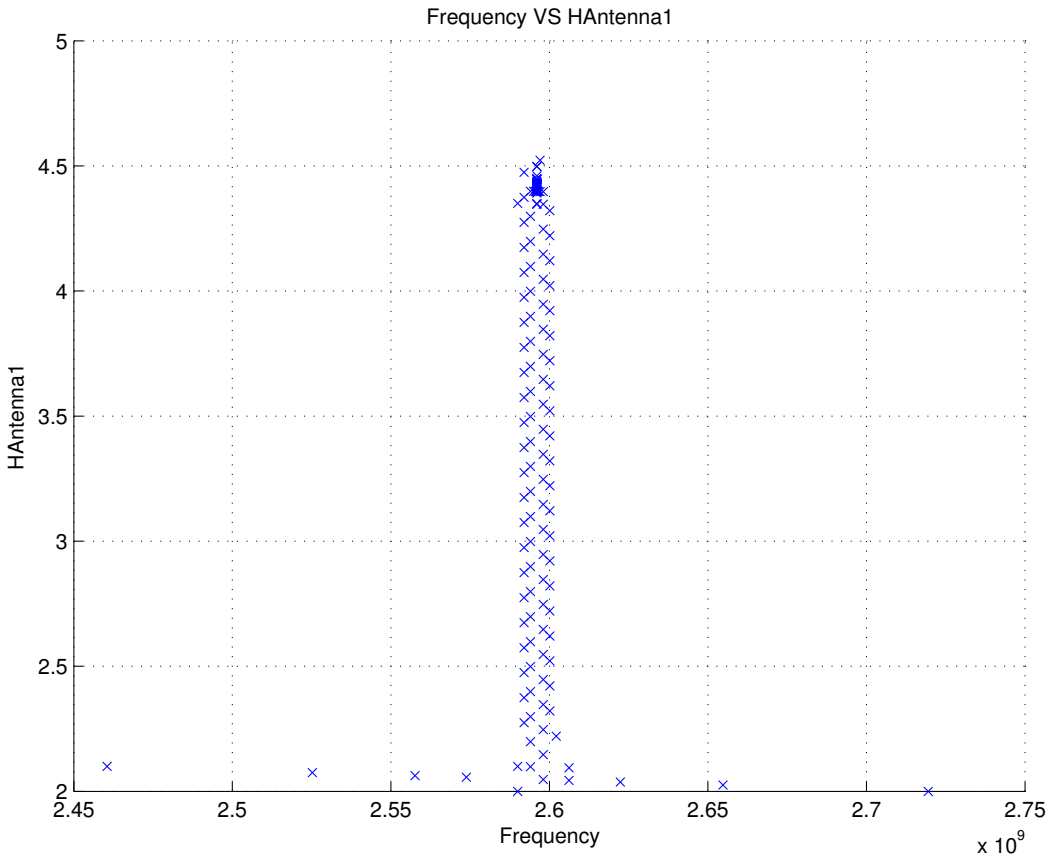

(c) Distribution of the search points of the supply frequency and antenna length

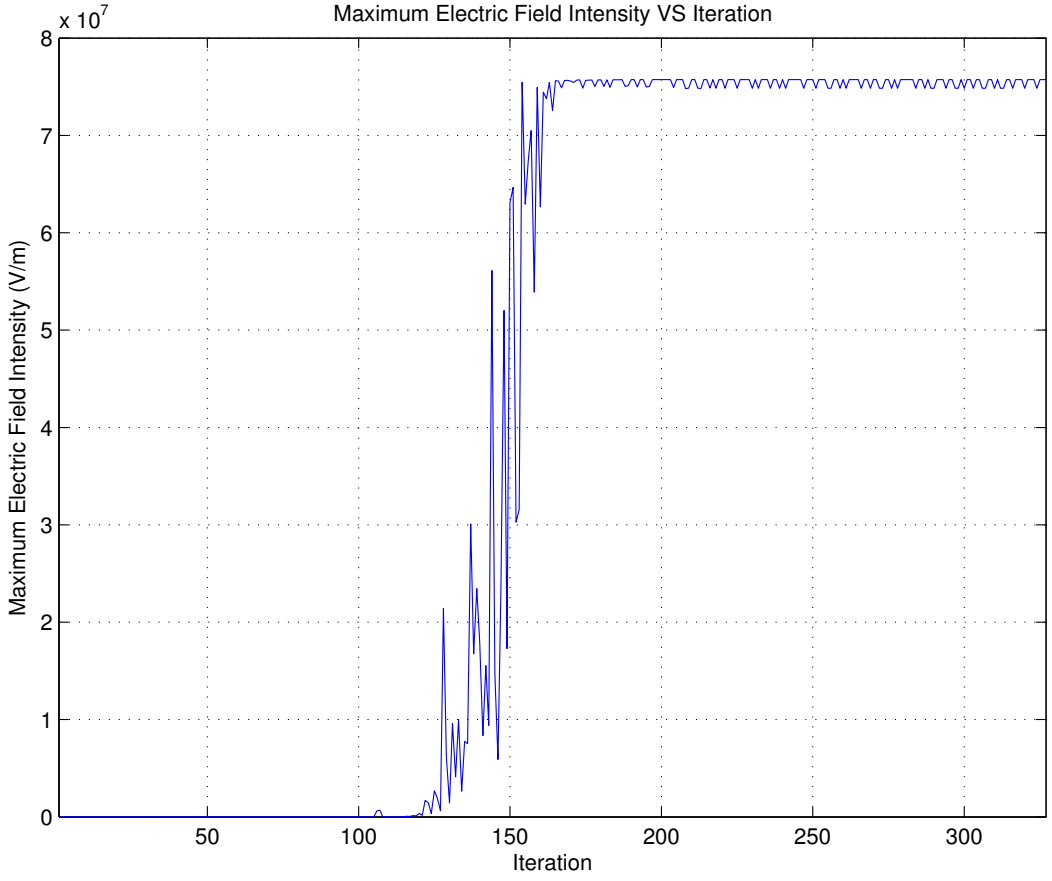

(d) Search trace for the maximum electric field intensity

Figure 5.5: NM search for the 2nd set of initial parameters of Table 5.1

3rd Search

The third search, employing the NM algorithm, uses the starting conditions defined in Table 5.1. The initial value for the frequency was defined as 2.5 GHz and the antenna length started at 10 mm. The initial value for the antenna length is not near to the known value that delivers the best propagation performance inside the engine cylinder, shown in section 4.3.4. The chosen starting value for the supply frequency is about 100 MHz lower than the known frequency which leads to resonance of the cavity.

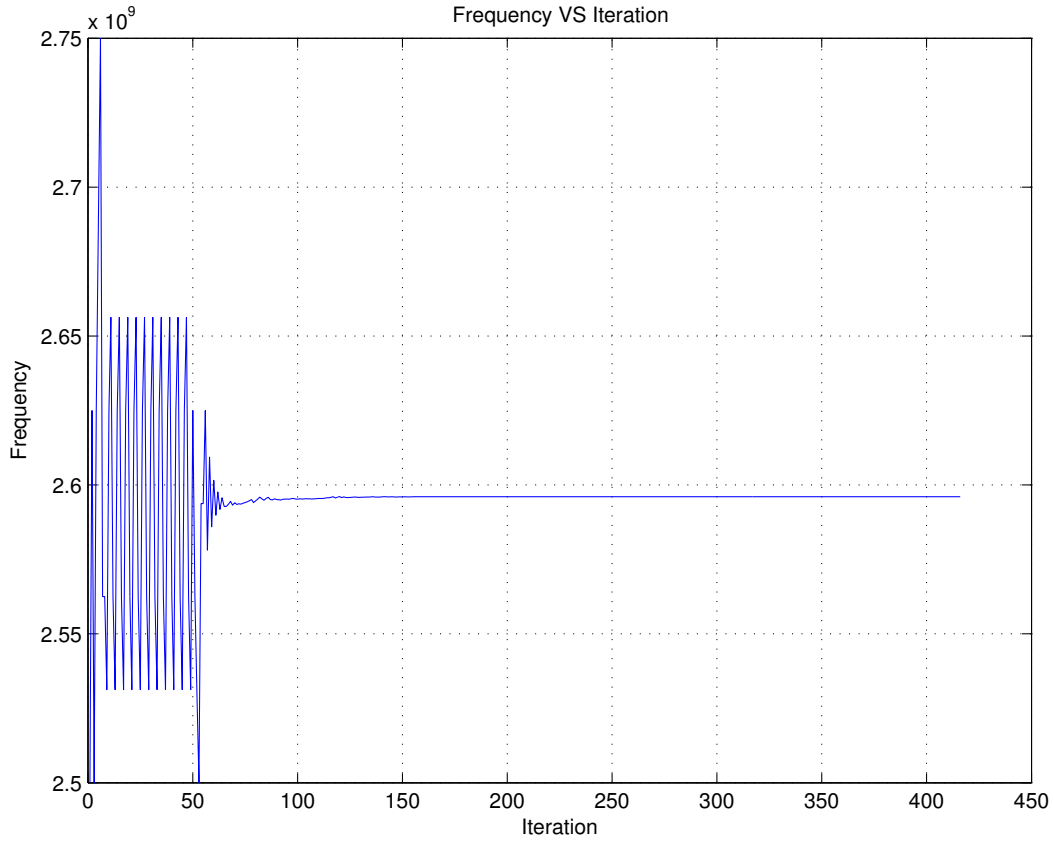

(a) Search trace for the supply frequency with the NM search method

Figure 5.6: NM search for the 3rd set of initial parameters of Table 5.1

Figure 5.6 shows the search trace and development of the different input variables and objectives by using the third set of initial parameters of Table 5.1. The search trace of the supply frequency, with an initial value of 2.5 GHz, is displayed in Fig. 5.6a. The figure was created by connecting the value after each evaluation during the search process. Figure 5.6b shows the search trace for the antenna length starting at 10 mm for each stop in the search process. The search point distribution between supply frequency and antenna length is presented in Fig. 5.6c. Figure 5.6d shows the maximum electric field intensity inside the cylinder during the search process.

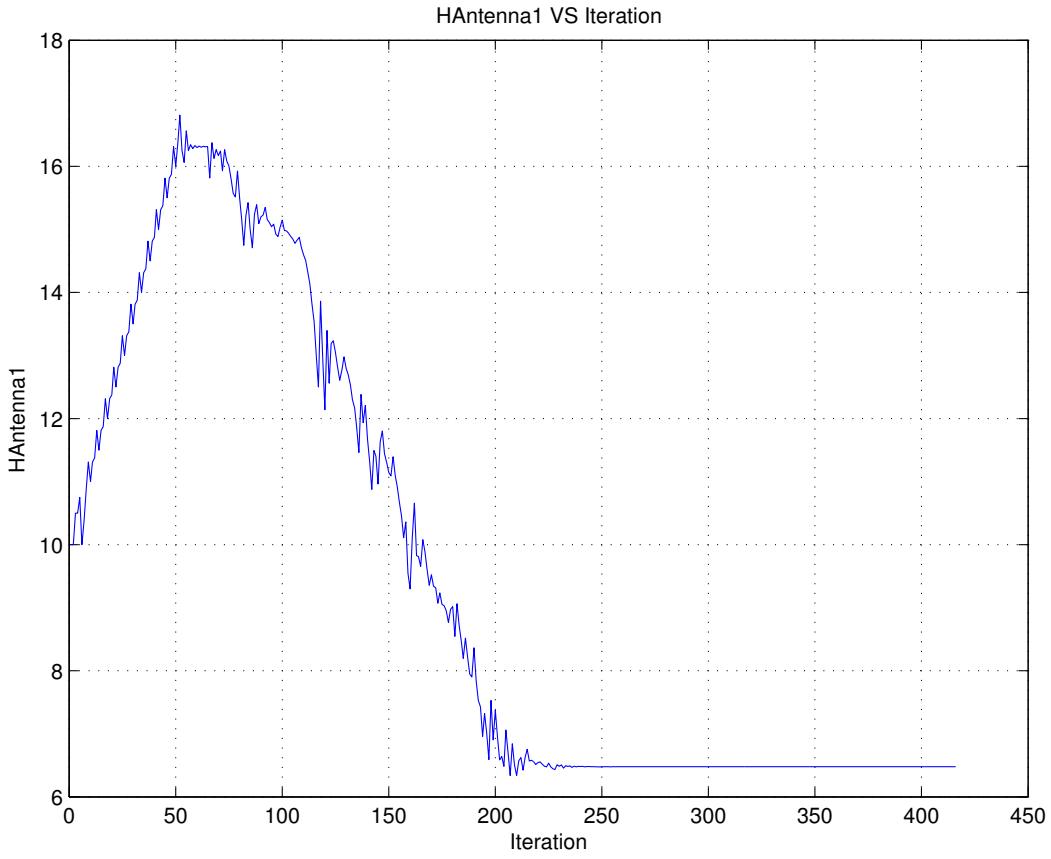

(b) Search trace for the antenna length with the NM search method

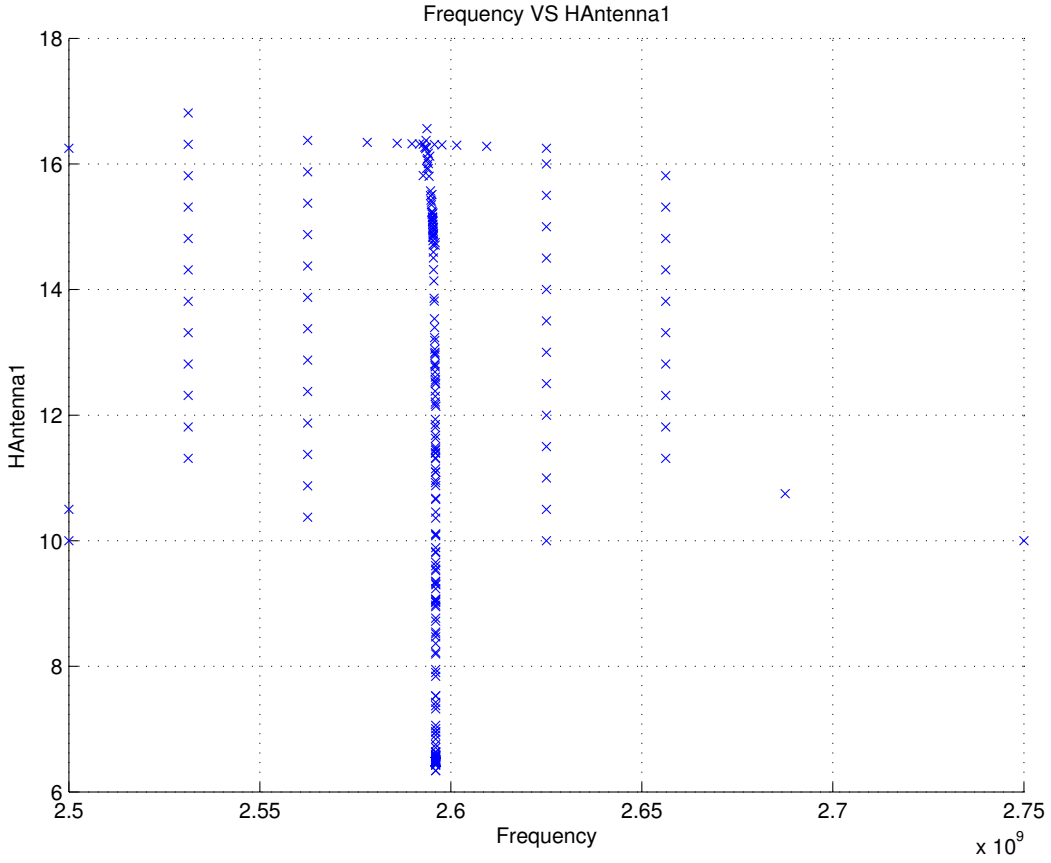

(c) Distribution of the search points of the supply frequency and antenna length

Figure 5.6: NM search for the 3rd set of initial parameters of Table 5.1

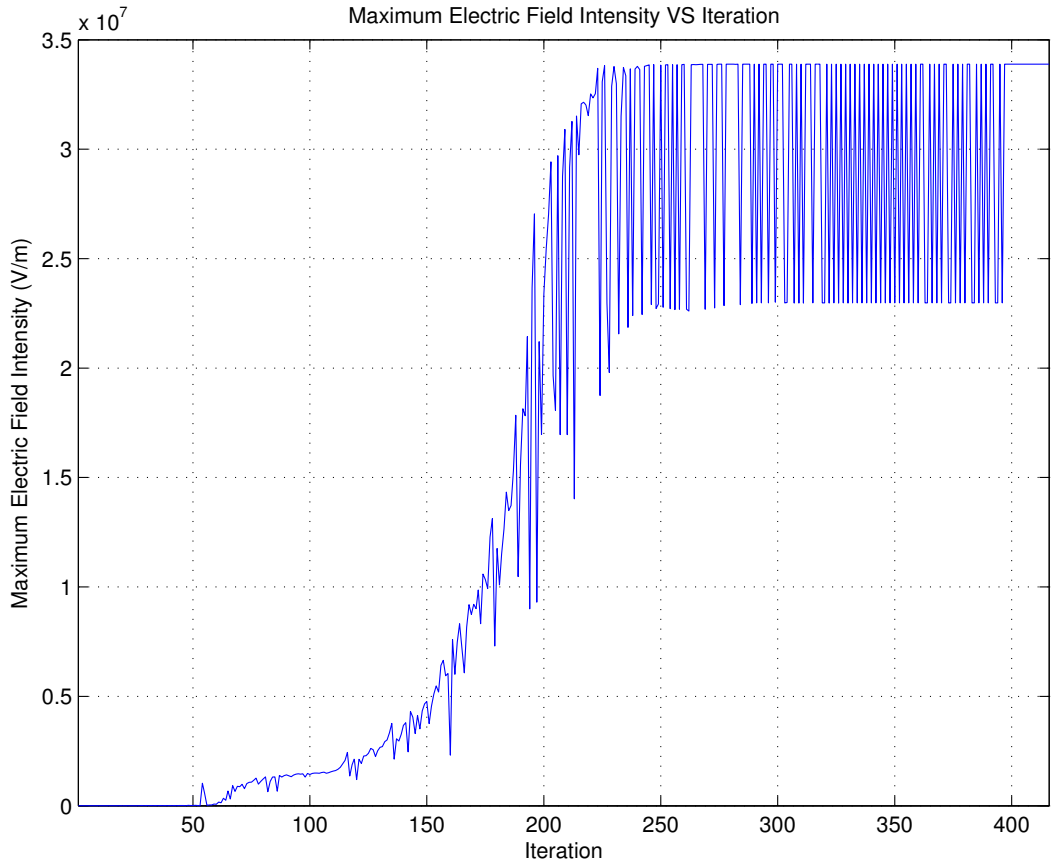

(d) Search trace for the maximum electric field intensity

Figure 5.6: NM search for the 3rd set of initial parameters of Table 5.1

4th Search

The fourth and last search, employing the NM algorithm, uses the starting conditions defined in Table 5.1. The initial value for the frequency was defined as 2.59 GHz and the antenna length started at 10 mm. The initial value for the antenna length is not close to the known antenna length of 1.25 mm which delivers the best propagation performance inside the engine cylinder, shown in section 4.3.4. The chosen starting value for the supply frequency is close and likely to obtain resonance inside the cavity.

Figure 5.7 shows the trace of search and development of the different input variables and objectives by using the fourth set of initial parameters of Table 5.1. The search trace of the supply frequency, with an initial value of 2.59 GHz, is displayed in Fig. 5.7a. The figure was created by connecting the value after each evaluation during the search process. Figure 5.7b shows the search trace for the antenna length starting at 10 mm for each step of the search process. The search point distribution between supply frequency and antenna length is presented in Fig. 5.7c. Figure 5.7d shows the maximum electric field intensity inside the cylinder during the search process.

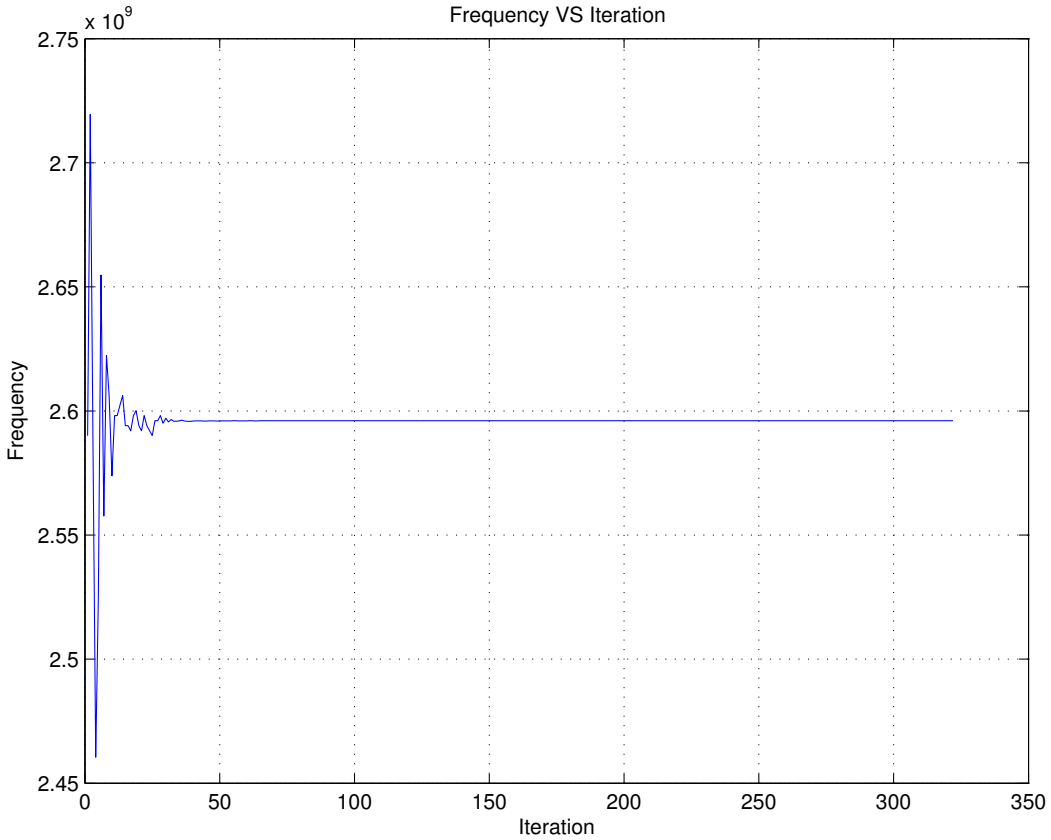

(a) Search trace for the supply frequency with the NM search method

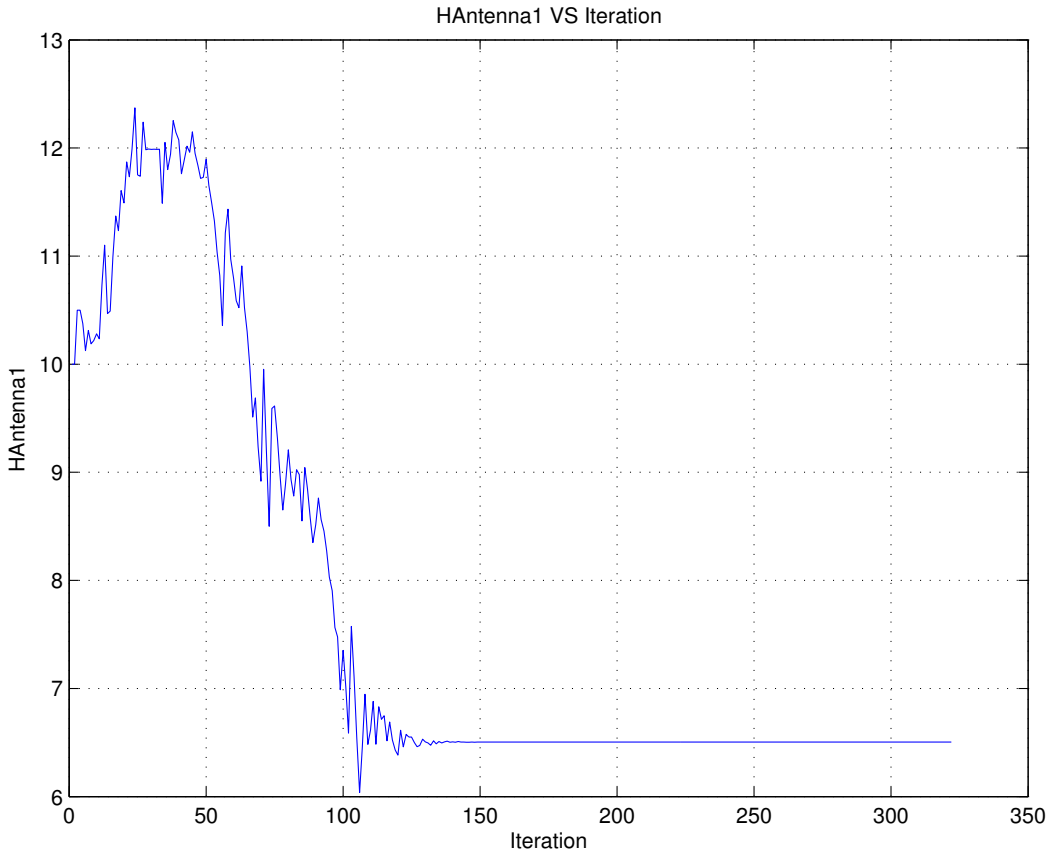

(b) Search trace for the antenna length with the NM search method

Figure 5.7: NM search for the 4th set of initial parameters of Table 5.1

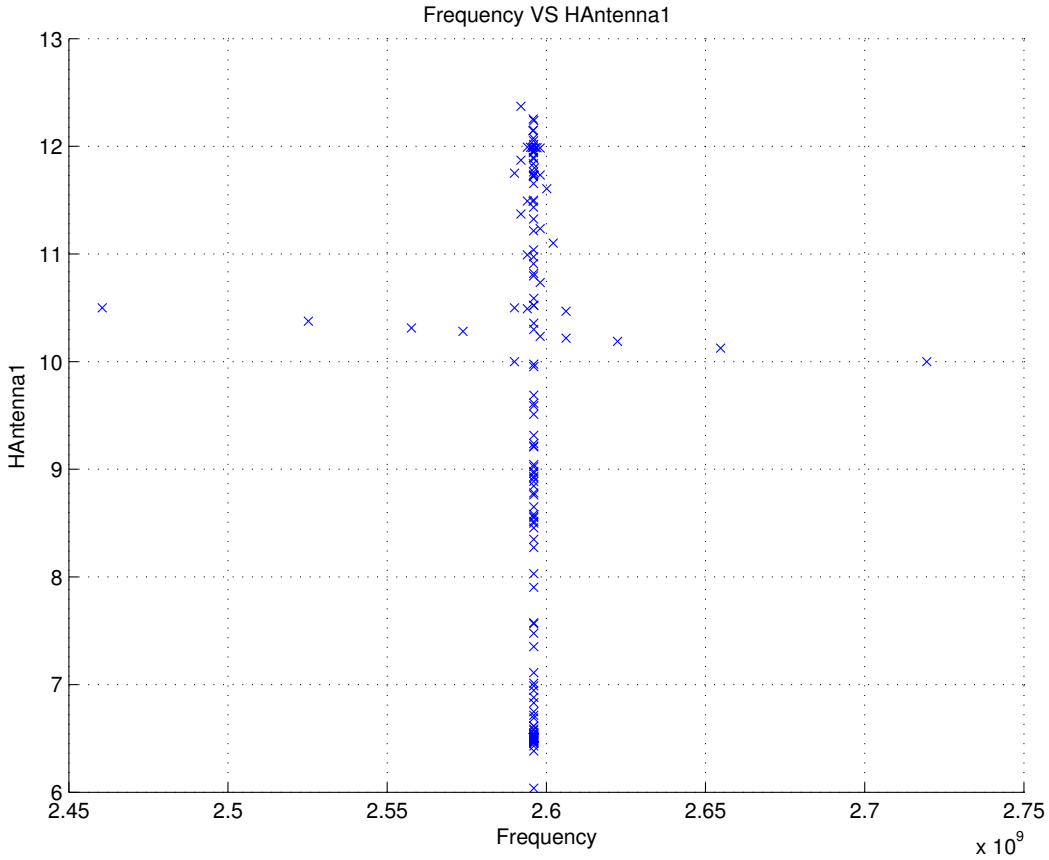

(c) Distribution of the search points of the supply frequency and antenna length

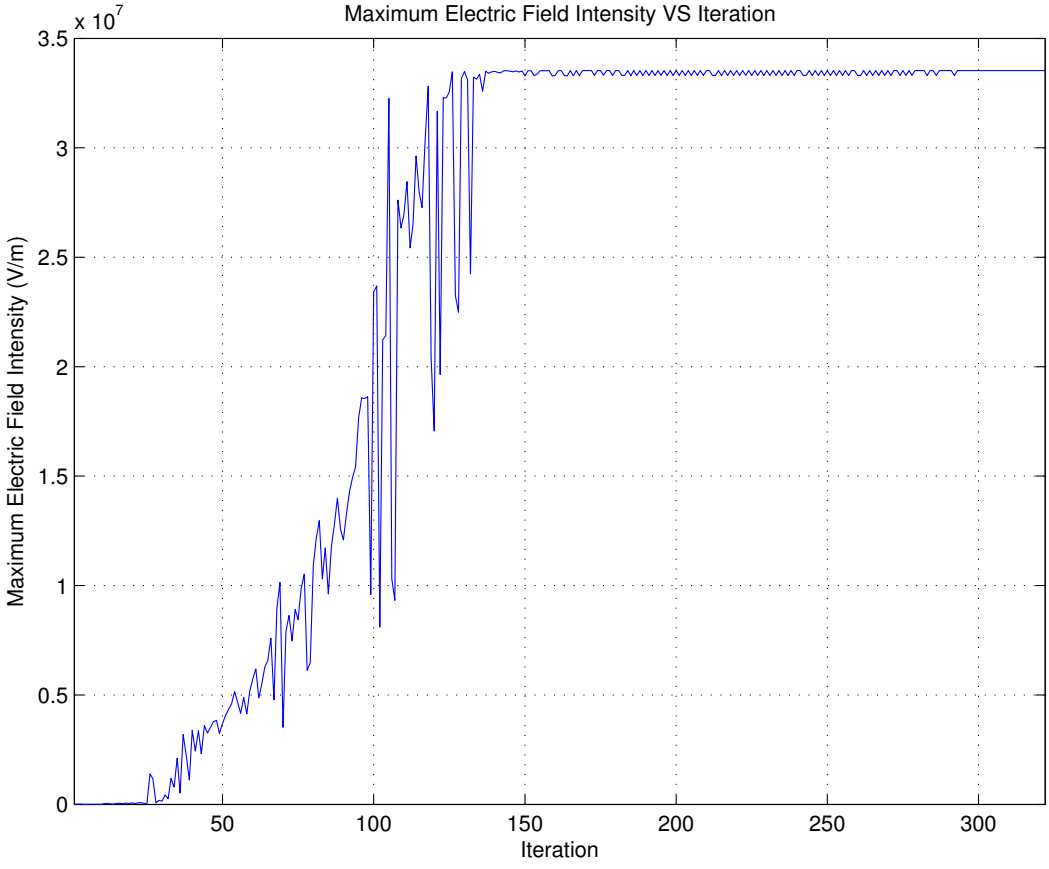

(d) Search trace for the maximum electric field intensity

Figure 5.7: NM search for the 4th set of initial parameters of Table 5.1

Comparison

Figure 5.4 to Fig. 5.7 present the approach of the NM search algorithm to the optimum solution for the optimisation problems. As the NM search algorithm is a deterministic optimisation method, it is unnecessary to run multiple simulations to achieve a reliable performance of the convergence speed. Table 5.2 lists the gathered search results for the different initial parameters. These results show that the initial values are highly relevant for the search to attain acceptable results. Furthermore, this confirms the problem of the NM algorithm. As mentioned in chapter 2, the algorithm strongly depends on the starting conditions to obtain reasonable results. The frequency of all four searches remains at approximately 2.596 GHz while the antenna length varies for every single search. The variable antenna length affects the maximum electric field intensity significantly.

Table 5.2: Search results of NM searches

Search	**Frequency** (GHz)	**Antenna length** (mm)	**Maximum Electric Field Intensity** (V/m)
1st	2.596 058	2.407	1.335×10^8
2nd	2.596 060	4.422	0.757×10^8
3rd	2.596 058	6.477	0.339×10^8
4th	2.596 058	6.503	0.335×10^8

For this simulation model a maximum electric field intensity of 1.473×10^8 V/m can be attained, as shown in section 4.3.4. An antenna length of 1.25 mm and a supply frequency of 2.5961 GHz is required to generate this maximum. This demonstrates that the first search nearly reaches the maximum with an electric field intensity of 1.355×10^8 V/m. Whereas the other three searches were unable to locate a sufficient electric field strength, they only reached a local extrema.

During the third and fourth searches the initial value for the antenna length was incapable of locating the possible maximum electric field intensity. The found maximum electric field intensity the searches reached was only a fraction of the maximum field strength possible.

5.3.2 Non-Deterministic search

In this section the non-deterministic optimisation search is implemented through the use of the Genetic Algorithm. The GA has some advantages and disadvantages as reviewed in section 3.6.2. In order to find the most suitable solution, the optimisation search will vary the supply frequency of the microwave generator and the antenna length ("HAntenna1") of the given simulation model in section 5.3. The investigation process includes two searches with the following starting conditions:

Table 5.3: Starting conditions of GA searches

Search	**Frequency** (GHz)	**Antenna length** (mm)
1st	2.55 - 2.65	0 - 10
2nd	2.5 - 2.7	0 - 20

Table 5.3 shows the initial values of the two searches. The chosen range for the supply frequency and the antenna length were influenced by the results of the single variable search for the antenna length in section 4.3.4. The optimisation settings and stopping criteria for the used algorithm were set to the following values:

- Display = final
- CrossoverFcn = crossoverscattered
- CrossoverFraction = 0.8
- MutationFraction = 0.2
- EliteCount = 2
- Generations = 40
- PopulationSize = 101
- SelectionFcn = selectionstochunif
- StallGenLimit = 20
- TimeLimit = Inf
- TolFun = 1E-6

These values are essential the default settings of the algorithm provided by the MATLAB optimisation toolbox. A change of these conditions at a later stage can improve the convergence and search performance or the overall search resolution.

1st Search

The first search employing the GA, uses the starting conditions defined in Table 5.3. The initial boundaries for the frequency are defined as 2.55 GHz to 2.65 GHz and the antenna length boundaries are 0 mm to 10 mm. The chosen range of the antenna length includes the value that delivers the best propagation performance inside the engine cylinder, see section 4.3.4. The defined frequency range covers the known frequency which leads to resonance of the cavity.

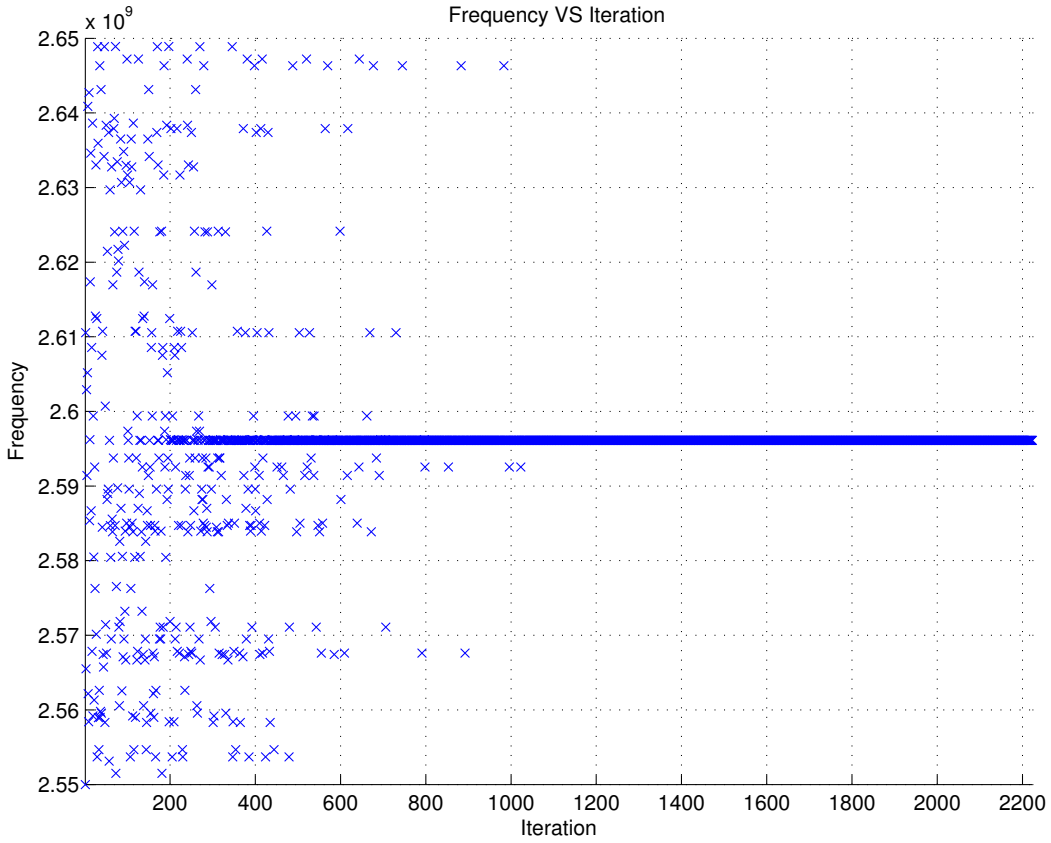

(a) Search trace for the supply frequency with the GA search method

Figure 5.8: GA search for the 1st set of initial parameters of Table 5.3

Figure 5.8 shows the trace of search and development of the different input variables and objectives by using the first set of initial parameters of Table 5.3. The search trace of the supply frequency, within a range of 2.55 GHz to 2.65 GHz, is displayed in Fig. 5.8a. The figure was built by connecting the values after each evaluation during the search process. Figure 5.8b demonstrates the search trace for the antenna length in the range from 0 mm to 10 mm for each step of the search process. The search point distribution between supply frequency and antenna length is presented in Fig. 5.8c. Figure 5.8d shows the maximum electric field intensity inside the cylinder during the search process.

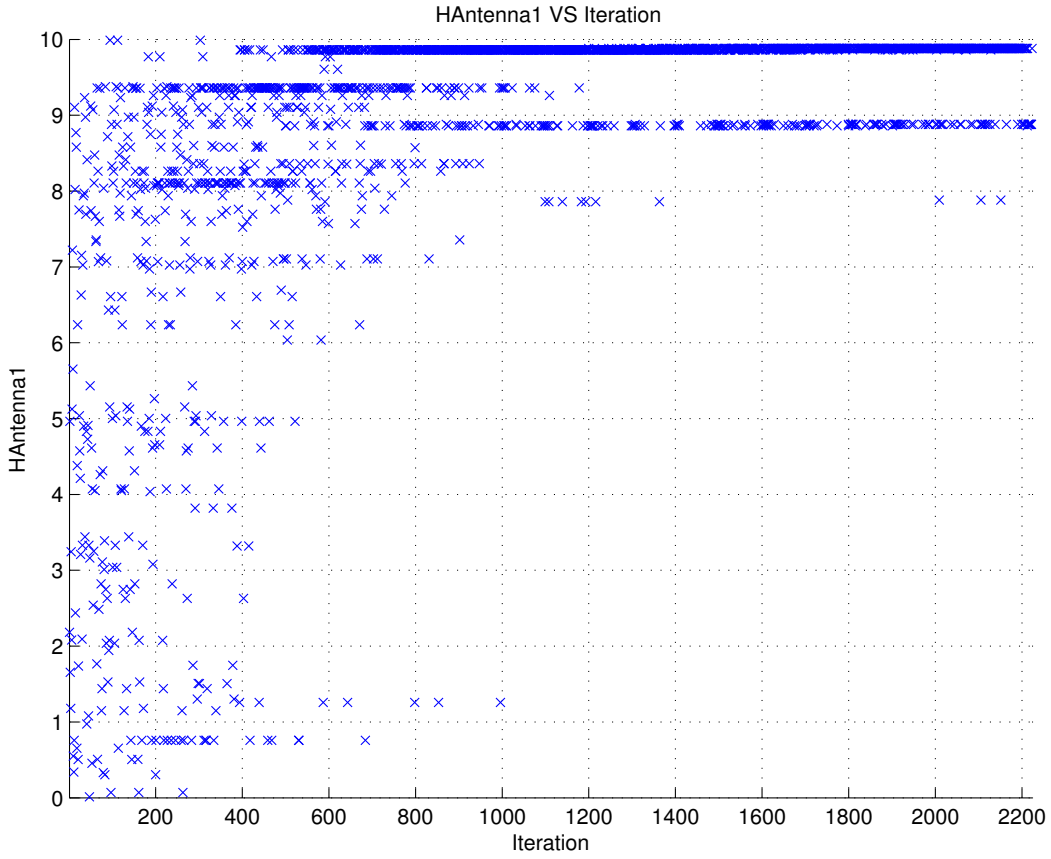

(b) Search trace for the antenna length with the GA search method

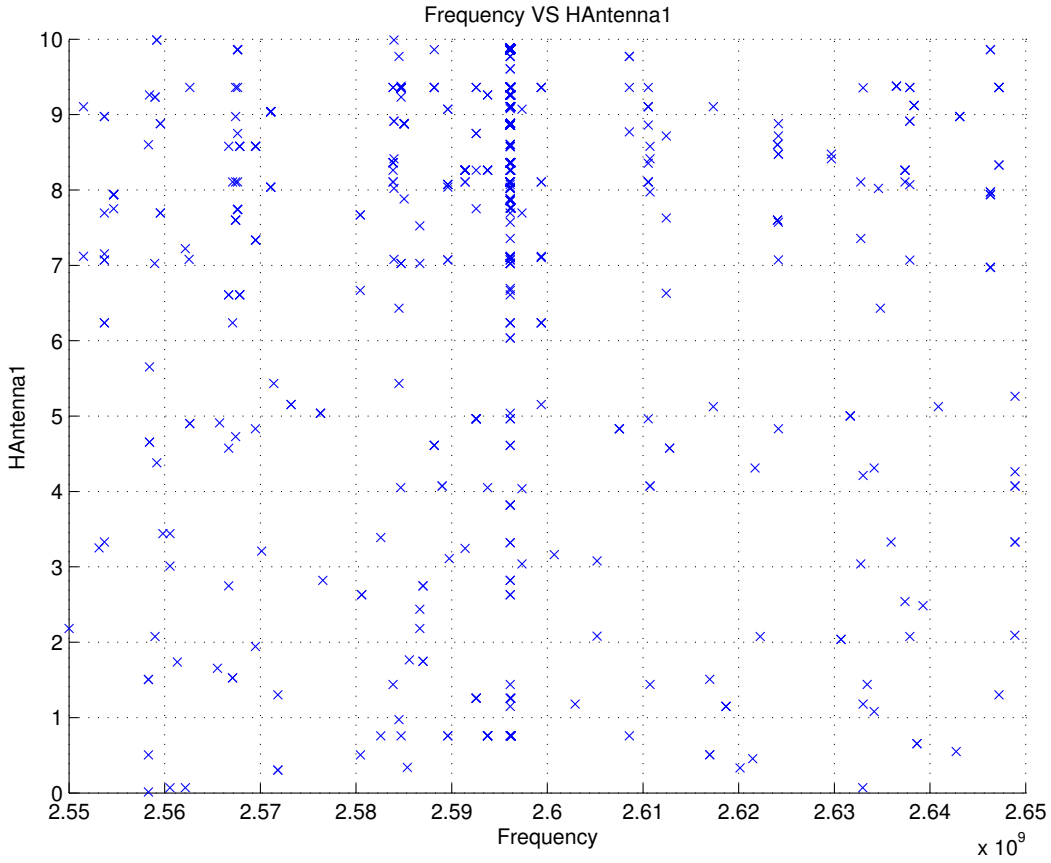

(c) Distribution of the search points of the supply frequency and antenna length

Figure 5.8: GA search for the 1st set of initial parameters of Table 5.3

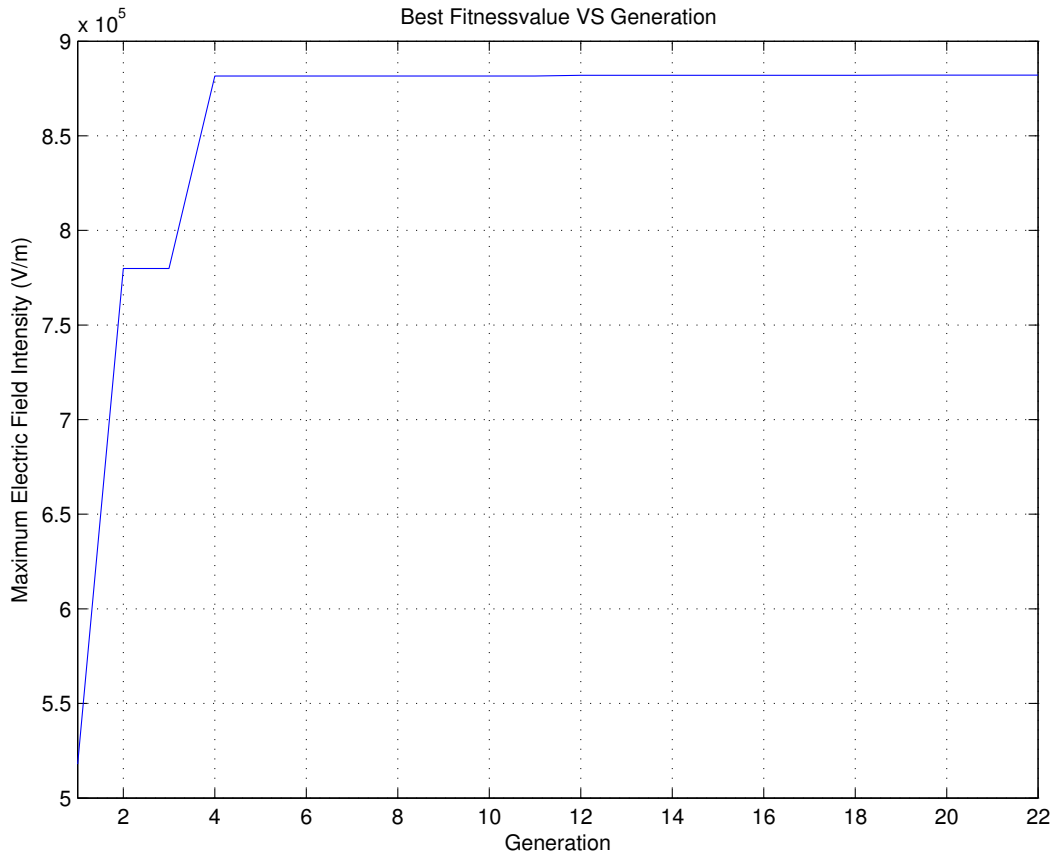

(d) Search trace for the maximum electric field intensity

Figure 5.8: GA search for the 1st set of initial parameters of Table 5.3

2nd Search

The second search employing the GA, uses the starting conditions defined in Table 5.3. The initial boundaries for the frequency are defined as 2.5 GHz to 2.7 GHz and the antenna length boundaries are 0 mm to 20 mm. The chosen range of the antenna length includes the value (1.25 mm) that delivers the best propagation performance inside the engine cylinder, see section 4.3.4. The defined frequency range covers the known frequency that causes resonance of the cavity.

Figure 5.9 shows the trace of search and development of the input variables by using the second set of initial parameters of Table 5.3. The search trace of the supply frequency, within a range of 2.5 GHz to 2.7 GHz, is displayed in Fig. 5.9a. The figure was built by connecting the values after each evaluation during the search process. Figure 5.9b shows the search trace for the antenna length in the range from 0 mm to 20 mm for every step of the search process. The search point distribution between supply frequency and antenna length is presented in Fig. 5.9c. Figure 5.9d shows the maximum electric field intensity inside the cylinder during the search process.

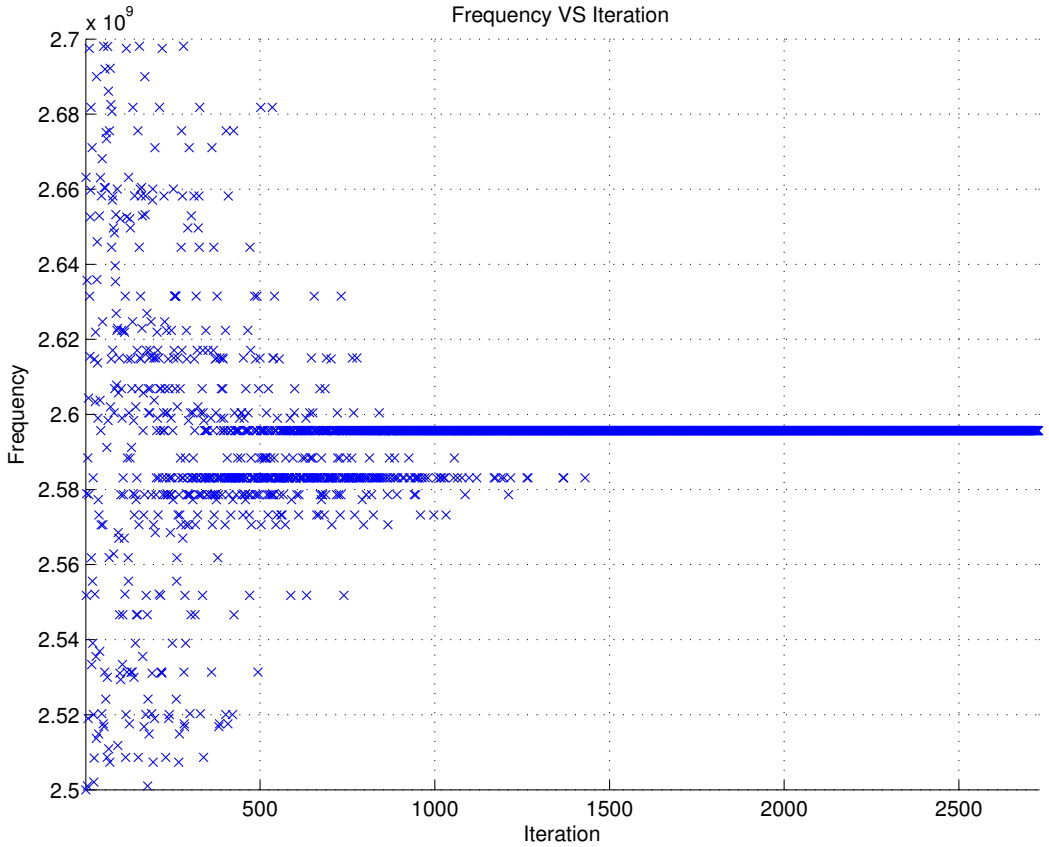

(a) Search trace for the supply frequency with the GA search method

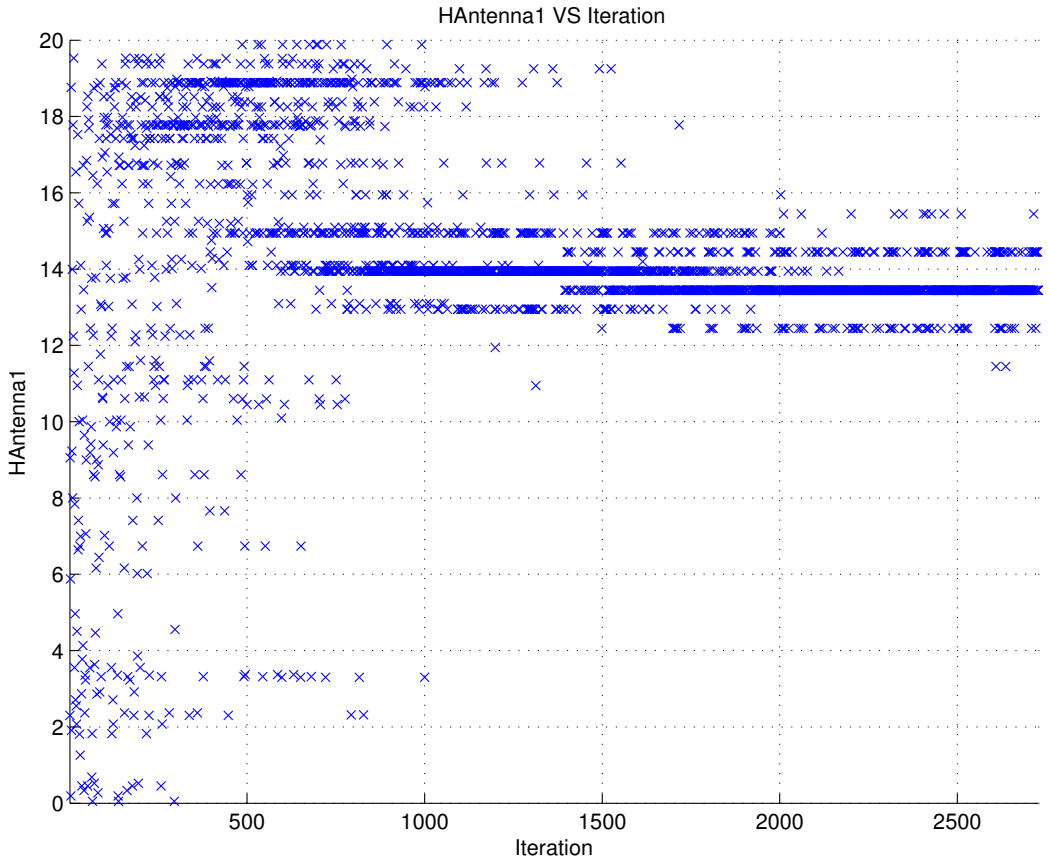

(b) Search trace for the antenna length with the GA search method

Figure 5.9: GA search for the 2nd set of initial parameters of Table 5.3

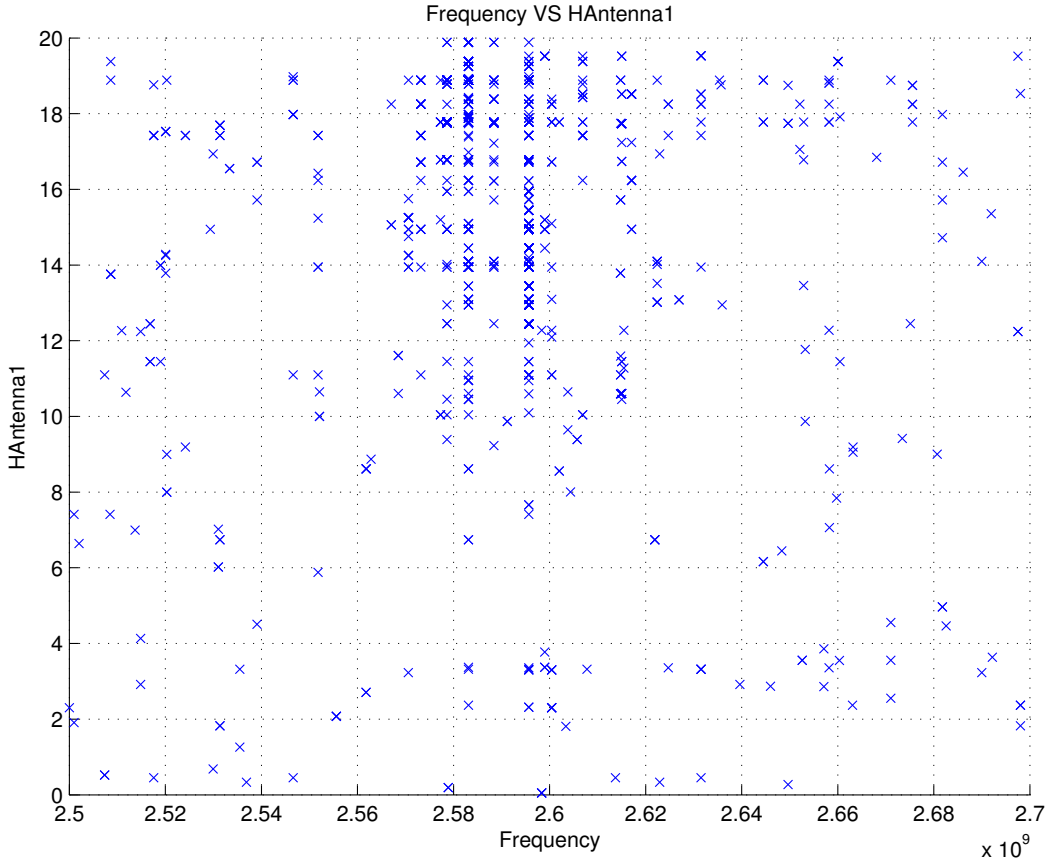

(c) Distribution of the search points of the supply frequency and antenna length

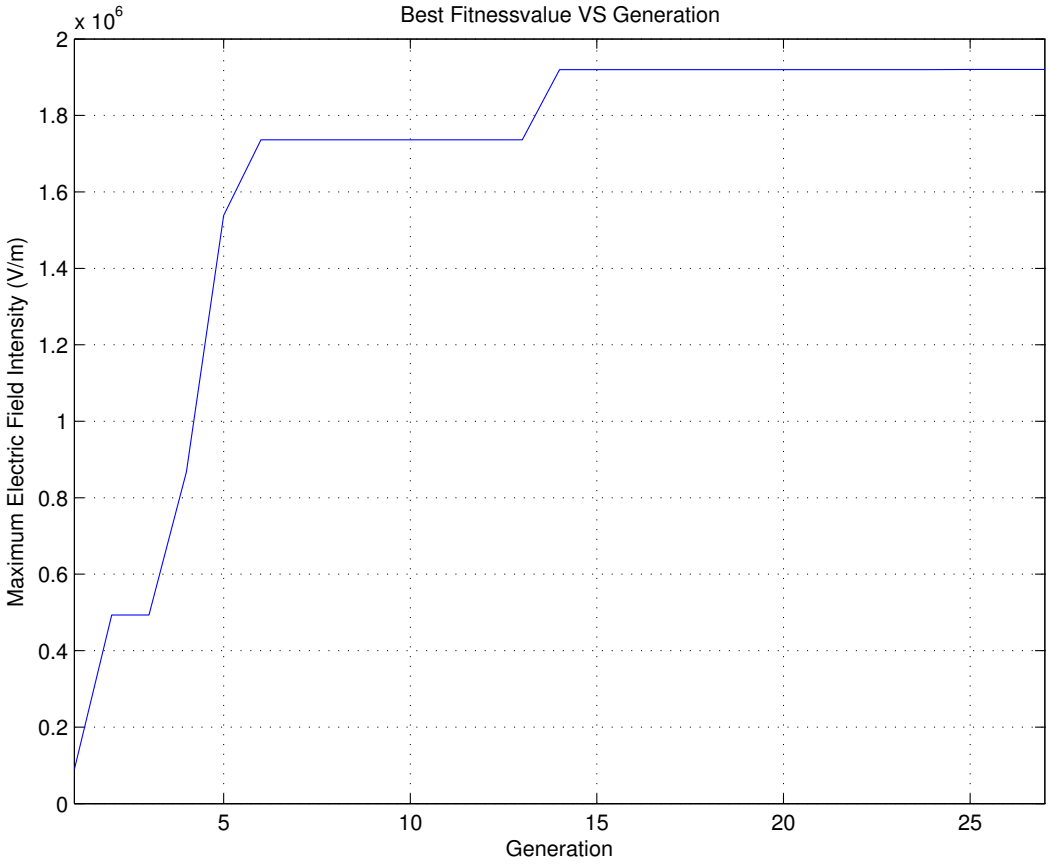

(d) Search trace for the maximum electric field intensity

Figure 5.9: GA search for the 2nd set of initial parameters of Table 5.3

Comparison

Figures 5.8 and 5.9 demonstrates how the GA search algorithm approaches the optimum solution. The GA search algorithm is a non-deterministic optimisation method and therefore the results will be inconsistent between different optimisation searches. Table 5.4 presents the results of the different searches, it can be seen that in contrast to the deterministic search in section 5.3.1 the gathered results are not sufficient.

Table 5.4: Search results of GA searches

Search	**Frequency** (GHz)	**Antenna length** (mm)	**Maximum Electric Field Intensity** (V/m)
1st	2.596 120	9.881	$0.882\,034 \times 10^6$
2nd	2.595 678	13.446	$1.920\,049 \times 10^6$

Previously mentioned in chapter 2, the GA requires more simulation evaluations than the NM algorithm in section 5.3.1. The resulted frequency of both optimisation searches is located at 2.596 120 GHz and 2.595 678 GHz, which can have a relatively high affect on the propagation performance. Even if the found supply frequencies are close, the antenna lengths vary between the searches which influences the electric field distribution inside the cavity.

For this simulation model, a maximum electric field intensity of 1.473×10^8 V/m can be attained (shown in section 4.3.4). To generate this maximum, an antenna length of 1.25 mm and a supply frequency of 2.5961 GHz is required. The two searches were unable to locate a sufficient electric field strength, they reached a local extrema. It can be summarised that both searches with the initial search range for the antenna length and the supply frequency were unsuitable for finding the global maximum electric field intensity. The maximum electric field intensity found is significantly less than the possible maximum field strength at the top of the cylinder for this model (see section 4.3.4).

5.3.3 Predefined search

Sections 5.3.1 and 5.3.2 employed the deterministic and non-deterministic searches to solve the optimisation problem of section 5.3. For the given problem, with two input parameters (supply frequency and antenna length), the NM optimisation search has shown a better performance than the GA search. This section uses the predefined

search algorithm, described in section 5.2, to analyse the performance of this newly designed search. This algorithm combines the advantages of both search techniques. The PGA algorithm will be applied in order to find the best solution by varying the supply frequency of the microwave generator and the antenna length ("HAntenna1") for the given simulation model in section 5.3. The whole search process includes two searches with the following starting conditions:

Table 5.5: Starting conditions of PGA searches

Search	**Frequency** (GHz)	**Antenna length** (mm)
1st	Not required	0 - 10
2nd	Not required	0 - 20

Table 5.5 shows the initial values of the two searches performed in this section. The selected starting condition for the antenna length was influenced by the results from the single variable change in the antenna length in section 4.3.4. It is not required to define a starting value for the supply frequency because the minimum necessary frequency range will be calculated during the search process. The optimisation settings and stopping criteria for the NM part of the combined search algorithm were set to the following:

- Display = final
- MaxFunEvals = 500
- MaxIter = 500
- TolFun = 1E-4
- TolX = 1E-4

The optimisation settings and stopping criteria for the GA part of the combined search algorithm were set to the following:

- Display = final
- CrossoverFcn = crossoverscattered
- CrossoverFraction = 0.8
- MutationFraction = 0.2
- EliteCount = 2

- Generations = 40
- PopulationSize = 101
- SelectionFcn = selectionstochunif
- StallGenLimit = 20
- TimeLimit = Inf
- TolFun = 1E-6

These values are essentially the default settings of the NM and GA provided by the MATLAB optimisation toolbox. A variation of these conditions at a later stage can improve the convergence and search performance or the overall search resolution.

1st Search

The first search employing the PGA uses the starting conditions defined in Table 5.5. The antenna length during this search can range from 0 mm to 10 mm. The defined

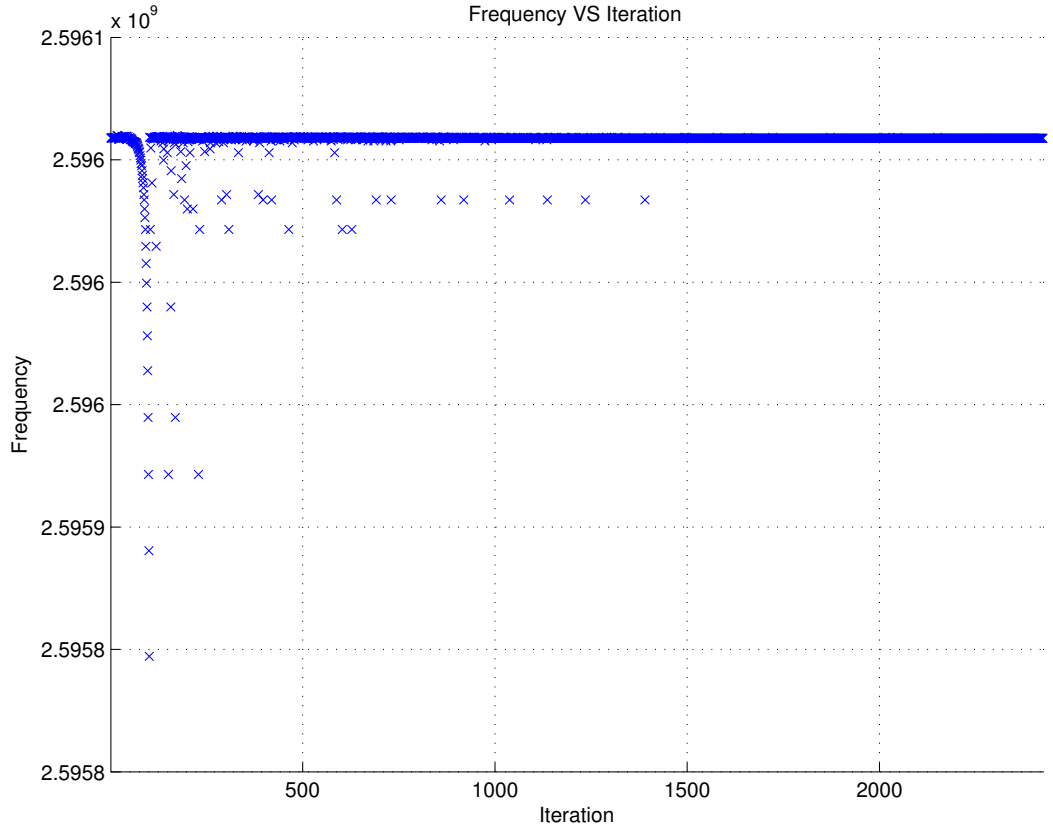

(a) Search trace for the supply frequency with the PGA search method

Figure 5.10: PGA search for the 1st set of initial parameters of Table 5.5

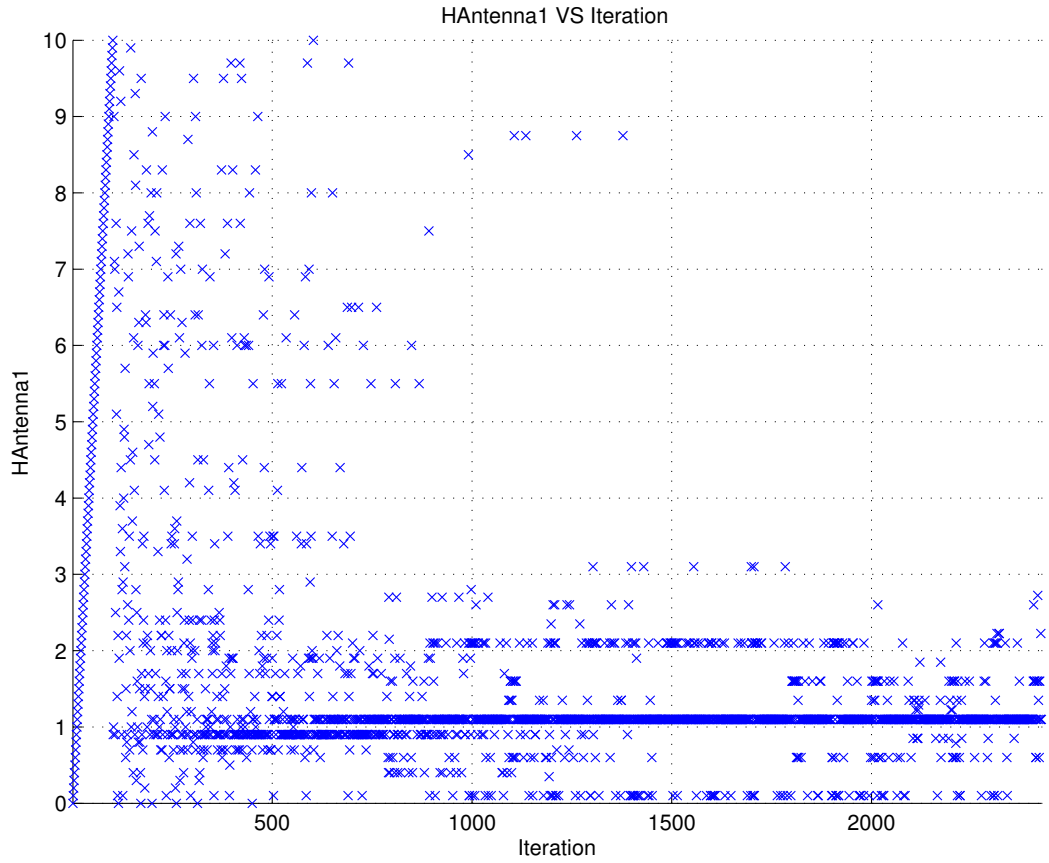

(b) Search trace for the antenna length with the PGA search method

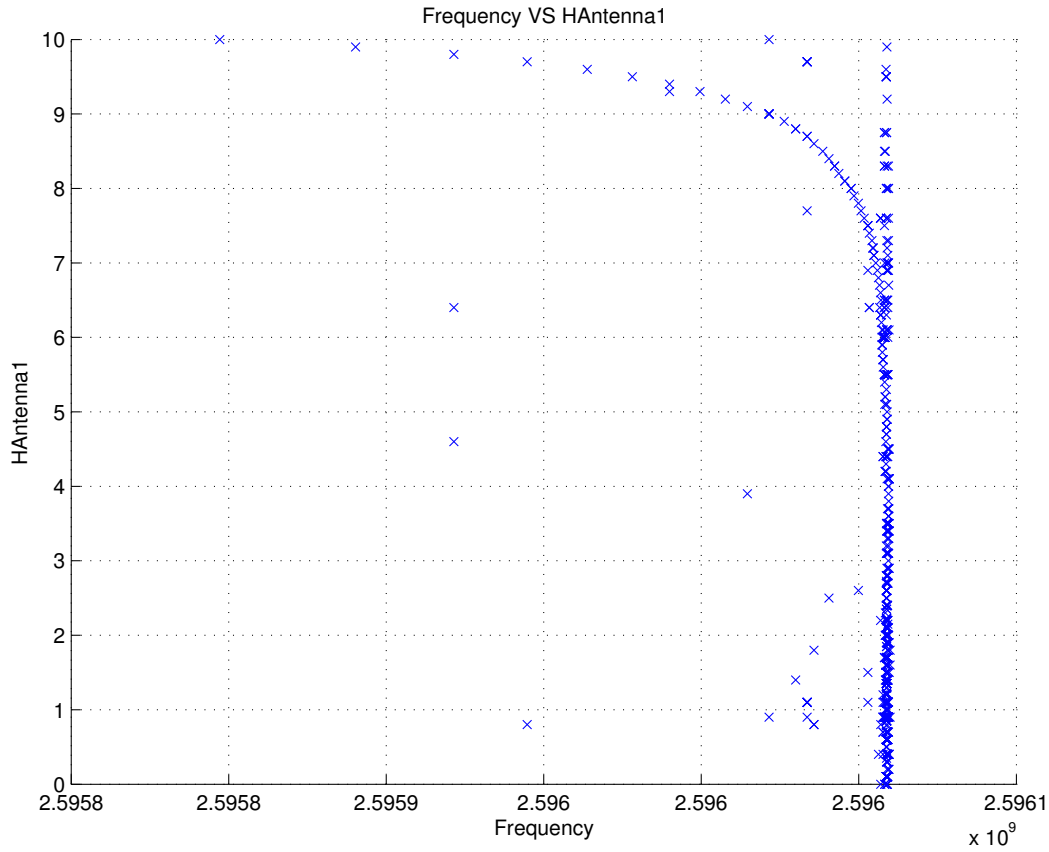

(c) Distribution of the search points of the supply frequency and antenna length

Figure 5.10: PGA search for the 1st set of initial parameters of Table 5.5

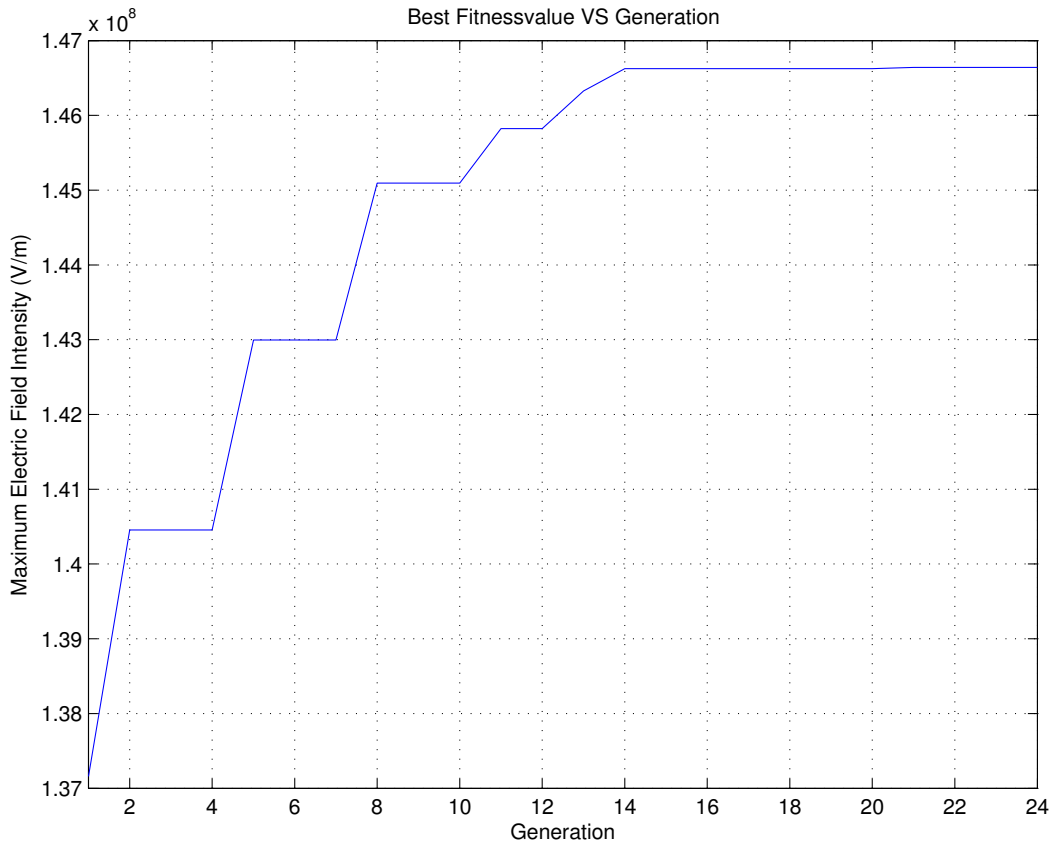

(d) Search trace for the maximum electric field intensity

Figure 5.10: PGA search for the 1st set of initial parameters of Table 5.5

range of the antenna length includes the already known antenna length of 1.25 mm which delivers the best propagation performance inside the combustion cylinder (see section 4.3.4). Aforementioned, a frequency range is not required and will be calculated prior to the optimisation search.

Figure 5.10 shows the search trace and development of the different input variables and objectives by using the first set of initial parameters of Table 5.5. The search trace of the supply frequency, within the previously calculated range, is displayed in Fig. 5.10a. The figure was built by connecting the values after each evaluation during the search process. Figure 5.10b shows the search trace for the antenna length in the range from 0 mm to 10 mm for every step of the search process. The search point distribution between supply frequency and antenna length is demonstrated in Fig. 5.10c. Figure 5.10d shows the maximum electric field intensity inside the cylinder during the search process.

2nd Search

The second search employing the PGA uses the starting conditions defined in Table 5.5. The antenna length during this search can range from 0 mm to 20 mm. The defined range of the antenna length includes the already known antenna length of 1.25 mm that renders the best propagation performance inside the combustion cylinder (see section 4.3.4). Aforementioned, a frequency range is not required.

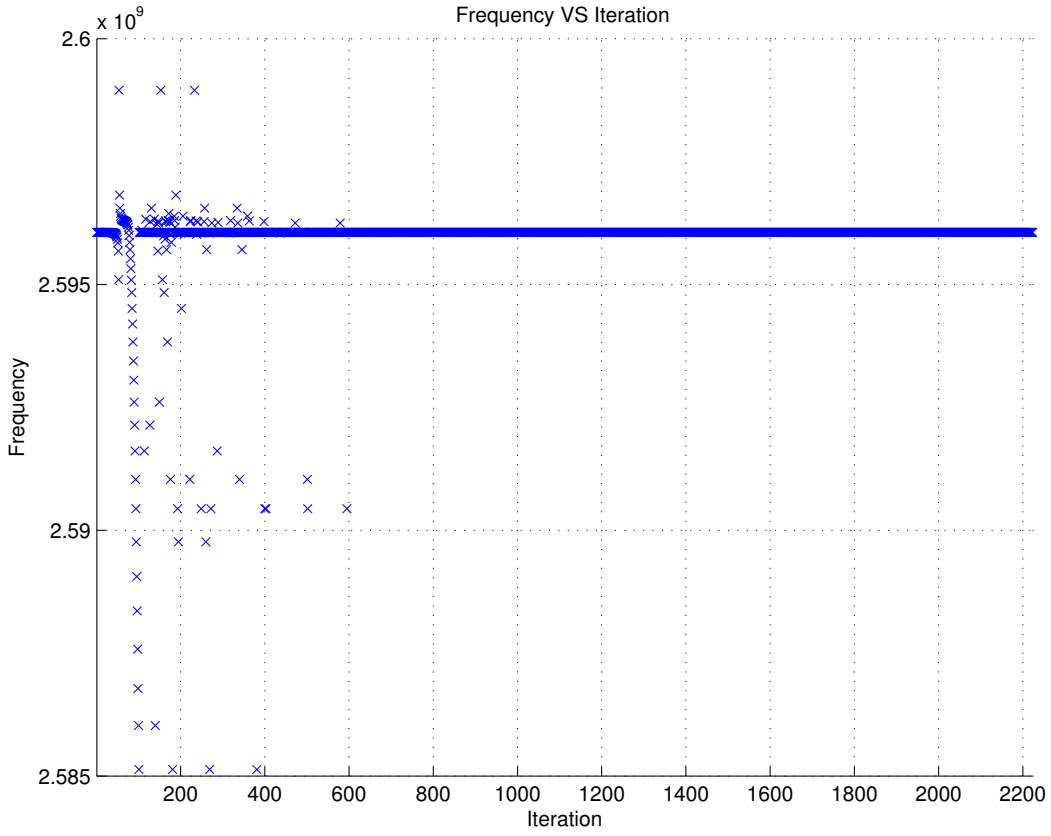

(a) Search trace for the supply frequency with the PGA search method

Figure 5.11: PGA search for the 2nd set of initial parameters of Table 5.5

Figure 5.11 shows the trace of search and development of the different input variables and objectives by using the second set of initial parameters of Table 5.5. The search trace of the supply frequency, within the previously calculated range, is displayed in Fig. 5.11a. The figure was built by connecting the values after each evaluation during the search process. Figure 5.11b shows the search trace for the antenna length in the range from 0 mm to 20 mm for each step of the search process. The search point distribution between supply frequency and antenna length is presented in Fig. 5.11c. Figure 5.11d shows the maximum electric field intensity inside the cylinder during the search process.

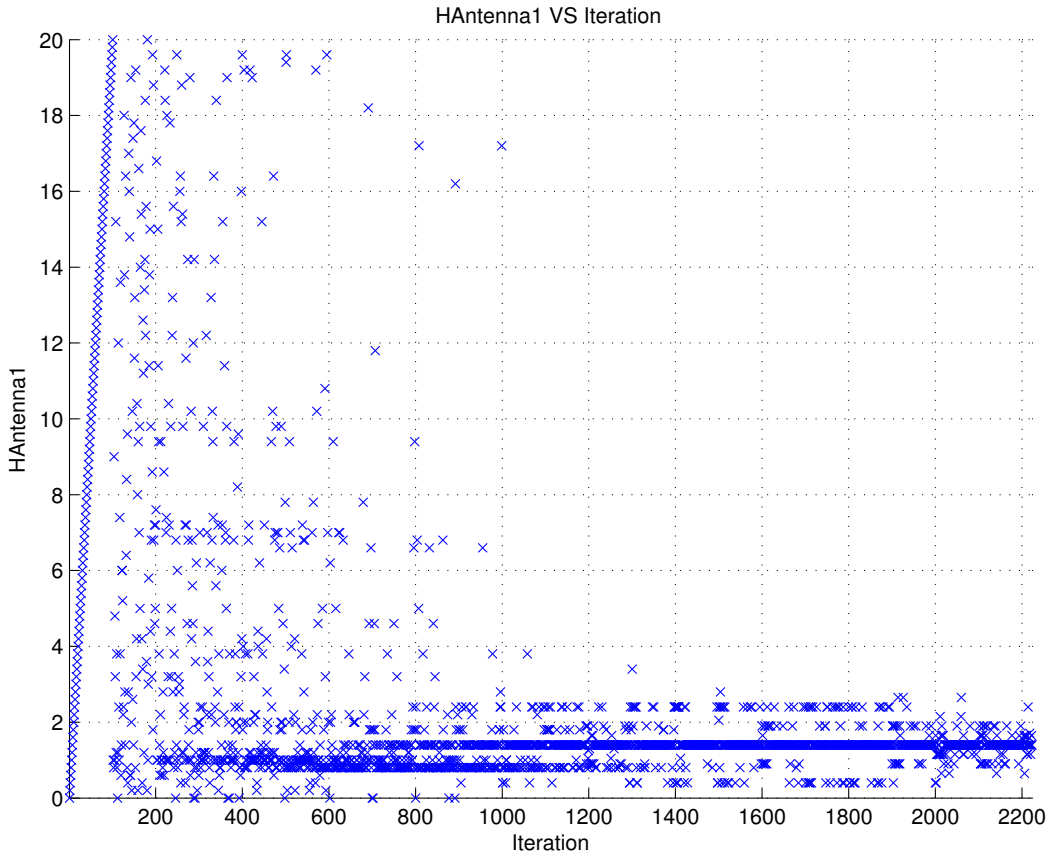

(b) Search trace for the antenna length with the PGA search method

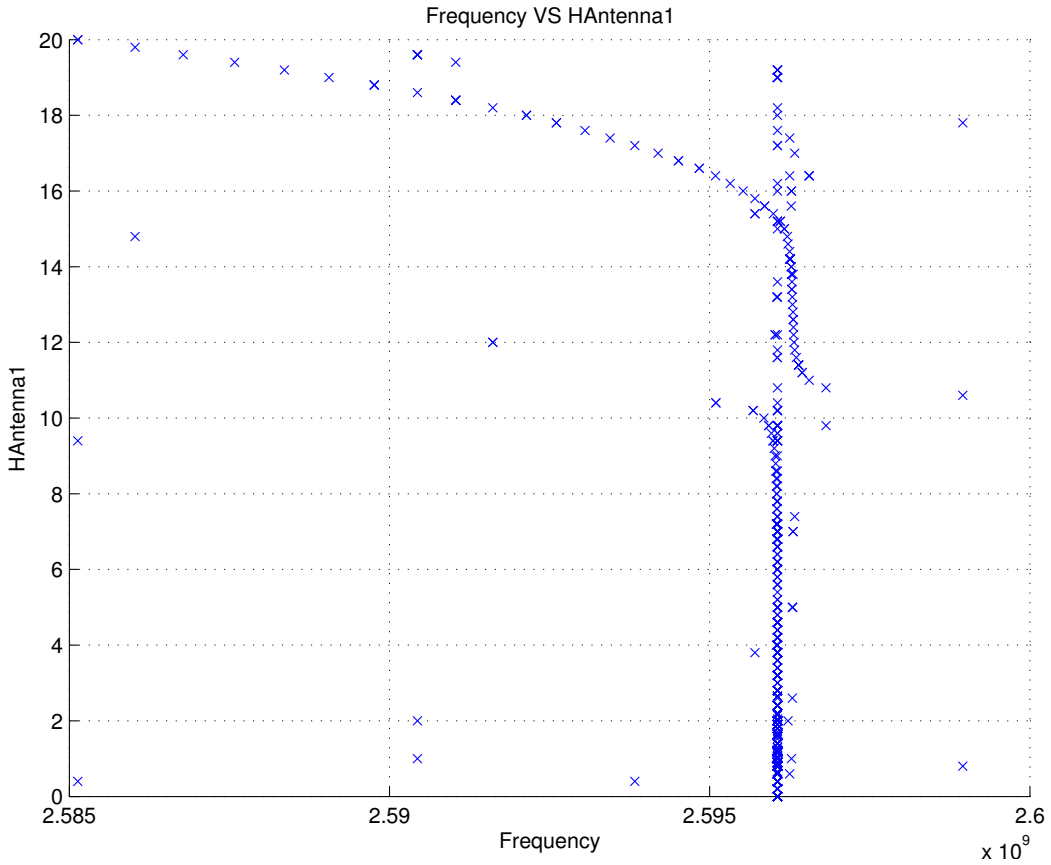

(c) Distribution of the search points of the supply frequency and antenna length

Figure 5.11: PGA search for the 2nd set of initial parameters of Table 5.5

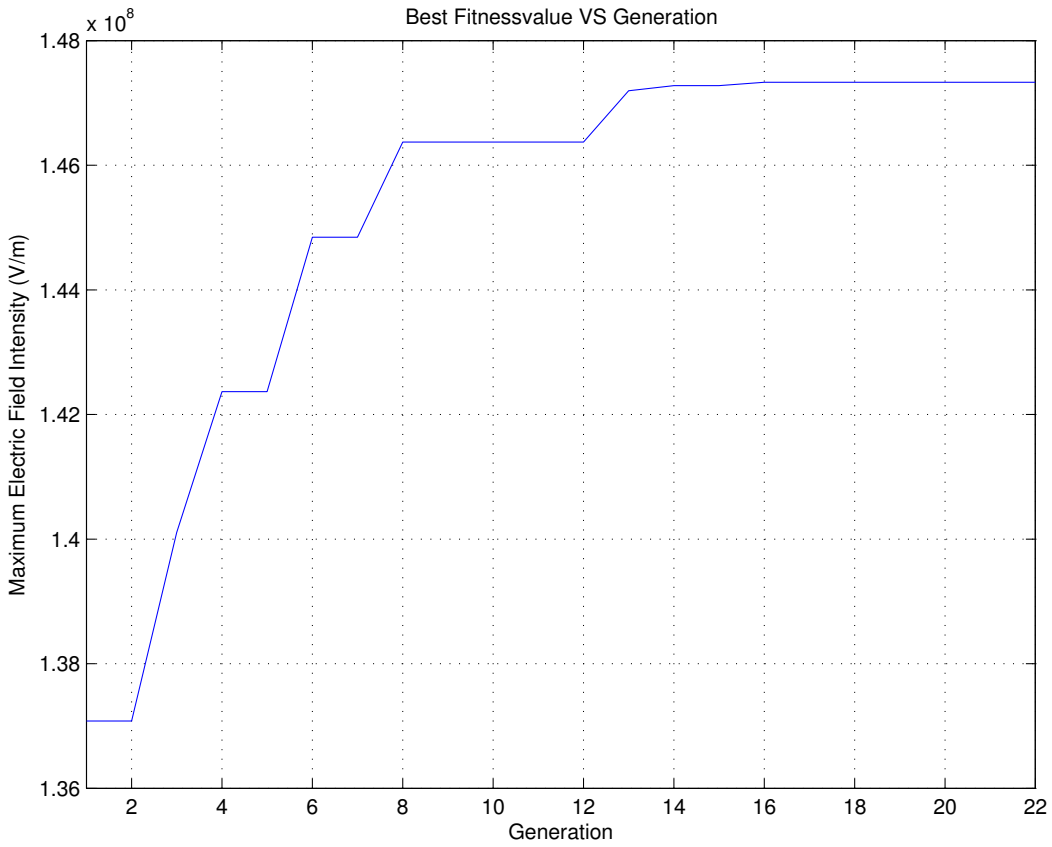

(d) Search trace for the maximum electric field intensity

Figure 5.11: PGA search for the 2nd set of initial parameters of Table 5.5

Comparison

Figures 5.10 and 5.11 demonstrates the way of how the PGA search algorithm approaches the optimum solution. The PGA search algorithm combines the deterministic and the non-deterministic optimisation methods, hence the results might alternate between multiple searches. Table 5.6 presents the search results. It can be seen that the PGA shows a much better performance than the GA in section 5.3.2, but is comparable to the NM algorithm in section 5.3.1.

Table 5.6: Search results of PGA searches

Search	**Frequency** (GHz)	**Antenna length** (mm)	**Maximum Electric Field Intensity** (V/m)
1st	2.596 059	1.154	1.466×10^8
2nd	2.596 059	1.401	1.473×10^8

As described in section 5.2, the PGA combines the advantages of the NM algorithm and the GA optimisation search to obtain the most suitable antenna design for a

given model. It can be seen in Table 5.6 that the found supply frequency of both searches is approximately 2.596 059 GHz. The found antenna lengths vary slightly which affects the maximum electric field intensity inside the engine cylinder. The maximum possible electric field intensity for this cylinder and antenna model was determined in section 4.3.4, and is approximately 1.473×10^8 V/m for an antenna length of 1.25 mm and a supply frequency of 2.5961 GHz.

The PGA is a combination of a deterministic and non-deterministic optimisation search and therefore the solution process includes a random factor. This factor makes it theoretically possible to achieve a better maximum electric field intensity inside the cylinder even if the search range for the input variables is larger. It can be summarised that both searches, with the given initial search range for the antenna length, were capable of finding the global maximum electric field intensity. The obtained maximum electric field intensity at the top of the cylinder is approximately the same as the global maximum inside the cavity, found in section 4.3.4.

5.4 Combination of Frequency, Antenna Length, Antenna Height, and Antenna Width

The combination of the frequency and the antenna length, in section 5.3, demonstrated a simple multivariable optimisation problem. The optimisation problem in this section, uses an extended antenna model which includes more input variables and determines the performance of the different optimisation methods for the application of the HCMI system. As previously mentioned, the supply frequency for the HCMI system is the most sensitive input, therefore it is essential to determine the starting conditions of the search algorithms very precisely.

The supply frequency together with the antenna length, the antenna height, and the antenna width are the input variables for the given system. The influence of the single variable changes were investigated in section 4.3.4 for the antenna length ("HAntenna1"), in section 4.4.1 for the antenna height ("HAntenna2"), and in section 4.4.2 for the antenna width ("WAntenna1").

Figure 5.12 shows the extended antenna model used for the optimisation search. Section 5.4.1 applies the deterministic NM algorithm to find the most advantageous propagation performance inside the combustion chamber. Sections 5.4.2 and 5.4.3 use the GA as well as the PGA to further analyse the optimisation problem and to compare the performance between the different search algorithms.

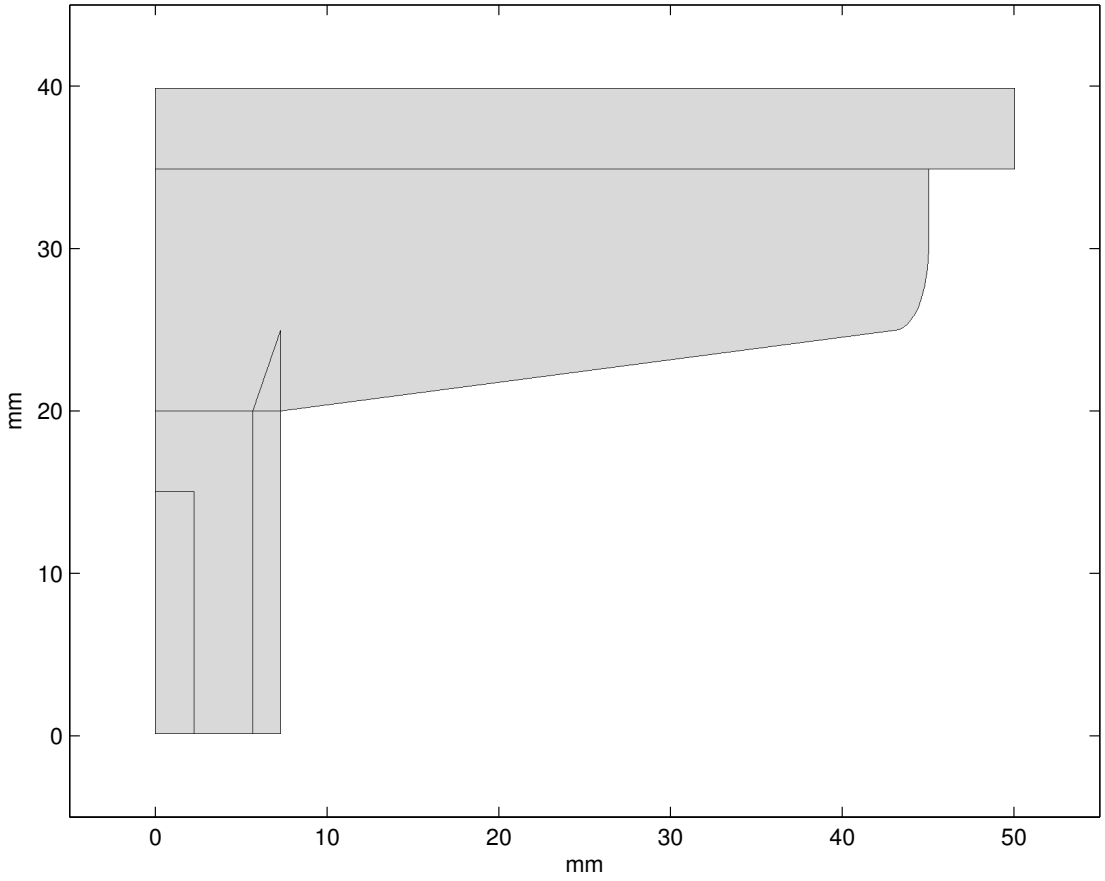

Figure 5.12: Extended antenna model

5.4.1 Deterministic search

The deterministic optimisation search in this section is implemented by using the NM simplex algorithm. The advantages and the disadvantages of the NM algorithm are reviewed in section 3.6.1. In order to find the most suitable solution, this optimisation search will vary the supply frequency of the microwave generator, the antenna length ("HAntenna1"), the antenna height ("HAntenna2"), and the antenna width ("WAntenna2") of the given simulation model in section 5.4. The whole investigation process includes four searches with the following starting conditions:

Table 5.7: Starting conditions of NM searches

Search	**Frequency** (GHz)	**Antenna length** (mm)	**Antenna height** (mm)	**Antenna width** (mm)
1st	2.55	5	5	2
2nd	2.55	10	7	5
3rd	2.59	5	5	2
4th	2.59	10	7	5

Table 5.7 shows the initial values of the four searches. The chosen starting conditions

for the supply frequency, the antenna length, the antenna height, and the antenna width were influenced by the results of the single variable searches in sections 4.3.4, 4.4.1 and 4.4.2. The optimisation settings and stopping criteria for the used algorithm were set to the following values:

- Display = final
- MaxFunEvals = 500
- MaxIter = 500
- TolFun = 1E-4
- TolX = 1E-4

These values are the default settings of the algorithm provided by the MATLAB optimisation toolbox. At a later stage varying these conditions can improve the convergence and search performance or the overall search resolution.

1st Search

The first search, employing the NM algorithm, uses the starting conditions defined in Table 5.7. The initial value for the frequency was defined as 2.55 GHz, the antenna length as 5 mm, the antenna height as 5 mm, and the antenna width started at 2 mm. The chosen starting value for the supply frequency is about 50 MHz lower than the approximate frequency that causes resonance of the cavity.

Figure 5.13 shows the trace of search and development of the different input variables and objectives by using the first set of initial parameters of Table 5.7. The search trace of the supply frequency, with an initial value of 2.55 GHz, is displayed in Fig. 5.13a. The figure was created by connecting the value after each evaluation during the search process. Figure 5.13b shows the search point distribution between the antenna length and antenna height with both starting at 5 mm. The search point distribution between the antenna height and antenna width is presented in Fig. 5.13c. Figure 5.13d demonstrates the maximum electric field intensity inside the cylinder during the search process.

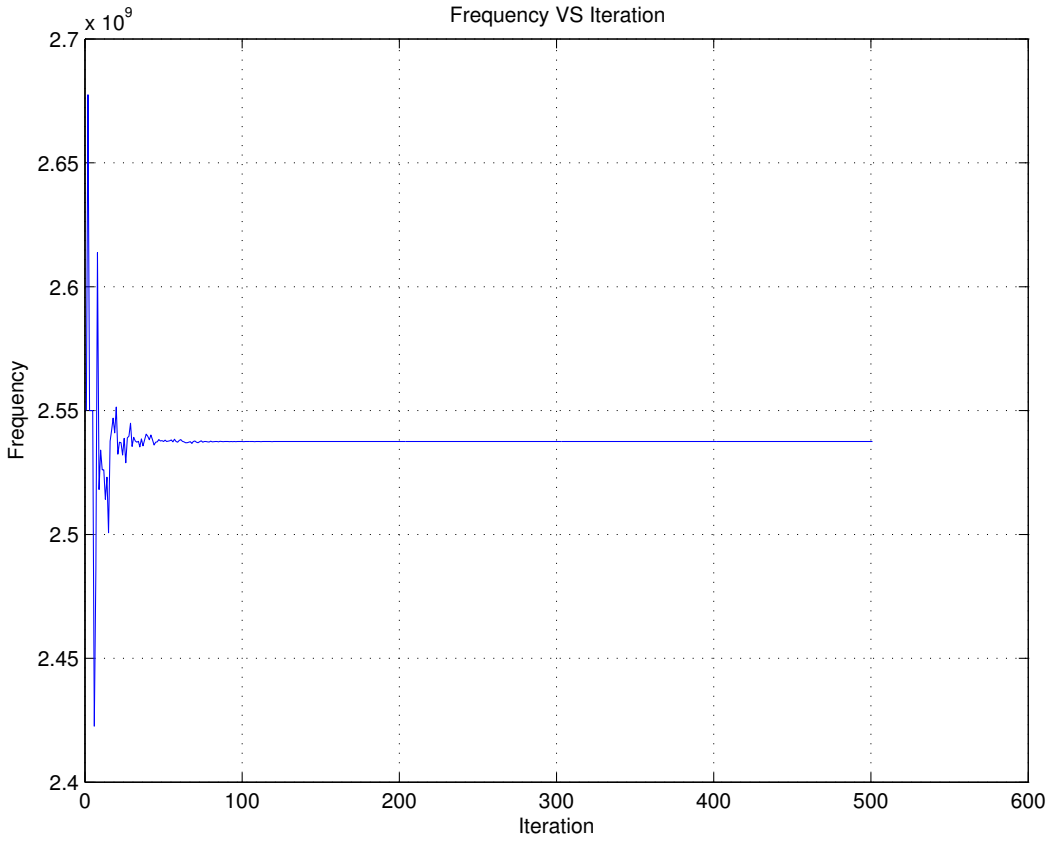

(a) Search trace for the supply frequency with the NM search method

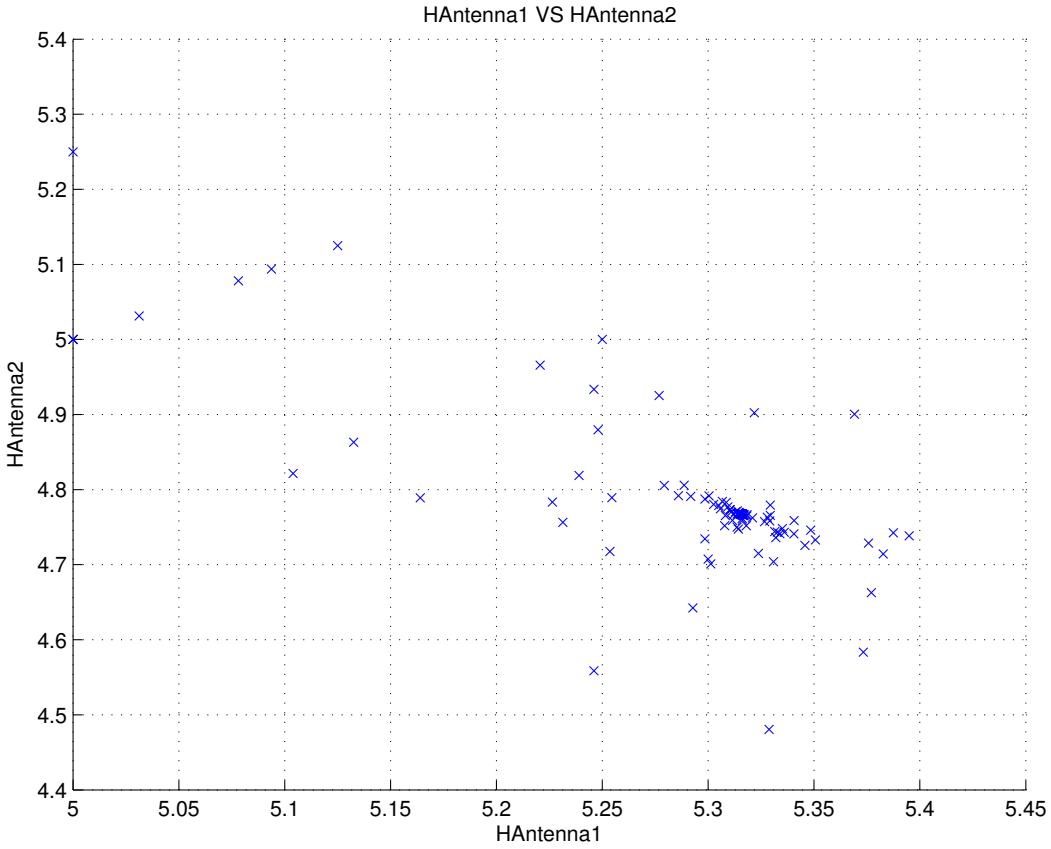

(b) Distribution of the search points of the antenna length and antenna height

Figure 5.13: NM search for the 1st set of initial parameters of Table 5.7

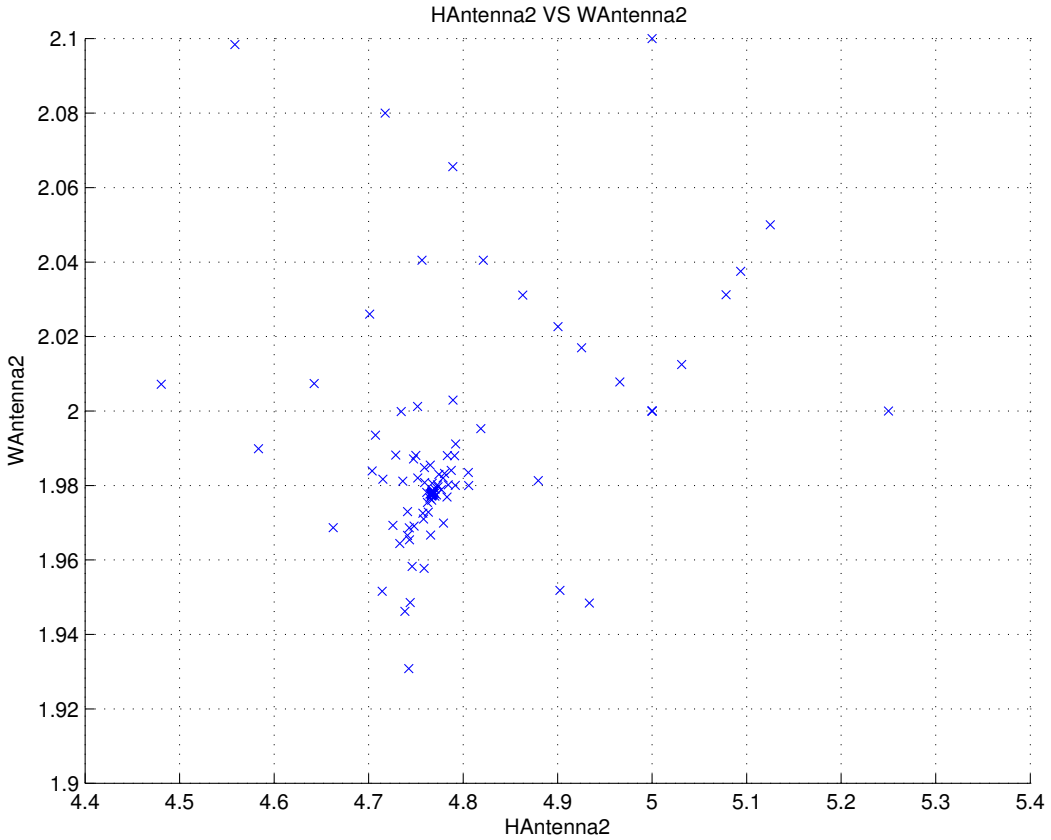

(c) Distribution of the search points of the antenna height and antenna width

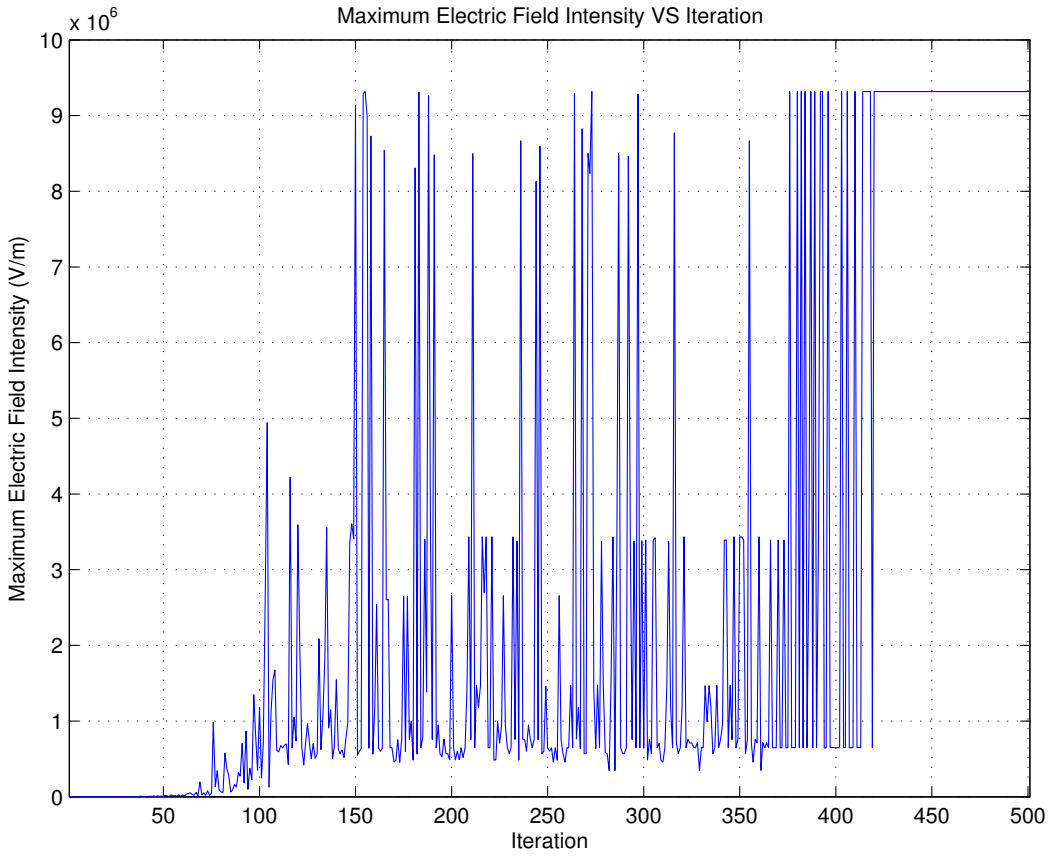

(d) Search trace for the maximum electric field intensity

Figure 5.13: NM search for the 1st set of initial parameters of Table 5.7

2nd Search

The second search employing the NM algorithm, uses the starting conditions defined in Table 5.7. The initial value for the frequency was defined as 2.55 GHz, the antenna length as 10 mm, the antenna height as 7 mm, and the antenna width started at 5 mm. The chosen starting value for the supply frequency is about 50 MHz lower than the approximate frequency which leads to resonance of the cavity.

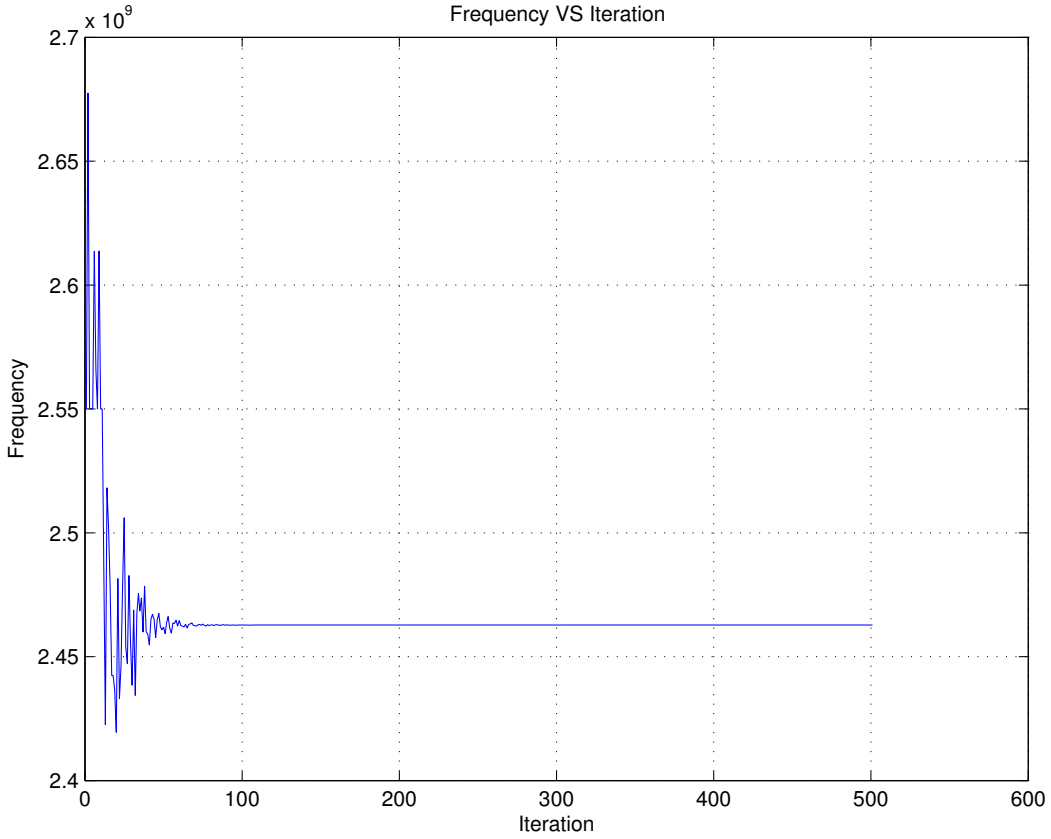

(a) Search trace for the supply frequency with the NM search method

Figure 5.14: NM search for the 2nd set of initial parameters of Table 5.7

Figure 5.15 shows the trace of search and development of the different input variables and objectives by using the second set of initial parameters of Table 5.7. The search trace of the supply frequency, with an initial value of 2.55 GHz, is displayed in Fig. 5.14a. The figure was created by connecting the value after each evaluation during the search process. Figure 5.14b shows the search point distribution between the antenna length and antenna height starting at 10 mm and 7 mm respectively. The search point distribution between the antenna height and antenna width is presented in Fig. 5.14c. Figure 5.15a shows the maximum electric field intensity inside the cylinder during the search process.

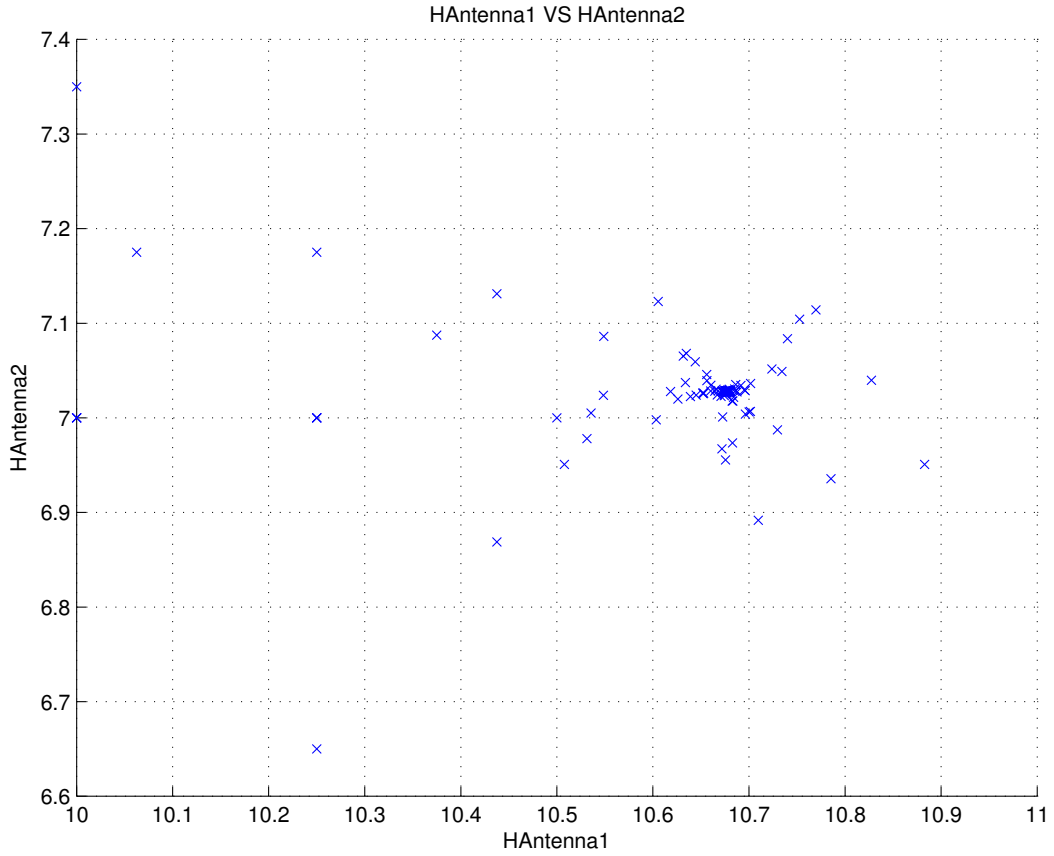

(b) Distribution of the search points of the antenna length and antenna height

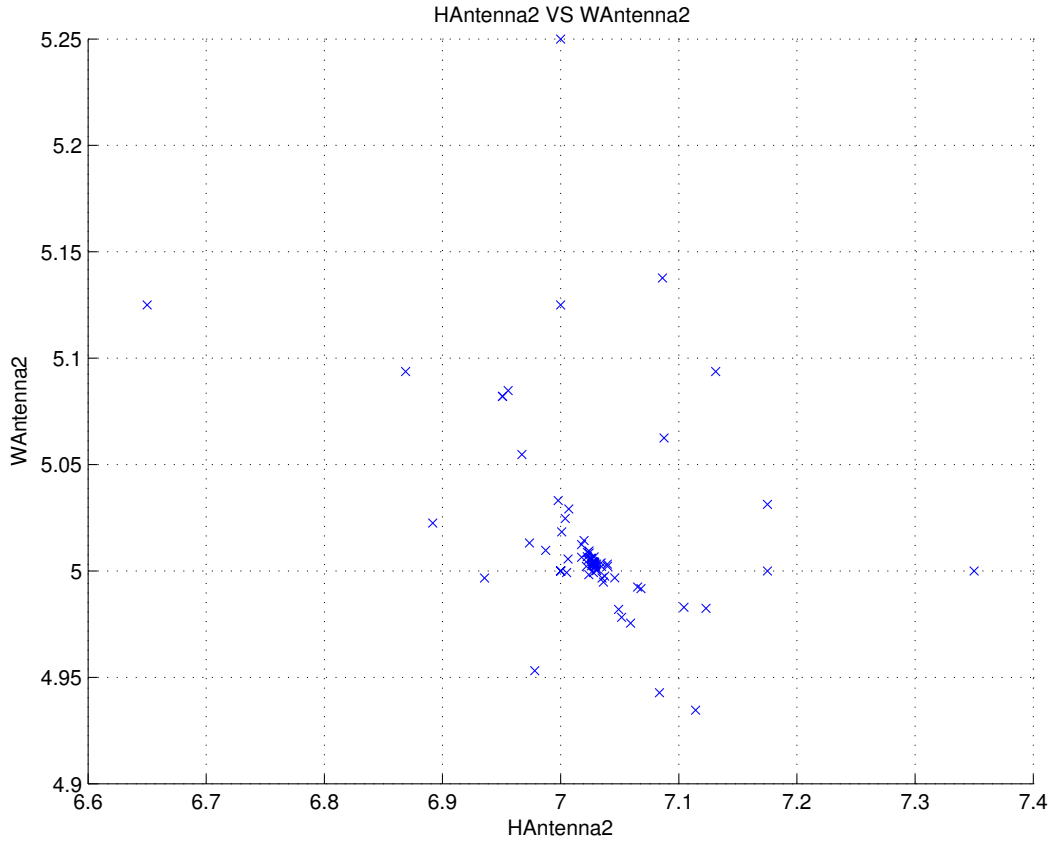

(c) Distribution of the search points of the antenna height and antenna width

Figure 5.14: NM search for the 2nd set of initial parameters of Table 5.7

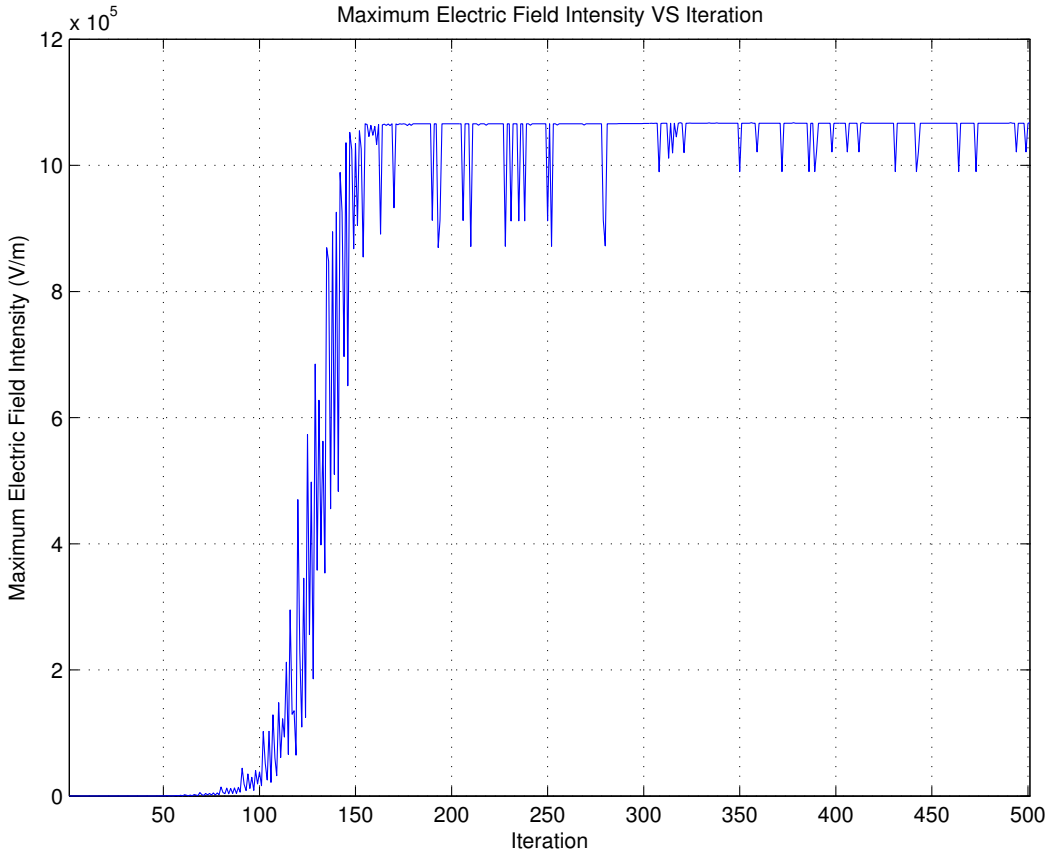

(a) Search trace for the maximum electric field intensity

Figure 5.15: NM search for the 2nd set of initial parameters of Table 5.7

3rd Search

The third search employing the NM algorithm, uses the starting conditions defined in Table 5.7. The initial value for the frequency was defined as 2.59 GHz, the antenna length as 5 mm, the antenna height as 5 mm, and the antenna width started at 2 mm. The chosen starting value for the supply frequency is about 50 MHz lower than the approximate frequency which leads to resonance of the cavity.

Figure 5.16 shows the trace of search and development of the different input variables and objectives by using the third set of initial parameters of Table 5.7. The search trace of the supply frequency, with an initial value of 2.59 GHz, is displayed in Fig. 5.16a. The figure was created by connecting the value after each evaluation during the search process. Figure 5.16b shows the search point distribution between the antenna length and antenna height both at 5 mm starting. The search point distribution between the antenna height and antenna width is presented in Fig. 5.16c. Figure 5.16d shows the maximum electric field intensity inside the cylinder during the search process.

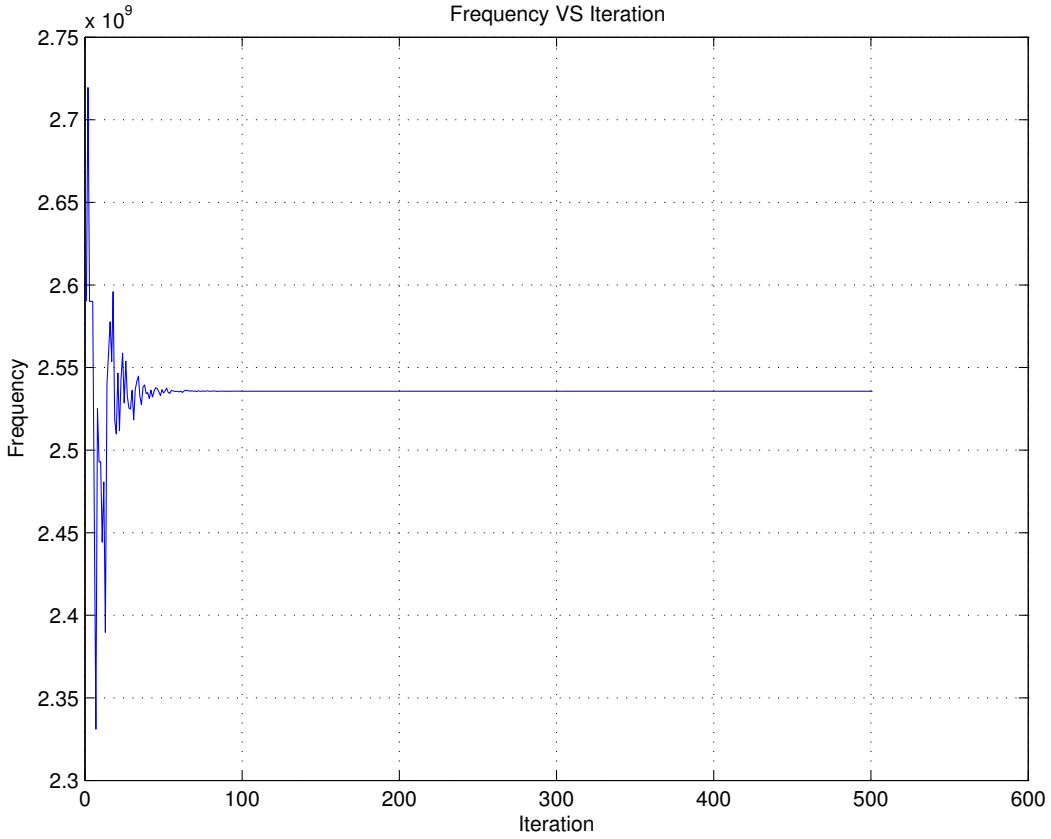

(a) Search trace for the supply frequency with the NM search method

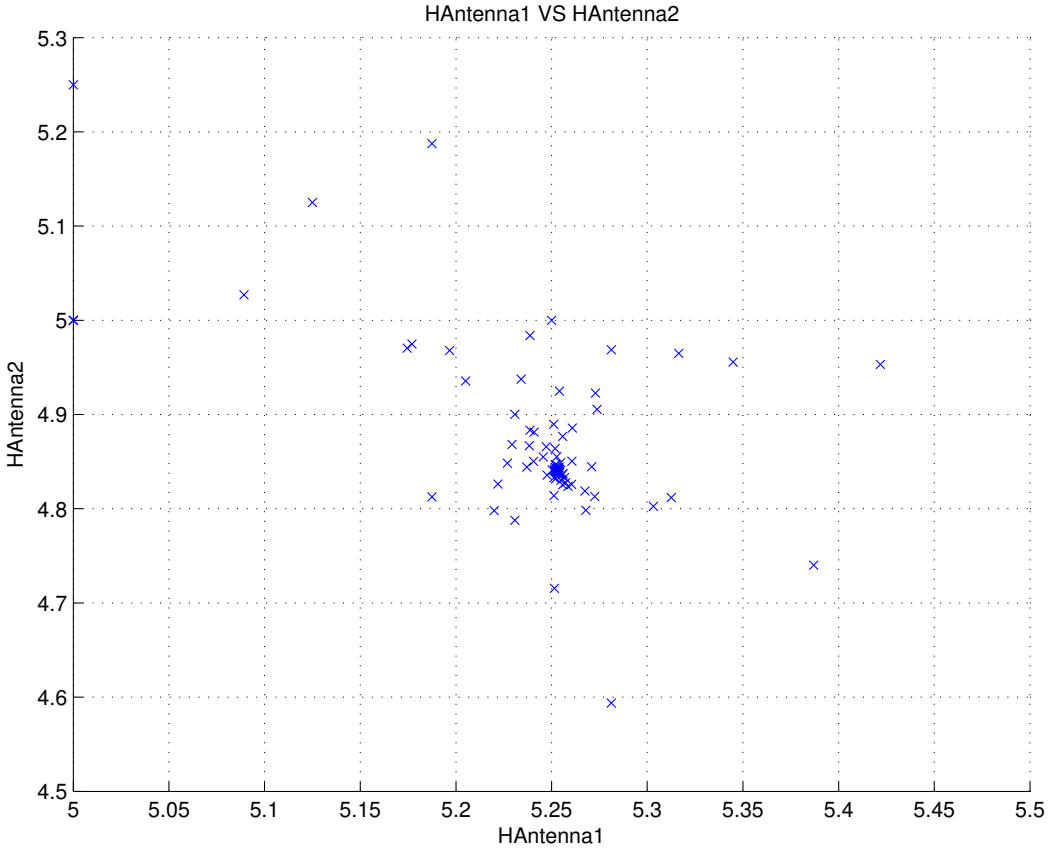

(b) Distribution of the search points of the antenna length and antenna height

Figure 5.16: NM search for the 3rd set of initial parameters of Table 5.7

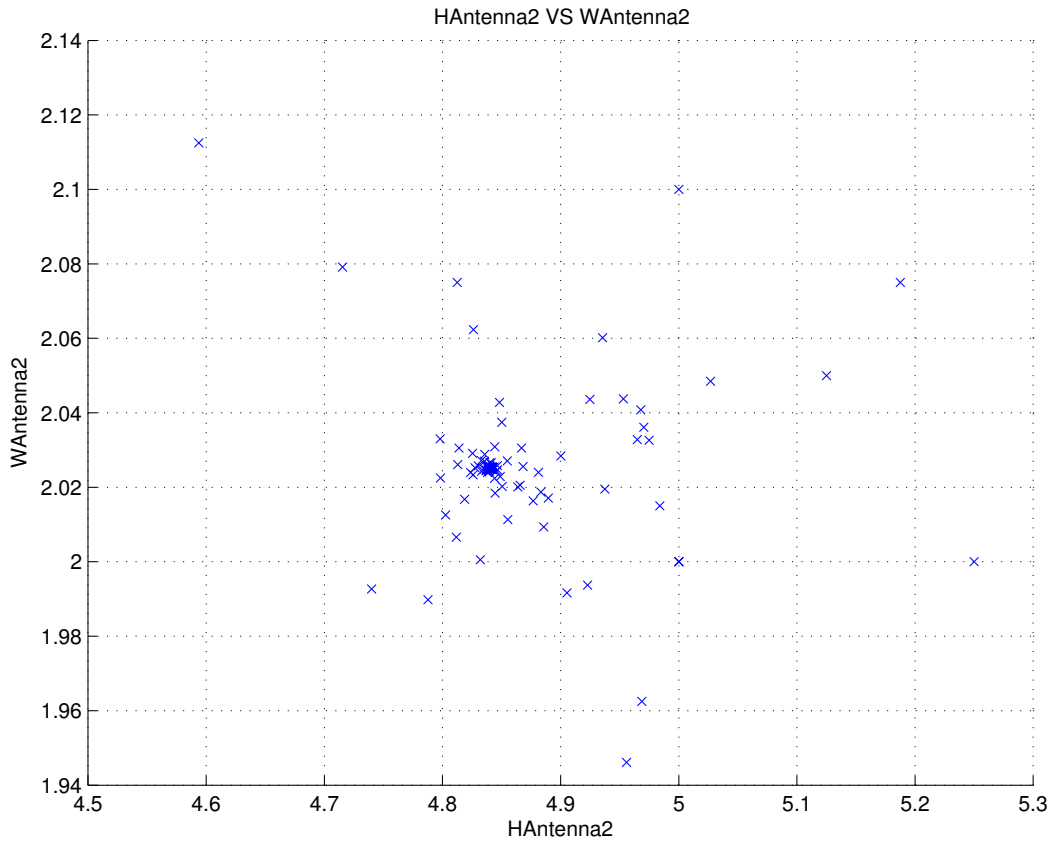

(c) Distribution of the search points of the antenna height and antenna width

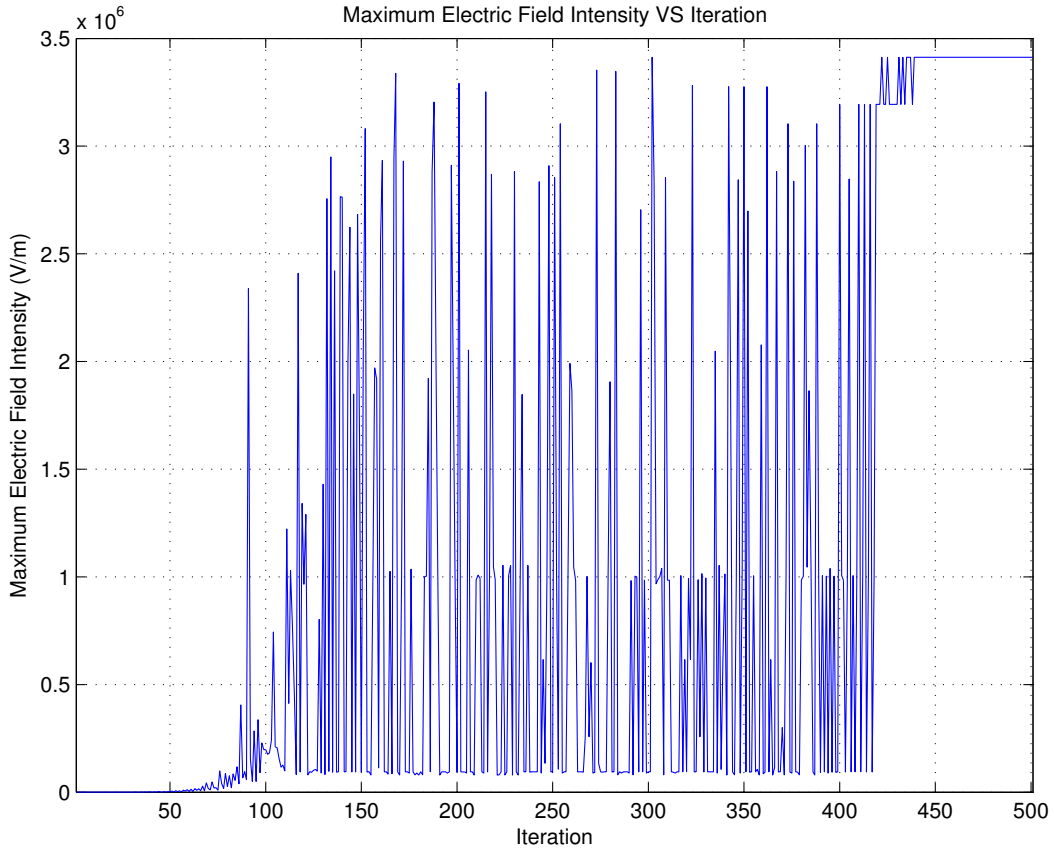

(d) Search trace for the maximum electric field intensity

Figure 5.16: NM search for the 3rd set of initial parameters of Table 5.7

4th Search

The fourth search employing the NM algorithm, uses the starting conditions defined in Table 5.7. The initial value for the frequency was defined as 2.59 GHz, the antenna length as 10 mm, the antenna height as 7 mm, and the antenna width started at 5 mm. The chosen starting value for the supply frequency is nearly 50 MHz lower than the approximate frequency that leads to resonance of the cavity.

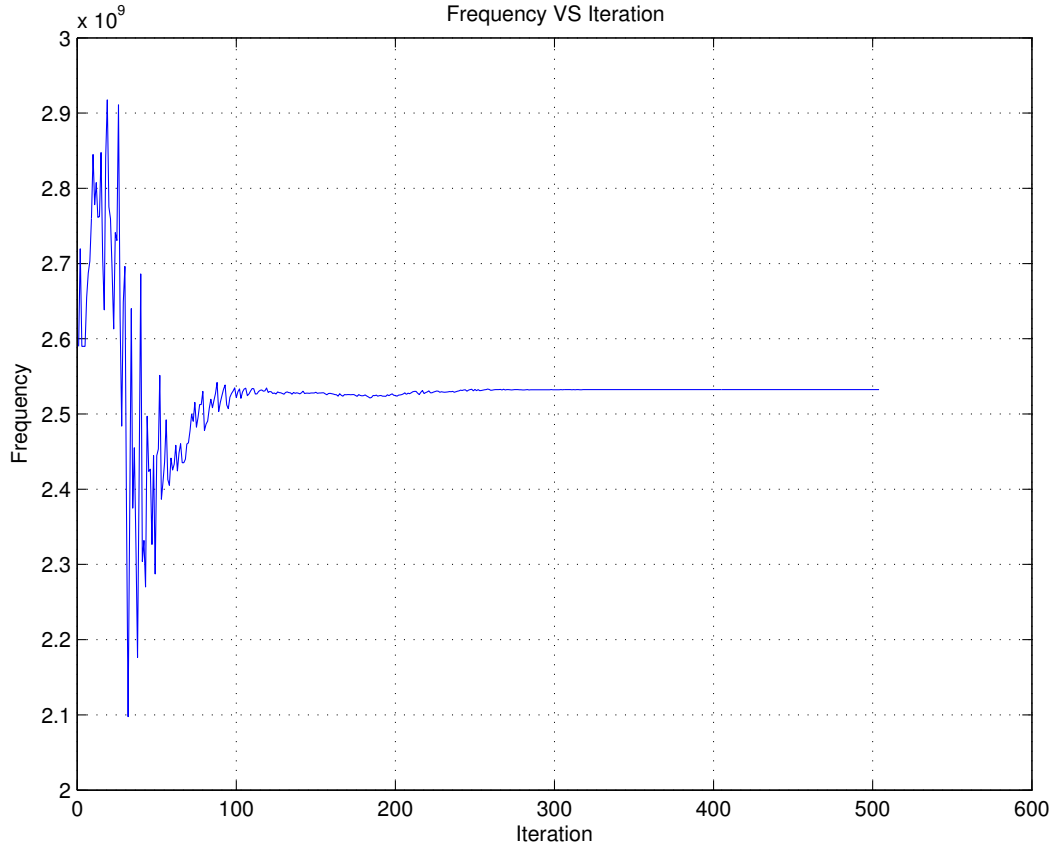

(a) Search trace for the supply frequency with the NM search method

Figure 5.17: NM search for the 4th set of initial parameters of Table 5.7

Figure 5.18 shows the trace of search and the development of the different input variables and objectives by using the fourth set of initial parameters of Table 5.7. The search trace of the supply frequency, with an initial value of 2.59 GHz, is displayed in Fig. 5.17a. The figure was created by connecting the value after each evaluation during the search process. Figure 5.18a shows the search point distribution between the antenna length and antenna height starting at 10 mm and 7 mm. The search point distribution between the antenna height and antenna width is presented in Fig. 5.18b. Figure 5.18c shows the maximum electric field intensity inside the cylinder during the search process.

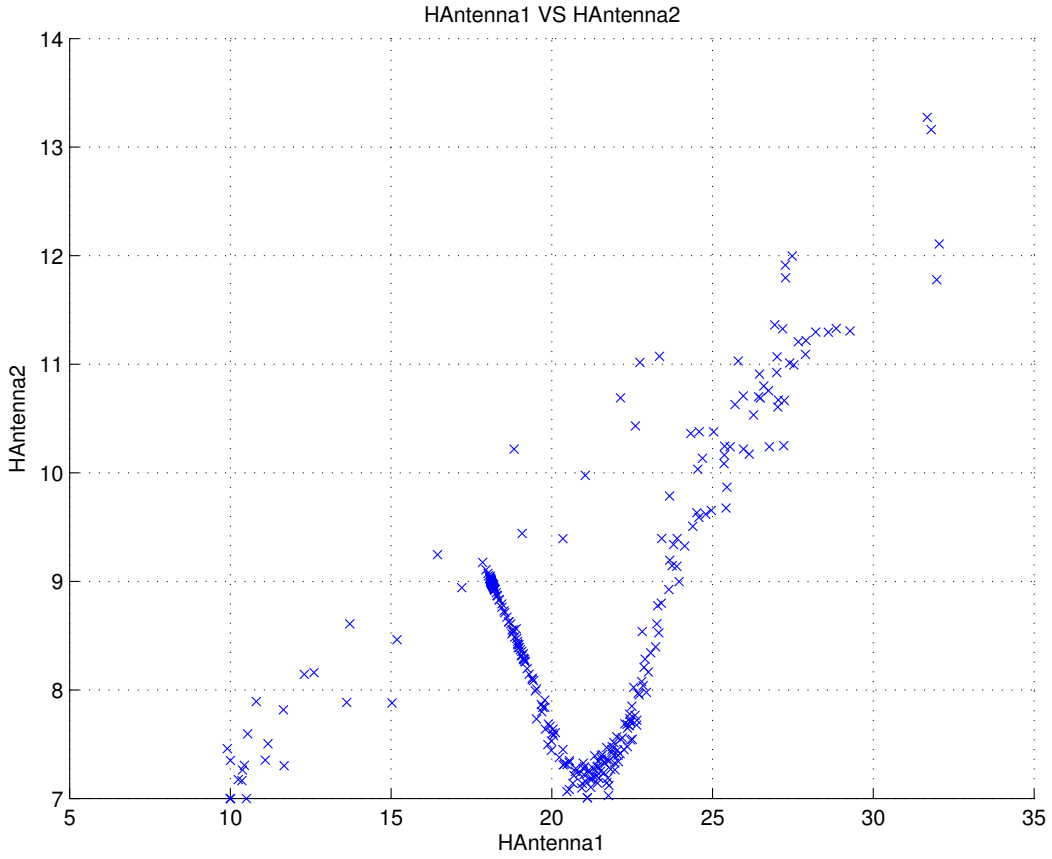

(a) Distribution of the search points of the antenna length and antenna height

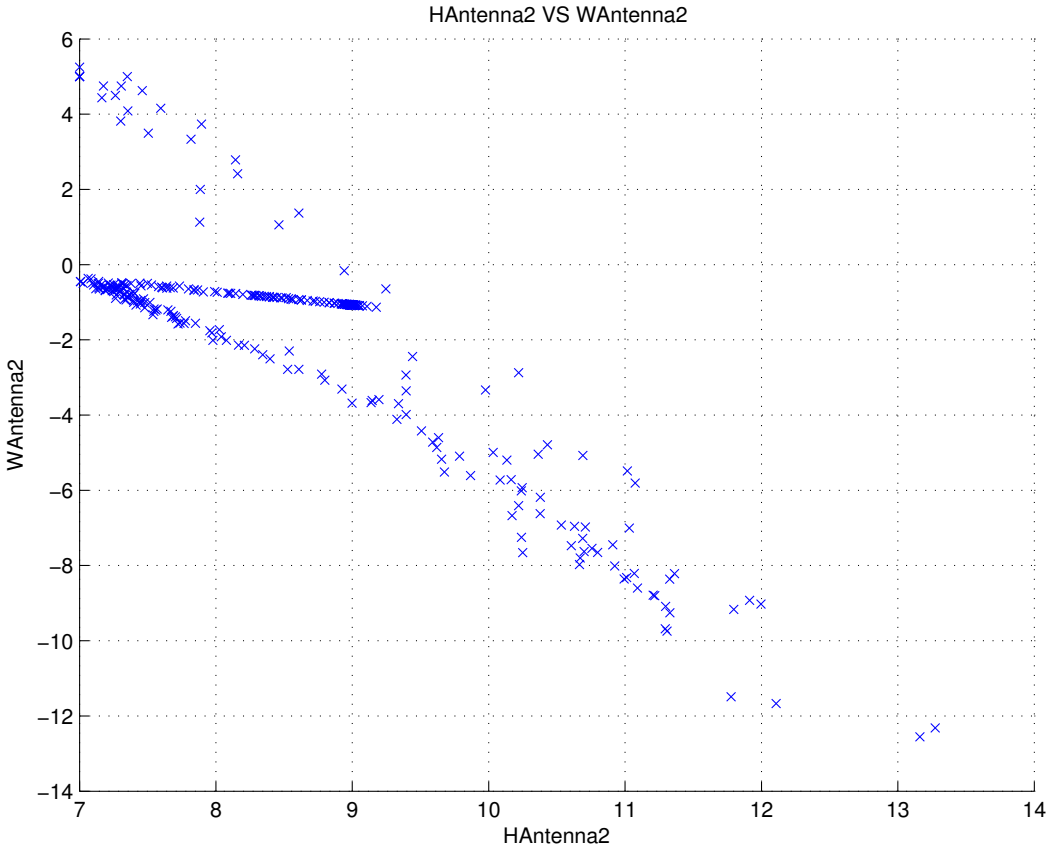

(b) Distribution of the search points of the antenna height and antenna width

Figure 5.18: NM search for the 4th set of initial parameters of Table 5.7

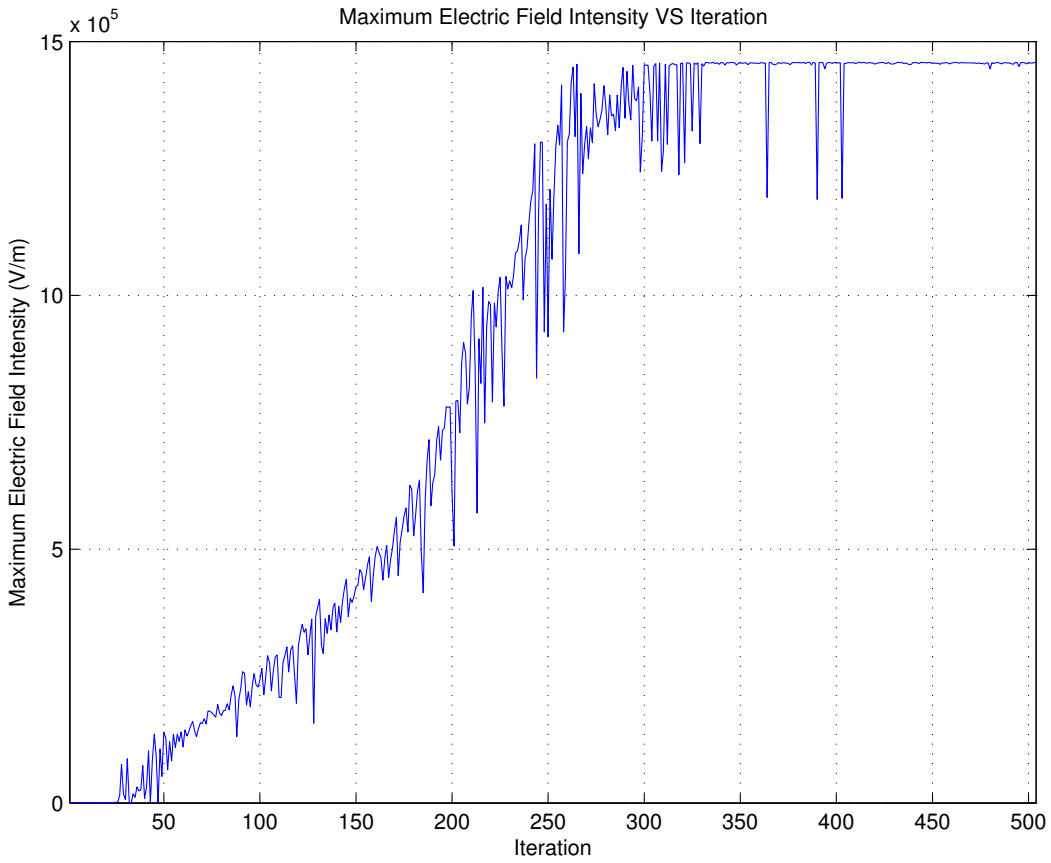

(c) Search trace for the maximum electric field intensity

Figure 5.18: NM search for the 4th set of initial parameters of Table 5.7

Comparison

Figure 5.13 to Fig. 5.18 present the approach of the NM search algorithm to the optimum solution for the optimisation problems. Table 5.8 lists the achieved search results for the different initial parameters and shows that none of them accomplished a sufficient electric field strength. As mentioned before and already demonstrated in sections 3.6.1 and 5.3.1, the NM algorithm relies on well defined starting values in order to obtain acceptable results.

For the four searches the found supply frequency is widely spread over the numerous range of 2.462 754 GHz to 2.537 480 GHz. In correspondence to the wide frequency range the antenna dimensions also vary from one search to another, depending on the starting conditions. This affects the maximum electric field intensity inside the engine cylinder. The maximum electric field intensity for this cylinder and antenna model is difficult to determine, sections 4.3.4, 4.4.1 and 4.4.2 have shown the field development during a single variable change. This search includes multiple variables and therefore it is impossible to know the global maximum.

Table 5.8: Search results of NM searches

Search	**Frequency** (GHz)	**Antenna length** (mm)	**Antenna height** (mm)	**Antenna width** (mm)	**Maximum Electric Field Intensity** (V/m)
1st	2.537 480	5.32	4.77	1.98	$9.318\,343 \times 10^6$
2nd	2.462 754	10.68	7.03	5.00	$1.067\,461 \times 10^6$
3rd	2.535 684	5.25	4.84	2.03	$3.412\,923 \times 10^6$
4th	2.532 301	18.11	8.99	−1.07	$1.459\,030 \times 10^6$

During the fourth search (Fig. 5.18) the boundary conditions of the antenna model have been exceeded for antenna width and therefore the search results are invalid. The minimum value for the antenna width is defined as 0 mm.

5.4.2 Non-Deterministic search

In this section, the non-deterministic optimisation search is implemented through the use of the Genetic Algorithm. The GA has some advantages along with disadvantages which are reviewed in section 3.6.2. In furtherance of finding the most suitable solution, this optimisation search will vary the supply frequency of the microwave generator, the antenna length ("HAntenna1"), the antenna height ("HAntenna2"), and the antenna width ("WAntenna2") of the given simulation model in section 5.4. The whole investigation process includes two searches with the following starting conditions:

Table 5.9: Starting conditions of GA searches

Search	**Frequency** (GHz)	**Antenna length** (mm)	**Antenna height** (mm)	**Antenna width** (mm)
1st	2.55 - 2.6	0 - 5	0 - 6	0 - 5
2nd	2.55 - 2.6	0 - 10	0 - 6	0 - 5

Table 5.9 shows the initial values of the two searches. The chosen range for the supply frequency as well as the antenna length were influenced by the results of the single variable search for the antenna length in section 4.3.4. The optimisation settings and stopping criteria for the algorithm used were set to the following values:

- Display = final
- CrossoverFcn = crossoverscattered

- CrossoverFraction = 0.8
- MutationFraction = 0.2
- EliteCount = 2
- Generations = 40
- PopulationSize = 101
- SelectionFcn = selectiontournament
- StallGenLimit = 20
- TimeLimit = Inf
- TolFun = 1E-6

These values are essentially the default settings of the algorithm provided by the MATLAB optimisation toolbox. A variation in these conditions at a later stage can improve the convergence and search performance or the overall search resolution.

1st Search

The first search employing the GA, uses the starting conditions defined in Table 5.9. The initial boundaries for the frequency are defined as 2.55 GHz to 2.65 GHz, the antenna length from 0 mm to 5 mm, the antenna height from 0 mm to 6 mm, and the antenna width boundaries are from 0 mm to 5 mm. The defined frequency range covers the known frequency which leads to resonance of the cavity.

Figure 5.19 shows the trace of search and development of the different input variables and objectives by using the first set of parameters from Table 5.9. The search trace of the supply frequency, within a range of 2.55 GHz to 2.65 GHz, is displayed in Fig. 5.19a. The figure was created by connecting the value after each evaluation during the search process. Figure 5.19b shows the search point distribution between the antenna length and antenna height in the range of 0 mm to 5 mm and 0 mm to 6 mm. The search point distribution between the antenna height and antenna width is presented in Fig. 5.19c. Figure 5.19d shows the maximum electric field intensity inside the cylinder during the search process.

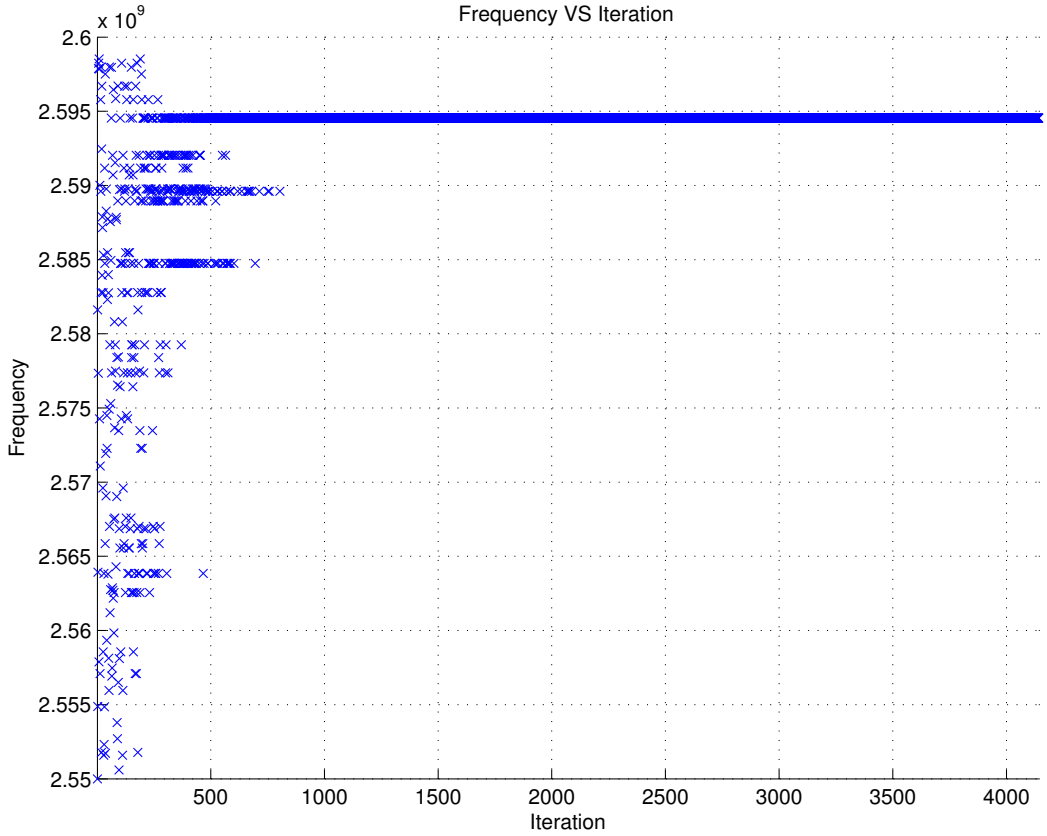

(a) Search trace for the supply frequency with the GA search method

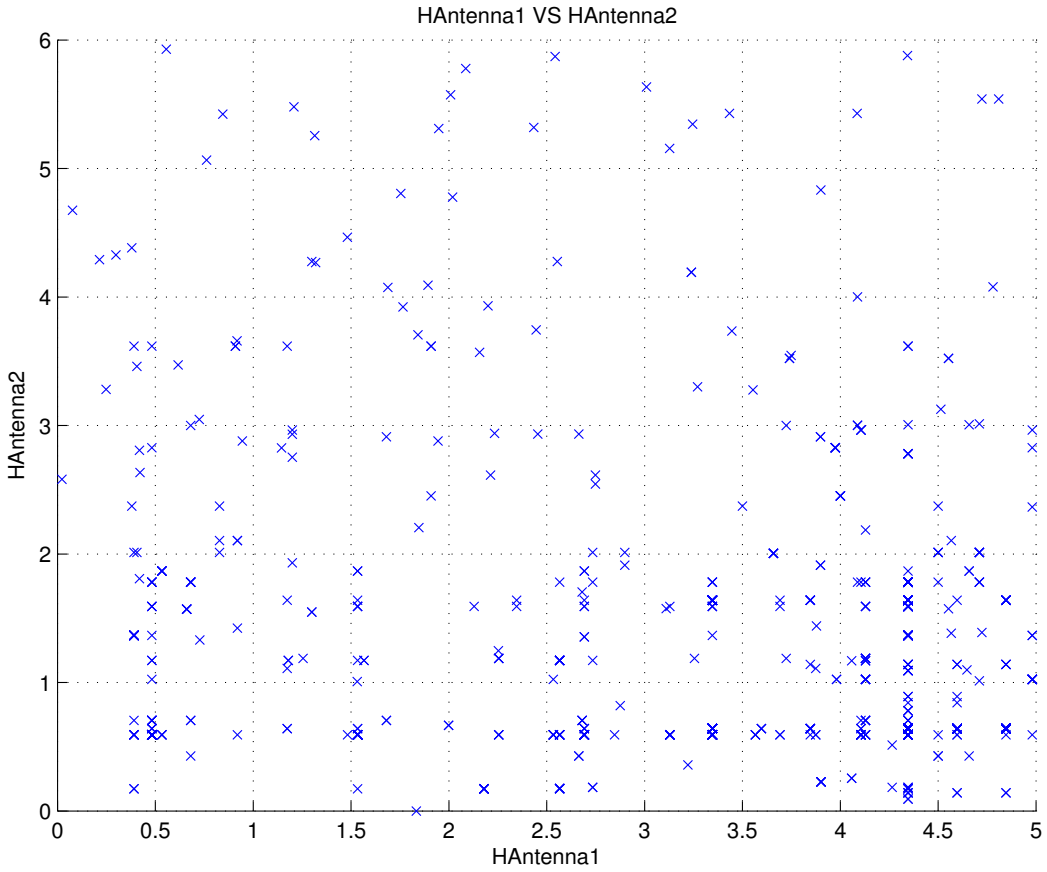

(b) Distribution of the search points of the antenna length and antenna height

Figure 5.19: GA search for the 1st set of initial parameters of Table 5.9

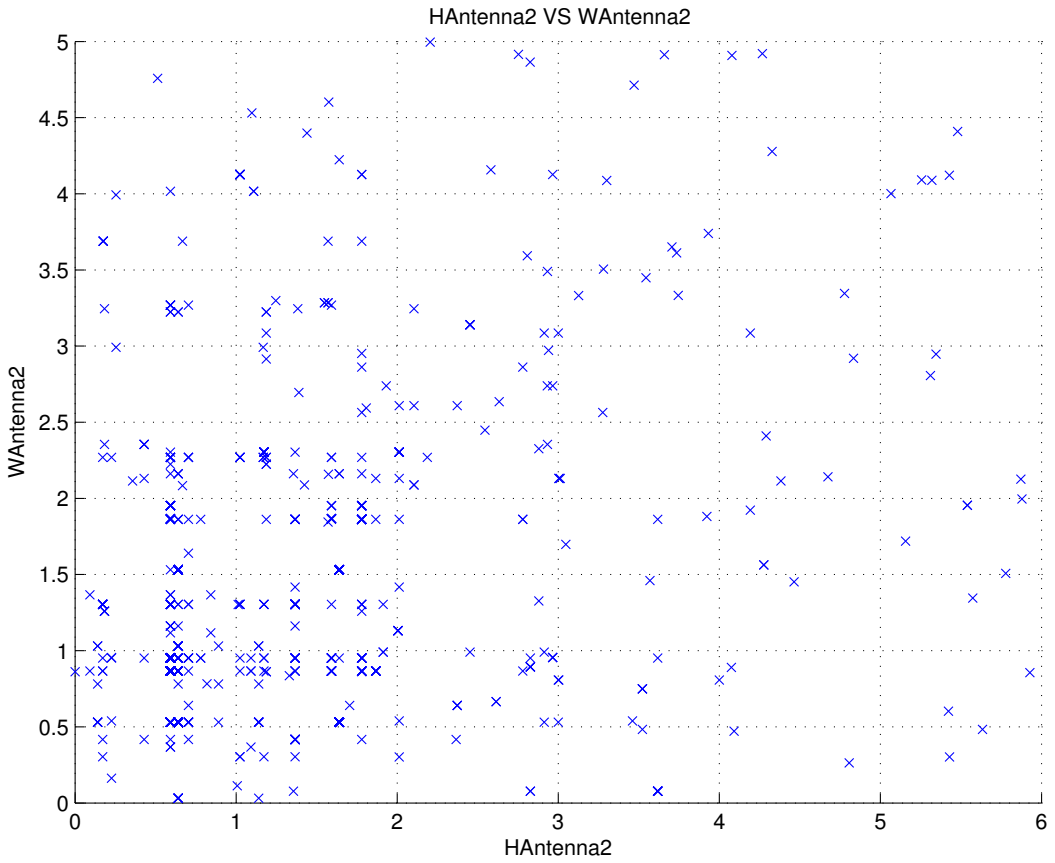

(c) Distribution of the search points of the antenna height and antenna width

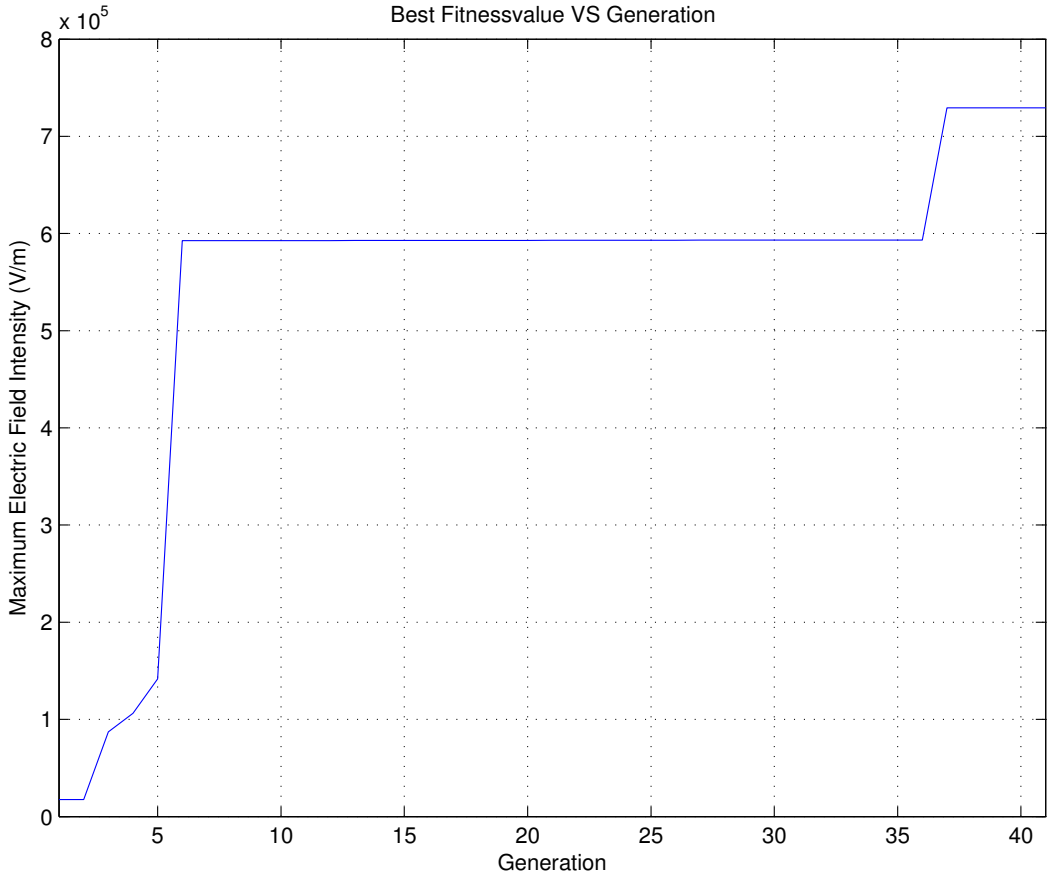

(d) Search trace for the maximum electric field intensity

Figure 5.19: GA search for the 1st set of initial parameters of Table 5.9

2nd Search

The second search employing the GA, uses the starting conditions defined in Table 5.9. The initial boundaries for the frequency are defined from 2.55 GHz to 2.6 GHz, the antenna length from 0 mm to 10 mm, the antenna height from 0 mm to 6 mm, and the antenna width boundaries from 0 mm to 5 mm.

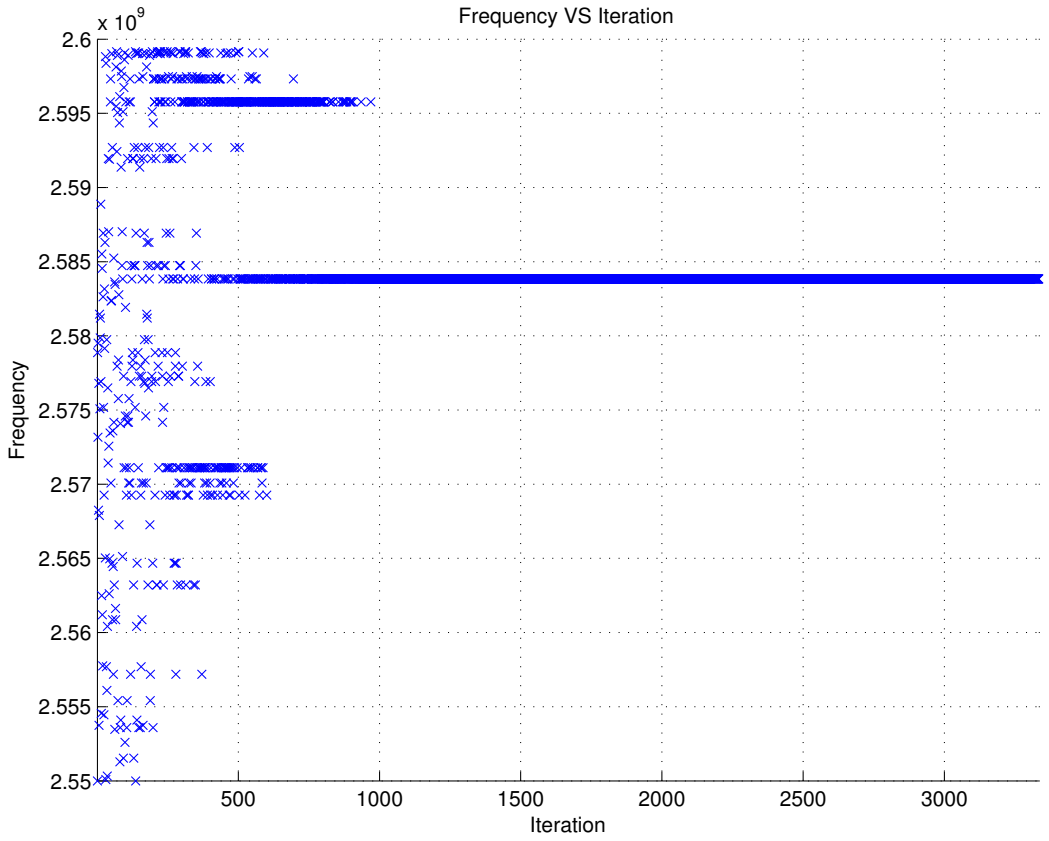

(a) Search trace for the supply frequency with the GA search method

Figure 5.20: GA search for the 2nd set of initial parameters of Table 5.9

Figure 5.20 shows the trace of search and development of the different input variables and objectives by using the second set of initial parameters of Table 5.9. The search trace of the supply frequency, within a range of 2.55 GHz to 2.65 GHz, is displayed in Fig. 5.20a. The figure was created by connecting the value after each evaluation during the search process. Figure 5.20b shows the search point distribution between the antenna length and antenna height in the range of 0 mm to 10 mm and 0 mm to 6 mm respectively. The search point distribution between the antenna height and antenna width is presented in Fig. 5.20c. Figure 5.20d shows the maximum electric field intensity inside the cylinder during the search process.

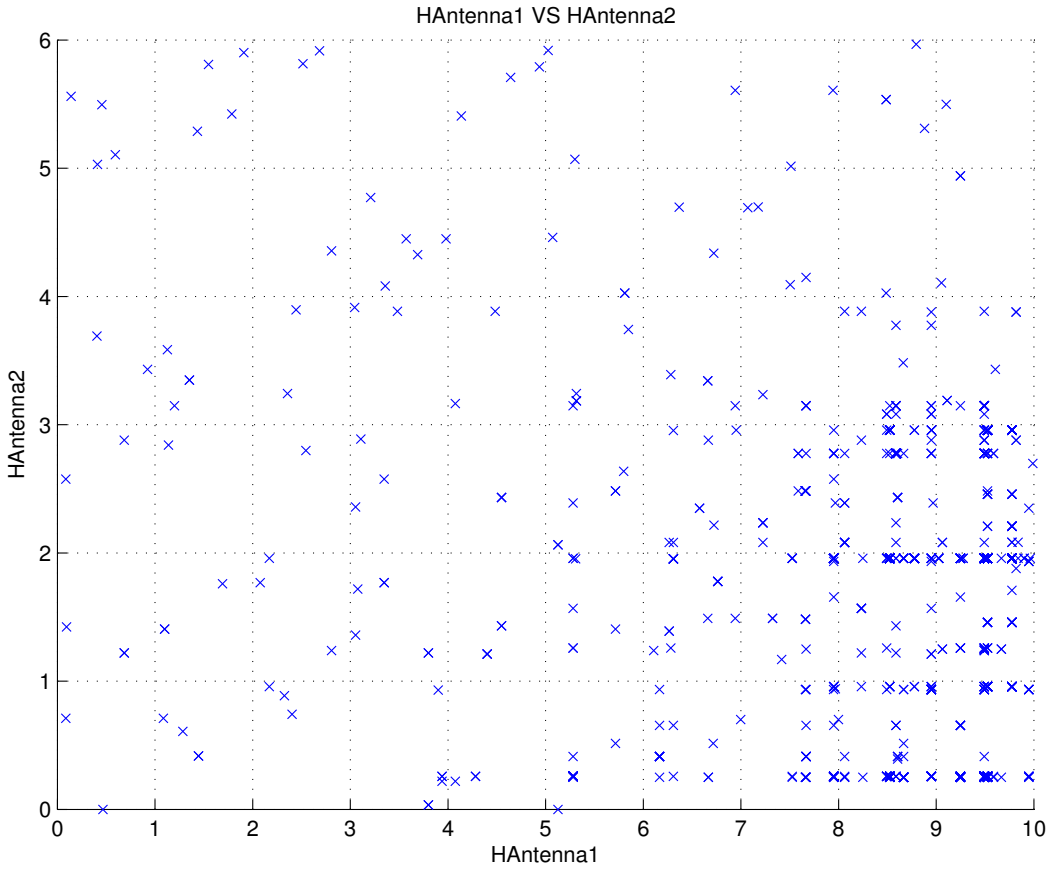

(b) Distribution of the search points of the antenna length and antenna height

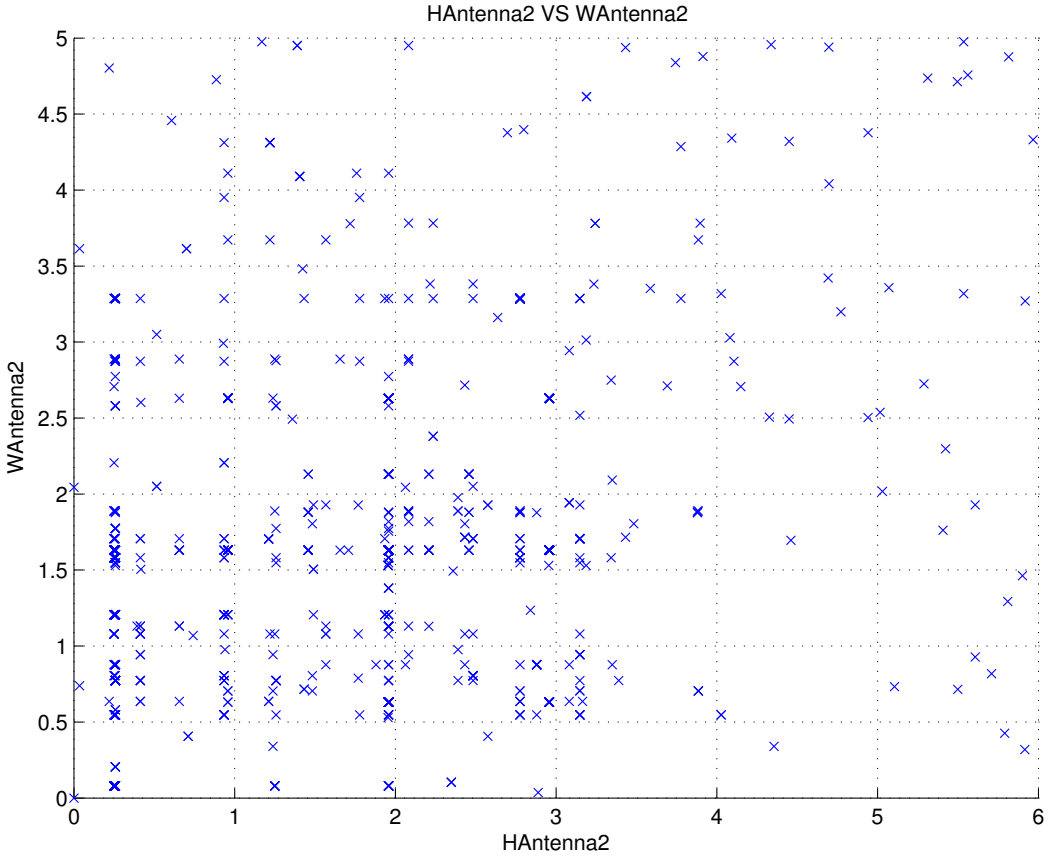

(c) Distribution of the search points of the antenna height and antenna width

Figure 5.20: GA search for the 2nd set of initial parameters of Table 5.9

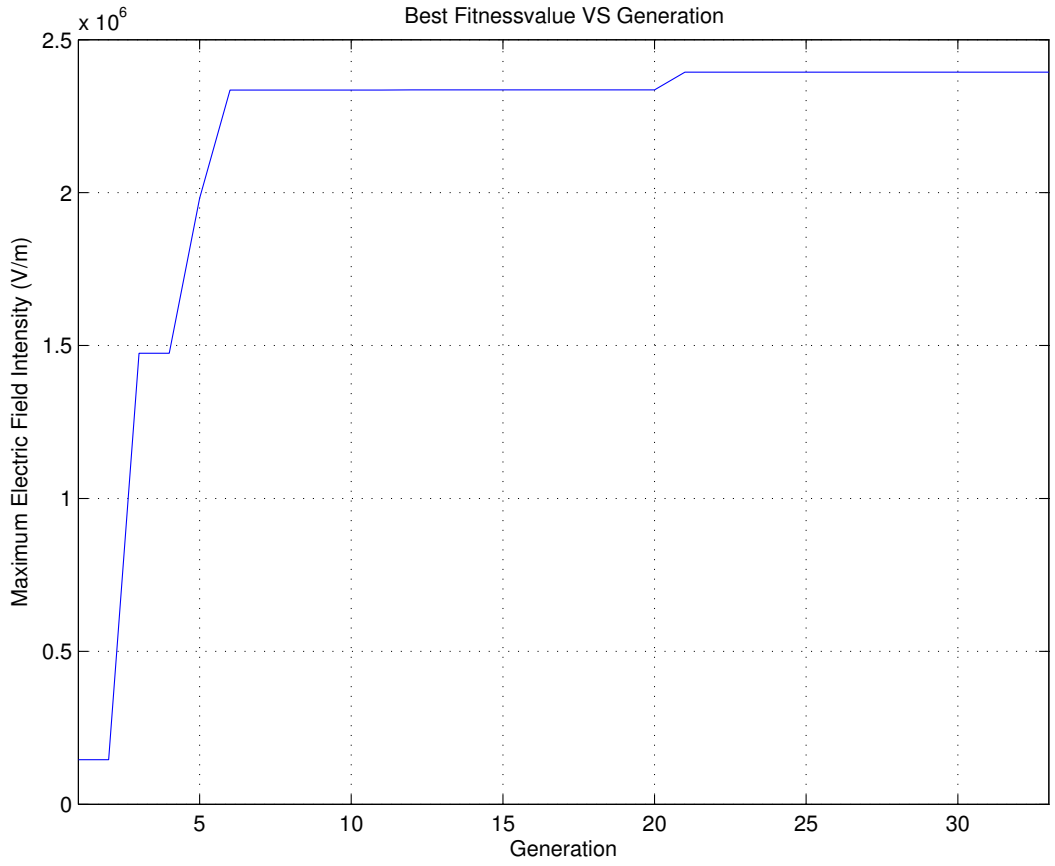

(d) Search trace for the maximum electric field intensity

Figure 5.20: GA search for the 2nd set of initial parameters of Table 5.9

Comparison

The figs. 5.19 and 5.20, present how the GA search algorithm approaches the optimum solution for the optimisation problems. The GA search is a non-deterministic optimisation method and therefore the results will be inconsistent between different optimisation searches. Table 5.10 presents the search results and established that in comparison to the deterministic search in section 5.4.1 the achieved results are unsatisfactory.

Table 5.10: Search results of GA searches

Search	**Frequency** (GHz)	**Antenna length** (mm)	**Antenna height** (mm)	**Antenna width** (mm)	**Maximum Electric Field Intensity** (V/m)
1st	2.594 545	4.85	0.64	0.53	$7.293\,665 \times 10^5$
2nd	2.583 839	9.78	1.96	1.63	$2.394\,119 \times 10^6$

Chapter 2 detailed that the GA requires many more simulation evaluations than the

NM algorithm in section 5.4.1. The found frequencies from both optimisation searches are located at 2.594 545 GHz and 2.583 839 GHz. These frequencies can have a relatively high affect on the propagation performance. Dependent on the supply frequency, the antenna dimensions vary significantly. This variation of the antenna length affects the maximum electric field intensity inside the engine cylinder. As seen in section 5.3.1, the maximum electric field intensity can reach at minimum $9.318\,343 \times 10^6\,\mathrm{V/m}$. The real maximum electric field intensity for this cylinder and antenna model is difficult to determine. Sections 4.3.4, 4.4.1 and 4.4.2 have shown the field development during a single variable change, this search includes multiple variables and therefore it is impossible to predetermine the global maximum. In conclusion, both searches with the initial search range for the frequency and the antenna dimensions were not conducive to finding the global maximum electric field intensity. The found maximum electric field intensity is, as before, a fraction of the possible maximum field strength at the top of the cylinder.

5.4.3 Predefined search

Section 5.4.1 and section 5.4.2 used the deterministic and the non-deterministic searches to solve the optimisation problem of section 5.4. For the given problem, with four input parameters (supply frequency, antenna length, antenna height, antenna width), the NM optimisation search has exhibited a better performance than the GA search. This section uses the predefined search algorithm described in section 5.2, to analyse the performance of this newly designed search. The algorithm combines the advantages of both search techniques. The PGA algorithm will be applied in order to find the most favourable solution by varying the supply frequency of the microwave generator, the antenna length ("HAntenna1"), the antenna height ("HAntenna2"), and the antenna width ("WAntenna2") of the given simulation model in section 5.4. The whole search process consists of two different searches with the following starting conditions:

Table 5.11: Starting conditions of PGA searches

Search	**Frequency** (GHz)	**Antenna length** (mm)	**Antenna height** (mm)	**Antenna width** (mm)
1st	Not required	0 - 5	0 - 6	0 - 5
2nd	Not required	0 - 10	0 - 6	0 - 5

Table 5.11 shows the initial values of the two searches in this section. The selected starting conditions for supply frequency, antenna length, antenna height, antenna width were influenced by the analysis of the single variable changes in sections 4.3.4, 4.4.1 and 4.4.2. The architecture of the PGA search do not required to define a search

range for the supply frequency because the minimum necessary frequency range will be calculated during the search process. The optimisation settings and stopping criteria for the NM part of the combined search algorithm were set to the following:

- Display = final
- MaxFunEvals = 500
- MaxIter = 500
- TolFun = 1E-4
- TolX = 1E-4

The optimisation settings and stopping criteria for the GA part of the combined search algorithm were set to the following:

- Display = final
- CrossoverFcn = crossoverscattered
- CrossoverFraction = 0.8
- MutationFraction = 0.2
- EliteCount = 2
- Generations = 40
- PopulationSize = 101
- SelectionFcn = selectionstochunif
- StallGenLimit = 20
- TimeLimit = Inf
- TolFun = 1E-6

These values are principally the default settings of the NM and GA provided by the MATLAB optimisation toolbox. A variation in these conditions at a later stage can improve the convergence and search performance or the overall search resolution.

1st Search

The first search employing the PGA uses the starting conditions defined in Table 5.11. The initial boundaries for the antenna length are defined as 0 mm to 5 mm, the antenna height as 0 mm to 6 mm, and the antenna width boundaries are 0 mm to 5 mm. Aforementioned, a frequency range is not required and will be calculated prior to the optimisation search. The given search range for the antenna dimensions cover the known values those delivers the best propagation performance inside the combustion chamber, investigated in sections 4.3.4, 4.4.1 and 4.4.2.

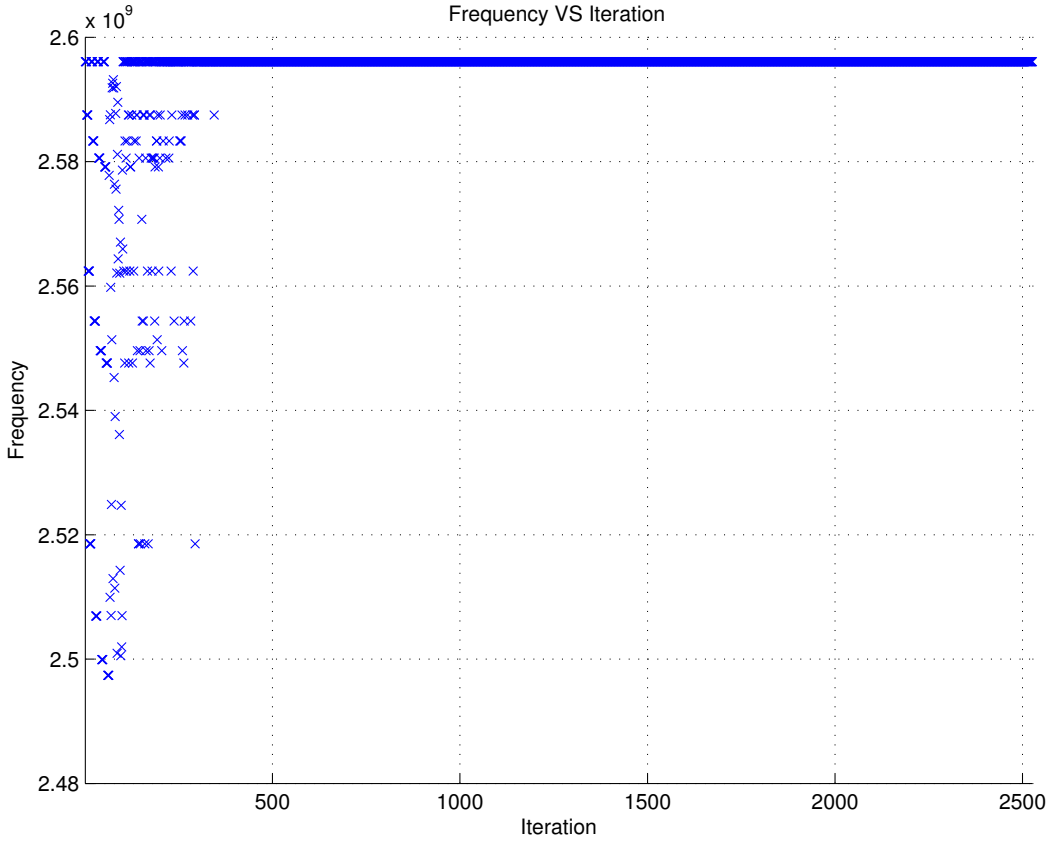

(a) Search trace for the supply frequency with the PGA search method

Figure 5.21: PGA search for the 1st set of initial parameters of Table 5.11

Figure 5.21 shows the trace of search and development of the different input variables and objectives by using the first set of initial parameters from Table 5.11. The search trace of the supply frequency, within the beforehand calculated range, is displayed in Fig. 5.21a. The figure was created by connecting the value after each evaluation and displays the parameter and the objective of each step during the search process. Figure 5.21b shows the search point distribution between the antenna length and antenna height in the range of 0 mm to 5 mm and 0 mm to 6 mm respectively. The search point distribution between the antenna height and antenna width is presented in Fig. 5.21c. Figure 5.21d illustrates the maximum electric field intensity inside the cylinder for the search process.

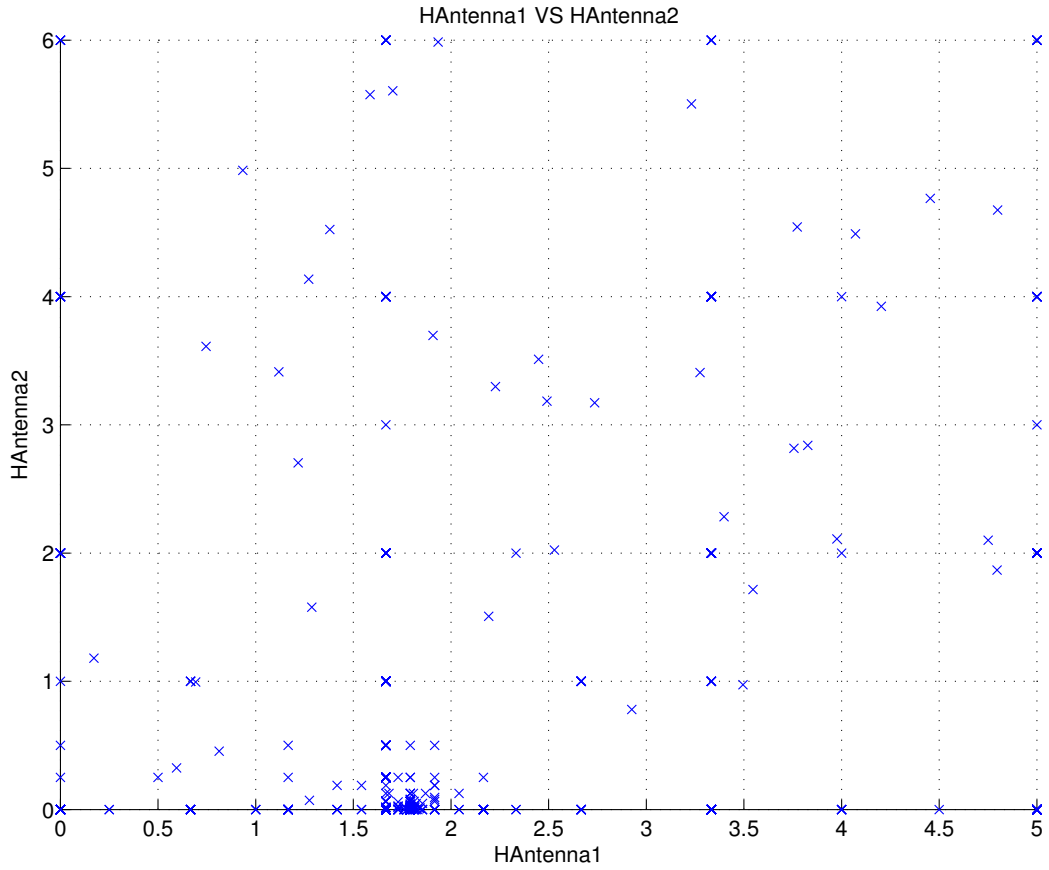

(b) Distribution of the search points of the antenna length and antenna height

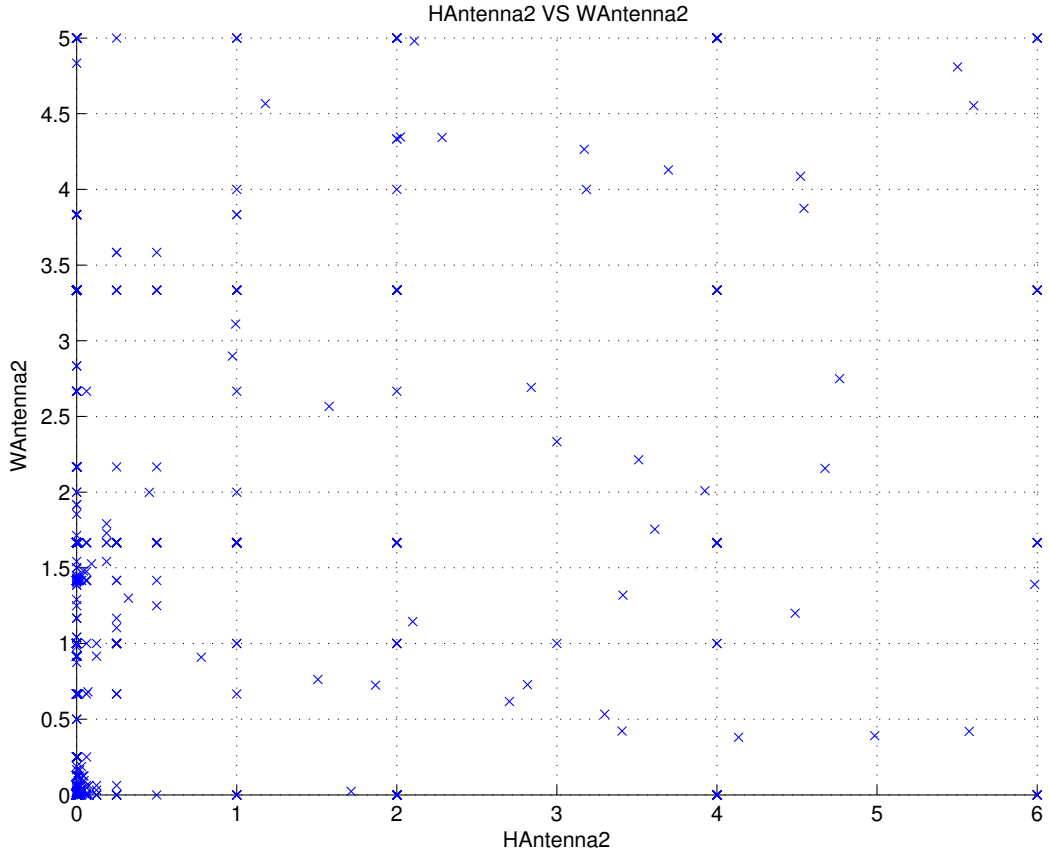

(c) Distribution of the search points of the antenna height and antenna width

Figure 5.21: PGA search for the 1st set of initial parameters of Table 5.11

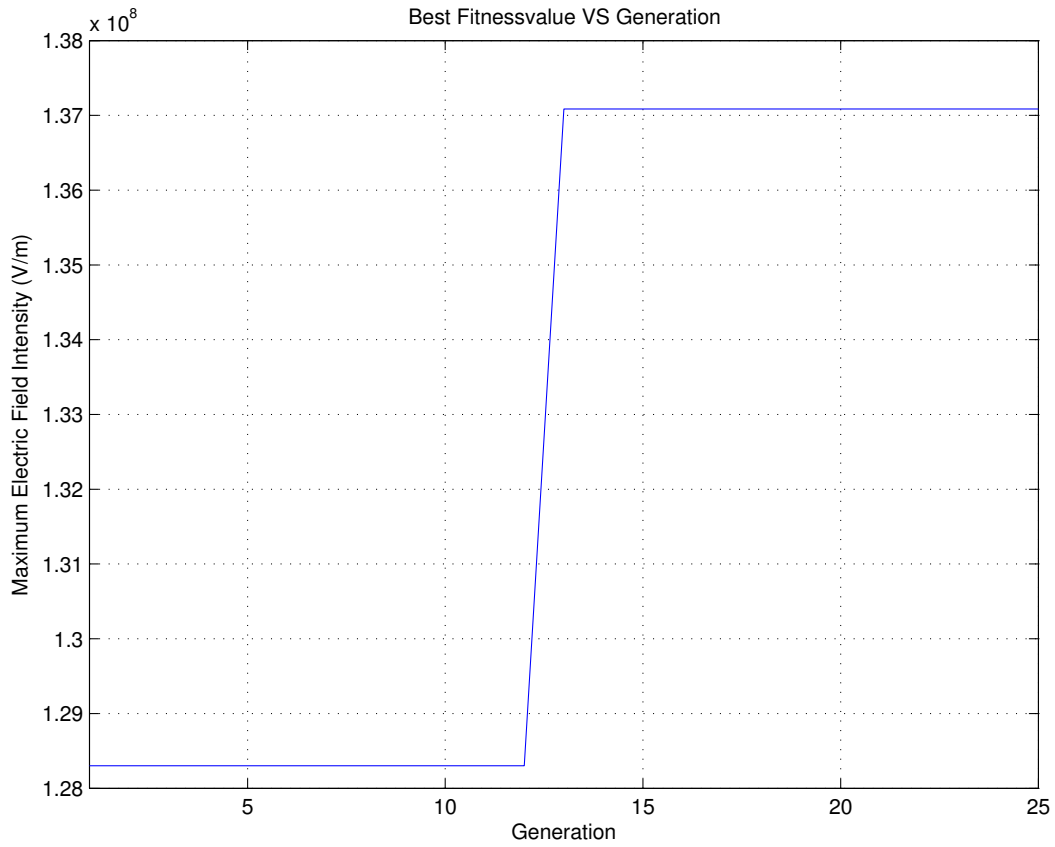

(d) Search trace for the maximum electric field intensity

Figure 5.21: PGA search for the 1st set of initial parameters of Table 5.11

2nd Search

The second search employing the PGA, uses the starting conditions defined in Table 5.11. The initial boundaries for the antenna length are defined as 0 mm to 10 mm, the antenna height as 0 mm to 6 mm, and the antenna width boundaries are 0 mm to 5 mm. Aforementioned, a frequency range is not required and will be calculated prior to the optimisation search. The given search range for the antenna dimensions covers the known values those who deliver the most suitable propagation performance inside the combustion chamber, sections 4.3.4, 4.4.1 and 4.4.2.

Figure 5.22 shows the trace of search and the development of the different input variables and objectives by using the second set of initial parameters from Table 5.11. The search trace of the supply frequency, within the previously calculated range, is displayed in Fig. 5.22a. The figure was created by connecting the value after each evaluation during the search process. Figure 5.22b shows the search point distribution between the antenna length and antenna height in the range of 0 mm to 10 mm and 0 mm to 6 mm. The search point distribution between the antenna height and antenna width is presented in Fig. 5.22c. Figure 5.22d shows the maximum electric

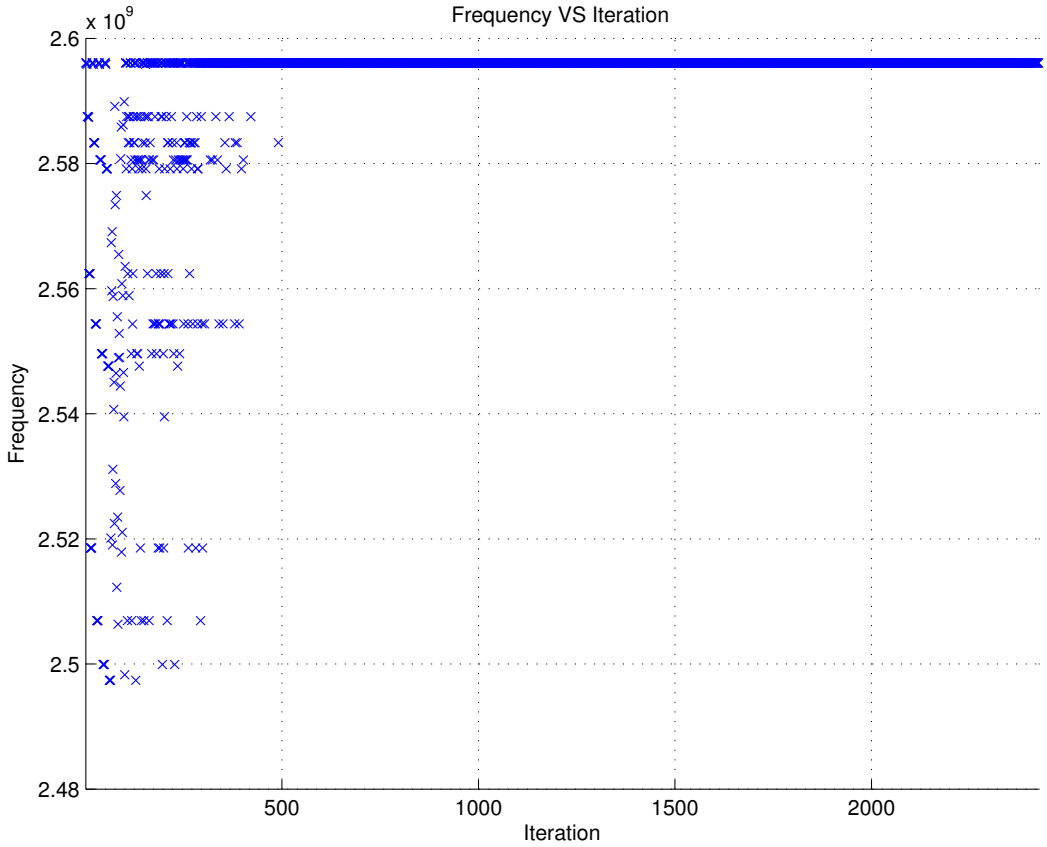

(a) Search trace for the supply frequency with the PGA search method

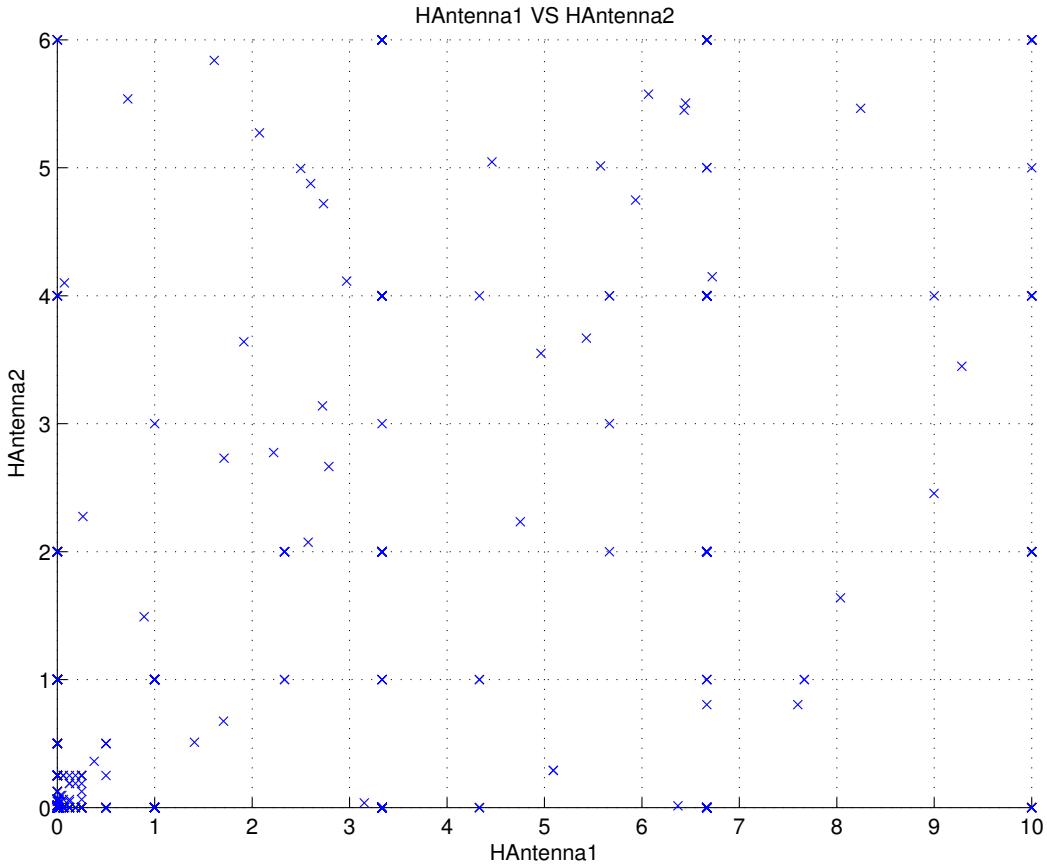

(b) Distribution of the search points of the antenna length and antenna height

Figure 5.22: PGA search for the 2nd set of initial parameters of Table 5.11

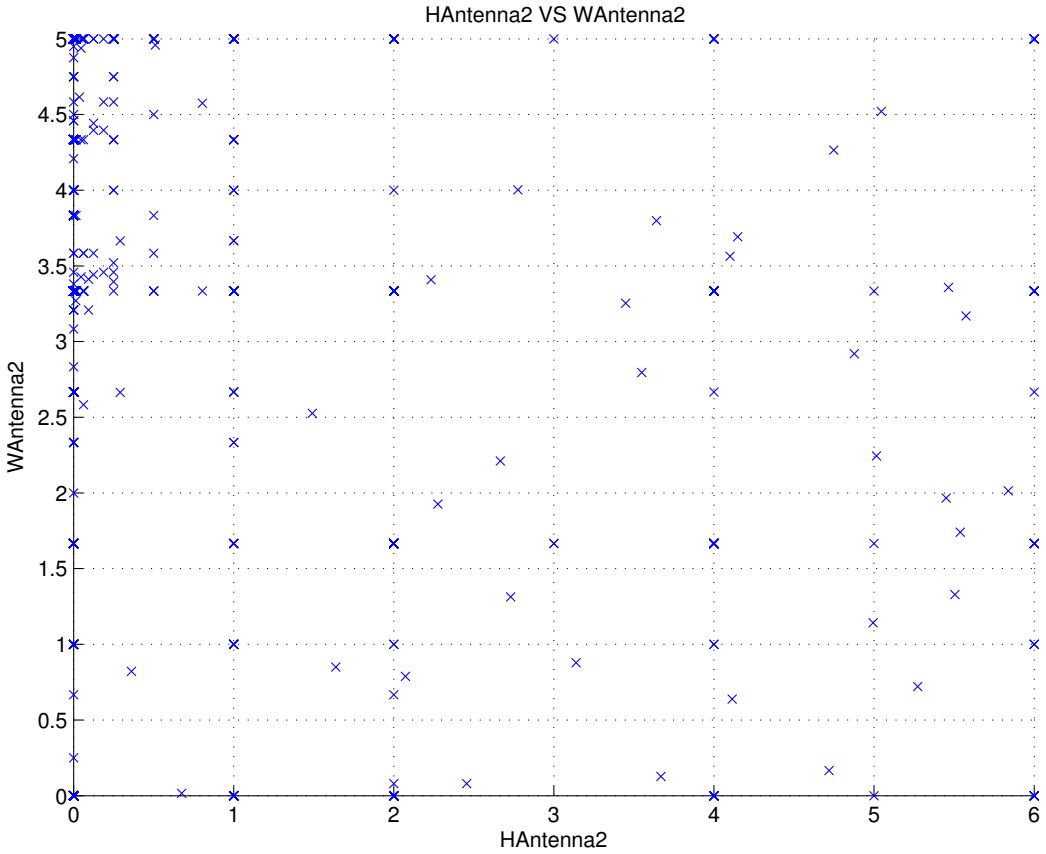

(c) Distribution of the search points of the antenna height and antenna width

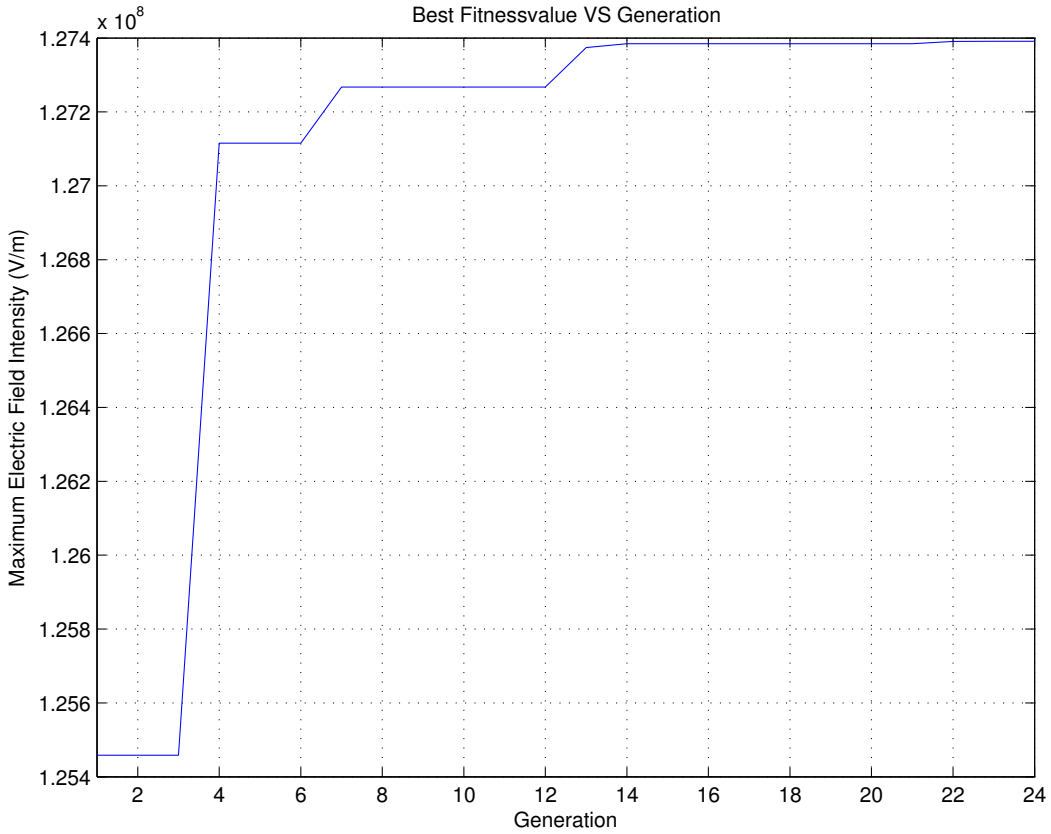

(d) Search trace for the maximum electric field intensity

Figure 5.22: PGA search for the 2nd set of initial parameters of Table 5.11

field intensity inside the cylinder during the search process.

Comparison

Figures 5.21 and 5.22 demonstrates the PGA search algorithm's approach to discovering the optimum solution. The PGA search algorithm combines the deterministic and the non-deterministic optimisation methods, hence the results will be inconsistent between multiple searches. Table 5.12 presents the search results. The PGA exhibits a significant better performance than the GA in section 5.4.2, but is comparable to the achieved results of the NM algorithm search in section 5.4.1.

Table 5.12: Search results of PGA searches

Search	**Frequency** (GHz)	**Antenna length** (mm)	**Antenna height** (mm)	**Antenna width** (mm)	**Maximum Electric Field Intensity** (V/m)
1st	2.596 060	1.79	0.0	1.42	$1.370\,861 \times 10^8$
2nd	2.596 059	0.12	0.0	3.33	$1.273\,914 \times 10^8$

As described in section 5.2, the PGA combines the advantages of the NM algorithm and the GA optimisation search to obtain the most suitable antenna design for a given model. Table 5.12 displays that the found supply frequency of both searches at nearly 2.596 059 GHz. The found antenna length varies slightly between the two searches, while the optimum value of the antenna height was found to be zero. That means, the PGA shows the most favourable performance in comparison to the deterministic and non-deterministic search in sections 5.4.1 and 5.4.2. The found maximum electric field intensity is nearly identical to the theoretically possible maximum field strength at the top of the cylinder, found in sections 4.3.4, 4.4.1 and 4.4.2.

5.5 Combination of Antenna Length, Antenna Height, and Antenna Width

The initial search, combining the frequency and the antenna length, in section 5.3 and the more complex search, combining the frequency and three antenna dimensions, in section 5.4, demonstrate a multivariable optimisation system in context of the HCMI system.

Previously obtained results have demonstrated that the location of the corresponding resonance frequency inside the cylinder leads to a problem. This dilemma is the to finding the most suitable antenna dimensions for obtaining the maximum electric field inside the combustion chamber. A solution to this problem is to exclude the frequency from the search, by using the relationship between the resonance frequency and Eigenfrequency of the engine cylinder. Therefore the search algorithm, introduced in section 5.1, will be employed in this section. The supply frequency of the microwave generation will not be an input of the multivariable optimisation problem any further. The changeable inputs of this search are the antenna length, antenna height, and antenna width of the two antennas. The influence of the single variable changes have been investigated in section 4.3.4 for the antenna length ("HAntenna1"), in section 4.4.1 for the antenna height ("HAntenna2"), and in section 4.4.2 for the antenna width ("WAntenna1").

Figure 5.12 presents the extended antenna model used for this optimisation search. In section 5.5.1 the deterministic NM algorithm will be employed to solve the optimisation problem. For further investigation of the same optimisation problem the non-deterministic GA (in section 5.5.2) will be applied.

5.5.1 Deterministic search

The deterministic optimisation search in this section is implemented by using the NM simplex algorithm. The advantages and disadvantages of the NM algorithm are reviewed in section 3.6.1. In furtherance of finding this most suitable solution, the optimisation search will vary the antenna length ("HAntenna1"), the antenna height ("HAntenna2"), and the antenna width ("WAntenna2") of the given simulation model in section 5.5. The whole investigation process includes two searches with the following starting conditions:

Table 5.13: Starting conditions of NM searches

Search	**Antenna length** (mm)	**Antenna height** (mm)	**Antenna width** (mm)
1st	5	5	2
2nd	10	7	5

Table 5.13 shows the initial values of the two searches. The chosen starting conditions for the antenna length, the antenna height, and the antenna width were influenced by the results of the single variable searches in sections 4.3.4, 4.4.1 and 4.4.2. The frequency will be calculated during the search process for each parameter pair by using

the Eigenfrequency of the cavity (see section 4.3.7). The optimisation settings and stopping criteria for the used algorithm were set to the following values:

- Display = final
- MaxFunEvals = 500
- MaxIter = 500
- TolFun = 1E-4
- TolX = 1E-4

These values are the default settings of the algorithm provided by the MATLAB optimisation toolbox. At a later stage a variation in these conditions can improve the convergence and search performance or the overall search resolution.

1st Search

The first search employing the NM algorithm, uses the starting conditions defined in Table 5.7. The initial value for the antenna length was defined as 5 mm, the antenna height as 5 mm, and the antenna width started at 2 mm. Aforementioned, a frequency is not required and will be calculated during the optimisation search.

Figure 5.23 shows the trace of search and development of the different input variables and objectives by using the first set of initial parameters of Table 5.13. Figure 5.23a shows the search point distribution between the antenna length and antenna height starting at 5 mm. The search point distribution between the antenna height and antenna length is presented in Fig. 5.23b. Figure 5.23c displays the search point distribution between the antenna height and antenna width. Figure 5.23d illustrates the maximum electric field intensity inside the cylinder during the search process.

2nd Search

The second search, employing the NM algorithm, uses the starting conditions defined in Table 5.7. The initial value for the antenna length was defined as 10 mm, the antenna height as 7 mm, and the antenna width started at 5 mm. Aforementioned, a frequency is not required and will be calculated during the optimisation search.

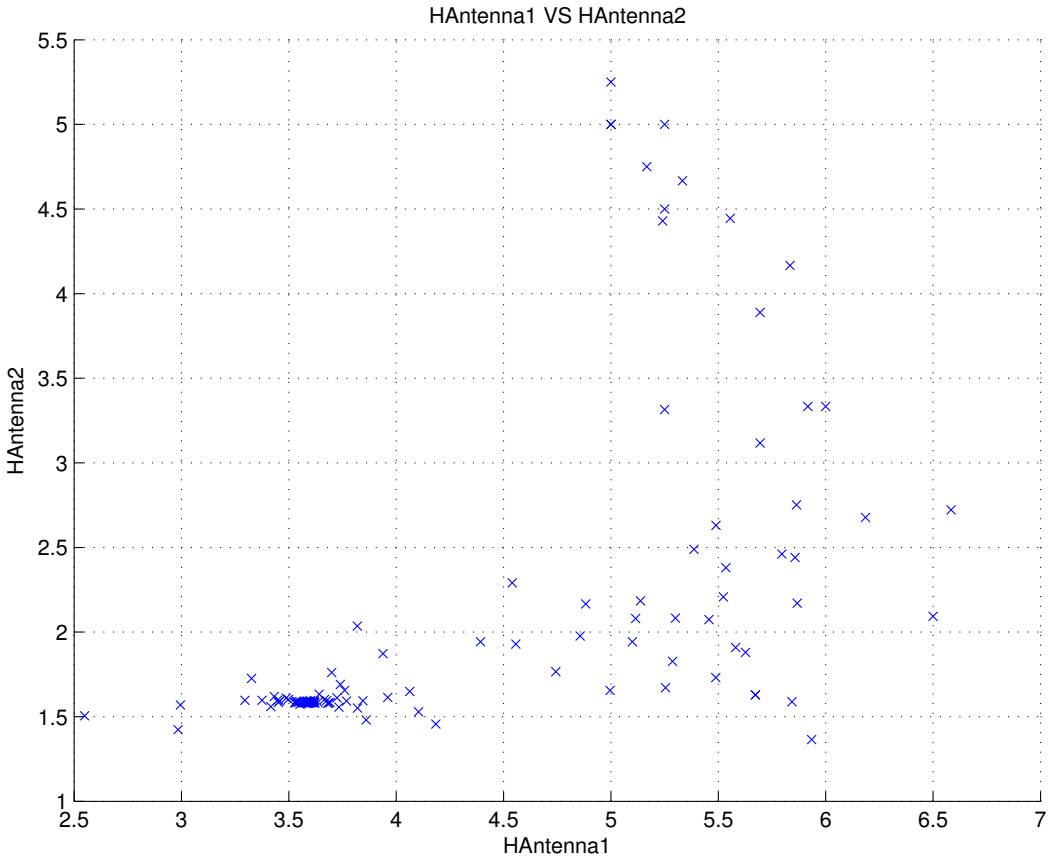

(a) Distribution of the search points of the antenna length and antenna height

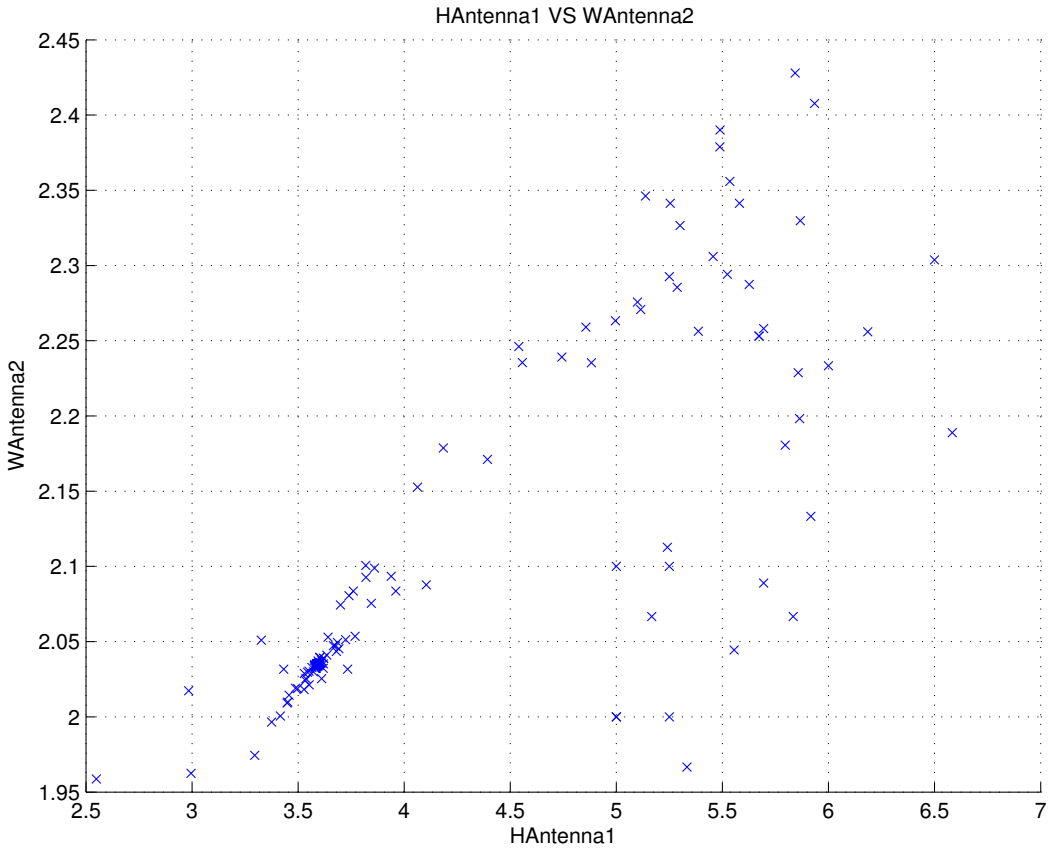

(b) Distribution of the search points of the antenna length and antenna weight

Figure 5.23: NM search for the 1st set of initial parameters of Table 5.13

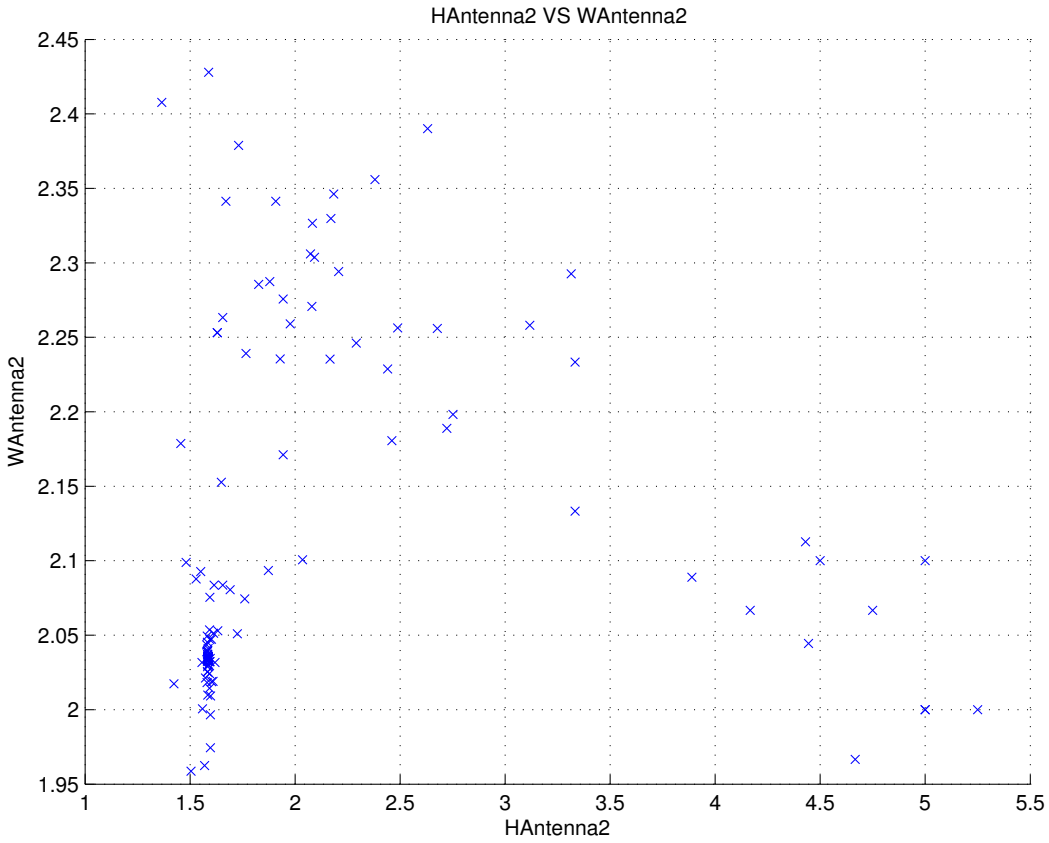

(c) Distribution of the search points of the antenna height and antenna width

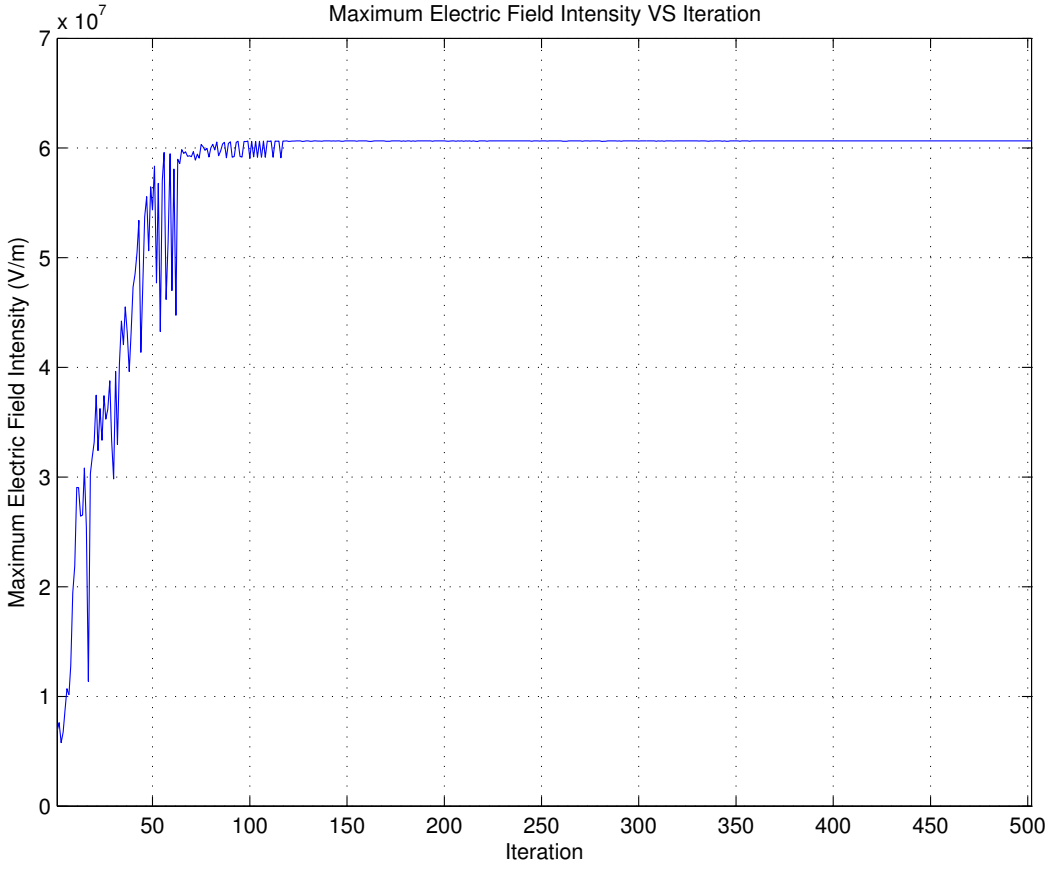

(d) Search trace for the maximum electric field intensity

Figure 5.23: NM search for the 1st set of initial parameters of Table 5.13

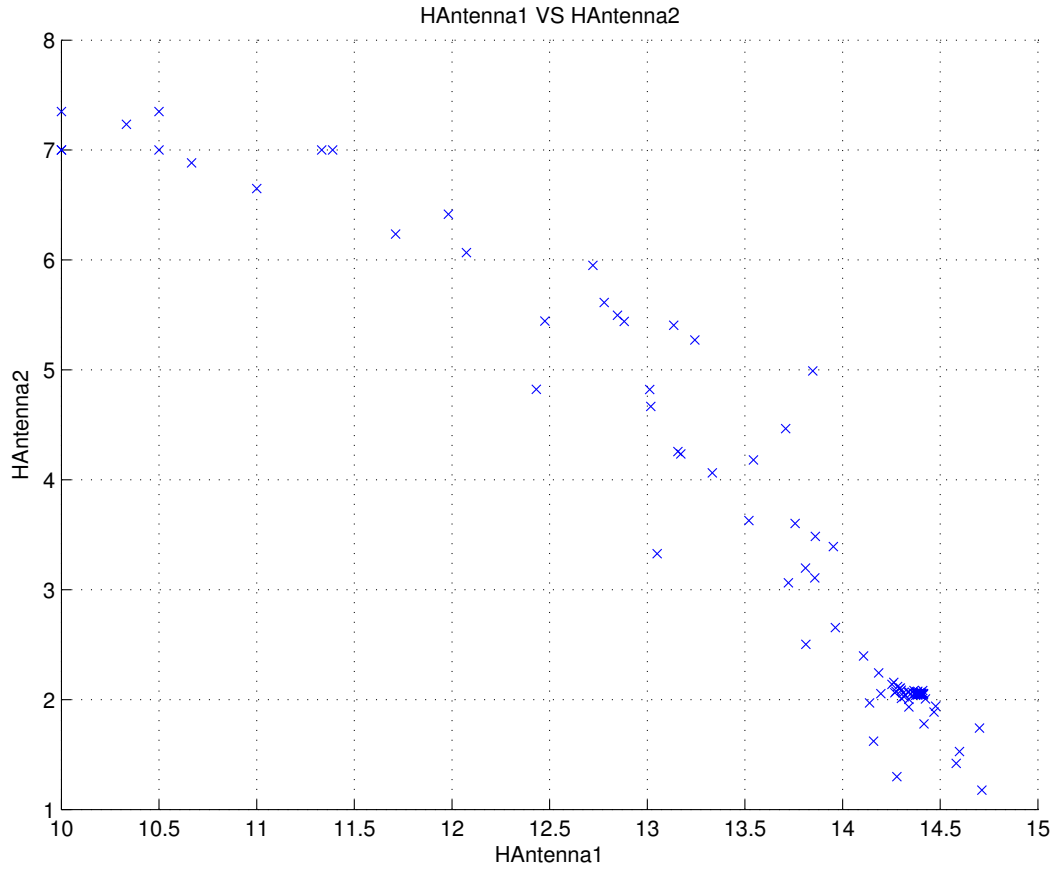

(a) Distribution of the search points of the antenna length and antenna height

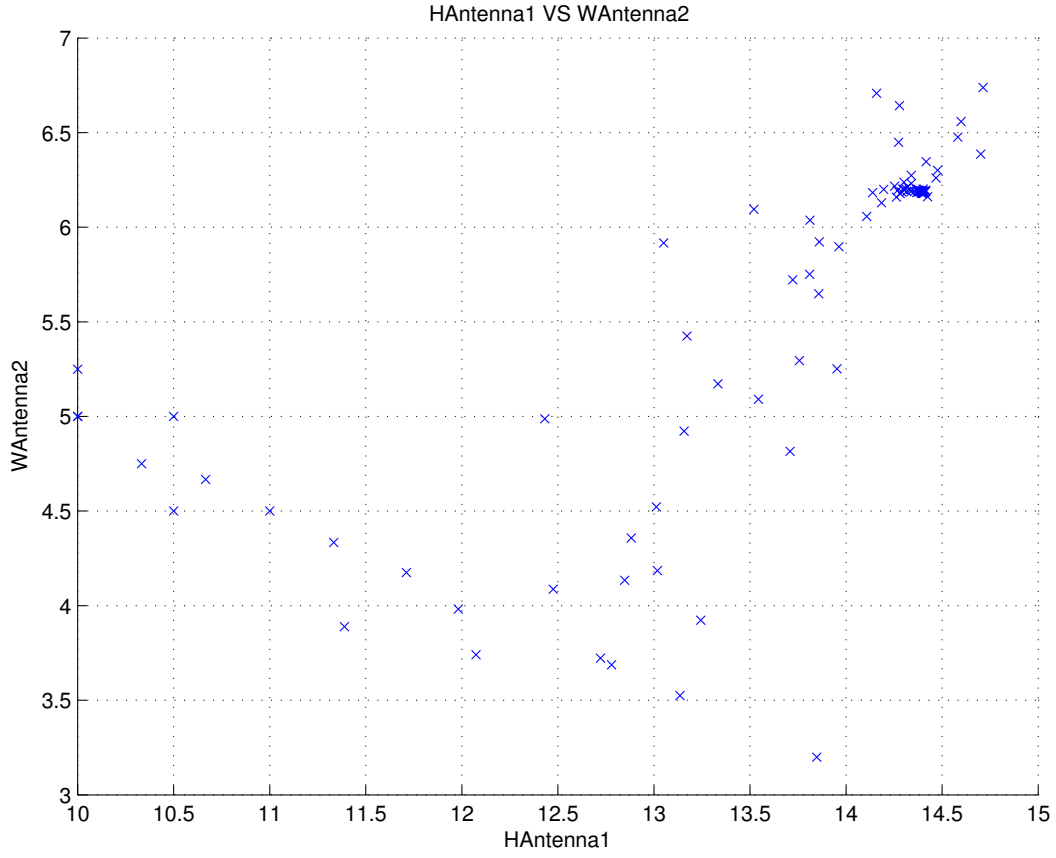

(b) Distribution of the search points of the antenna length and antenna weight

Figure 5.24: NM search for the 2nd set of initial parameters of Table 5.13

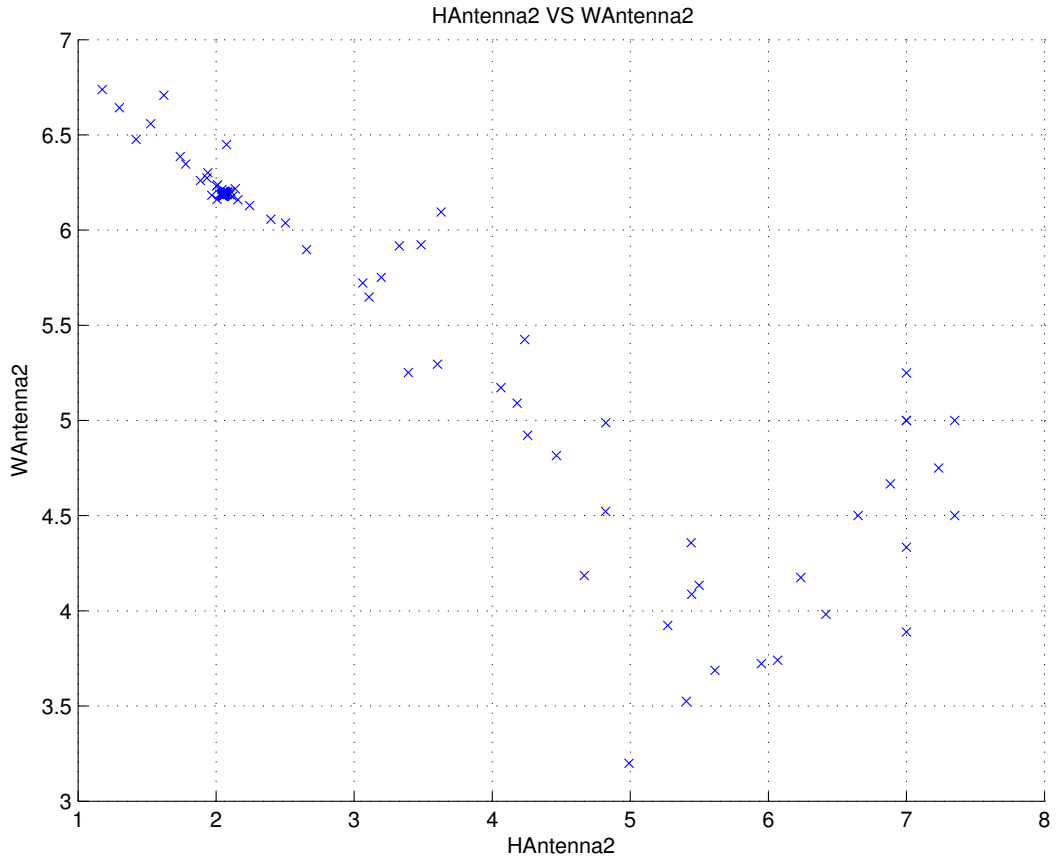

(c) Distribution of the search points of the antenna height and antenna width

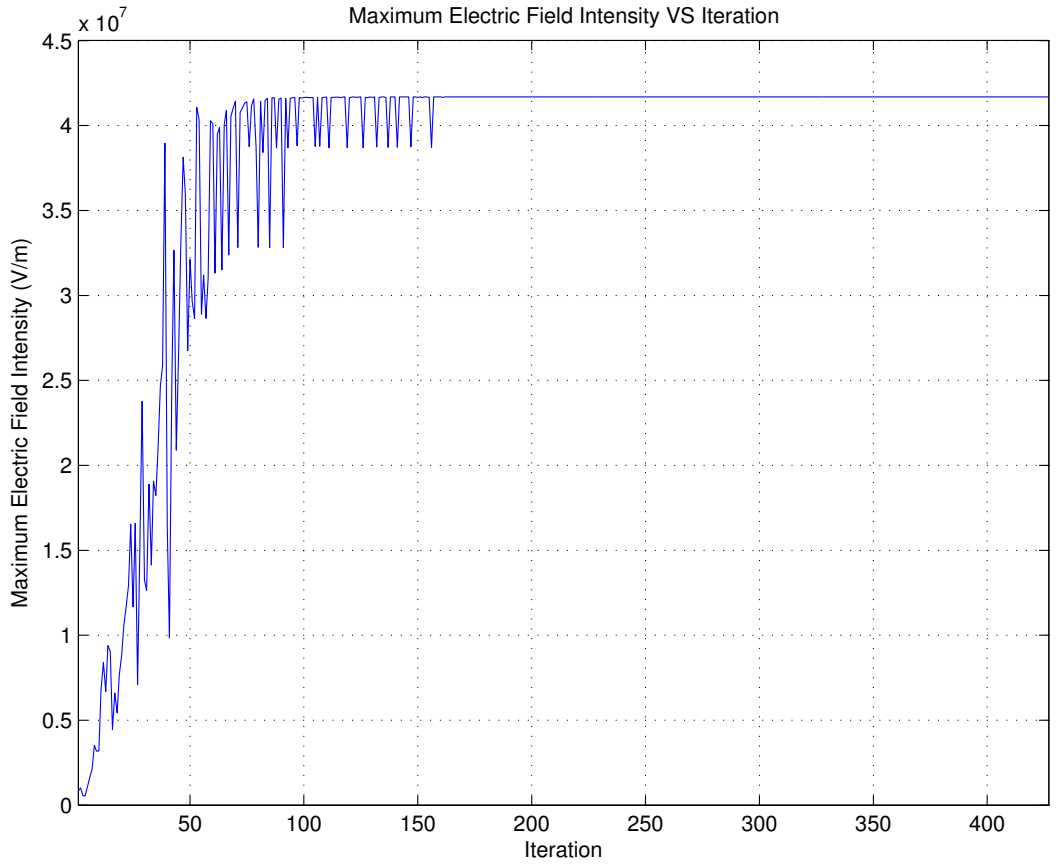

(d) Search trace for the maximum electric field intensity

Figure 5.24: NM search for the 2nd set of initial parameters of Table 5.13

Figure 5.24 represents the trace of search and development of the different input variables and objectives by using the second set of initial parameters of Table 5.13. Figure 5.24a shows the search point distribution between the antenna length and antenna height starting at 5 mm. The search point distribution between the antenna height and antenna length is presented in Fig. 5.24b. Figure 5.24c displays the search point distribution between the antenna height and antenna width.Figure 5.24d illustrates the maximum electric field intensity inside the cylinder during the search process.

Comparison

Figure 5.23 and Fig. 5.24 present the approach of the NM search algorithm to the optimum solution for the optimisation problems. Table 5.14 lists the search results gathered for the different initial parameters. As previously mentioned and demonstrated in sections 3.6.1, 5.3.1 and 5.4.1, the NM algorithm relies on well defined starting values in order to obtain acceptable results.

Table 5.14: Search results of NM searches

Search	**Antenna length** (mm)	**Antenna height** (mm)	**Antenna width** (mm)	**Maximum Electric Field Intensity** (V/m)
1st	3.59	1.58	2.04	$6.065\,497\,6 \times 10^7$
2nd	14.40	2.05	6.19	$4.168\,517 \times 10^7$

Table 5.14 presents the different search results, it can be seen that the performance is superior in comparison to the results achieved in the earlier searches. The results presented do not include a solution to the supply frequency of the microwave generator. Therefore it is required to use the found antenna dimensions to determine the exact frequency for obtaining resonance.

Table 5.15: Resonance frequency results of the NM searches

Search	**Frequency** (GHz)	**Maximum Electric Field Intensity** (V/m)
1st	2.586 624	$6.684\,422 \times 10^7$
2nd	2.578 305	$5.160\,787 \times 10^7$

As mentioned earlier, this search uses the Eigenfrequency to calculate a corresponding frequency for the input variables instead of applying the supply frequency as an input

variable to the search process. After the optimisation search, a single variable deterministic search will be applied. The search will utilise the found antenna dimensions to obtain the correct resonance frequency of the cylinder as well as the maximum electric field intensity. Table 5.15 presents the result of the resonance frequency search for the found antenna dimensions in Table 5.14. The search demonstrated that the found maximum electric field intensities are nearly as the found field strength in section 5.3.1.

5.5.2 Non-Deterministic search

In this section, the non-deterministic optimisation search is implemented by the use of the Genetic Algorithm. The GA has some advantages and disadvantages which were reviewed in section 3.6.2. In order to find the most favourable solution, this optimisation search will vary the antenna length ("HAntenna1"), the antenna height ("HAntenna2"), and the antenna width ("WAntenna2") of the given simulation model in section 5.5. The whole investigation process includes two searches with the following starting conditions:

Table 5.16: Starting conditions of GA searches

Search	**Antenna length** (mm)	**Antenna height** (mm)	**Antenna width** (mm)
1st	0 - 5	0 - 6	0 - 5
2nd	0 - 10	0 - 6	0 - 5

Table 5.16 shows the initial values of the two searches. The chosen starting conditions for the antenna length, the antenna height, and the antenna width were influenced by the results of the single variable searches in sections 4.3.4, 4.4.1 and 4.4.2. The frequency will be calculated during the search process for each parameter pair by using the Eigenfrequency of the cavity (see section 4.3.7). The optimisation settings and stopping criteria for the used algorithm were set to the following values:

- Display = final
- CrossoverFcn = crossoverscattered
- CrossoverFraction = 0.8
- MutationFraction = 0.2
- EliteCount = 2

- Generations = 40
- PopulationSize = 101
- SelectionFcn = selectiontournament
- StallGenLimit = 20
- TimeLimit = Inf
- TolFun = 1E-6

These values are essentially the default settings of the algorithm provided by the MATLAB optimisation toolbox. A variation in these conditions at a later stage can improve the convergence and search performance or the overall search resolution.

1st Search

The first search employing the GA, uses the starting conditions defined in Table 5.9. The initial boundaries for the antenna length are defined as 0 mm to 5 mm, the antenna height as 0 mm to 6 mm, and the antenna width boundaries are 0 mm to 5 mm. As aforementioned, a frequency is not required and will be calculated during the optimisation search.

Figure 5.25 shows the trace of search and development of the different input variables and objectives by using the first set of initial parameters from Table 5.16. Figure 5.25a shows the search point distribution between the antenna length and antenna height in the range from 0 mm to 5 mm and 0 mm to 6 mm. The search point distribution between the antenna length and antenna width is presented in Fig. 5.25b. Figure 5.25c displays the search point distribution between the antenna height and antenna width. Figure 5.25d shows the maximum electric field intensity inside the cylinder during the search process.

2nd Search

The second search employing the GA uses the starting conditions defined in Table 5.9. The initial boundaries for the antenna length are defined as 0 mm to 10 mm, the antenna height as 0 mm to 6 mm, and the antenna width boundaries are 0 mm to 5 mm. As

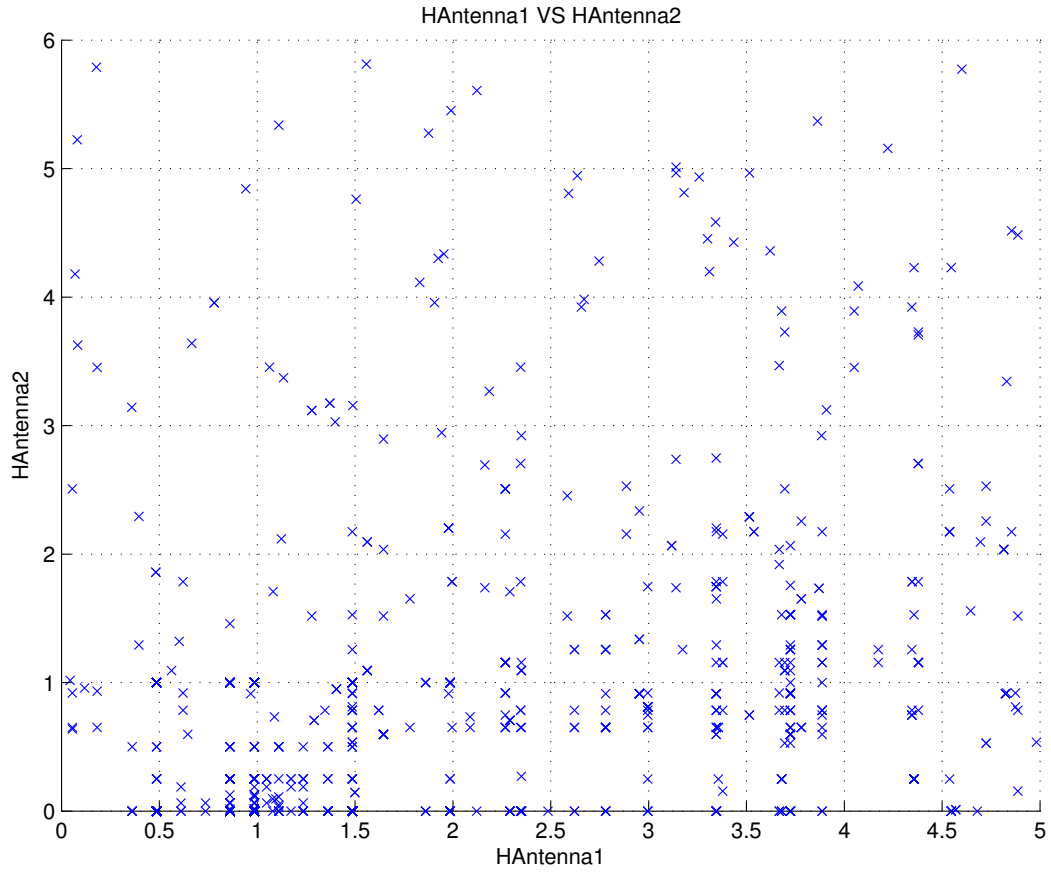

(a) Distribution of the search points of the antenna length and antenna height

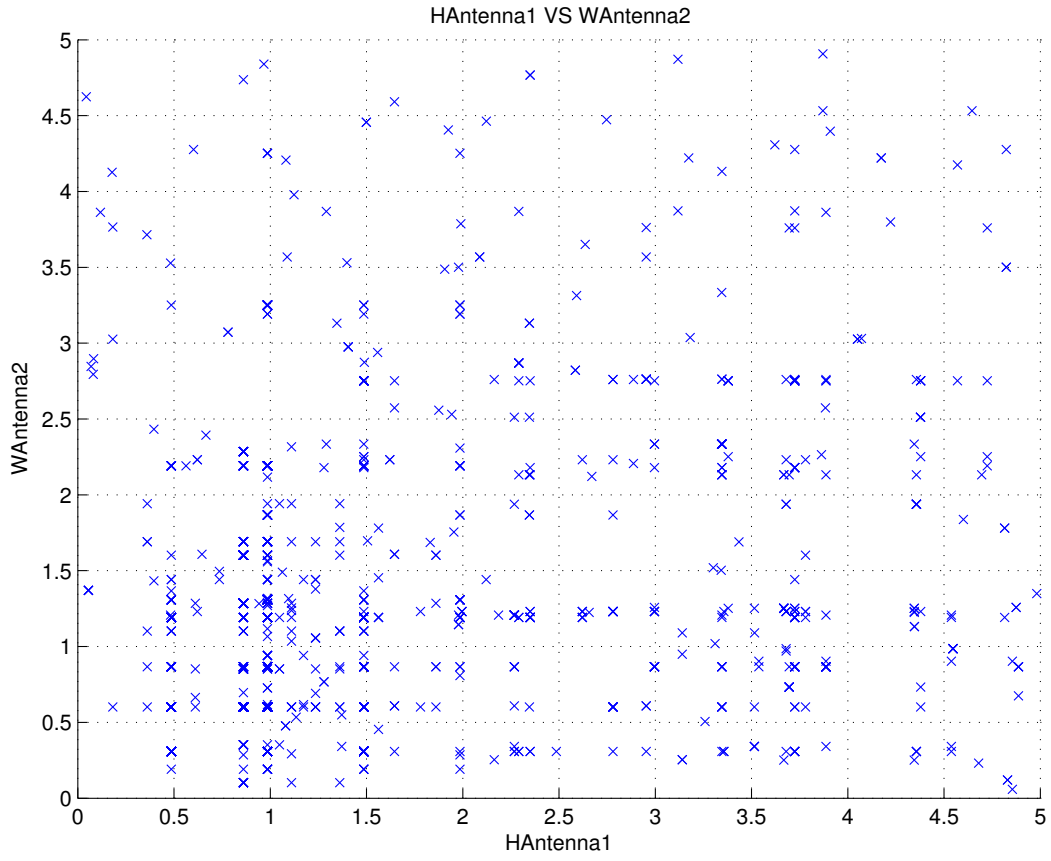

(b) Distribution of the search points of the antenna length and antenna weight

Figure 5.25: GA search for the 1st set of initial parameters of Table 5.16

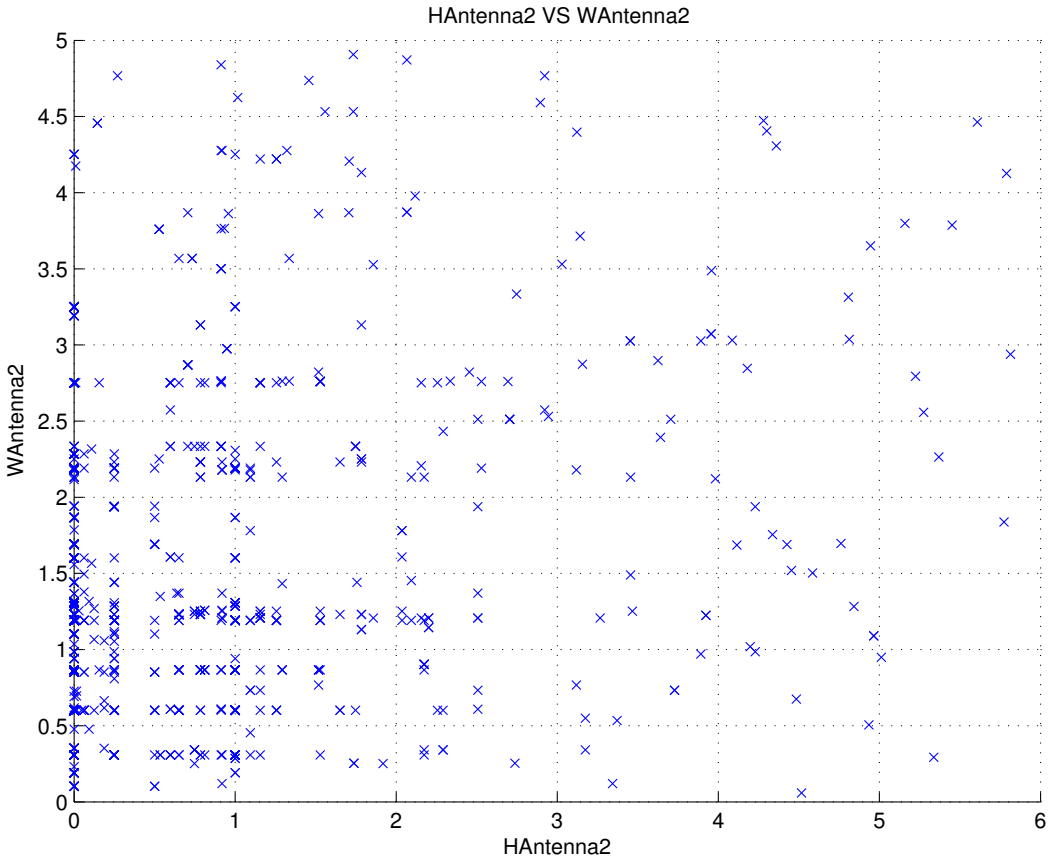

(c) Distribution of the search points of the antenna height and antenna width

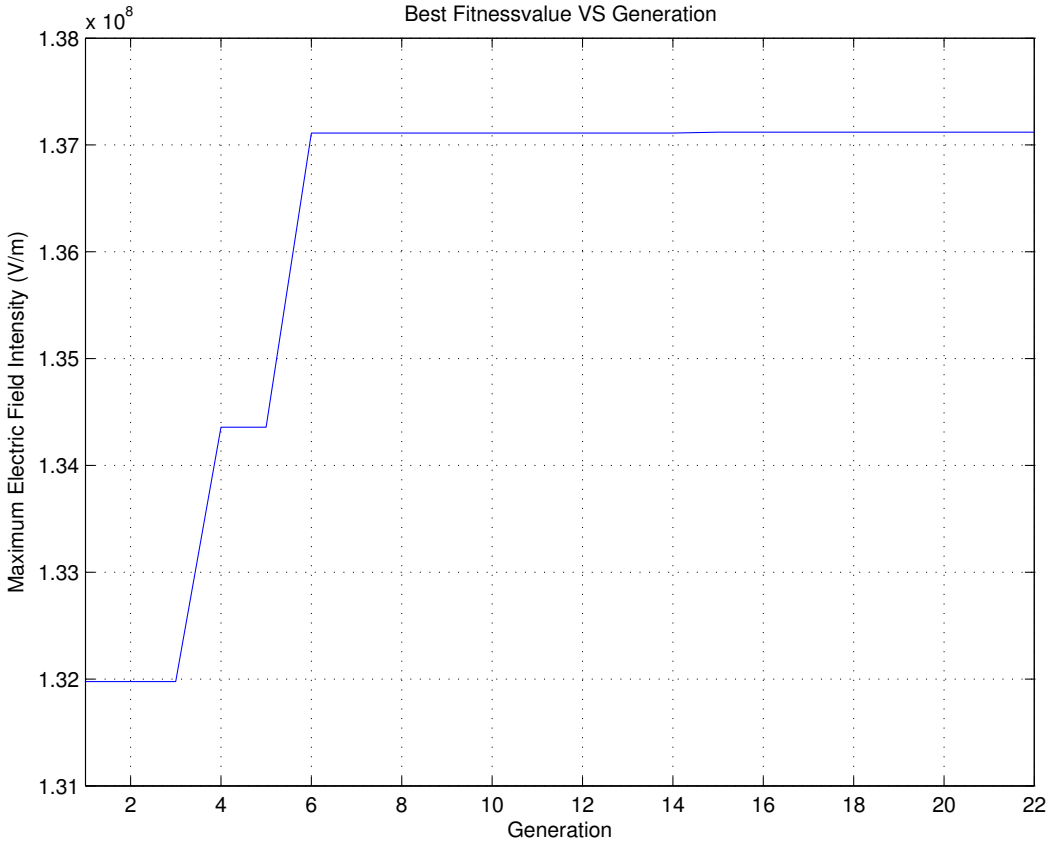

(d) Search trace for the maximum electric field intensity

Figure 5.25: GA search for the 1st set of initial parameters of Table 5.16

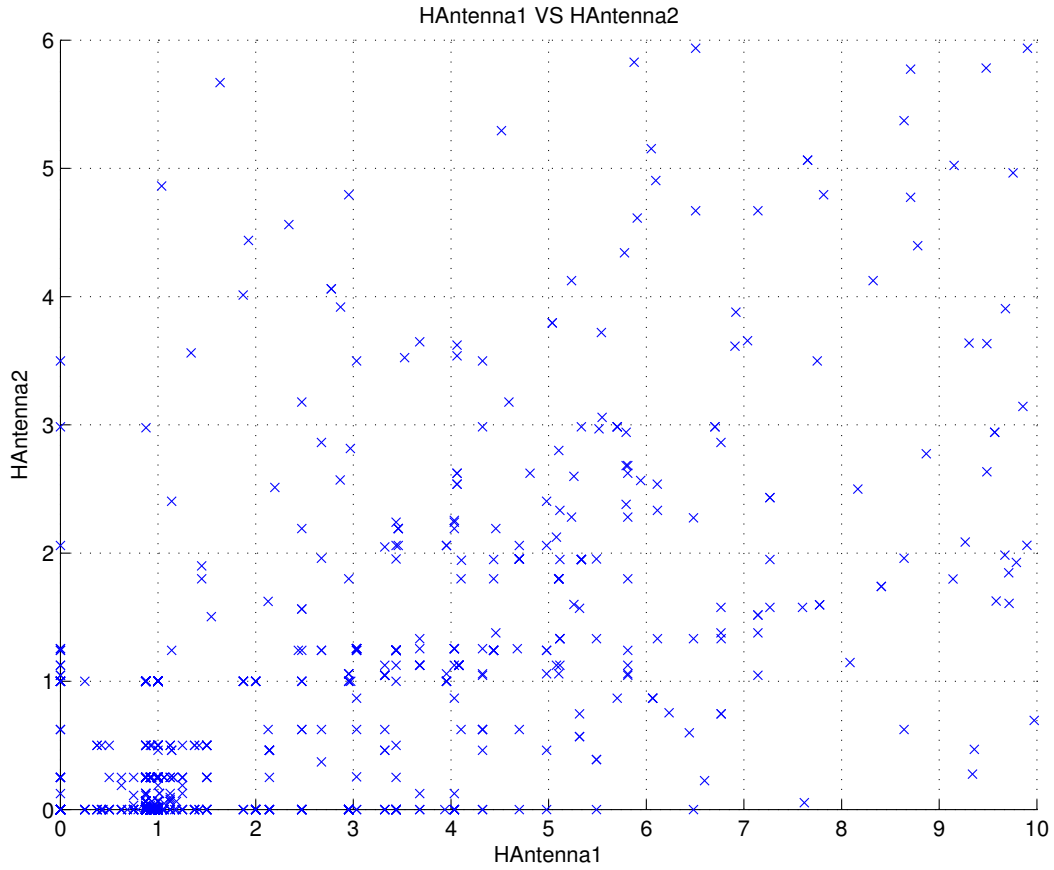

(a) Distribution of the search points of the antenna length and antenna height

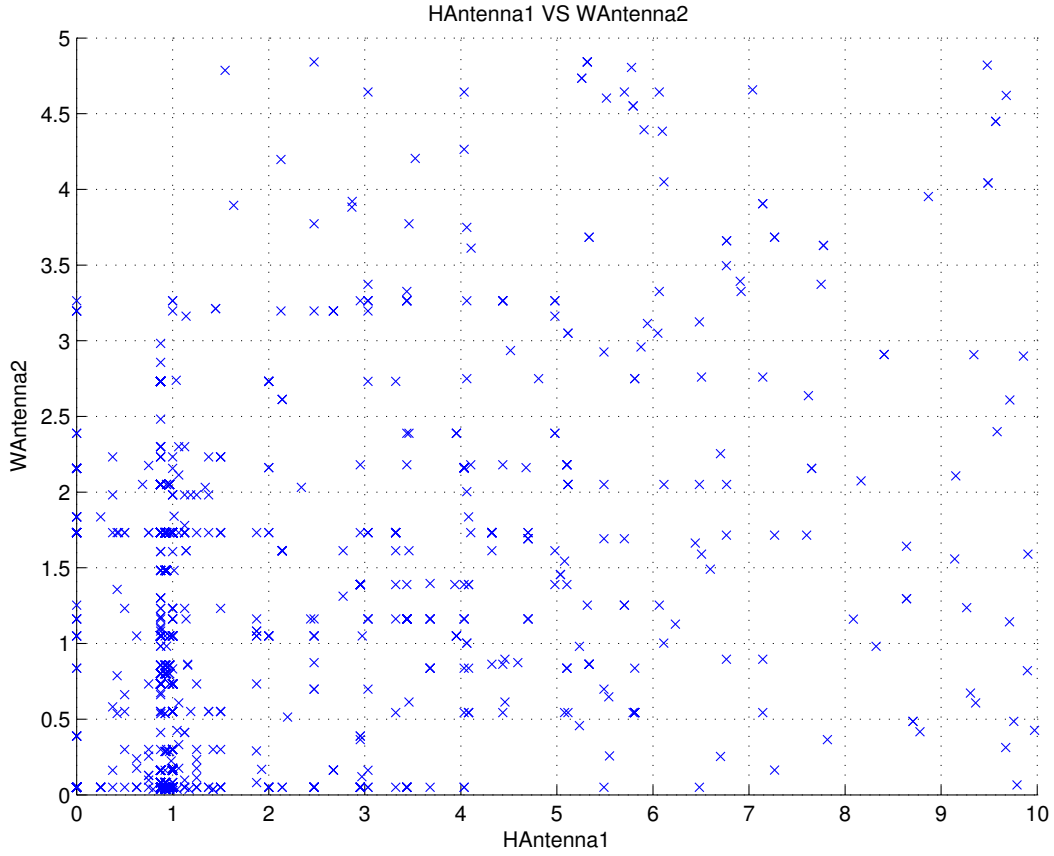

(b) Distribution of the search points of the antenna length and antenna weight

Figure 5.26: GA search for the 2nd set of initial parameters of Table 5.16

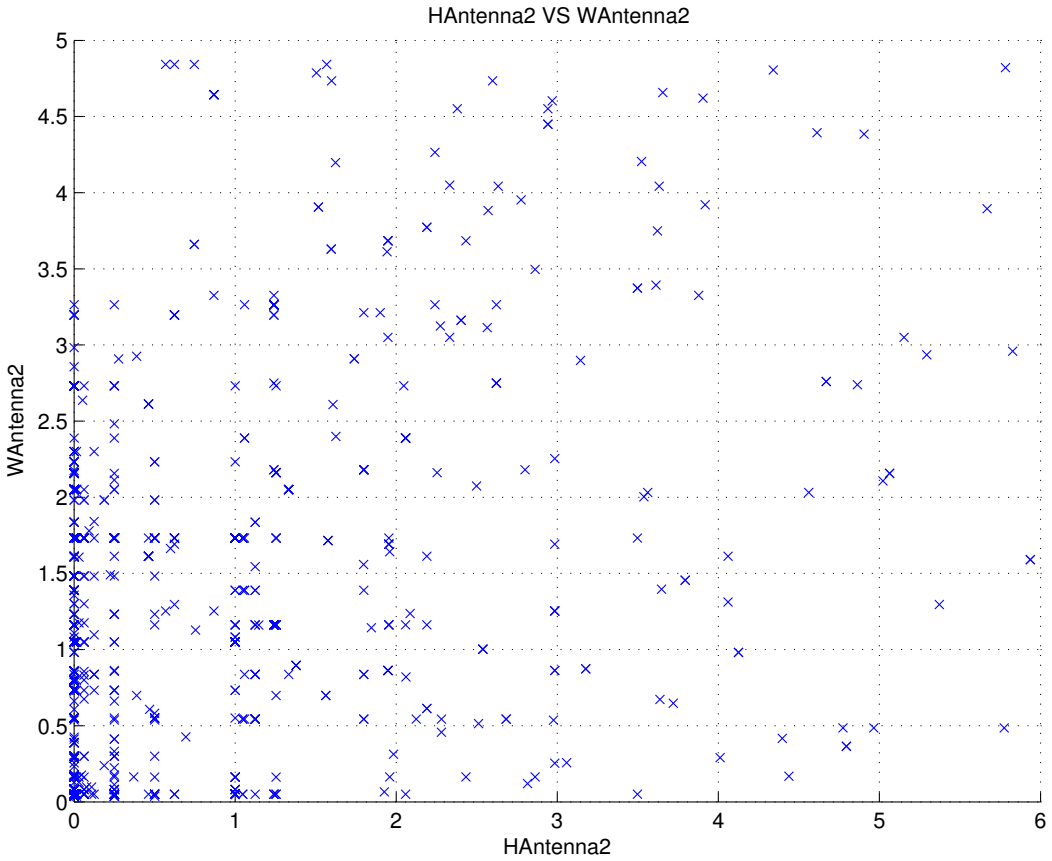

(c) Distribution of the search points of the antenna height and antenna width

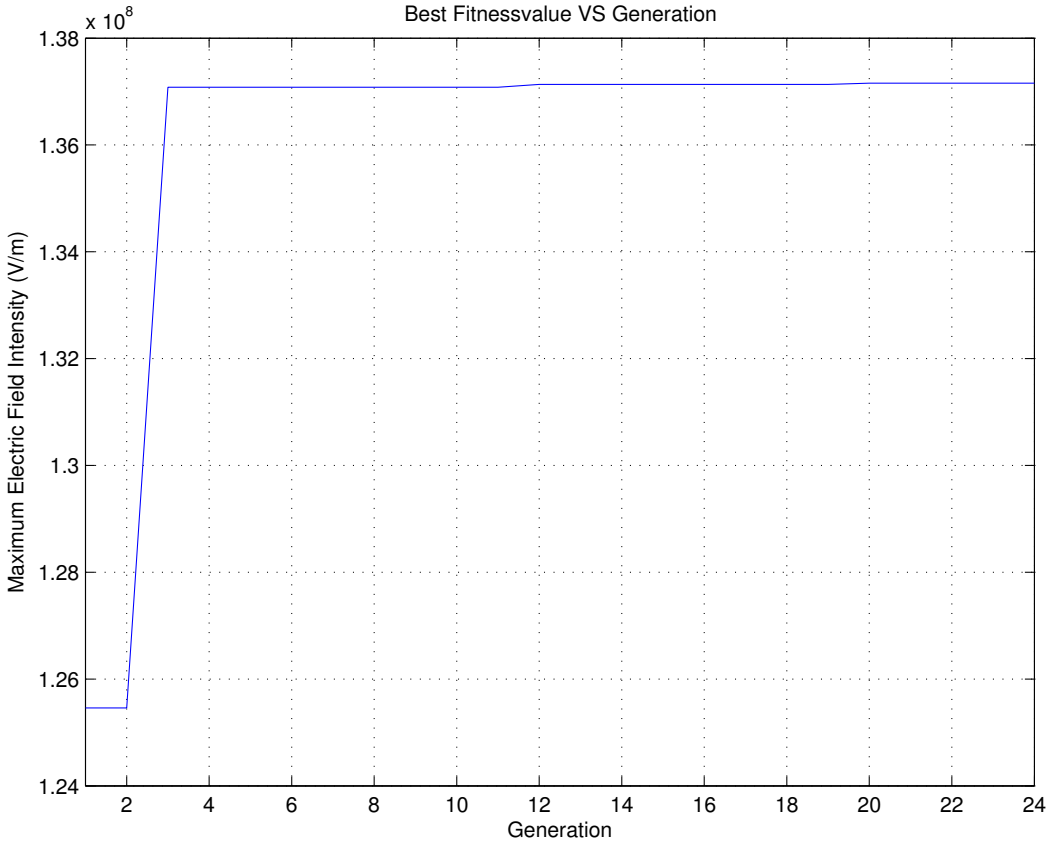

(d) Search trace for the maximum electric field intensity

Figure 5.26: GA search for the 2nd set of initial parameters of Table 5.16

previously mentioned, a frequency is not required and will be calculated during the optimisation search.

Figure 5.26 shows the trace of search and development of the different input variables and objectives by using the second set of initial parameters from Table 5.16. Figure 5.26a shows the search point distribution between the antenna length and antenna height in the range of 0 mm to 10 mm and 0 mm to 6 mm. The search point distribution between the antenna length and antenna width is presented in Fig. 5.26b. Figure 5.26c displays the search point distribution between the antenna height and antenna width. Figure 5.26d shows the maximum electric field intensity inside the cylinder during the search process.

Comparison

In the figs. 5.25 and 5.26 how the GA search algorithm approaches the optimum solution for the optimisation problems is presented. The GA search is a non-deterministic optimisation method and therefore the results will be inconsistent between different optimisation searches.

Table 5.17: Search results of GA searches

Search	**Antenna length** (mm)	**Antenna height** (mm)	**Antenna width** (mm)	**Maximum Electric Field Intensity** (V/m)
1st	0.86	0.0	1.60	$1.371\,203 \times 10^8$
2nd	0.92	0.0	0.50	$1.371\,585 \times 10^8$

Table 5.17 presents the different search results, the performance is superior in comparison to results achieved in earlier searches. The most suitable solution was found for an antenna height of zero. The presented results do not include a solution for the supply frequency of the microwave generator. Therefore it is required to use the found antenna dimensions to determine the exact frequency for obtaining resonance.

Table 5.18: Resonance frequency results of the GA searches

Search	**Frequency** (GHz)	**Maximum Electric Field Intensity** (V/m)
1st	2.596 059	$1.445\,262 \times 10^8$
2nd	2.596 059	$1.452\,231 \times 10^8$

As previously mentioned, this search uses the Eigenfrequency to calculate a corresponding frequency for the input variables applying the supply frequency as an input variable to the search process. After the optimisation search, a single variable deterministic search will be applied. The search will use the found antenna dimensions to obtain the correct resonance frequency of the cylinder as well as the maximum electric field intensity. Table 5.18 presents the result of the resonance frequency search for the antenna dimensions from Table 5.17. The found maximum electric field intensities are nearly as strong as the global maximum field strength found in sections 4.3.4 and 5.4.3.

Conclusion

In contrast to chapter 4, which used exhaustive searches to analyse the signal characteristics and the electric field intensity inside the engine cylinder, the chapter used different optimisation search algorithms to find the optimum antenna design for the best propagation performance. The complete search process was separated in three different scenarios: the combination of frequency and antenna length, the combination of frequency antenna length, antenna height, and antenna width, and the combination of combination of antenna length, antenna height, and antenna width.

Each scenario, which also included various antenna designs, was analysed with multiple deterministic as well as non deterministic algorithm searches. It has been shown that the deterministic search algorithms require less evaluations in comparison to the non-deterministic searches but achieve a lower overall search performance. The non-deterministic search algorithms on the other hand require significantly more evaluations but offer a better search performance to find the global extrema of the optimisation problem. Some results have shown negative values for the various antenna dimensions or exceeded the physical boundaries of the cylinder head during the search process. Therefore the use of the NM optimisation search can be problematic because no boundaries can be set. The enhanced search terminologies, presented in section 5.1 and section 5.2, and applied in section 5.5, tried to focus on the problem of finding the resonance frequency of the cavity. As shown, the supply frequency for the ignition device of a HCMI system is mandatory to generate a strong electric field inside the combustion cylinder to break down the air-fuel mixture. The results have shown a significant improvement of the convergence speed and the maximum electric field propagation performance inside the engine cylinder for the different antenna geometries and search conditions.

Chapter 6

Conclusions and Further Work

The research into a microwave ignition for internal combustion engines has been advanced in this thesis through simulations and Computer-Automated Design based virtual prototyping. This thesis has verified the feasibility of a microwave ignition system in terms of electromagnetic field strengths inside the cylinder. Furthermore, it addressed the design and prototyping problems concerning the homogeneous charge microwave ignition system through systematic virtual prototyping.

Primary to any simulation, the FEM simulation software COMSOL Multiphysics had been validated using a regular cylinder. The compared results agreed with the theoretical optimum. Various simulations have shown that the cylinder design, the antenna length, and the piston position can significantly affect the propagation performance inside the cavity as well as the resonance condition of the system. This has served as a pilot test of the Computer-Automated Design, to determine the most suitable cylinder and antenna design in terms of electromagnetic field propagation performance. This search has permitted analysis on the influence of the factors not related to the antenna design, e.g. the Air-Fuel Ratio of the mixture and the cylinder radius. It has been found that the Air-Fuel Ratio is not a requirement for the optimisation search. This is because the connection between Air-Fuel Ratio and maximum electric field intensity is proportional. Therefore it is possible to choose the Air-Fuel Ratio, based on the optimum value for the application. The systematic study of single and multivariable changes of the antenna dimensions have been analysed in furtherance of understanding the relationship between the different input variables. Two antenna designs were used for variable simulations and it was discovered that the inner antenna length has a significant impact on the maximum electric field intensity inside the engine cylinder.

The extension of an additional antenna had shown more non-linearities inside the

combustion cylinder. Subsequent to the single variable changes, the search had been successfully extended to a multivariable search to detect the relation between different input parameters. For example, it had been possible to observe that the resonance frequency is affected more by the piston position than by the antenna length. This discovery underlines the importance of the correct and exact timing advance and control of the ignition event.

The systematic search was extended by an intelligent CAutoD optimisation search with various algorithms. The first optimisation problem started from the supply frequency and the length of the first antenna. During the optimisation of this problem the Nelder–Mead algorithm and the Genetic Algorithm had presented some challenges due to the high influence of a correct resonance frequency. It was found, that often the bandwidth of resonance is just a few hundred kHz. Therefore a new search technique, as presented in section 5.2, had been developed to assist in the definition of the search range of the frequency and to improve the search performance. After the first search, the default antenna model was extended by an additional antenna with the intention of improving the propagation performance inside the combustion chamber at certain antenna dimensions. The second optimisation problem started from the supply frequency, the antenna length of the default antenna, and the antenna height and width of the extended antenna. It had been shown that both search techniques were challenged by the problem of reaching a reasonable electric field intensity inside the cylinder, to break down the air-fuel mixture. Therefore a new search technique, as presented in section 5.1, was designed to avoid the high influence of the resonance frequency and rendered it possible to solve optimisation problems without using the frequency as an input variable. This search technique can be used with the Nelder–Mead search and Genetic Algorithm, and was fully applied in section 5.5.

During the second optimisation, the Nelder–Mead as well as Genetic Algorithm optimisation had found an insufficient field strength compared to the global maximum. However, the Predefined Genetic Algorithm optimisation found an equivalent field strength compared to the first optimisation search with an antenna height of zero. The third search then, applied the advanced search technique which calculated the resonance frequency by using the Eigenfrequency. The non-deterministic algorithm has shown that the best propagation performance was achieved with an antenna height of zero and the width of the second antenna below 2 mm.

One issue that had been addressed during the automated search in this research, was the overhead time of communications between the FEM simulation platform and the optimisation algorithm. As a solution to this problem, a new interface between Multiphysics and MATLAB had been developed, which led to a significantly faster data exchange rate. This interface, FEM Solver, had been able to access COMSOL Multi-

physics via the Java Application Programming Interface and hence, port the optimisation algorithms used, to Java.

For fully-fledged CAutoD virtual prototyping of the electromagnetic propagation, the default antenna model had been extended with an additional antenna. The CAutoD algorithms using this more sophisticated model had the best performance with an antenna height of zero and a width of the second antenna below 2 mm. This determined, that any antenna at the outer shield of the coaxial cable and inside the cylinder head, will interfere with the electromagnetic propagation inside the cavity and lower the propagation performance. Therefore the use of this kind of antenna on an ignition device is not preferable. The gain of design flexibility stands in no reasonable relation to the loss of maximum electric field performance inside the engine cylinder.

In addition to the achievements in virtual prototyping, a new optimisation technique, the Heredity Algorithm, had been developed. Its convergence speed had been analysed using independent benchmark functions and it had been shown that the algorithm provides a significantly better performance in comparison with the Genetic Algorithm for all benchmark functions tested. This needs to be further researched with more tests and benchmark functions outside of this thesis.

Further work would involve the physical prototyping of a microwave ignition device to confirm the simulation based results obtained in this thesis. The achieved results, due to virtual prototyping, will be beneficial to the physical design process. At the current stage, the simulation carried out the electromagnetic field simulations in furtherance of creating a sufficient electromagnetic field inside the combustion chamber to initiate the breakdown of the air-fuel mixture. The next stage would be to model the chemical breakdown process of the air-fuel mixture, which allows the investigation of the behaviour of pressure and temperature in connection with microwave induced plasma inside the engine cylinder. In this way, it would be possible to gain more knowledge about the potential increase of the overall efficiency of the HCMI system.

Appendix A

Model Structure

To design a combustion chamber of and ICE as COMSOL Multiphysics model several steps are required, the initialisation, parameter, geometry, mesh, physics, material, selection, study, and result part. This section gives a few source code examples for the model structure and eventual dependences to other parts.

Listing A.1: COMSOL Multiphysics model initialisation

```
1  Model model = ModelUtil.create("Model");
2  model.name("Default_2D.mph");
3  model.param().set("A", "15");
4  model.param().set("B", "1.97");
```

The initialisation part created a new, empty, model object on line 1 and give this model a unique name on line 2. The variable *model* is used at any later stage to access the saved data or to extend the model partially. The use of parameters is optimal but useful while implementing a CAutoD system. This is the global position inside of the model structure to save and define all later required parameters and can be simple matched against possible input variables. It is possible to save every type of numbers throughout the model like a length for the geometry or just a material constant like the relative permittivity of the air-fuel mixture inside the cavity.

Listing A.2: COMSOL Multiphysics model geometry

```
5  model.geom().create("geom1", 2);
6  model.geom("geom1").axisymmetric(true);
7  model.geom("geom1").lengthUnit("mm");
8  model.geom("geom1").feature().create("r1", "Rectangle");
9  model.geom("geom1").feature("r1").set("size", new String[]{"A", "B"});
10 model.geom("geom1").run();
```

Prior simulation it is required to implementation the geometry of the combustion chamber and antenna design. In this example here a regular cylinder was created as a two dimensional simulation. If it is required to model a more complex cylinder design it is alternatively possible to import a geometry model directly from CAD applications like AutoCAD or Solidwords. The benefits of using a two dimensional simulation model is a simplified calculation and shorter simulation time compared to a three dimensional model implementation. Therefore this will be used for this project as long as nothing else is required. The disadvantage of using a axially symmetric implementation is that the model results are not providing any three dimensional informations. The cylinder shape cannot be irregular and no exact data of the location and behaviour of the electric field in the three dimensional cylindrical cavity are available.

Listing A.3: COMSOL Multiphysics model material and mesh

```
19  model.material().create("mat1");
20  //
21  model.material("mat1").selection().named("box1");
22  model.material("mat1").name("Dielectric");
23  model.material("mat1").propertyGroup("def").set("electricconductivity",
24        new String[]{"0","0","0","0","0","0","0","0","0"});
25  model.material("mat1").propertyGroup("def").set("relpermittivity",
26        new String[]{"2.713","0","0","0","2.713","0","0","0","2.713"});
27  model.material("mat1").propertyGroup("def").set("relpermeability",
28        new String[]{"1","0","0","0","1","0","0","0","1"});
29  //
30  model.mesh().create("mesh1", "geom1");
31  model.mesh("mesh1").run();
```

Every model component needs to be assigned with a material as well as a mesh size prior simulation. The mesh defined the element resolution for the whole mode, if so required it is also possible to define different mesh sizes within a simulation model. The change of the mesh size effects the results accuracy and also the calculation time of the simulation. A finer mesh size results in more elements to calculate for each step and therefore impacts the performance of every single simulation step within a CAutoD system. For a reliable and efficient implementation it is required to find a compromise between the element resolution and the simulation time.

Listing A.4: COMSOL Multiphysics model physics and study

```
31  model.physics().create("emw", "ElectromagneticWaves", "geom1");
32  //
33  model.physics("emw").feature().create("port1", "Port", 1);
34  model.physics("emw").feature("port1").selection().named("box6");
35  model.physics("emw").feature("port1").set("PortExcitation", "on");
36  model.physics("emw").feature("port1").set("PortType", "Coaxial");
```

```
37    model.physics("emw").feature("port1").set("E_src", "root.mod1.tEr");
38    //
39    model.study().create("std1");
40    //
41    model.study("std1").feature().create("eig", "Eigenfrequency");
42    model.study("std1").feature("eig").set("neigs", "1");
43    model.study("std1").feature("eig").set("shift", "2.6E9");
44    model.study("std1").run();
```

The physics part describes the behaviour and will be executed with the model while solving the simulation. For this project the main focus is laid on the EM calculation inside the combustion chamber. Prior the implementation as API it is useful to build and evaluate the used physics inside COMSOL with the advantage that COMSOL provides reasonable default values for the equations. The study will solve the given model by applying the defined physics and solution steps. This example here shows a calculation of the Eigenfrequency inside the cylindrical cavity. After solving the simulation model successfully the available results can be accessed and analysed on variable ways by using the extensive COMSOL API.

Bibliography

Bellenoue, M, S A Labuda, and M Engles (2005). "Corona discharge ignition and combustion promotion of methane/air mixtures". In: *Proceedings of the European Combustion Meeting*.

Birchak, J R et al. (1974). "High dielectric constant microwave probes for sensing soil moisture". In: *Proceedings of the IEEE* 62.1, pp. 93–98. ISSN: 0018-9219.

Bradley, D et al. (2004). "Fundamentals of high-energy spark ignition with lasers". In: *Combustion and Flame*, pp. 55–77.

Britannica Encyclopædia Online (2011). *Internal Combustion Engine*. URL: http://www.britannica.com/EBchecked/topic/290504/internal-combustion-engine (visited on 03/15/2012).

Comsol (2011a). *LiveLink^{TM} for MATLAB® User's Guide for COMSOL 4.2*.

Comsol (2011b). *Multiphysics Reference Guide for COMSOL 4.2*.

Comsol (2012). *RF Module User's Guide for COMSOL 4.2*.

Controls, Clipper (2012). *Dielectric Constant Values*. URL: http://www.clippercontrols.com/pages/Dielectric-Constant-Values.html.

Dana Corporation (2005). *Dana Corporation's AtmoPlas(TM) Technology Uses Pulsed Microwave Energy to Initiate Engine Combustion*. URL: http://www.thefreelibrary.com/Dana%20Corporation's%20AtmoPlas(TM)%20Technology%20Uses%20Pulsed%20Microwave...-a0136153394 (visited on 05/10/2014).

Davis, James A (1989). *Multipoint spark ignition system*. US Patent 4805570.

Davis, Lawrence David (1999). *Evolutionary algorithms*. Springer.

Dawkins, Richard (1996). *The Blind Watchmaker: Why the Evidence of Evolution Reveals a Universe without Design*. W. W. Norton & Company.

Deb, Kalyanmoy (2001). *Multi-Objective Optimization Using Evolutionary Algorithms*. Wiley.

DeFreitas, Dennis Michael et al. (1997). *Ignition methods and apparatus using microwave energy*.

Epping, Kathi et al. (2002). "The Potential of HCCI Combustion for High Efficiency and Low Emissions". In: *Society of Automotive Engineers*.

Gallatz, Armin and Nikita Hirsch (2010). *Micro Wave Ignition AG*. URL: http://www.mwi-gmbh.com.

Gallatz, Volker (2004). "Method for igniting combustion of fuel in a combustion chamber of an engine, associated device and engine".

Gallatz, Volker, Nikita Hirsch, and Irina Tarasova (2010). "Method for igniting combustion of fuel in a combustion chamber of an engine, associated device and engine".

Gesche, R, S Kühn, and C Andrei (2008). "Plasma ignition in a quarter-wavelength microwave slot resonator". In: *Journal of Physics D: Applied Physics* 41.19.

Ghanea-Hercock, Robert (2003). *Applied evolutionary algorithms in Java*. Springer.

Gilles, T (2011). *Automotive Service: Inspection, Maintenance, Repair*. New Automotive and Truck Technology Titles! Series. Cengage Learning. ISBN: 9781111128616.

Gundeisen, Martin (2004). *Energy efficient transient plasma Iignition and combustion*. Tech. rep. University of Southern California.

Gundeisen, Martin (2007). *Energy efficient transient plasma ignition physics and technology*. Tech. rep. University of Southern California.

Gurnett, Donald A., Amitava Bhattacharjee, and E.J. Zita (2006). "Introduction to Plasma Physics with Space and Laboratory Applications". In: *American Journal of Physics* 74, p. 462.

Hagen, J. von, Y. Venot, and W. Wiesbeck (2001). "Microwave-generated plasma in air under standard conditions". In: *IEEE Transactions on Plasma Science* 29.4, pp. 604–608. ISSN: 00933813. URL: http://ieeexplore.ieee.org/lpdocs/epic03/wrapper.htm?arnumber=940954.

Hartman, J (2004). *How to Tune and Modify Engine Management Systems*. Motorbooks Workshop. MBI Publishing Company. ISBN: 9780760315828. URL: http://books.google.co.uk/books?id=RYsglAO9f8gC.

Haupt, Randy L and Sue Ellen Haupt (2004). *Practical genetic algorithms*. Hoboken, N.J.: J. Wiley.

Jacobs, Christopher A. (1996). *The doctor's step-by-step guide to optimizing your ignition*. Jacobs Electronics, p. 160. ISBN: 0965085600.

Jalopnik (2007). *GM Rolls out Prototypes Powered by HCCI*. URL: http://jalopnik.com/293027/gm-rolls-out-prototypes-powered-by-hcci.

Jimenez, Francisco, Samuel D Ekpe, and Steven K Dew (2007). "Modeling of Low Pressure Magnetron Plasma Discharge". In: *COMSOL Conference*.

Johansson, Rolf et al. (2008). "HCCI Engine Modeling and Control using Conservation Principles". In: *Society of Automotive Engineers*.

Katsuhiro, K, A Endo, and J Takezaki (1981). *Ignition system for internal combustion engine*.

Kutlar, Osman Akin, Hikmet Arslan, and Alper Tolga Calik (2005). "Methods to improve efficiency of four stroke, spark ignition engines at part load". In: *Energy Conversion and Management*, pp. 3202–3220.

Lackner, Maximilian, Franz Winter, and Avinash K Agarwal (2010). *Handbook of combustion 5, New technologies*. Weinheim: Wiley-VCH.

Langmuir, Irving (1928). "Oscillations in Ionized Gases". In: *Proceedings of the National Academy of Science*, pp. 627–637.

Lichtenecker, K and K Rother (1931). "Die Herleitung des logarithmischen Mischungsgesetzes aus allgemeinen Prinzipien der stationären Strömung". In: *Physikalishce Zeitschrift* 31, pp. 255–260.

Liu, G.R. and S. S. Quek (2013). *The Finite Element Method: A Practical Course*. Butterworth-Heinemann.

Liu, Jianbang et al. (2005). "Transient Plasma Ignition". In: *IEEE TRANSACTIONS ON PLASMA SCIENCE* 33.2, pp. 326–327.

Looyenga, H (1965). "Dielectric constants of mixtures". In: *Physica* 31, Physica.

Makita, Minoru and Yuji Ikeda (2010). *Ignition or Plasma Generation Apparatus*.

Manning and M P (1995). "Plasma ignition system reduces NOx emissions". In: *Pipeline and Gas Journal* 222.10, pp. 26–30.

Martin, Tracy (2012). *How to Tune and Modify Motorcycle Engine Management Systems*. MotorBooks International, p. 192. ISBN: 0760340730.

Mitchell, Tom M. (1997). *Machine Learning*. McGraw-Hill Science/Engineering/Math. ISBN: 0070428077.

Moon, John F (1974). *Rudolf Diesel and the Diesel Engine*. London, United Kingdom: London:Priory Press.

Nelder, J A and R Mead (1965). "A Simplex Method for Function Minimization". In: *Computer Journal* 7, pp. 308–313.

Paschen, Friedrich (1889). "On the potential difference required for spark initiation in air, hydrogen, and carbon dioxide at different pressures". In: *Annalen der Physik* 273.5, pp. 69–96. (Visited on 10/30/2013).

Pepper, D W and J C Heinrich (1992). *The Finite Element Method: Basic Concepts and Applications*. Series in Computational and Physical Processes in Mechanics and Thermal Sciences. Hemisphere Publishing Corporation. ISBN: 9781560321040.

Pertl, F A and J E Smith (2009). "Electromagnetic design of a novel microwave internal combustion engine ignition source, the quarter wave coaxial cavity igniter". In: *Automobile Engineering* 223.11, pp. 1405–1417.

Potts, H and J Hugill (2000). "Studies of high-pressure, partially ionized plasma generated by 2.45GHz microwaves". In: *Plasma Sources Science and Technology* 9, pp. 18–24.

Qiao, J et al. (2003). "The development of microwave systems to reduce diesel exhaust emissions". In: *ICSE*, pp. 570–574.

Rajput, R K (2005). *Internal Combustion Engines*. Laxmi Publications.

Rao, S. S. (2005). *The Finite Element Method in Engineering*. Butterworth-Heinemann.

Ross, Brian (1999). "A Lamarckian Evolution Strategy for Genetic Algorithms". In: *L. Chambers (Ed.), The Practical Handbook of Genetic Algorithms*. CRC Press.

Schaus, Ropert J (2003). "Spark plug with multi-point firing cap". 660 8430.

Schleupen, Richard (2002). *Ignition Device for a High-Frequency Ignition*.

Schmidt, E, K Linkenheil, et al. (2003). *Induction driven igntion*.

Schmidt, E and H O Ruoss (2003). *Device for igniting an air-fuel mixture in an internal combustion engine*.

Seely, Samuel and Alexander D Poularikas (1979). *Electromagnetics : classical and modern theory and applications*. New York, United States of America: Dekker.

Sequeira, Brian (2011). *Table of Time-Harmonic Model Properties in Circular Cylindrical Waveguide*.

Smith, James E, R Stile, and G Thompson (1997). "Investigation of a Radio Frequency Plasma Ignitor for Possible Internal Combustion Engine Use". In: *International Congress & Exposition*. Detroit.

Spears, William M (2000). *Evolutionary algorithms: the role of mutation and recombination*. Springer.

Starikovskaia, S M (2006). "Plasma assisted ignition and combustion". In: *Journal of Physics D: Applied Physics* 39.16, pp. 265–299.

Stegun, Irene A., Milton Abramowitz, and David Miller (1965). *Handbook of Mathematical Functions With Formulas, Graphs and Mathematical Tables (National Bureau of Standards Applied Mathematics Series No. 55)*.

Taylor, C F (1985). *The Internal-combustion Engine in Theory and Practice: Combustion, fuels, materials, design*. Vol. 2. The MIT press.

U.S. Department of Energy (2013). *Fuel Economy*. URL: http://www.fueleconomy.gov/feg/atv.shtml (visited on 10/01/2013).

Ward Michael, A V (1991). *Reverse stratified, ignition controlled, emissions best timeing learn*.

Ward, Michael (1974). *Combustion in an internal combustion engine*.

Warnatz, Jürgen, Ulrich Maas, and Robert W Dibble (2006). *Physical and Chemical Fundamentals, Modeling and Simulation, Experiments, Pollutant Formation*. Berlin: Springer.

Wiener, O (1910). "Zur theorie der refraktionskonstanten". In: *Berichte über die Verhandlungen der Königlich-Sächsischen Gesellsschaft der Wissenschaften zu Leipzig* -, pp. 256–277.

Yasar, Osman (2001). "Plasma Modeling of Ignition for Combustion Simulations". In: *Proceedings of the International Conference on Computational Sciences-Part I*, pp. 1147–1158.